DESIGN REPORT FOR AN INDIRECTLY COOLED 3-m DIAMETER SUPERCONDUCTING SOLENOID FOR THE FERMILAB COLLIDER DETECTOR FACILITY

DO NOT DISTRIBUTE

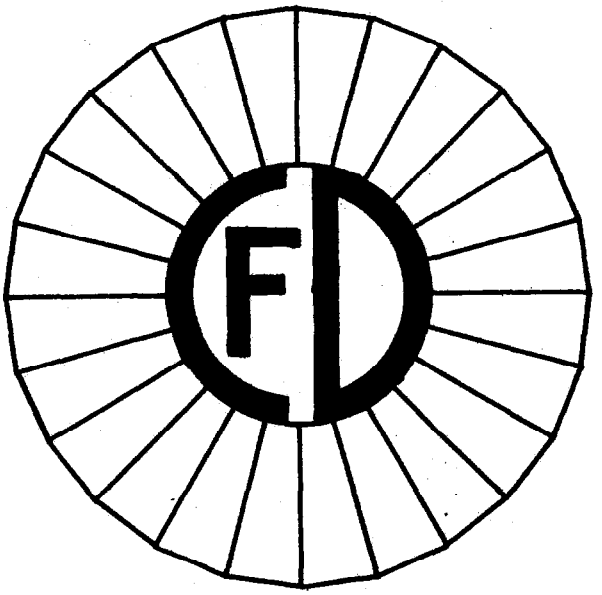

FERMILAB

OCTOBER, 1982

Fermilab

Fermi National Accelerator Laboratory
P.O. Box 500 • Batavia, Illinois • 60510

TM-1135
2750.000
October 1, 1982

DESIGN REPORT FOR AN INDIRECTLY COOLED 3-m DIAMETER SUPERCONDUCTING SOLENOID FOR THE FERMILAB COLLIDER DETECTOR FACILITY

R. Fast, J. Grimson, R. Kephart, E. Leung
L. Mapalo, R. Wands and R. Yamada
Research Services Department - Collider Detector Department
Fermi National Accelerator Laboratory

H. Minemura, S. Mori, M. Noguchi and R. Yoshizaki
Institute of Applied Physics, University of Tsukuba

K. Kondo
Institute of Physics, University of Tsukuba

TABLE OF CONTENTS

		PAGE
CHAPTER I.	INTRODUCTION	
	General Requirements	1
	Operational Guidelines	3
CHAPTER II.	YOKE DESIGN	
	General Features	7
	Magnetic Field Calculations	13
	Electromagnetic Forces on Detector Components	17
	Decentering Forces on Coil	24
	Testing of Coil Without Yoke	25
	Interaction of Yoke and Coil Upon Fast Coil Discharge	26
	Deflections and Stresses in Yoke	27
CHAPTER III.	COIL DESIGN	
	General Features	37
	Conductor	38
	Outer Support Cylinder	42
	Fabrication of Coil	42
	Eddy Current Analysis	46
	Analytical Stress Analysis	51
	Finite Element Stress Analysis of Coil Including Supports	56
	Computer Analysis of Quench Properties	60
CHAPTER IV.	CRYOSTAT	
	General Features	71
	Vacuum Vessel	71
	Support System	75
	Attachment of Cryostat to Yoke	79
	Liquid Helium Cooling Tube	81
	Radiation Shields and Thermal Intercepts	85
CHAPTER V.	CHIMNEY AND CONTROL DEWAR DESIGN	
	Chimney	89
	Control Dewar	91
	Transition Joints	91
	Assembly/Disassembly Joints	93
CHAPTER VI.	REFRIGERATION SYSTEM	
	Description	95
	Flow Diagram	95
	Hardware Components	98
	System Heat Loads and Capacity	100
	Steady-State Operation of Helium System	102

PAGE

Non Steady-State Operation of Helium System 102
Liquid Nitrogen System Operation 104

CHAPTER VII. DC CIRCUIT, POWER SUPPLY, BUS CONDUCTOR AND DUMP RESISTORS
DC Circuit 105
Prime Mover 105
Bus Circuit 107
Fast Dump Resistor 108
Slow Dump Resistor 109
5000 A Switches 109
Magnet Charge Time 109

CHAPTER VIII. INSTRUMENTATION AND CONTROLS
Magnet and Refrigeration Instrumentation 113
Power Suppy Instrumentation Package 121
Control System 123

CHAPTER IX. TESTING 127

ACKNOWLEDGMENTS 129

APPENDIX A: SYSTEM PARAMETERS 131

APPENDIX B: MATERIAL PROPERTIES 137

APPENDIX C: COMPUTER ANALYSIS OF QUENCHES 139

APPENDIX D: MAGNETIC FORCES ON DETECTOR COMPONENTS 151

APPENDIX E: RESIN IMPREGNATION 159

APPENDIX F: CODE DESIGN OF VACUUM SHELLS 165

APPENDIX G: MECHANICAL ANALYSIS OF SUPPORTS 175

APPENDIX H: FINITE ELEMENT THERMAL ANALYSIS OF SOLENOID 185

APPENDIX I: PRESSURE RISE DURING QUENCH 195

APPENDIX J: THERMAL ANALYSIS OF RADIATION SHIELD AND LN_2 INTERCEPTS 199

APPENDIX K: DESIGN OF CHIMNEY AND CONTROL DEWAR 205

APPENDIX L: RECOMMENDED THERMAL INSULATION SCHEME 217

APPENDIX M: HEAT LOAD INTO CRYOGENIC SYSTEMS 221

PAGE

APPENDIX N: PRESSURE RELIEFS 235

APPENDIX O: PRESSURE DROP DURING NORMAL OPERATION 239

APPENDIX P: LOCAL HEAT SOURCE INSIDE THE CDF SOLENOID COIL 245

CHAPTER I: INTRODUCTION

General Requirements.

The Fermilab Collider Detector Facility (CDF) is a large detector system designed to study $\bar{p}p$ collisions at very high center of mass energies. The central detector for the CDF* shown in Fig. I(1) employs a large axial magnetic field volume instrumented with a central tracking chamber composed of multiple layers of cylindrical drift chambers and a pair of intermediate tracking chambers. The purpose of this system is to determine the trajectories, sign of electric charge, and momenta of charged particles produced with polar angles between 10 and 170 degrees. The magnetic field volume required for tracking is approximately 3.5 m long and 3 m in diameter. To provide the desired $\Delta p_T/p_T \leq 1.5\%$ at 50 GeV/c using drift chambers with $\sim$ 200μ resolution the field inside this volume should be 1.5 T. The field should be as uniform as is practical to simplify both track finding and the reconstruction of particle trajectories with the drift chambers.

Such a field can be produced by a "cylindrical current sheet" solenoid with a uniform current density of 1.2×10^6 A/m (1200 A/mm) surrounded by an iron return yoke. For practical coils and

*"Design Report for the Fermilab Collider Detector Facility," Fermilab, Batavia, Illinois (August 1981).

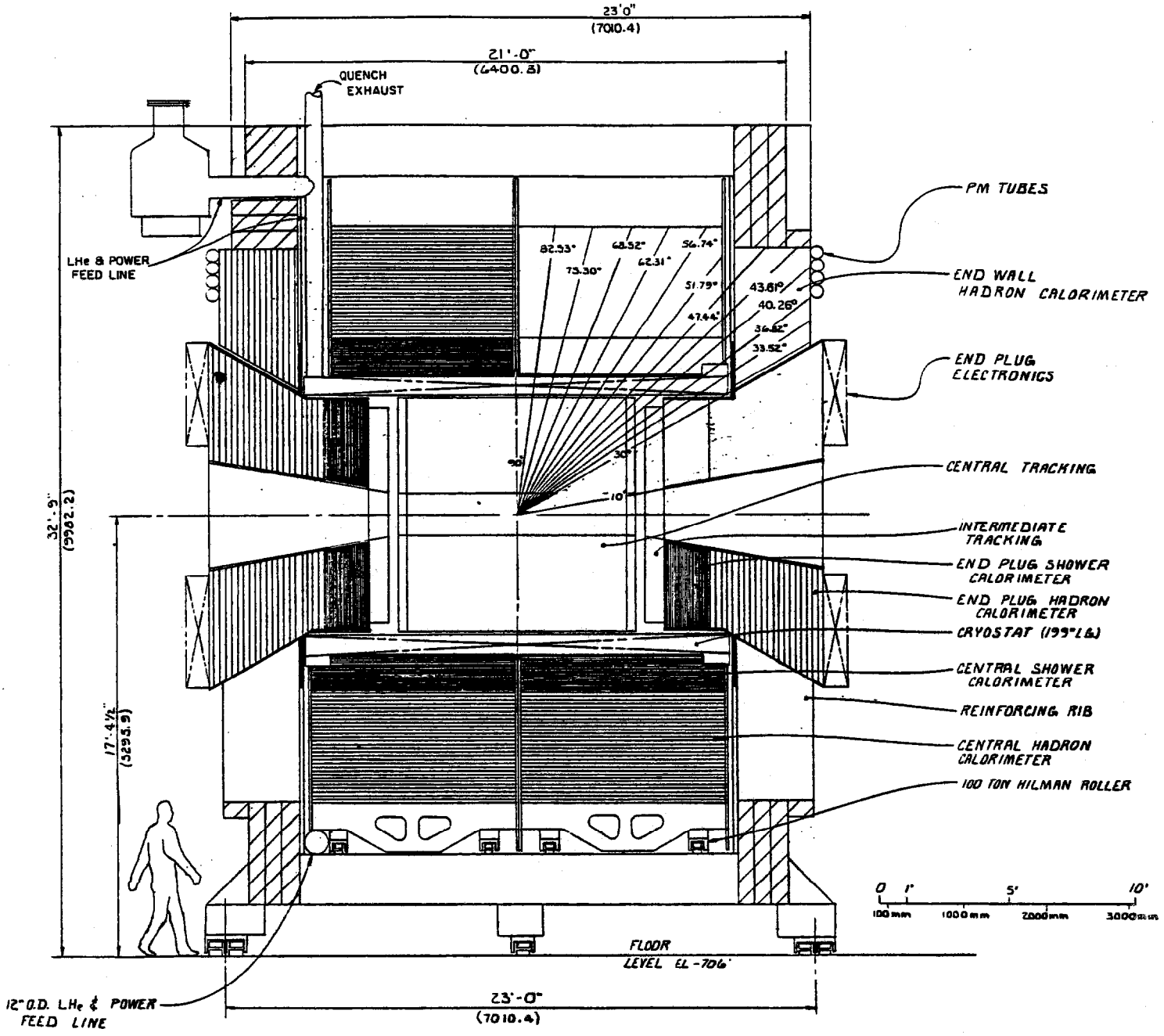

Fig. I(1). Side view of detector

return yokes, both central electromagnetic and central hadronic calorimetry must be located outside the coil of the magnet. This geometry requires that the coil and the cryostat be "thin" both in physical thickness and in radiation and absorption lengths. This dual requirement of high linear current density and minimal coil thickness can only be satisfied using superconducting technology. In this report we describe the design for an indirectly cooled superconducting solenoid to meet the requirements of the Fermilab CDF.

The components of the magnet system are discussed in the following chapters, with a summary of parameters listed in Appendix A. Additional operational guidelines used for the design are discussed below.

Operational Guidelines.

The central detector weighs 2400 short tons (2.18×10^6 kg). It must be capable of operation in either of two locations; the Collision Hall or an adjacent Assembly Hall*, with a moving time between the two areas of approximately 16 hours. The move is a straight-line translation of 98.25 ft (30 m). The superconducting magnet will be mounted in the detector and should remain cold (less than 77 K) for up to two days, giving a factor of three cushion to accommodate unforeseen difficulties during a move. The

*W. Nestander, et. al., "Colliding Beam Experimental Area at B0 Straight Section," Title 1 Design Report, Fermilab, Batavia, Illinois (August 28, 1981).

detector rolls on recirculating machinery rollers using hydraulic cylinders as prime movers. The areas are shown in Fig. I(2).

Power supply and refrigeration systems must be located outside the radiation area along the east wall of the Assembly Hall. The power bus and liquid helium/liquid nitrogen transfer line will enter the Collision Hall through 12" x 20" (300 mm x 500 mm) duct. A separate transfer line and power bus will exist for testing and operation of the magnet in the Assembly Hall.

During normal operation, the magnet is capable of being charged to full field in approximately 10 minutes. Under fault conditions, it must be possible to remove the large stored magnetic energy ($\sim$ 30 MJ) without damaging the magnet or detector in a manner that insures the safety of personnel. Moreover, the magnet and all of its auxiliary cryogenic and electrical systems must meet Fermilab and DOE safety requirements.

Auxiliary equipment necessary for operation or installation of the magnet, such as dewars, dump resistors, transfer lines, etc., must be compatible with other parts of the detector. In particular, the magnet system must not interfere with the central hadron and EM shower calorimeters and their removal for service, the mounting of the central tracking chamber and its service, end plug removal, intermediate tracking chambers, end wall calorimeters, and forward and end wall muon chambers.

The coil support structure must be designed to safely handle the large electromagnetic forces which act on the coil. Finally, since the coil is an essential component of the only general

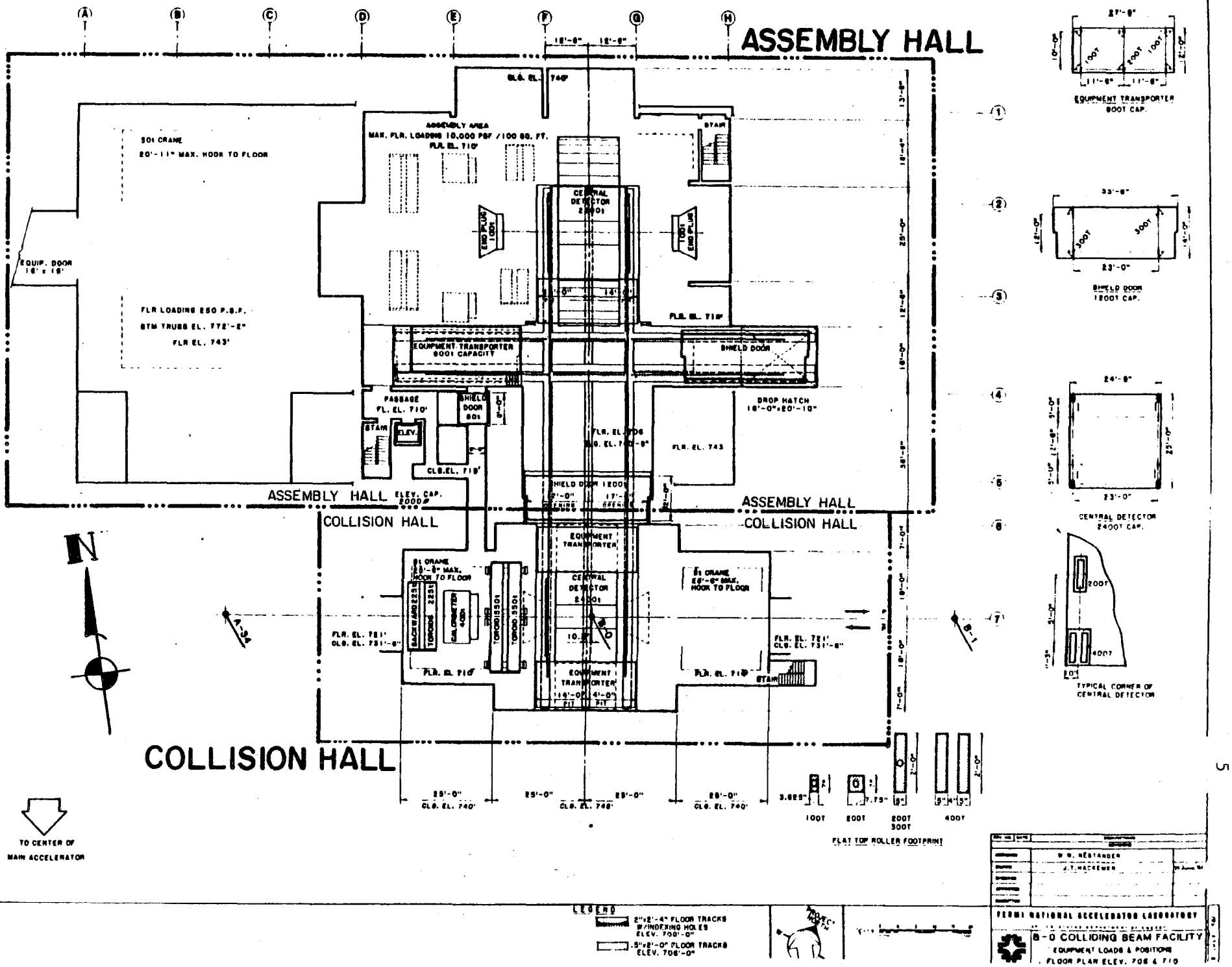

Fig. I(2). Plan view of facility

purpose detector that will in the forseeable future investigate $\bar{p}p$ collisions at center-of-mass energies of 2 Tev, it is crucial that the design goals are met, and that it be as trouble free and reliable in operation as possible.

CHAPTER II: YOKE DESIGN

General Features

The function of the yoke is to provide a flux return path for the central solenoidal field. The magnet yoke also provides the structural support for most of the modules of the central detector. An isometric view of the bare yoke is shown in Fig. II(1). The basic structure is that of two end walls and four return legs, constructed primarily of distressed steel (i.e., scrap low carbon steel plates) approximately 8" (200 mm) thick, cut to size, machined on appropriate surfaces, and welded into pieces weighing a maximum of 50 tons each.

The four return legs are made of this distressed steel plate and connect the end walls. The two lower return legs act as the supporting structure for the four "Roman" arches that carry the central calorimetry. The elevation of the upper surface of these lower return legs is set at 710 ft., the same as the predominant floor level in both the Collision Hall and Assembly Hall. This allows the arches to be rolled out onto the floor in the Assembly Hall or onto the transporter carts for servicing.

The two end walls are used as the structural support for the superconducting solenoid and for the calorimeter modules between 10° and 50° with respect to each beam. The edges are distressed steel plates. Extending in from the edges are twelve reinforcing ribs of 2" (50.8 mm) thick steel plate welded to a 2" (50.8 mm)

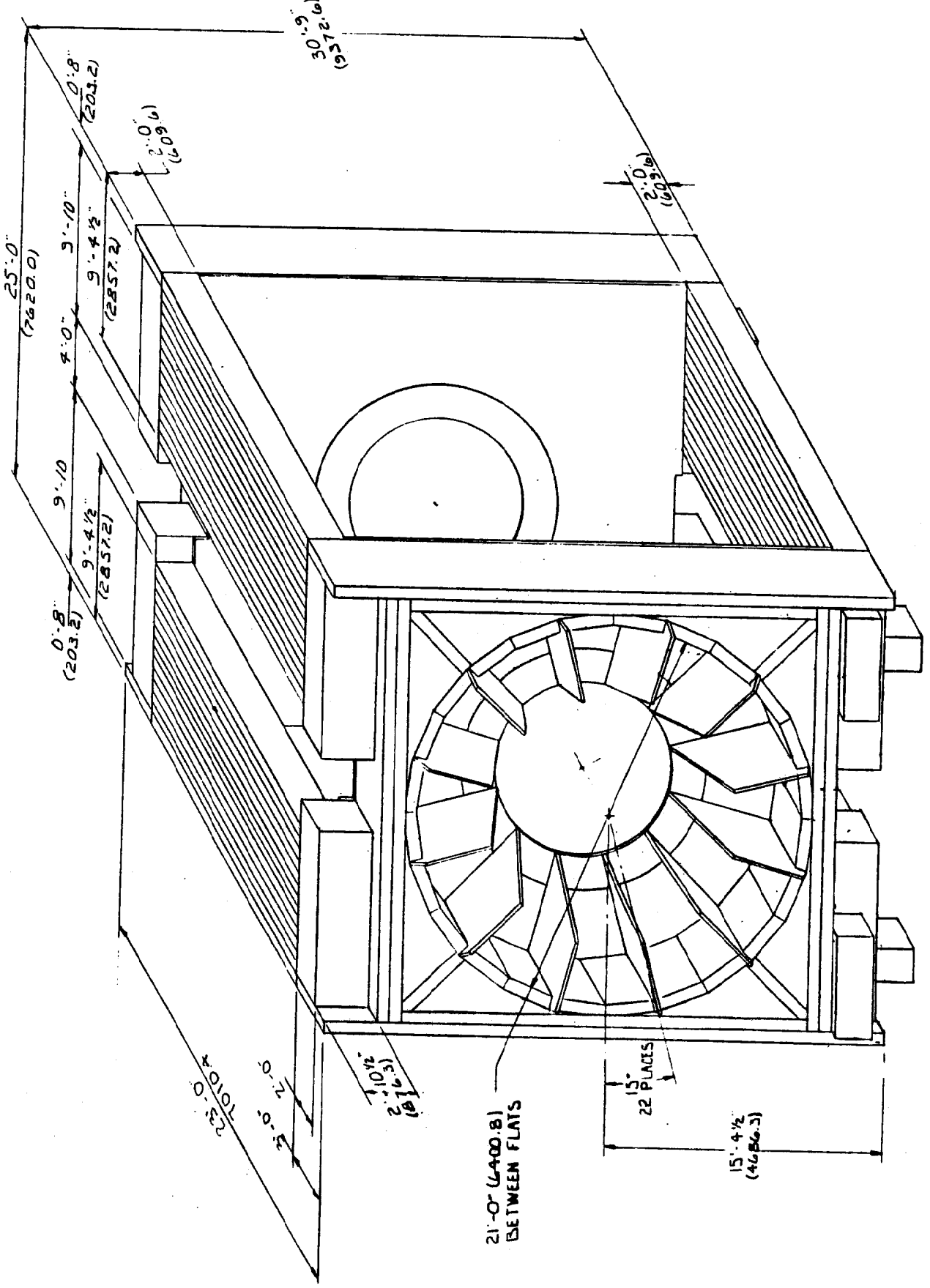

Fig. II(1). Isometric view of bare yoke

thick stainless back plate that serves as support for the solenoid and for the conical end plug.

The entire yoke will be assembled in the Assembly Hall with the help of the 50 ton crane. When the end wall and end plug calorimetry are in place, the yoke, coil, and cryostat can be tested and the field mapped without the central calorimetry.

The annular region between 30° and 50° is covered by end wall hadron calorimeter modules mounted between the twelve ribs of the end wall as shown in Fig. II(2). The annular region between 10° and 30° is covered by the end plug hadron calorimeter. These calorimeters are discussed in the next section. Both of these hadron calorimeters are used in the flux return path for the central solenoidal field. Since the axial forces on these calorimeters are large (approximately 460 metric tons total on each end), the calorimeters are fabricated from 2" (50 mm) thick steel plates. The axial compressive force on the conical end plug will be carried through the twelve radial reinforcing ribs to the yoke end wall.

Another function of the magnet yoke is to provide the support structure to roll the entire central detector between the Assembly Hall and the Collision Hall. The actual rolling mechanism is provided by eight 500 ton Hillman rollers.

Access to all phototubes is from the outside of each of the central and end wall calorimetry modules. The end plug calorimetry electronics is mounted on the outside surface of the end plug itself. The only parts of the central detector that must

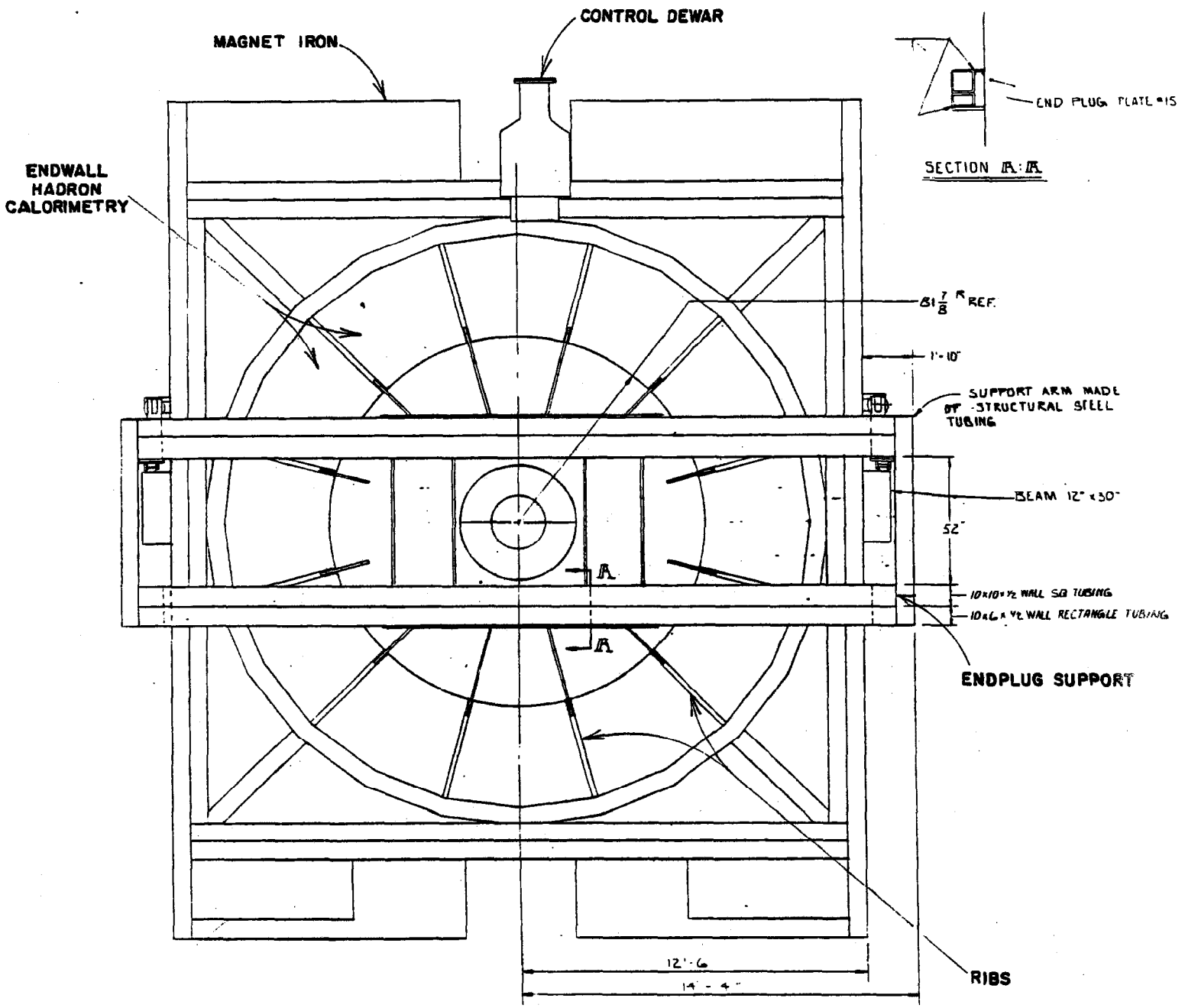

Fig. II(2). End view of yoke, end wall calorimetry, and solenoid

move for service access are the central arches (to service the central EM position chambers) and the end plugs (to provide service access to the central and intermediate tracking chambers).

A side view of the detector is shown in Fig. II(3) with the end plug extended. The detector consists of a stationary end wall hadron calorimeter and a movable end plug hadron calorimeter. Both parts are made up of a series of 2" (50.8 mm) steel plates separated by 3/4" (19.0 mm) air gaps. The stationary portion consists of 24 modules. The weight of the end plug hadron calorimeter is supported by horizontal beams traversing the vertical end wall frame members and attached to the plug on the outermost steel plate. This allows the end plug to be moved for access to the central tracking chamber. This frame is shown in Fig. II(2).

The outer portion of the end plug is cone shaped with the outside having an included angle of 60° with its vertex at the center of the detector. The bore of the end plug also is conical in shape, uses the same vertex, and has an included angle of 20°. The four innermost plates of the end plug hadron calorimeter form a cylinder with a diameter slightly smaller than the inner diameter of the bore of the solenoid. The end plug electromagnetic shower counter will be mounted to the innermost plate of the end plug hadron calorimeter.

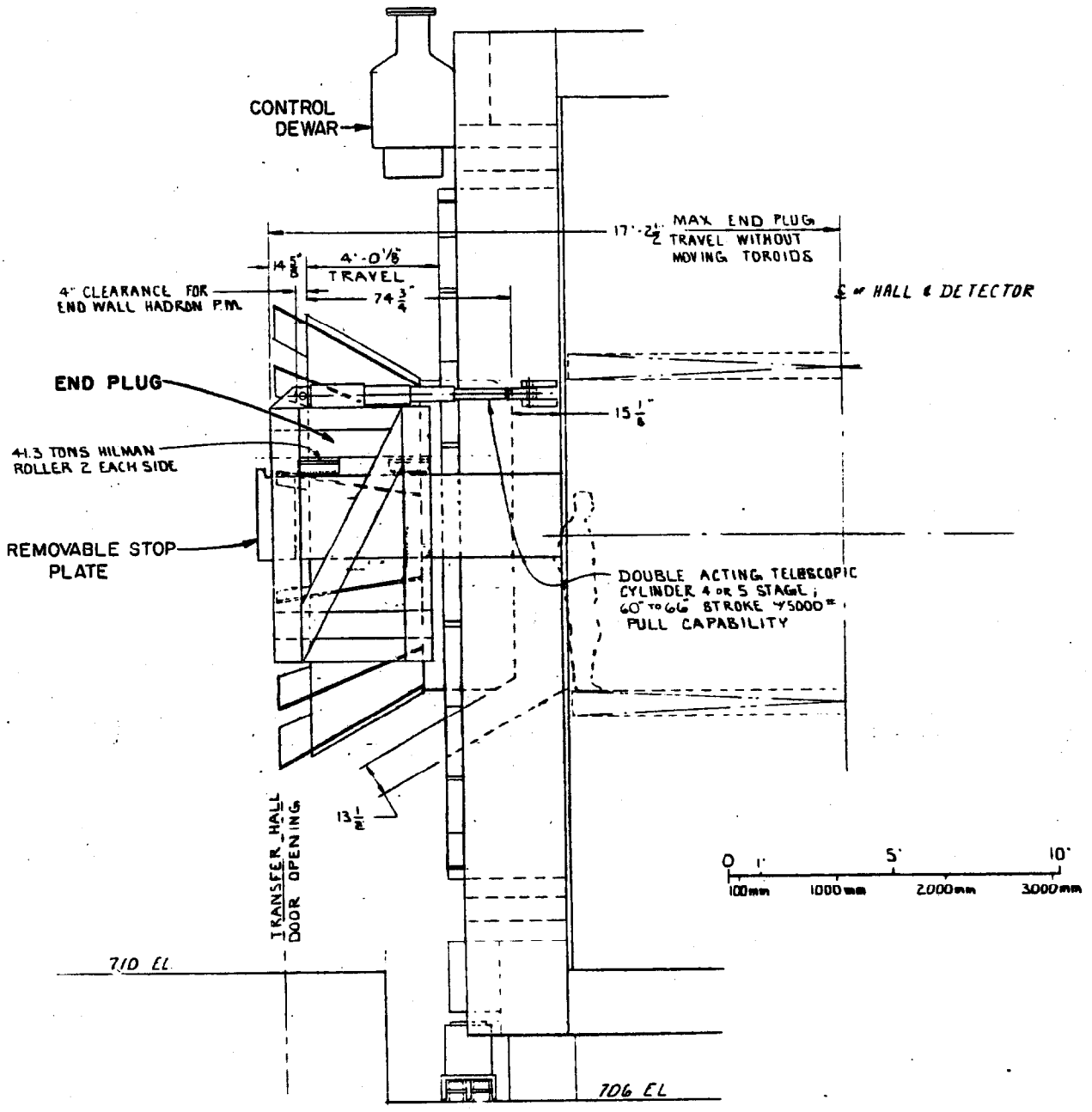

Fig. II(3). Side view of detector with end plug pulled back

Magnetic Field Calculations

Two-Dimensional Magnetic Field Calculations. A two dimensional magnetostatic program called TRIM* was used to calculate the magnetic field distribution of the CDF magnet. Its accompanying subroutine FORGY** was applied to estimate forces on the calorimetry, the yoke and the coil. These programs are useful for axisymmetrical cases, but do not actually calculate in three dimensions.

The geometry used for the calculation (Run "H14 CDF") is shown in Fig. II(4) (only a quadrant is shown). The CDF detector is not completely axisymmetric, but the main parts of the magnetic structure including the central calorimeter, end plugs, end wall, and the superconducting solenoid coil are axisymmetric. The return legs of the yoke which are far away from the central solenoid are nonaxisymmetric. For the calculation we have assumed perfect axisymmetry and have taken into account the non-symmetric yoke by using an effective width for the yoke of 10.7 inches (272 mm). As a result the calculated field around the yoke should be regarded as an average value with more accurate values to be determined in the future using three-dimensional programs.

* R.J. Lari and J.K. Wilhelm, Computer Program TRIM for Magnet Design, Argonne Internal Report, unpublished (May 22, 1972).

**T.K. Khoe and R.J. Lari, "FORGY" A Companion Computer Program of "TRIM" to Calculate Forces and Energy in Electromagnets, an Argonne Internal Report, unpublished (January 4, 1972).

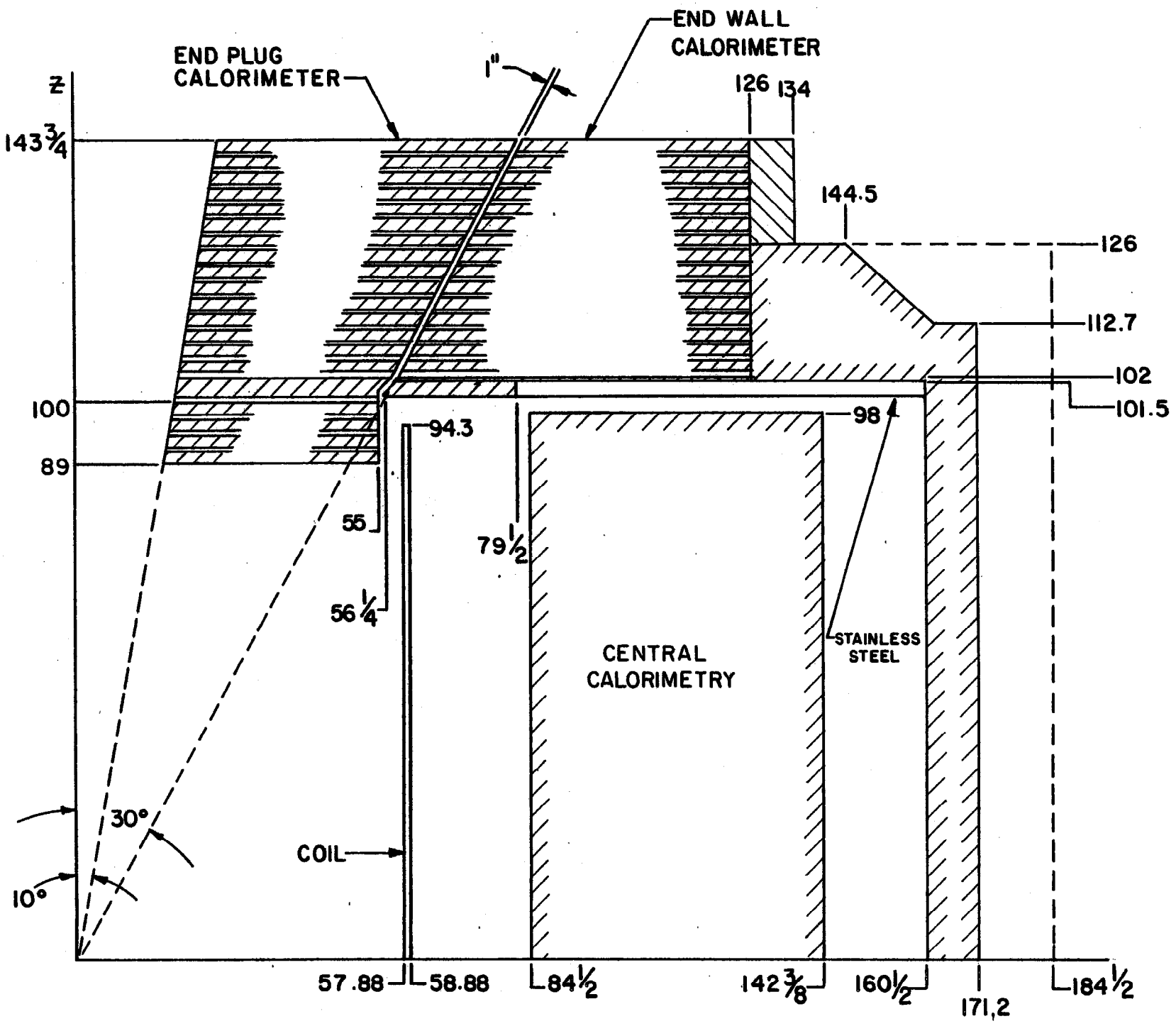

Fig. II(4). Iron and coil geometry for TRIM run "H14 CDF"

The field shape around the end of the superconducting coil depends strongly on several factors, as will be discussed. To achieve the most uniform axial field distribution, it is preferable to put the end of the conductor layer as close to the yoke surface as possible. However, with a superconducting coil, some gap is required between coil and yoke for insulation and structure. To improve the axial field uniformity, several steel plates (which act also as part of the end plug hadron calorimeter) extend into the bore of the coil.

To optimize the magnetic field uniformity and reduce the magnetic forces on the coil, the following major parameters can be adjusted. The numbers for the run "H14 CDF" are added in parenthesis.

1. Number of the re-entrant iron plates in the coil bore (4 plates).
2. Axial gap between the end of the superconducting conductor and the surface of the yoke (5.70 inches/145 mm).
3. Radial gap between the re-entrant iron plates and the superconducting conductor (3.38 inches/86 mm).
4. B-H curves of iron plates.

The dependence of magnetic forces on these parameters as well as their values for the proposed "best" geometry are presented in Appendix D. The flux distribution in the iron for "H14 CDF" is shown in Fig. II(5). The axial component of the magnetic field is uniform to $\leq$ 2%. The flux density at the center of the coil and in the return legs are about 1.49 T and 1.36 T, respectively. The

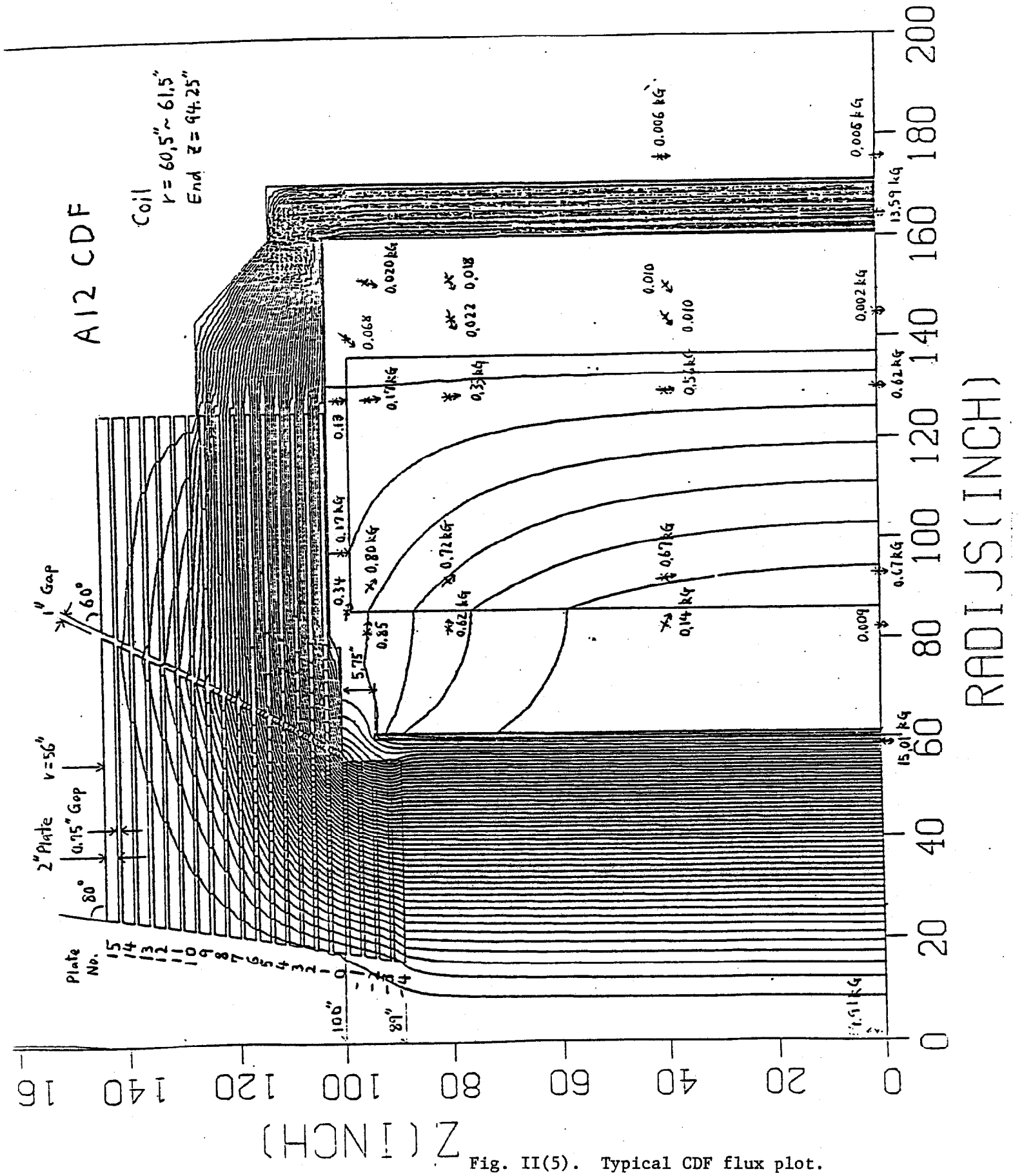

Fig. II(5). Typical CDF flux plot.

central hadron calorimeter was modeled as a solid iron block instead of a multiple-plate structure due to a shortage of regions in TRIM program. The flux density inside this block is estimated to be 0.07 T. In reality the front few plates of the multiple plate calorimeter may be driven to high flux density. However the field outside the calorimeter should be well represented by this model. Most of the area where the photomultipliers will be placed will be in a field of ∿ 20 gauss (2 mT) or less.

The detailed flux density in the iron around the end of the coil and in the re-entrant plates is shown for "H14 CDF" in Fig. II(6). The maximum flux density reaches 2.5 T in a limited corner area. Eventually we will measure the B-H curve of the iron to be used around the end plug, and recalculate the magnetic field using those numbers.

Electromagnetic Forces on Detector Components

There are five major components of the CDF detector which are affected by the magnetic forces. They are the superconducting solenoid coil itself, the end plug calorimeters, the end wall calorimeters, the yoke, and the central calorimeters. The forces on these components were calculated by using run "H14 CDF" and are given in Table II(1).

Some components, especially the thick iron yoke, and the aluminum disks and cylinders of the central tracking chamber and the coil cryostat, are subject to magnetic forces due to eddy currents generated in them when the magnet is discharged rapidly. There are also gravitational forces on each component and a force

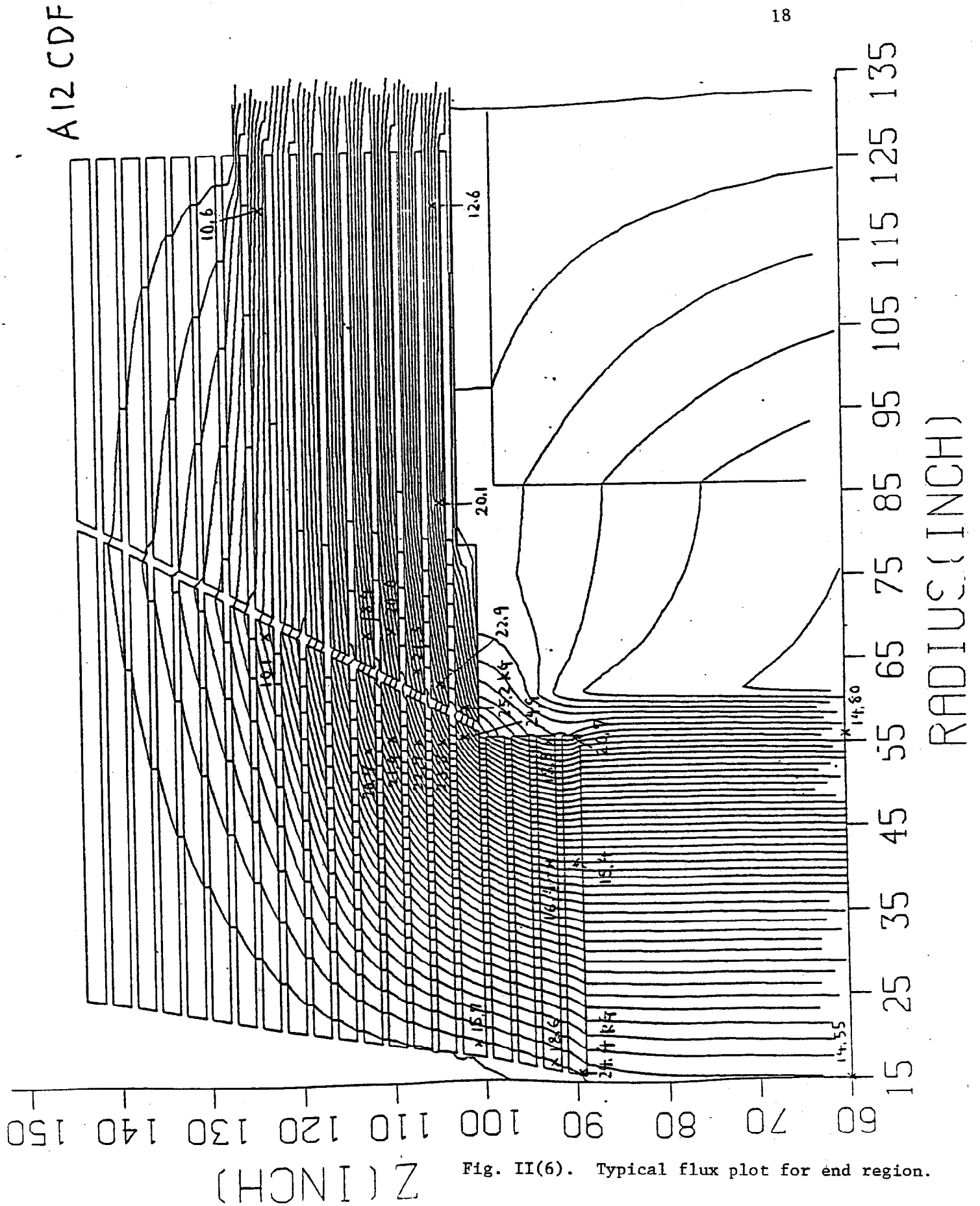

Fig. II(6). Typical flux plot for end region.

Table II(1). The distribution of axial forces among the components of solenoid magnet. The major parameters are 3 m ϕ, 5 m long. All forces A_z are given in metric tons.

Run No.	Major Characteristics	B_o (Tesla)	R (in.)	A_z on Coil	A_z on End Plug	A_z on End Wall	A_z on Calorimeter	A_z on Back Leg	Total A_z
A12	10^o opening	1.491	60.5	-123.2	-481.5	-26.3	+0.5	$\sim$ +0.2	-630.3
H14	10^o opening	1.494	58.38"	-95.4	-476.9	+18.6	+0.6	$\sim$ +0.15	-553
A200	Air core	$\sim$ 1.3	60.0	-537.5					-537.5
(A200)		(normalized to 1.49)		(-706 .1)					(-706.1)
CSL0126	Ideal Case No Hole	1.51	60.0	-4.2	-678.7	$\sim$ 0			-678.7

due to atmospheric pressure on components which are under vacuum. The superconducting coil is subject to $\vec{I} \times \vec{H}$ forces while ferromagnetic components experience the $(\vec{m}.\nabla)\vec{H}$ force.

Force on Coil. The force on the coil during magnetic excitation has been studied in detail and reported elsewhere.* There are two force components. One is the radial component which corresponds to a magnetic pressure of about 130 psi (0.9 MPa, 9 kg/cm^2), and the other is an axial force component caused by the radial component of the fringing field at the end of the conductor. This axial force can be minimized by choosing the optimum iron/coil geometry. The H14 CDF case calculated has an axial force of 0.94 MN (9.54 metric tons) toward the coil midplane. The forces from both ends of the coil compress the coil but do not result in a net force on the coil if the coil is axially centered in the iron yoke.

Force on End Plug. The end plug hadron calorimeter is made of a stack of 2 inch (50.8 mm) thick washer-shaped iron plates. The end plug is pulled as a unit into the center of the coil during magnet excitation. The total inward force calculated for

*R. Yamada, Can We Test Large Solenoid Coils Safely Without Yoke, January 26, 1981, Fermilab Internal Report, CDF-86, unpublished.

"H14 CDF" is 4.49 MN (458 metric tons) for each end plug. The distribution of the total force on individual plates is shown in Table II(2) for "H14 CDF" case. Interestingly the innermost re-entrant plates are not being pulled inwards strongly, because they are in a nearly uniform field. The radial forces on these plates are also shown in the table.

Force on End Wall. The forces on the end wall calorimeter, which is also made of two inch (50.8 mm) thick iron plates, are also listed in Table II(2). Only the second and the third plates are being pulled inwards. The remaining plates are being pushed moderately outward. The total outward force is 0.18 MN (18.6 metric tons), for the total structure of the end wall calorimeter. There are structural iron plates perpendicular to the two inch plates for the end wall calorimeter, which were not taken into account in the field calculation, and which will cause some change in the force on the end wall calorimeter.

The radial force on the end wall is also listed in the Table II(2). As is expected, its total radial force of 3.18 MN (324 metric tons), matches that of the end plug.

Force on Central Calorimeter. The forces on the central calorimeter are also listed in Table II(2). The total radial inward force is 0.018 MN (1.8 metric tons) corresponding to roughly 750 N (77 kg)/15^{o} unit. The axial force is 6.3 kN (640 kg) toward the end wall calorimeter for the 2.5 m long circular

Table II(2). Forces on End Plates of A12 CDF
FORCE ON PLATES OF H14 CDF

Parameters

4 re-entrant iron plates, r = 56"

2" iron plates and 3/4" gaps, 10^{o} opening

Coil R_{AVE} = 58.38" (R = 57.88 " ∿ 58.88") Gap between coil and plate = 3.38"

End at Z = 94.3" Gap between coil and 100" plate = 5.70"

Forces on End Plates

	End Plug		End Wall	
	FZ	FR	FZ	FR
Plate No.	Total Axial Force per plate (N)	Total Radial Force per plate (N)	Total Axial Force per plate (N)	Total Radial Force per plate (N)
Re-entrant				
-4	$+16.5 \times 10^{4}$	$+1.7 \times 10^{4}$		
-3	-18.8	+4.3		
-2	-32.9	+14.8		
-1	-38.0	+17.1		
Regular				
0	-75.1	+39.4	$+9.8 \times 10^{4}$	-59.6×10^{4}
1	-73.3	+35.0	-15.5	-52.0
2	-51.8	+41.2	-2.8	-40.0
3	-48.2	+41.0	+1.8	-45.8
4	-42.8	+35.1	+4.7	-35.1
5	-37.6	+27.1	+6.8	-28.5
6	-26.4	+20.1	+4.6	-19.9
7	-15.6	+11.9	+3.6	-13.3
8	-8.9	+8.2	+1.5	-8.1
9	-5.7	+5.0	+1.4	-5.4
10	-3.4	+3.4	+0.7	-3.4
11	-2.2	+2.2	+0.6	-2.4
12	-1.4	+1.6	+0.3	-1.6

Regular				
13	-1.0	+1.2	+0.3	-1.2
14	-0.6	+1.0	+0.3	-0.9
15	-0.3	+0.9	+0.1	-0.8
	-467.5×10^4	$+312.2 \times 10^4$	$+18.2 \times 10^4$	-318.0×10^4

Forces on Central Calorimeter

Radial	Total	-1.8×10^4 N	Pulling inwards
Axial	Total	$+0.63 \times 10^4$ N	Pulling out in 8

assembly. Thus, the forces on the central calorimeter can be easily handled.

Total Axial Force. The calculated total axial force on these four components for "H14 CDF" is 5.4 MN for 1.5 T, which seems a little low than expected. The corresponding number for the case of "A12 CDF" which has a slightly different geometry, is 6.4 MN. There is some convergency problem with "H14 CDF", while "A12 CDF" does not have this problem. It is expected future calculation will immprove the value of the axial force A_z on the end wall. In the case of "A12 CDF" the total for is the same as as that for the ideal case with no hole in the end plug. If the coil has a big internal axial force, then the axial force on the end plug becomes correspondingly smaller, as is explained in Appendix D.

Decentering Forces on Coil

There are two decentering forces on the solenoid, one axial and the other radial. These forces occur if the coil is not axially symetric, if the coil axis does not coincide with the magnetic axis, or if the coil is not symetric with respect to the radial field distribution.

Axial Decentering Force. The axial decentering force was estimated from two computer runs with TRIM and FORGY. In one case the coil is made one inch longer toward the end wall, "G14 CDF", and in the other one inch shorter, "D14 CDF". The axial spring constant for the proposed design was calculated from these two runs. It is 17.6 MN/m (10.1×10^4 lbf/inch). The magnitude of this spring constant is almost independent of small changes in the

configuration of the magnet. It is not much affected by the number of the re-entrant plates, nor by the length of the coil.

Radial Decentering Force. The radial decentering force was also estimated from two computer runs. In this case the diameter of the coil was made one inch bigger for one case and one inch smaller for the other. Then the case with one inch displacement with correct radius was assumed to be composed of a half of the small coil and the matching half of the big coil.

The radial spring constant was taken as the difference between the forces acting on each half coil. The value obtained in this way for the proposed design is 12.3 MN/m (7.0×10^4 lbf/inch) toward the bigger coil (i.e., decentering). This may be an over-estimation for the following reasons: If the contribution from two two-inch segments connecting these two half coils (assuming the average field over these segments is half the central field B_o) is taken into account, then the total force will cancel to zero. Therefore, the actual spring constant must be somewhere from 0 to 12.3 MN/m. For design purposes 12.3 MN/m was used, but a more correct number will eventually be determined from a three-dimensional calculation.

Testing of Coil Without Yoke

It is desirable to test the finished coil without the iron yoke. But, the force distribution in this case is quite different from that with yoke, and a detailed study is reported elsewhere.*

*R. Yamada, op cit.

This fact must be considered both in designing the solenoid coil and when testing it without the yoke.

If the solenoid coil were excited to the design current of 5000 A without the yoke, the radial field component at the end of the coil would be much larger and the total compressive force on the coil would be too large. Although differential compressive force on each conductor would diminish toward the center of the coil as usual, the accumulated force on the coil would increase toward the midplane, where it would be 5.3 MN (540 metric tons). Roughly speaking the accumulated axial compression on the coil without the yoke at half the design current still exceeds that with the yoke at full current. Thus we will not test the coil without iron to more than half the design current (seet Chapter IX).

Interaction of Yoke and Coil Upon Fast Coil Discharge

In a previous report the possibility of a tensile force on the coil during fast coil discharge is described.* It is reasoned that in the event of a quench the field from the coil might die out faster than eddy currents would permit the field from the iron to die out, thus the coil would experience a net axial tension sometime during the decay. We must also take into account the eddy current effects in the outer support cylinder and cryostat components. This problem should be worked out in detail.

*D. Cline, et. al., "Conceptual Design of a Large, Thin Coil Superconducting Solenoid Magnet for Colliding Beam Experiments at Fermilab," Technical Memo TM-826, Fermilab, Batavia, IL (October 25, 1978).

Deflections and Stresses in Yoke

The general purpose finite element program ANSYS was used to analyze the deflection and stresses in the yoke resulting from the electromagnetic loadings and structural weight.* Two three dimensional models of one quarter of the yoke were generated to analyze the following conditions:

1. Detector operation in the Collision Hall.
2. Transportation of yoke and instrumentation to and from the Assembly Hall.

The finite element models are shown in Fig. II(7). Under these conditions, some or all of the following loads will be present:

1. Weight of yoke.
2. Axial electromagnetic load on end plug and end wall.
3. Weight of "Roman Arch" hadron calorimetry on lower return legs.
4. Weight of end wall hadron calorimetry on end wall structure.

These loadings are summarized in Table II(3). The axial magnetic force which tends to compress the yoke was calculated from the equation

*R. Wands, J. Grimson, R. Kephart and D. Theriot, "Finite Element Stress and Deflection Analysis of CDF Yoke and End Plug", Fermilab TM-2750.1113, May, 1982.

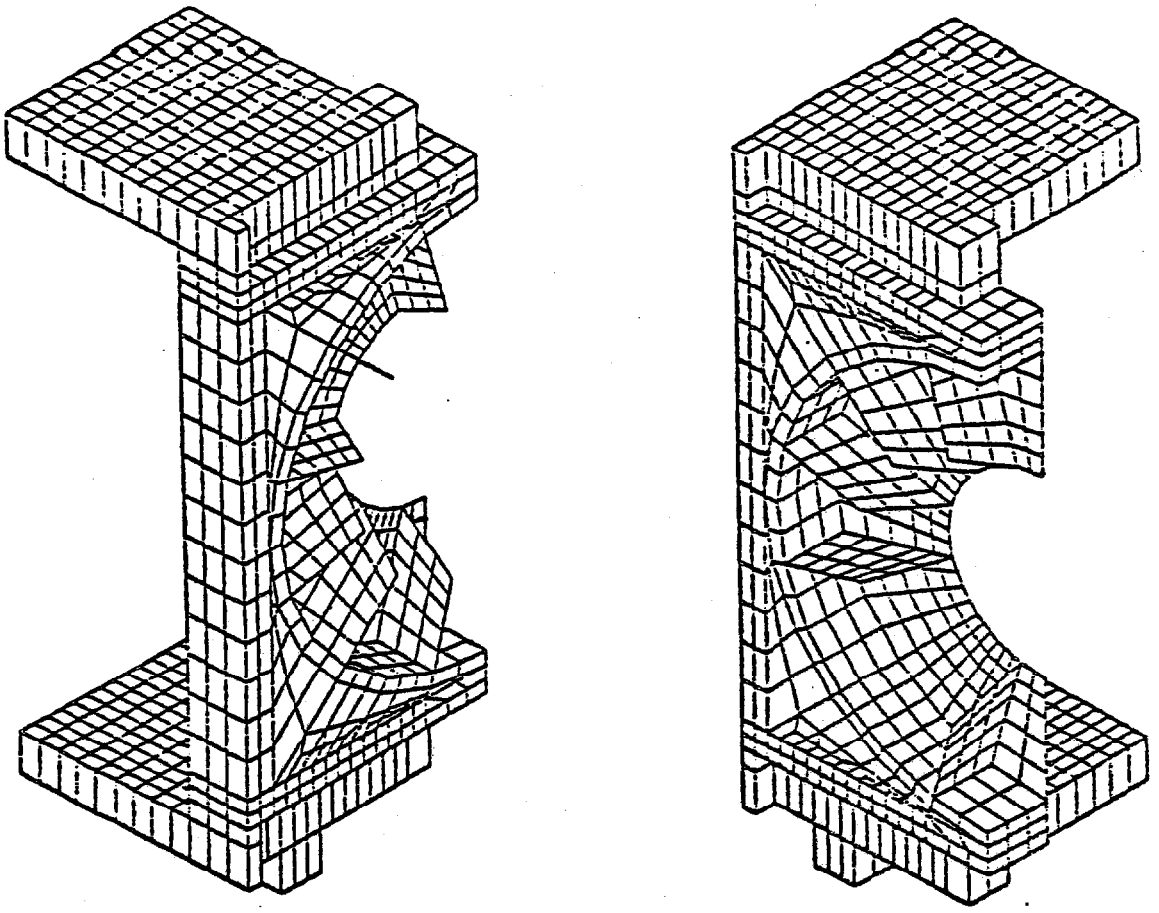

a) Operation model

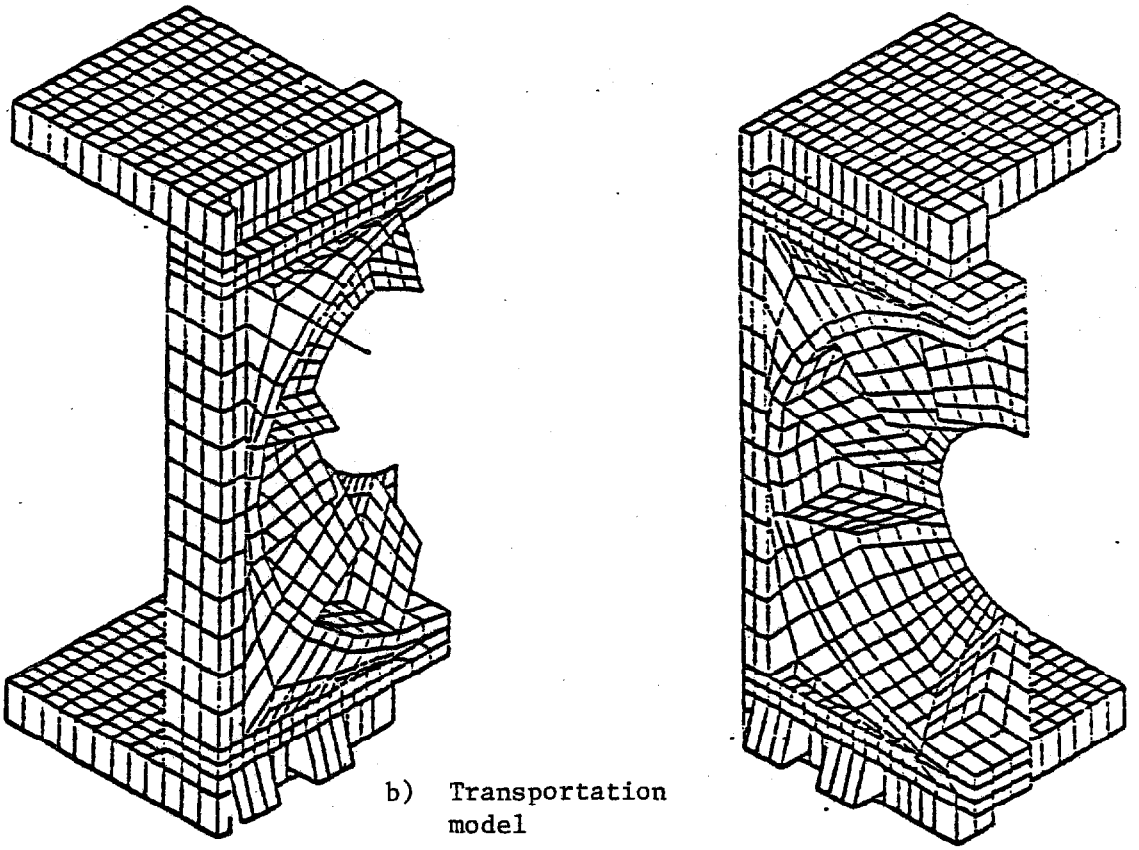

b) Transportation model

Fig. II(7). Yoke finite element models

Table II(3)

Loading of Yoke Finite Element Models

(Magnitudes correspond to load on one-fourth of yoke)

Load	Magnitude	Method of Application	Operation	Transportation	Thermal
Weight of yoke	$4(10^5)$ lbs	Coordinate acceleration	X	X	
Axial magnetic	$7(10^5)$ lbs	Nodal forces	X		
Weight of "Roman Arch" Hadron calorimetry	$3.6(10^5)$ lbs	Nodal forces	X	X	
Weight of endwall Hadron calorimetry	$3.12(10^5)$ lbs	Nodal forces	X	X	
Thermal	$\Delta T = 40^{\circ}$ F	Uniform ΔT			X

$$F = \frac{B^2 A}{2\mu_o}$$

where F = electromagnetic force

B = magnetic field

A = cross sectional area of solenoid

μ_o = permeability of vacuum

For a coil radius from centerline to current sheet of 157.5 cm (62 in) and a magnetic field of 1.5 T, the force F is 7.0 MN (784 short tons). A portion of this force appears as axial compression of the coil itself, and is not felt by the end wall since axial supports exist only at one end of the coil. Assuming this portion to be the 0.86 MN (94 short tons) calculated for the case of four reentrant plates, the total axial magnetic force felt by the end wall is 6.14 MN (690 short tons) at each end. A load of 6.23 MN (700 short tons) was used in this analysis to introduce some conservatism. Fig. II(8) shows the loading locations on the model.

The yoke deformations resulting from the four loading present during detector operation are shown in Fig. II(9). Maximum deflections for both the operation and transportation modes are summarized in Table II(4).

The axial deflection during operation is 2.7 mm (0.106 in) and should not interfere with detector function. The relative deformation of the backing plate of the end wall by which the

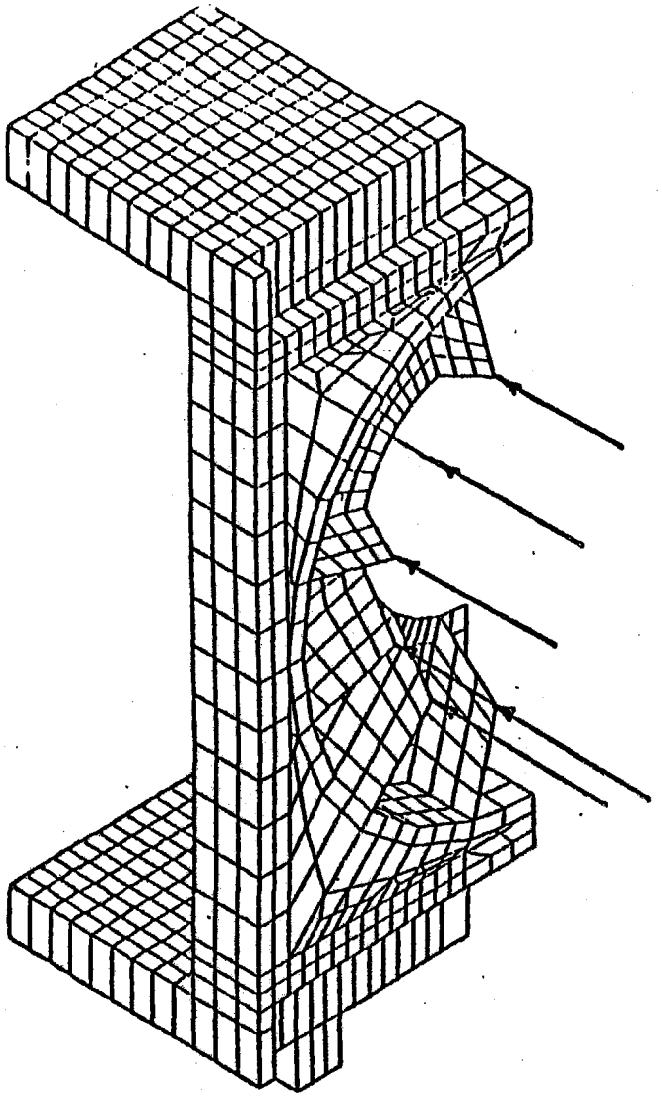

Axial Loading
Total Force = $7(10^5)$ lbs.

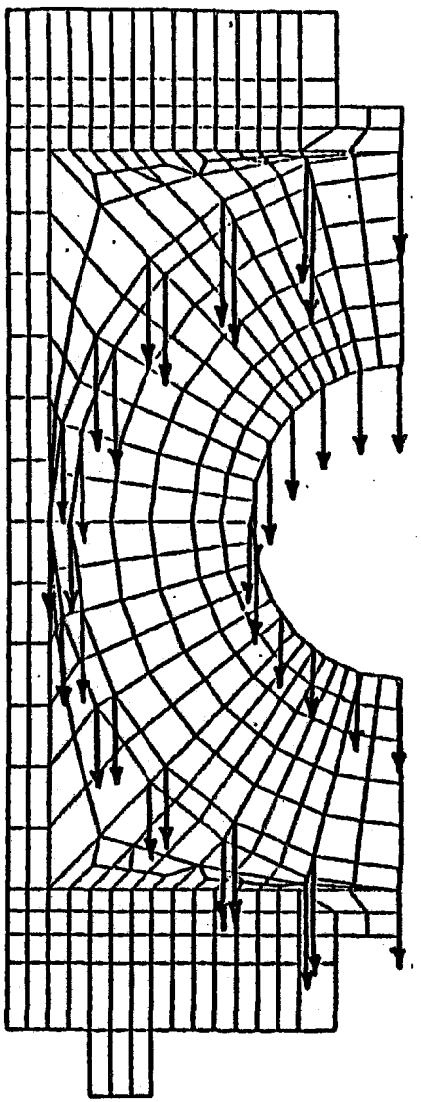

End Module Loading
Total Force = $3.12\ (10^5)$ lbs.

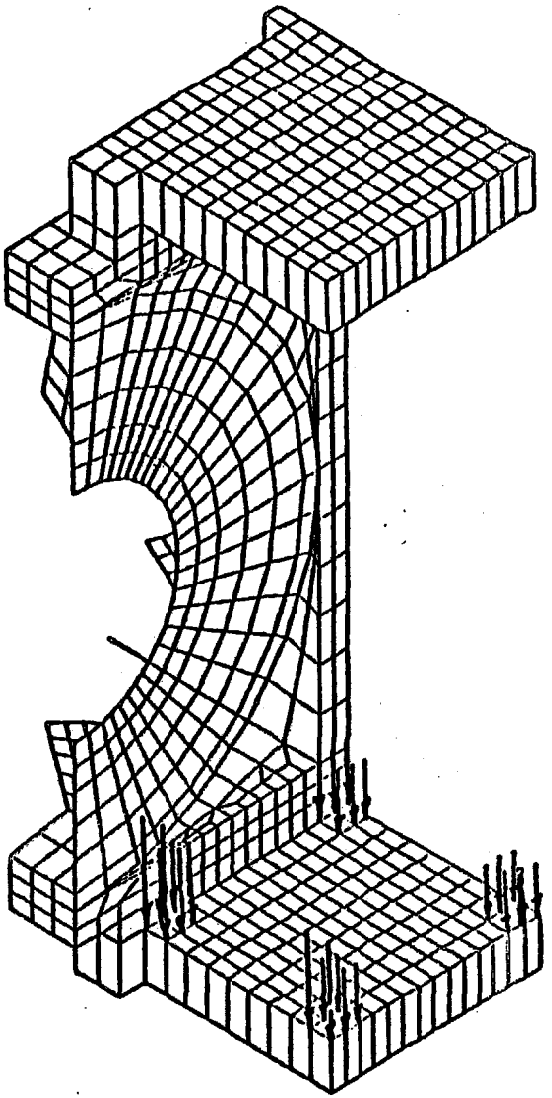

"Roman Arch" Central Calorimetry Loading
Total Force = $3.6(10^5)$ lbs.

Fig. II(8). Location and magnitude of loadings

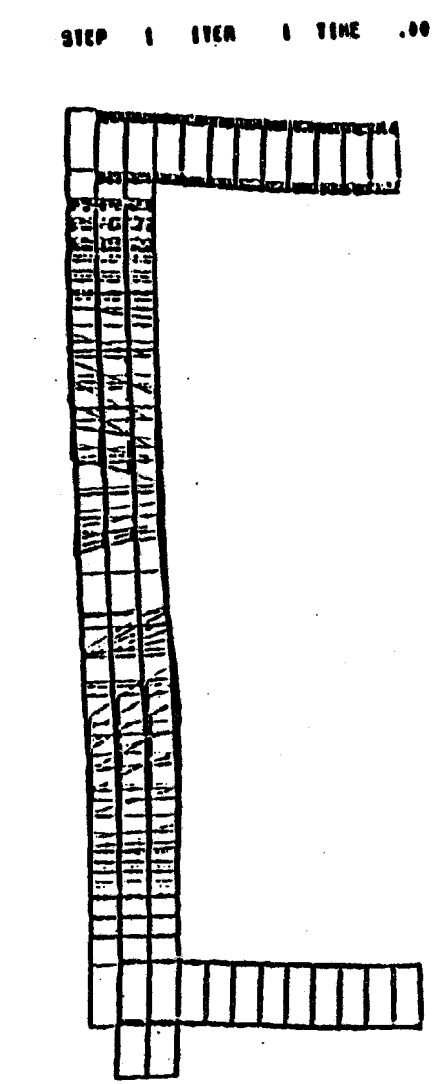

(a)

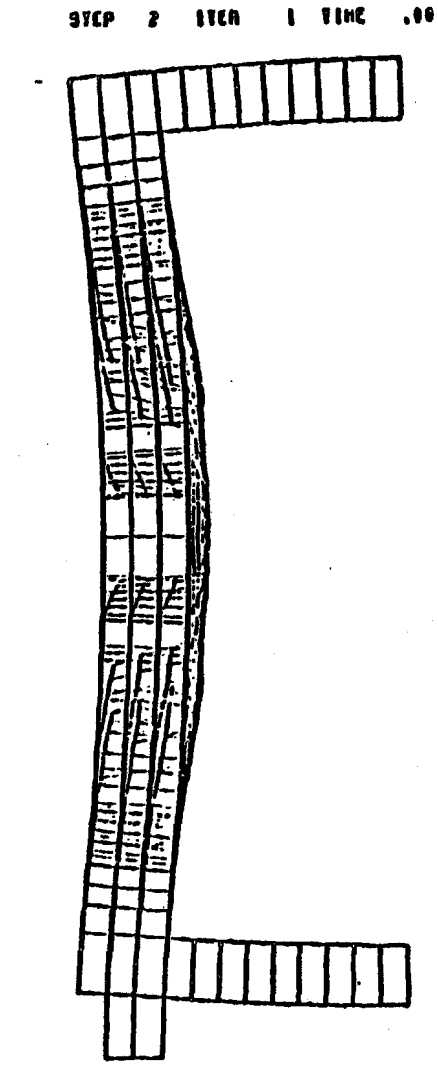

(b)

Fig. II(9). Deflected Shape of Yoke Under its Own Weight and Axial Magnetic Loading

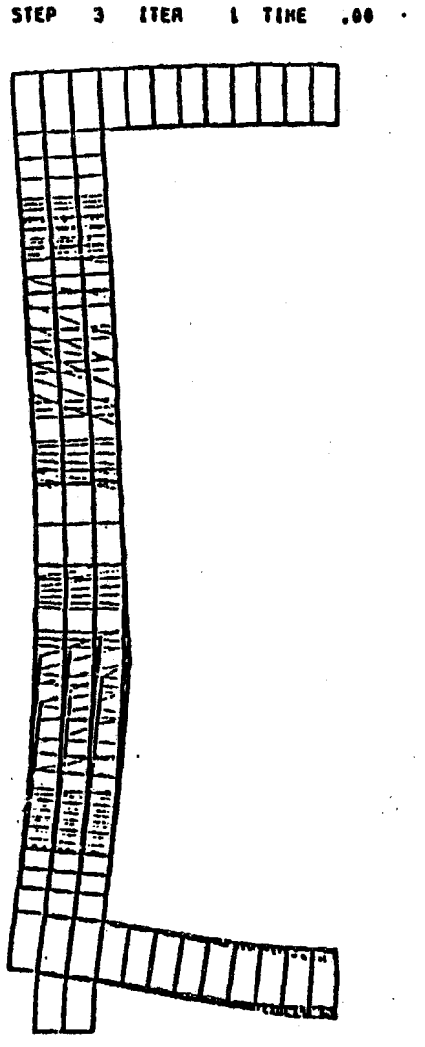

(c)

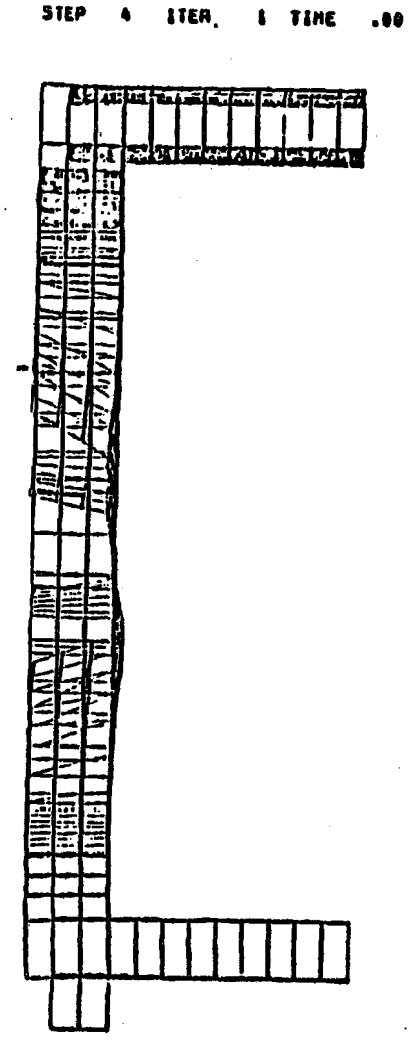

(d)

Fig. II(9). Deflected Shape of Yoke Under "Roman Arch" and End Module Gravitational Loads

Table II(4)

Maximum Deflections in Yoke Finite Element Models

Model	Load Type	Maximum Deflection (in.) X (Horizontal)	Y (Vertical)	Z (Axial)
Operation	Gravity	-.003	-.007	.002
	Axial magnetic	.010	-.028	-.100
	"Roman Arch" hadron calorimetry	.002	-.016	-.010
	Endwall hadron calorimetry	-.002	-.005	-.001
	Combined	.010	-.045	-.106
Transportation	Combined weight, "Roman Arch" hadron calorimetry and endwall hadron calorimetry	-.006	-.035	-.032
Thermal	Thermal	.046	.12	.038

solenoid is supported is approximately 0.51 mm (.02 in). The solenoid supports will allow this relative motion and ensure coil package integrity.

The most highly stressed components during operation will be the twelve support ribs, which restrain the end wall calorimetry against the axial magnetic force. Stresses of 43.4 MPa (6300 psi) were calculated by ANSYS for the support ribs near the loading points. Actual rib stresses will probably be lower, however, since the load in the actual structure is applied over some finite area and not at a single point as in the model.

Large y (vertical) and z (axial) deflections are produced during transportation. This is due chiefly to the weight of the "Roman Arch" central hadron calorimetry on the lower return legs, and the fact that during transportation the yoke and instrumentation are supported on feet several inches outward (axially) from the feet upon which the yoke rests during operation, see Fig. II(1) . Deflections are not critical during the period when the yoke is being transported, however. Stresses are of more importance, and the finite element results indicate that stresses during transportation are negligible, not exceeding 13.8 MPa (2000 psi).

The CDF yoke is adequate to withstand the electromagnetic and weight loadings present both during the operation of the detector in the Collision Hall and during transportation to and from the Assembly Hall.

CHAPTER III: COIL DESIGN

General Features

The superconducting coil consists of a single layer helical winding of aluminum stabilized superconductor mounted inside an aluminum support cylinder. The conductor is "indirectly cooled" by conduction from a cooling loop attached to this support cylinder.

No helium contacts the surface of the conductor in the coil. For stability, the coil relies on the specific heat and high thermal conductivity of the high purity aluminum stabilizer. Such a coil exhibits less thermal stability than standard cryostable designs and thus requires careful engineering and construction techniques for its proper operation. However, this type of design offers the following important advantages:

1. A large He cryostat is not required. This simplifies the construction and reduces the LHe inventory required and thus reduces safety related problems.
2. The total thickness of the coil can be reduced improving the "Physics" performance and reducing the cold mass.
3. By using an outer support cylinder the need for banding is eliminated. This further reduces the material required and simplifies the coil construction.
4. The liquid helium cooling loop is simple and permits rapid yet well controlled cooldown of the coil.
5. Since the inside surface of the coil is exposed, it can be easily instrumented and if necessary repaired.

We describe in this chapter the fabrication, stress analysis and quench behavior of this coil. The main parameters of the coil are summarized in Appendix A. Of particular significance is the "thinness" of the coil, namely 0.83 radiation lengths and 0.19 absorption lengths.

Conductor

The conductor that will be used consists of a monolithic copper/superconductor matrix surrounded by a high purity aluminum stabilizer.

The conductor will be produced by Hitachi, Ltd using the extrusion with front tension (EFT) method. Detailed characteristics of this conductor as well as results from a 1 m ϕ x 1 m long R&D solenoid have been reported elsewhere.[1)]

A cross section of the conductor is shown in Fig. III(1). The volume ratio of Al : Cu : NbTi is 21 : 1 : 1. Figure III(2) shows standard magnetic field (H) versus critical current (I_c) data for this conductor, together with the load line for the solenoid with yoke. Conductor parameters are summarized in Table III(1). The critical current is 10.4 kA at 4.2 K and 1.5 tesla. The guaranteed solenoid operating current is 4.5 kA and the design operating current is 5 kA. The conductor width of 2 cm is determined primarily by the maximum voltage to ground and the maximum temperature rise during a quench as will be discussed in later sections.

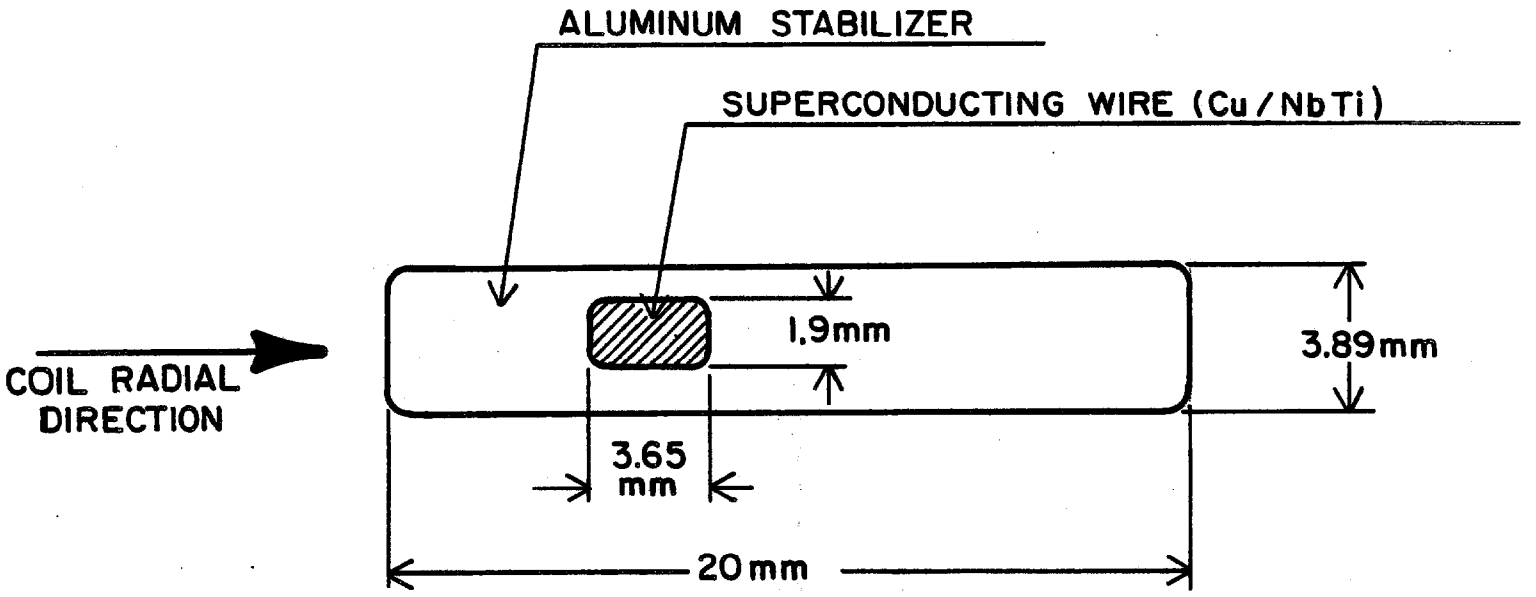

SUPERCONDUCTING WIRE: 50μmϕ x 1700
MATERIAL RATIO: Al :Cu: NbTi = 21 :1 :1
ALUMINUM PURITY: > 99.99%

Fig. III(1). Cross section of conductor

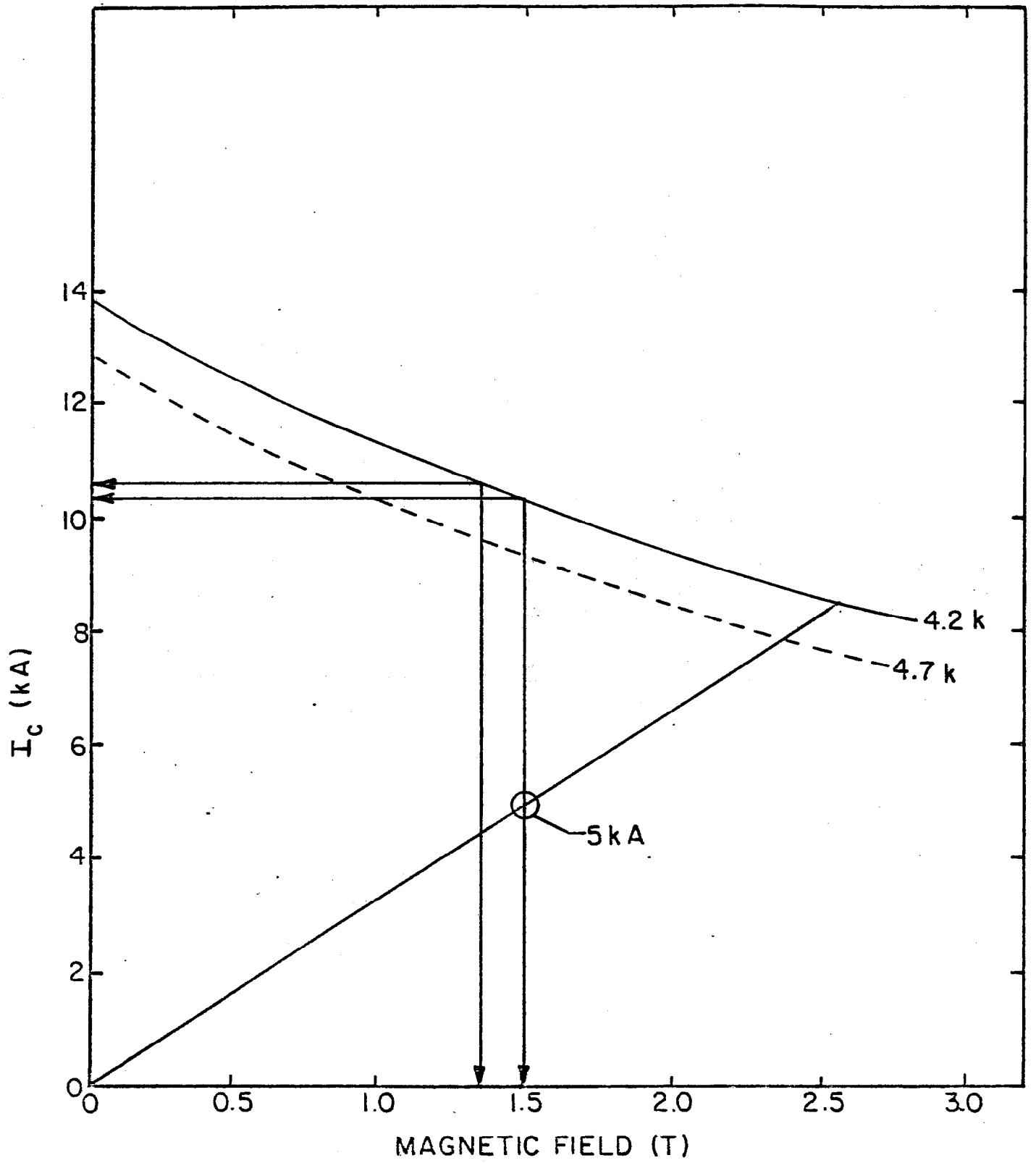

Fig. III(2). Conductor short sample and magnet load line

Table III(1) Conductor Parameters

Items	Value
Filament Diameter	50 μmϕ
Number of Filaments	1700
SC Filament Area	3.34 mm^2
Cu/SC Ratio	1 : 1
Al/SC Ratio	21 : 1
Purity of Al Matrix	$\gtrsim$ 99.99 %
RRR of Al	$\gtrsim$ 1000
Short Sample Data at 1.5 tesla, 4.2 K	10.4 kA
Unit Length	> 1000 m

Outer Support Cylinder

The coil does not have a permanent inner bobbin; the radial electromagnetic forces are supported as a hoop stress in a cylinder outside the coil. This cylinder, made of 5083 aluminum, is slipped over the completed coil and the radial gap between the coil and cylinder filled with a filled epoxy. The helium cooling pipe is attached to the outside of the support cylinder and so the coil is cooled through this epoxy layer. Therefore it is very important to keep the gap between the coil and the support cylinder as small as possible and the epoxy free of voids.

Fabrication of the Coil

Construction of the coil consists of the following major steps:

1. Winding of the conductor on a temporary mandrel whose radial dimension can be reduced later for removal.
2. Insertion of the coil into the outer support cylinder.
3. Filling the gap between the coil and the support cylinder.
4. Removal of the temporary inner mandrel for the final assembly.

Coil Winding. Figure III(3) shows the schematic diagram of a proposed arrangement for winding of the coil. A very similar arrangement was employed for the R&D solenoid coil in which the layer-taping process was done manually.

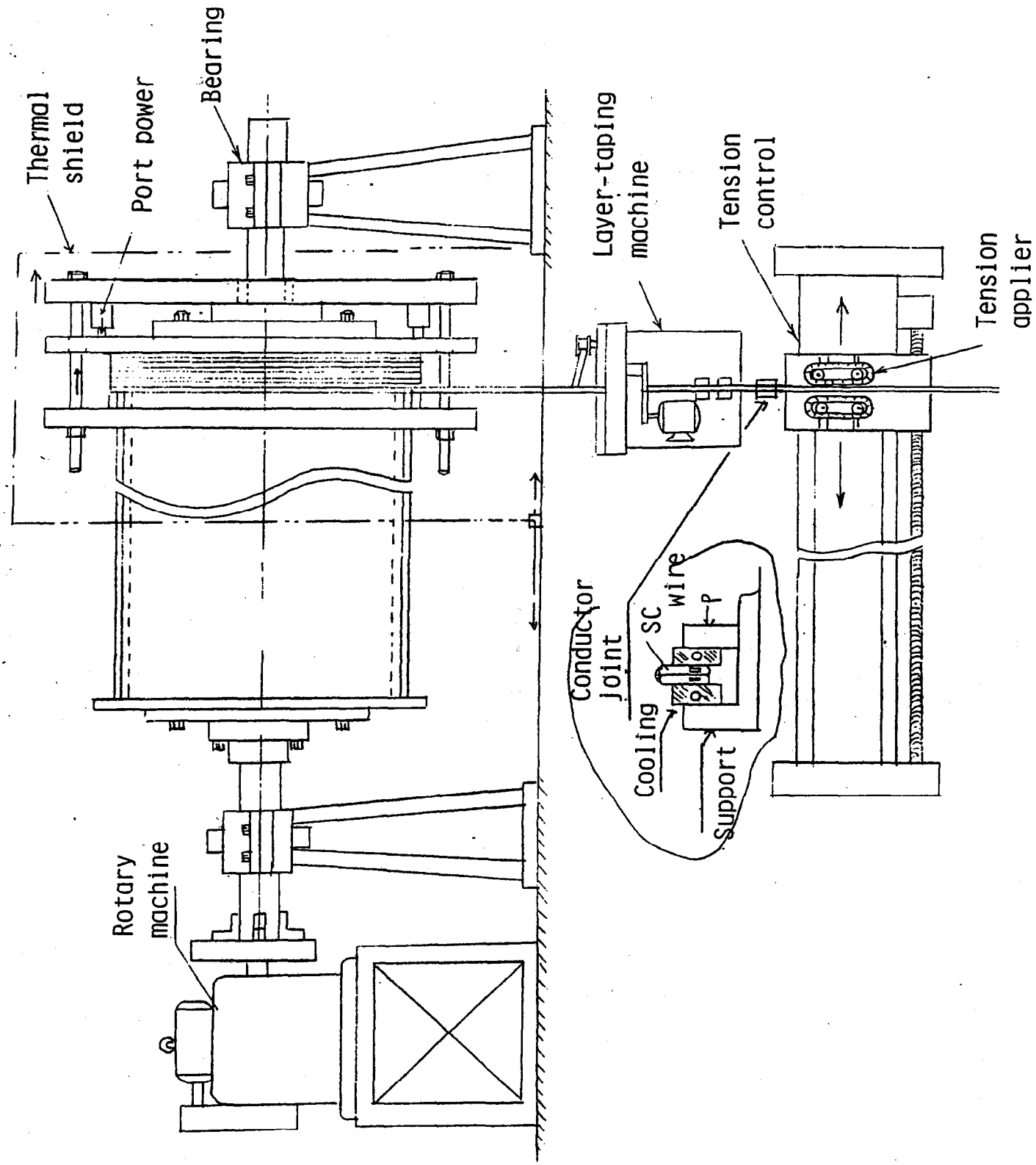

Fig. III(3). Coil winding arrangement

Since the tolerance of the radial dimension of the coil determines the uniformity of thickness of insulating materials between the coil and the support cylinder, the radial dimension will be checked continuously. R&D work will be carried out by using a mandrel 3 m in diameter and dummy conductor in order to establish the procedure for coil winding.

The cooling tube will be welded on the outside surface of the support cylinder. A brace structure will be used outside the support cylinder to improve the mechanical rigidity of the cylinder during machining of the inside surface of the cylinder. The brace structure will be kept until assembly of the coil and the support cylinder is completed and then removed.

Conductor Joints. The maximum length of a single EFT conductor segment is determined by the maximum length of NbTi/Cu wire that can be manufactured. This length is approximately 1 km for the conductor that will be used for the CDF solenoid. Thus the CDF solenoid will have about 12 conductor joints. In order to develop techniques to make good conductor joints two conductor joints were made and tested successfully in the R&D solenoid.[1] Figure III(4) shows a schematic diagram of the cross section of a conductor joint made with this newly developed welding method. The thickness of the welded area is about 2 mm. The conductor joints in the R&D solenoid used a full turn of double layers of the normal conductor and two welded sections of 40 cm each. The net resistance for such a joint is about $7 \times 10^{-10}\Omega$ at 4.2 K.

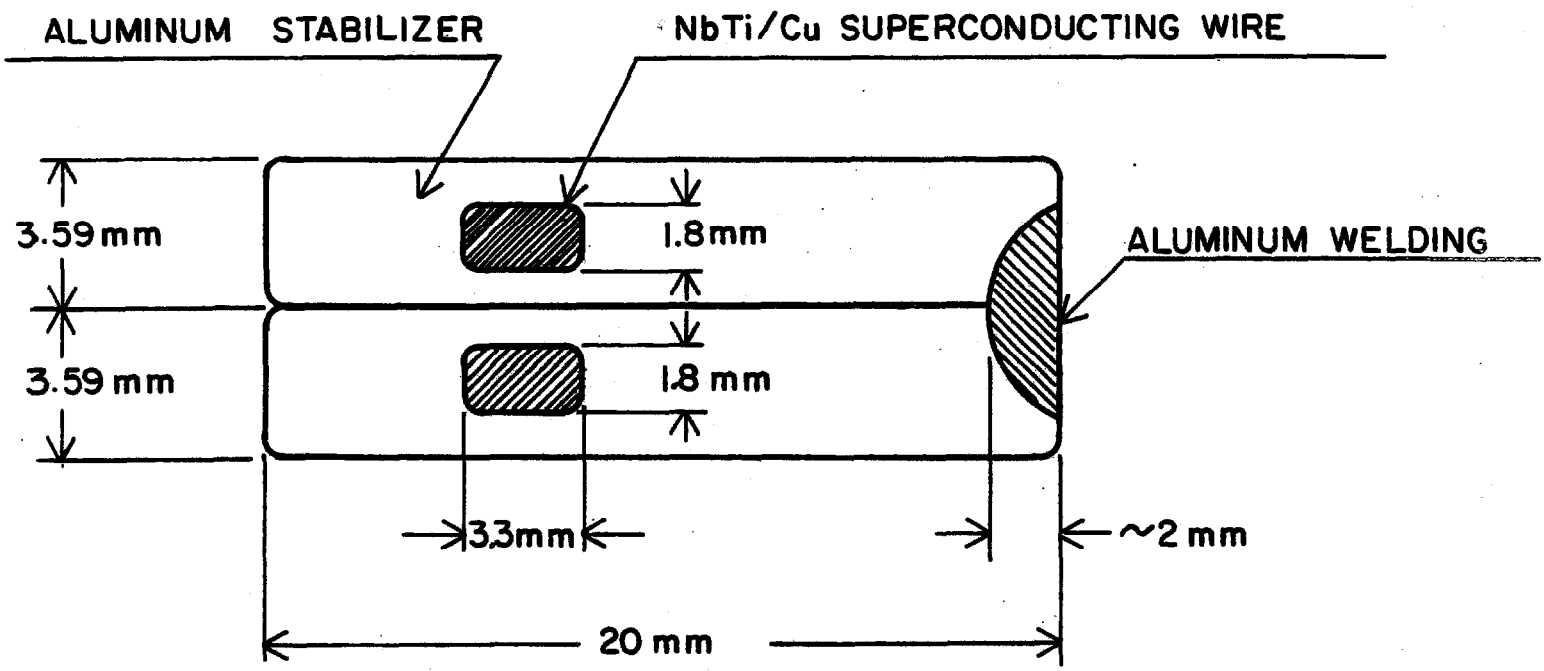

Fig. III(4). Conductor joint
for R&D solenoid

Filling the Coil-Support Cylinder Gap. The space between the coil and the support cylinder will be vacuum impregnated with epoxy resin after filling with porous insulating materials. The thickness of the gap is estimated to be approximately 3 mm. Figure III(5) shows a schematic drawing of the arrangement for vacuum impregnation. Details are found in Appendix E.

Extensive R&D will be carried out in order to determine properties of epoxy and insulating materials and also to establish the method of vacuum impregnation. Various tests will be carried out using dummy cylinders of about 50 cm in diameter and 5 m in length.

Insulation Scheme. The exact insulation scheme for the CDF solenoid will not be determined until new R&D programs are completed. Table III(2) gives insulation thickness, insulation materials, and resins used for the R&D solenoid and those presently considered for the CDF solenoid. The turn-to-turn insulation may be changed to polyimide (Kapton) in order to improve the efficiency of the automated layer-taping machine.

Eddy Current Analysis

Induction Currents in the Support Cylinder. We estimate effects due to eddy currents in the support cylinder during the charging period of the CDF solenoid.

Thickness of the support cylinder	1.6 cm
Mutual inductance between the coil and support cylinder, M	2.0 mH

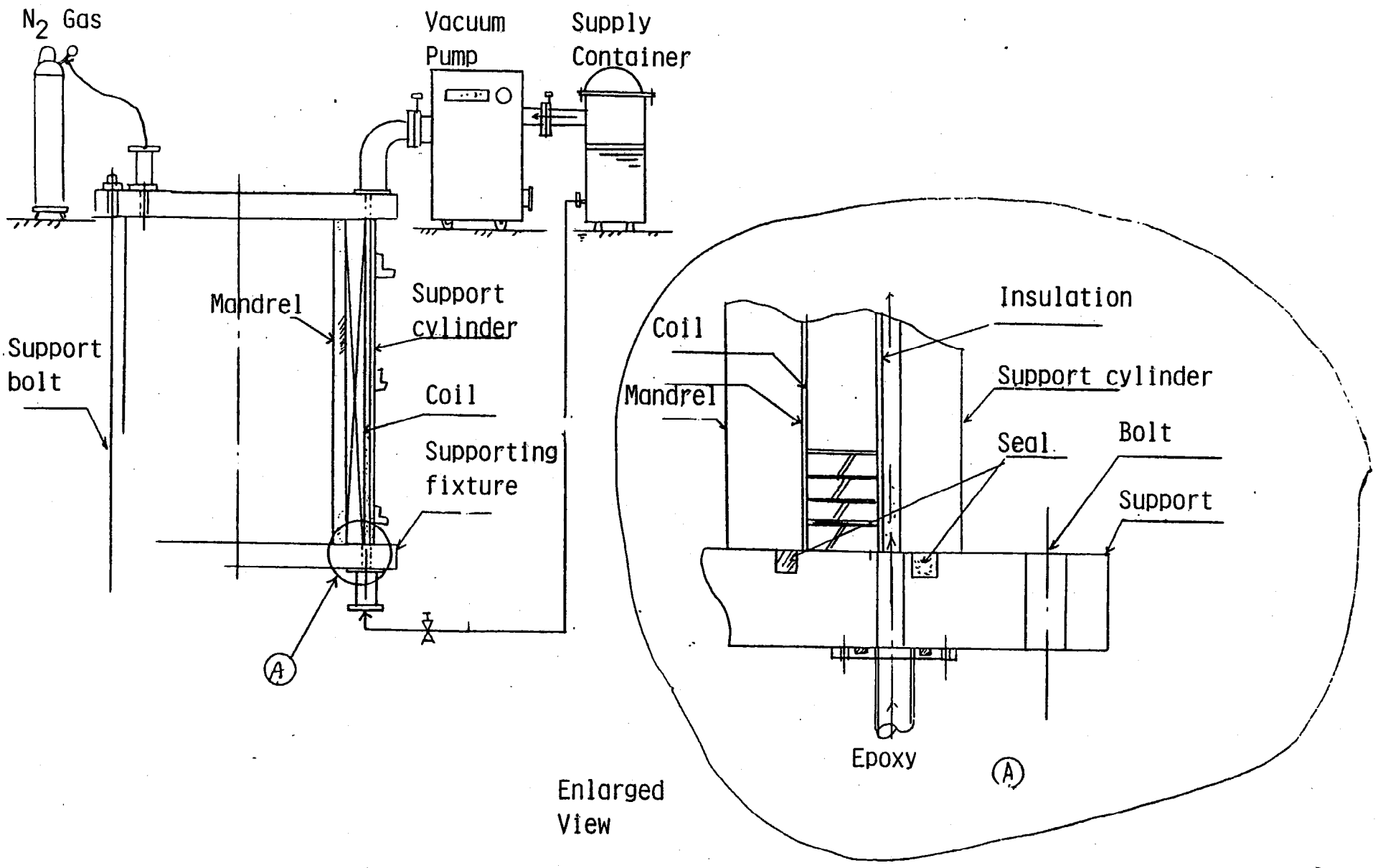

Fig. III(5). Vacuum impregnation arrangement

Table III-2. Insulation thicknesses, insulation materials, and resins used for the R&D solenoid and those under consideration for the CDF solenoid.

Solenoid	Item	Turn-to turn	Outside of the coil	Inside of the coil	Coil end	Coil-support cylinder
R&D	Thickness (mm)	0.1	0.36	1.0	20	--
	Materials	50μm polyamied: half overwrap	mica tape and polyimide tape	mica sheet and glass tape	epoxy G-10 plate	--
	Resins	semicured epoxy	polyester (room temp. curing)	polyester (high temp. curing)	epoxy	--
CDF	Thickness (mm)	0.1	0.36	under study	20	to be decided after tests in R&D work
	Materials	50μm polyimide or polyamied: half overwrap	mica tape and polyimide tape		epoxy G-10 plate	
	Resins	semicured epoxy	polyester (room temp. curing)		epoxy	

Electrical resistivity of the support cylinder material (aluminum alloy A5083) at 4.2 K — 3.05 μΩ cm

We consider the support cylinder as a plate of 300 π cm x 500 cm x 1.6 cm. The stiffening rings at the coil ends are considered as plates of 300 π cm x 40 x 2.8 cm. Eddy currents are induceed circumferentially on the support cylinder.

Then the resistance of the support cylinder, R, is given by

$$R = \frac{3.05 \times 300\ \pi \times 10^{-6}}{(500 \times 1.6)+(80 \times 2.8)} = 2.8\ \mu\Omega$$

Joule heating power due to induction current in the support cylinder, P, is given by

$$P = \frac{1}{R} \left(M \frac{dI}{dt}\right)^2$$

For a charging time of 10 minutes we get

$$P = \frac{1}{2.8 \times 10^{-6}} \times \left(2.0 \times 10^{-3} \times \frac{5000}{10 \times 60}\right)^2$$

$$= 99\ W$$

We note that the induced heating power is inversely proportional to the square of the charging time.

The total eddy current power in the support cylinder during a quench is estimated to be approximatey 10% of the total thermal power induced in the coil.

Induction Currents in the Conductor. Eddy current power loss in the conductor during charging time can be estimated by using a model given in CDF-SDS-11[2].

The eddy current power loss in the coil, P_{coil}, is estimated by

$$P_{coil} = N_t \frac{1}{R_c} \left(A_{eff} \frac{dB}{dt}\right)^2$$

where

N_t = number of turns

R_c = effective resistance of one turn

A_{eff} = effective conductor area of magnetic flux crossing per turn

For the CDF solenoid we have

N_t = 1200

R_c = 1.0×10^{-5} Ω ($\rho = 4 \times 10^{-11}$ Ωm)

A_{eff} = 7×10^{-2} m^2, see Fig. III (1)

Therefore, for the charging time of 10 minutes we get

$$P_{coil} = \frac{1200}{1.0 \times 10^{-5}} \left(7 \times 10^{-2} \times \frac{1.5}{10 \times 60}\right)^2$$

$$\sim 4 \text{ W}$$

Analytical Stress Analysis

Hoop Stress.

The conductor will be wound with an axial compression but there will be no substantial radial preloading on the conductor. The gap between the conductor winding and the outer support cylinder is filled up with an epoxy resin, loaded to have a thermal contraction coefficient approximately equal to that of aluminum. During cool-down no gap should be developed between the conductor and the cylinder.

When the coil and support cylinder are cooled from room temperature to 4.2 K, the radius is reduced by $\Delta R_1 = 4.3 \times 10^{-3} \times R = 6.5$ mm and the total length is reduced by $\Delta L_1 = L \times 4.3 \times 10^{-3} = 21$ mm. The chimney end of the support cylinder is fixed to the iron yoke and therefore the other end moves toward the chimney end by 21 mm (0.81").

When the magnet is excited, the conductor pushes the support cylinder outward with a magnetic pressure P.

$$P = \frac{B^2}{2\mu_o} \ (N / m^2) = 4.06 \times B^2 \ (kg/cm^2)$$

where B is the magnetic field given in tesla. With B = 1.5 T, the magnetic pressure is 9.14 kg/cm^2 (130 psi).

The thickness of the support cylinder can be determined by Procedure 4.1 of Japanese Industrial Standard, JIS B8243,

$$t \geq \frac{P\ D_i}{200\ \sigma_a \eta - 1.2\ P}$$

where

t = wall thickness (mm)

D_i = inner diameter of the cylinder (mm)

σ_a = acceptable tensile stress (kg/mm^2)

η = welding efficiency

For D_i = 3032 (mm), P = 9.14 (kg/cm^2), σ_a = 10 (kg/mm^2), and η = 0.9, we get

$$t \geq 16 \text{ (mm)}$$

Since the coil itself absorbs some of the magnetic pressure, we choose the thickness of the support cylinder to be 16 mm.

The radius of the conductor and the support cylinder is increased by ΔR_2 due to the hoop stress, σ.

$$\epsilon = \frac{\Delta R_2}{R} = \frac{\sigma}{E} = \frac{1}{E} \frac{PR}{(t_c + t_s)}$$

where E is the Young's modulus of aluminum 8.3 x 10^5 kg/cm^2, 1.8 x 10^6 psi) at 4.2 K, and t_c and t_s are the radial thickness of the conductor and support cylinder, respectively. For t_c = 2 cm and t_s = 1.6 cm,

$$\varepsilon = 4.1 \times 10^{-4} \text{ and } \Delta R_2 = .067 \text{ cm.}$$

When the magnet is energized, the total thickness of the coil which $(t_c + t_s)$, is reduced by ΔW due to the Poisson ratio ν (= 0.36),

$$\Delta W = (t_c + t_s) \frac{\Delta R_2}{R} \nu = 5.4 \times 10^{-4} \text{ cm}$$

and the total length of the coil is reduced by ΔL_2,

$$\Delta L_2 = L \frac{\Delta R_2}{R} \nu = 7.5 \times 10^{-2} \text{ cm}$$

Stress-Strain Curve. The estimated stress-strain curves of the coil components are shown in Fig. III(6). The stress-strain curve of the 2cm conductor, which was used for the R and D coil, was measured at 77 K.[3] Its Young's modulus is 700×10^3 kg/cm^2, and its yield stress is 450 kg/cm^2. The estimated stress-strain curve for the 5083-0 aluminum data is also shown in Fig. III(6).[4] Its Young's modulus and yield stress at 77K are 820×10^3 and 1410 kg/cm^2, respectively. Its acceptable design stress is 10 kg/mm^2

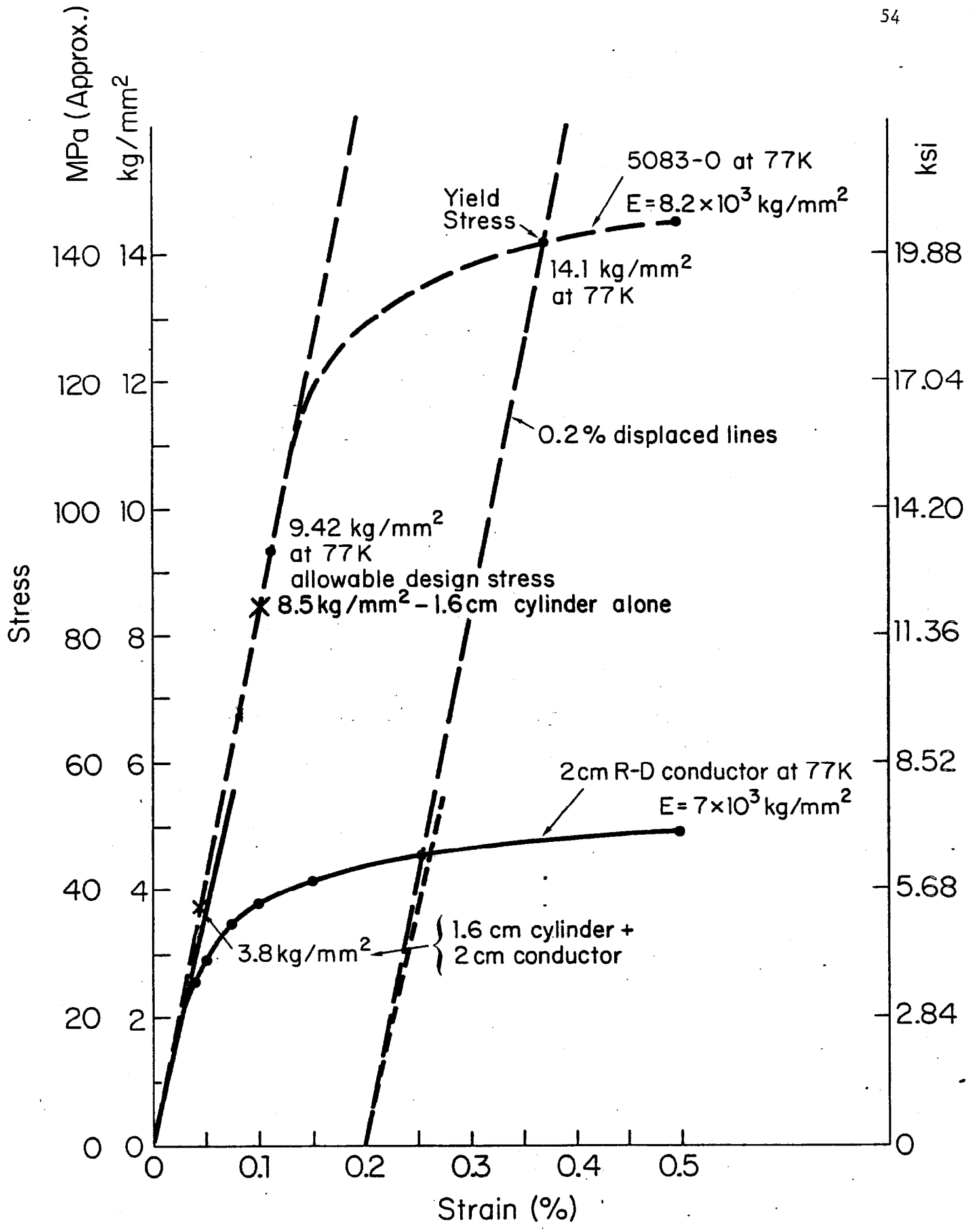

Fig. III(6). Estimated stress-strain curve

at 5 K.

The estimated operation points are also shown in Fig. III(6). If we consider the contribution of the 1.6 cm support cylinder and the 2 cm conductor together, the hoop stress in the coil structure is

$$\sigma = P \times \frac{R}{(t_c + t_s)}$$

$$\sigma = 380 \text{ kg/cm}^2$$

If we assume that only the support cylinder bears the magnetic force, the hoop stress in the cylinder is 860 kg/cm^2, which is still below the acceptable design stress of aluminum 5083-0.

Since the maximum strain of the conductor is well below the 0.1% level, there should be no significant increase in the resistivity of the pure aluminum stabilizer due to the cyclic strain.[5] Also we expect there will be no additional increase in the magneto-resistivity of the pure aluminum due to the strain as observed elsewhere.[6]

Axial Compression. During solenoid excitation, the conductor winding as a whole is axially under compression due to the fringing field. The accumulative compressive force is calculated to be about 100 metric tons on the conductor. If we assume this force is absorbed only by the 2 cm thick conductor layer and not by the support cylinder, then the uniform force of 100 tons in the

axial direction corresponds to a compressive pressure P = 53 kg/cm^2. To prevent conductor motion and to increase the effective Young's modulus of the conductor layer in the axial direction, the conductor should be preloaded with an axial compressive force larger than this pressure.

During this preloading the coil length is reduced roughly by ΔL_3.

$$\Delta L_3 = \frac{P}{E_{eff}} \times \frac{tc}{t_c+t_s} \times L = \frac{53}{700 \times 10^3} \times \frac{2}{1.6+2} \times 5 \times 10^2 = .02 \text{ cm}$$

where E_{eff} is the assumed effective Young's modulus in the axial direction of the coil structure composed of the conductor, insulation and the support cylinder.

Finite Element Stress Analysis of Coil Including Supports

Operation of the central detector will impose large electromagnetic decentering forces on the solenoid. These forces, originating in the current sheet, are transmitted from the conductor to the support cylinder, then to the yoke endwalls through the radial and axial support system. The mechanical analysis of the supports alone is presented in Appendix G, and simple analytical calculations dealing with the support cylinder under magnetic pressure have been presented previously in this chapter. To analyze the more complicated case of support cylinder/support rod interaction, a finite element model was created. Three loadings were considered.

1. Axial electromagnetic decentering force.
2. Radial electromagnetic decentering force.
3. Axial preloading.

The axial and radial decentering forces, which result from an axisymmetrical placement of the solenoid within the magnet iron, are described in Chapter II. For the purposes of this analysis, it is assumed that an initial off center displacement of 1" exists in both the axial and radial directions, resulting in forces of 101000 lbs (axial) and 70000 lbs (radial). (45.9 metric tons and 31.8 metric tons respectively.)

The axial preloading force occurs when the conductor is preloaded to assume an initial axial compressive strain equal to what will occur when the magnet is excited. This preloading is applied by numerous bolts in each of the support cylinder stiffening rings, and produces a tension in the support cylinder, as well as localized stresses in the stiffening rings.

Finite Element Model. A three dimensional model of 180° segment of one stiffening ring was generated using eight node solid elements, and is shown in Fig. III(7). Two elements were used through the radial thickness of the ring, and 18 elements along the axial length. A total of 6111 nodes were used with 18000 active degrees of freedom. The support pads were modeled by using thick bar elements originating at the support pad bolt locations and terminating at the ball end of the support rod.

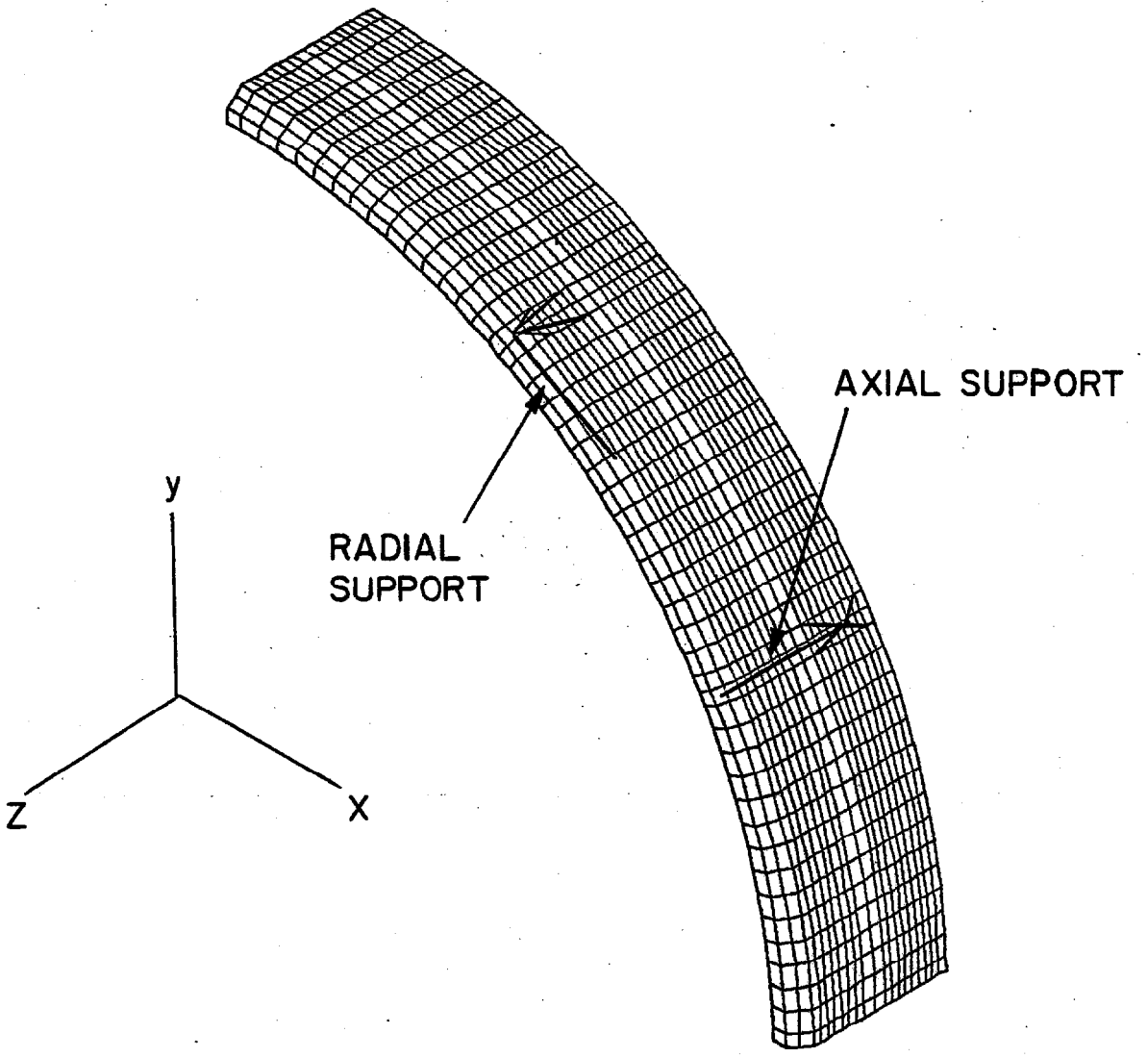

Fig. III(7). Portion of three dimensional finite element model of support cylinder stiffening ring

This is an approximation which sacrifices stress information in the support pad, but which should emulate the stiffness and load transfer characteristics of the pad sufficiently to give meaningful deflection and stress figures for the ring. The Inconel 718 support rods were input as bar elements, which is an exact modeling of these components.

Constraints were applied to enforce symmetry. Electromagnetic loads in the directions indicated in Fig. III(7) were simulated by designating the appropriate coordinate accelerations. The pre-load force was applied by fixing the nodes lying nearest the actual preload bolt centers, and applying concentrated nodal loads in the axial direction to the nodes at which the stiffening ring will meet the thinner bulk of the support cylinder in the actual structure.

The orientations for the decentering loads were chosen to coincide with the position of greatest support loading, which is demonstrated in Appendix G.

The stress results were compared to the maximum acceptable stress for 5083-0 Al at 5.0 K. (10 kg/mm^2, 14.2 ksi).

Results. The stresses calculated for the axial and radial support rods under the electromagnetic loading are 45407 N/cm^2 (65840 psi) and 46314 N/cm^2 (67157 psi) respectively. These figures agree within a few percent with those presented in Appendix G. Calculated maximum axial and radial deflections are 0.084 cm (0.033 in) and .084 cm (.033 in) respectively. These

values exceed those of Appendix G due to deformation of the stiffening ring. Deflections at the nodes to which the support rods attach are 0.074 cm (0.029 in) and 0.074 cm (0.029) for the axial and radial loadings, respectively, and agree well with the Appendix G values.

The normal and shearing stresses calculated by ANSYS for the three loadings are given in Table III(3). Stress directions are in the global coordinate system shown in Fig. III(7). The normal stresses are seen to be the greatest under the radial load, but do not exceed the maximum acceptable stress. Combined stress effects can be estimated by adding the absolute values of a given stress for the three load cases. The largest value obtained in this way is, for normal stress, 7495 N/cm^2 (10870 psi) and for shear stress, 5140 N/cm^2 (7450 psi). The normal stress does not exceed the maximum acceptable stress. Although the shear stress value is somewhat high, it should be noted that stress contributions from preload will diminish greatly during operation as the coil is compressed by the magnetic field. Therefore, no stress in the stiffening ring will exceed the maximum allowable stress during operation.

Computer Analysis of Quench Properties

Quench properties of the CDF solenoid have been extensively studied by computer simulations. We present here results of calculations in which the quench-back effects were taken into account for the final parameters of the CDF solenoid. The detailed methods of the calculations is described elsewhere[7] and

Table III(3). Maximum Stresses in Stiffening Ring (N/cm^2)

Loading	σ_x	σ_y	σ_z	τ_{xy}	τ_{yz}	τ_{xz}
Axial Electromagnetic	-1900	2094	-1787	1050	943	-850
Radial Electromagnetic	4592	-3850	-4528	1660	2920	-3724
Coil Preload	882	963	1180	-596	533	565

in Appendix C.

Figure III(8) shows computed maximum voltages and maximum temperatures as a function of the external protection resistance. The maximum temperatures correspond to those at 30 sec after the onset of a quench at the middle of the solenoid.

The temperature of the conductor as a function of time at the origin of a quench (and at an axial distance of 1.25 m away from the origin,) and the temperature of the support cylinder as a function of time for $R_{ext} = 0.04$ are shown in Fig. III(9). In this calculation the cooling effects of the liquid helium is neglected. For simplicity we assumed a homogeneous temperature for the support cylinder and no heat flow between the coil and the support cylinder. Since a temperature difference arises between the coil and the support cylinder as seen in Fig. III(9), some thermal energy flows from the coil to the support cylinder. In order to estimate the time constant to reach an equilibrium temperature between the coil and the support cylinder we consider the case in which the coil and support cylinder have uniform temperatures of 80 K and 40 K, respectively. This can be reached in about 15 sec after the onset of a quench in the case of Fig III(9). The thickness and thermal conductivity of the insulator between the coil and the support cylinder are assumed to be 3 mm and 1 mW K^{-1} cm^{-1}, respectively. Figure III(10) shows computed temperatures of the coil and the support cylinder as a function of time. The time constant is substantially longer than those for temperature rises during a quench shown in Fig. III(9). This

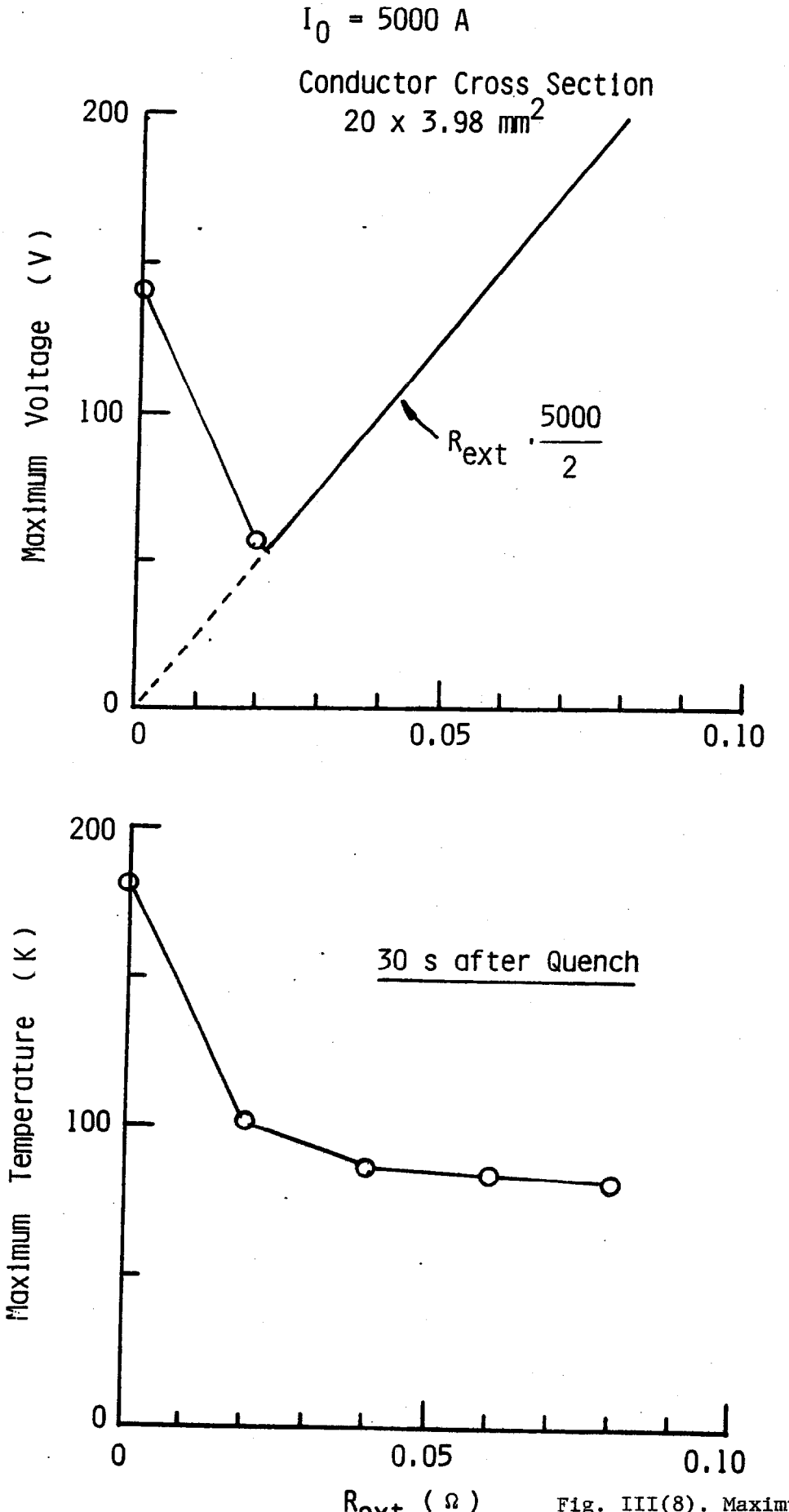

Fig. III(8). Maximum quench voltage and temperature vs external resistance

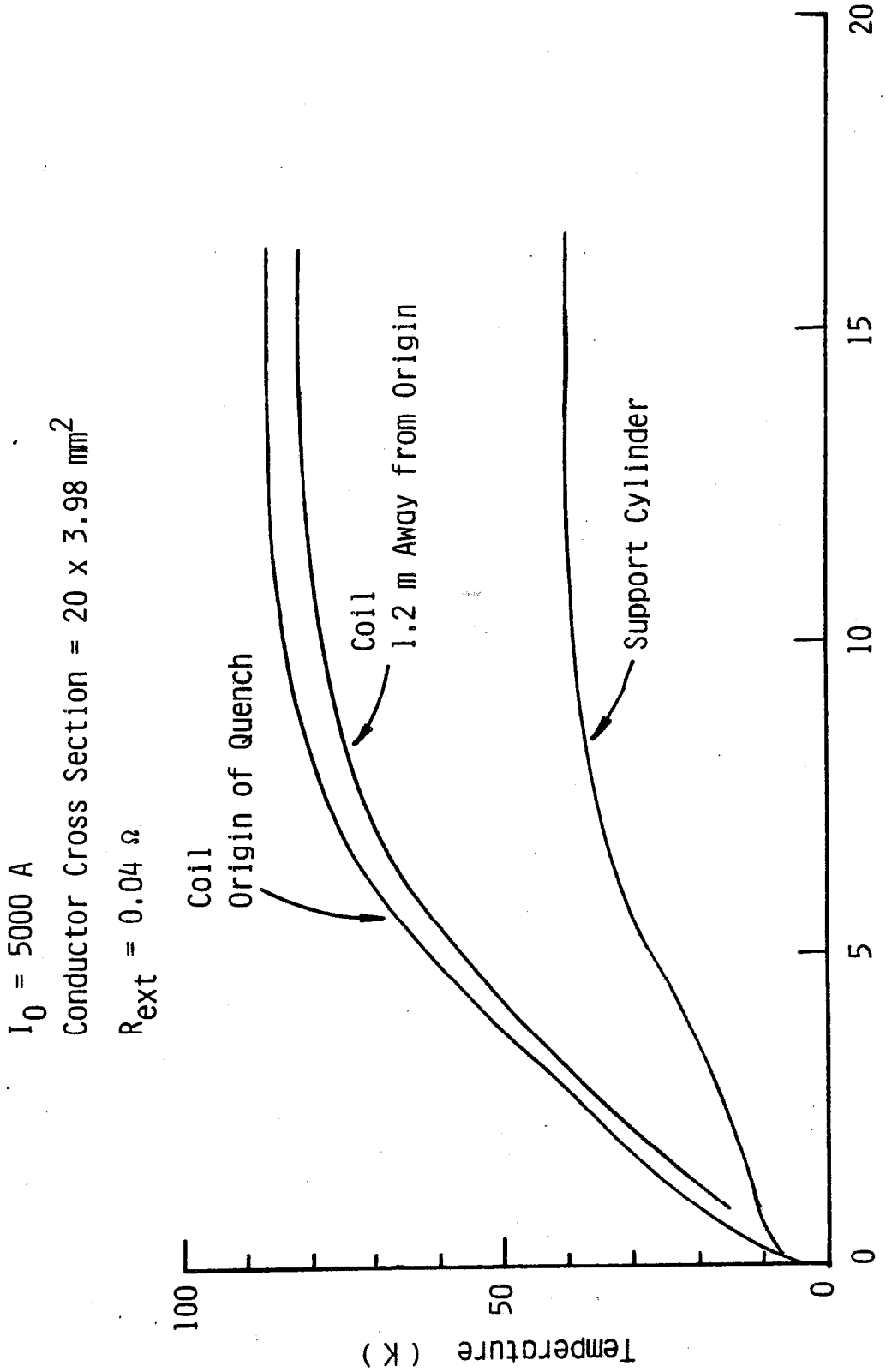

Fig. III(9). Temperature vs time following quench

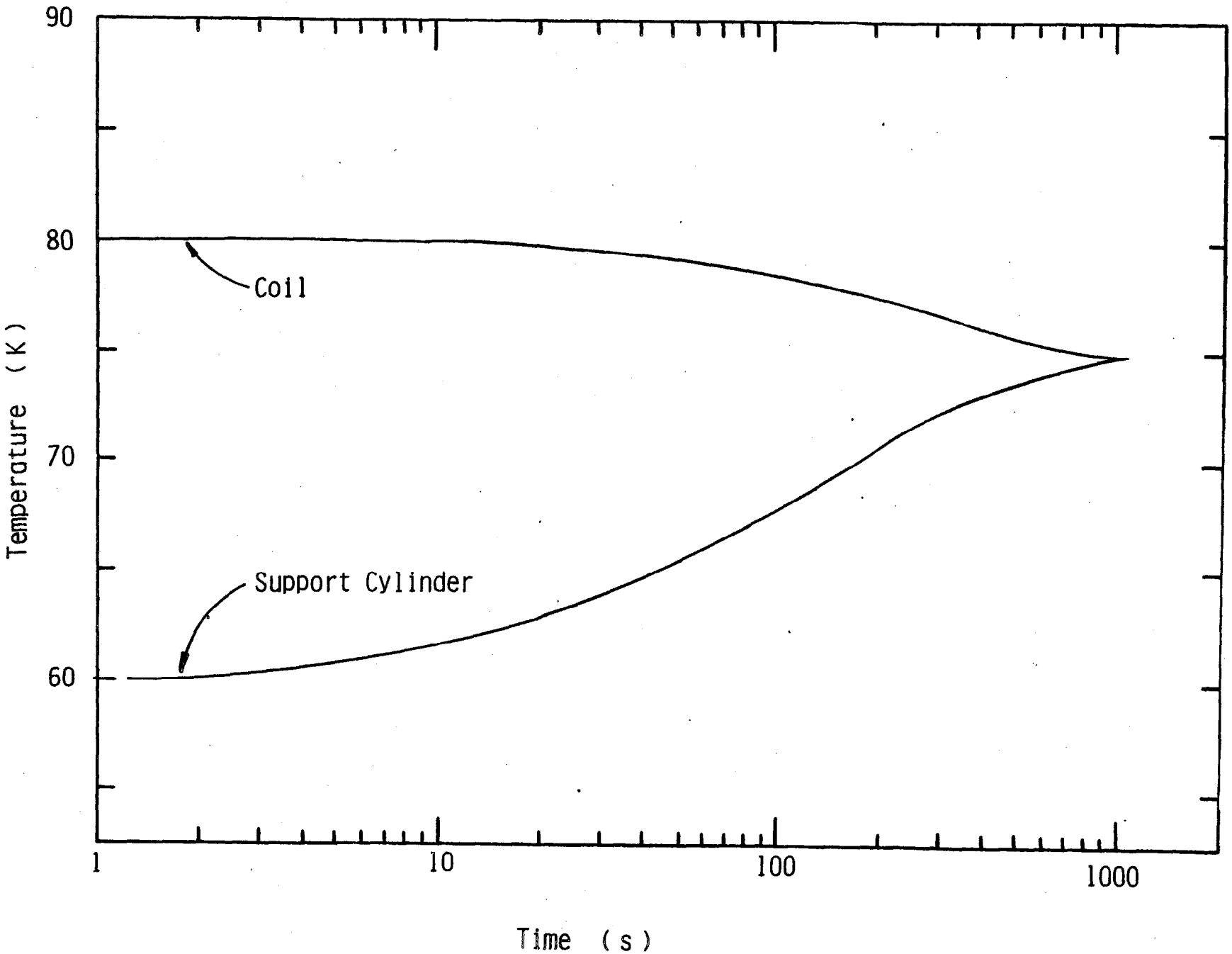

Fig. III(10). Temperature of coil and support cylinder vs time after quench

supports the assumption of no heat flow between the coil and the support cylinder during a quench.

The magnet currents as a function of the time after the onset of a quench are shown in Fig. III(11) for various external resistors.

Figure III(12) shows the equilibrium temperature of the cold mass of the solenoid, namely of the coil and support cylinder, as a function of the external resistor. As seen in Fig III(10), the equilibrium temperature is reached in about 10 minutes after a quench starts. Also shown are the energies deposited directly in the coil, support cylinder, and external resistors.

References

1. T. Kishimoto et al., "Design Report for an Indirect Cooling Superconducting Solenoid Magnet for the CDF Detector", Internal Report of Institute of Applied Physics, Univ. of Tsukuba, HEAP-4, March 1982 (unpublished), also H. Hirabayaski et al., Jpn. J. Appl. Phys. 20, 2243 (1981) and 21, 1149 (1982).

2. R. Yamada and M. Wake, "Eddy Current Loss in Conductor during Charging-up and Quench", Fermilab Internal Report, CDF-SDS-11, March, 1982.

3. Hitachi Engineering Sheet 1423-0-48, July, 1982.

4. Handbook on Materials for Superconducting Machinery, 4.3.1-4/(11/75).

5. H.R. Segal, Reinforced Aluminum as a Superconducting Magnet Stabilizer" IEEE Trans. on Mag., Vol. Mag-13, 109, 1977.

6. S.H. Kim and S.T. Wang "Measurements of Mechanical and Electrical Properties of High Purity Aluminum", Advances in Cryogenic Engineering, 24, 485, 1977.

7. T. Kishimoto, S. Mori and M. Noguchi, "Computer

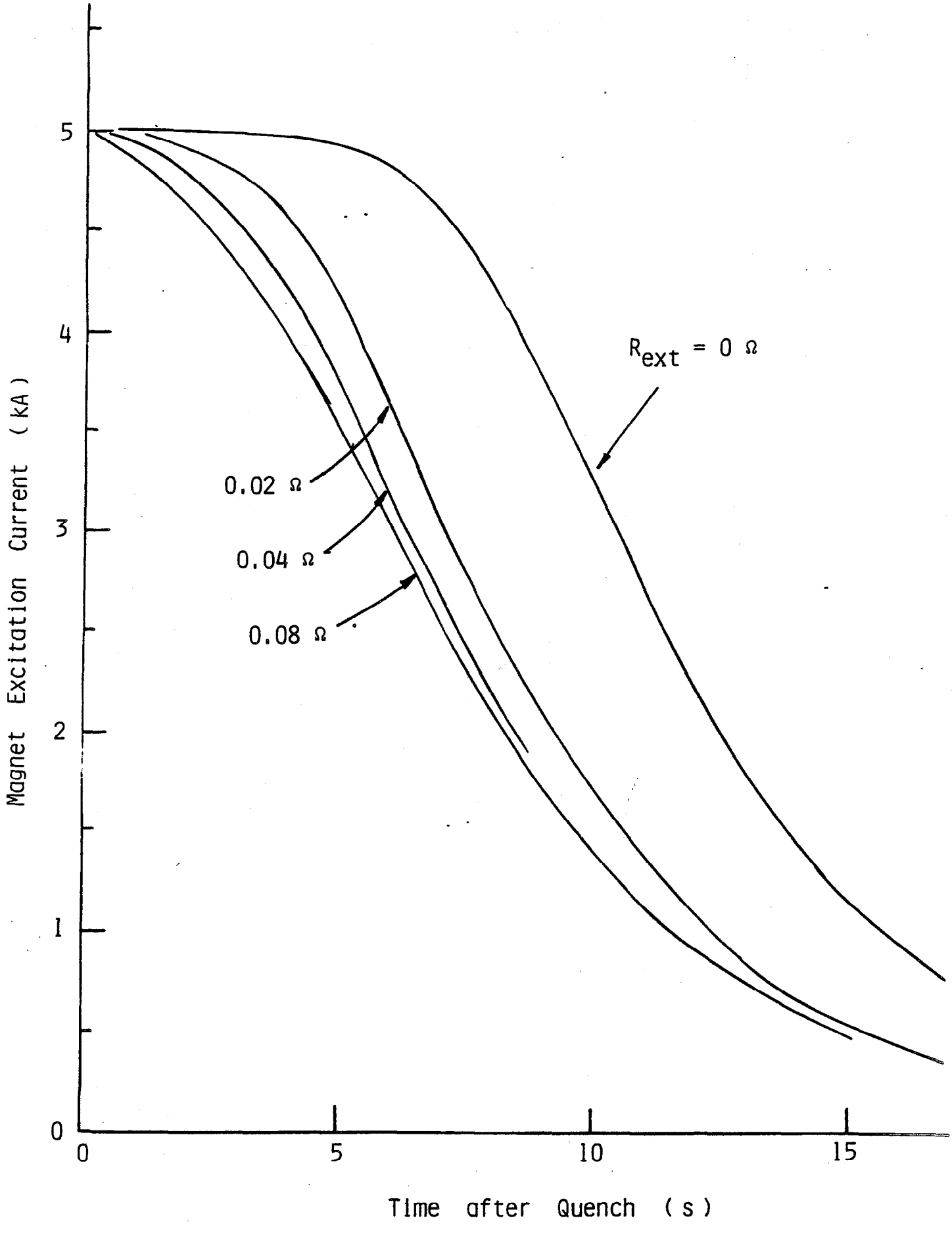

Fig. III(11). Magnet current vs time after quench

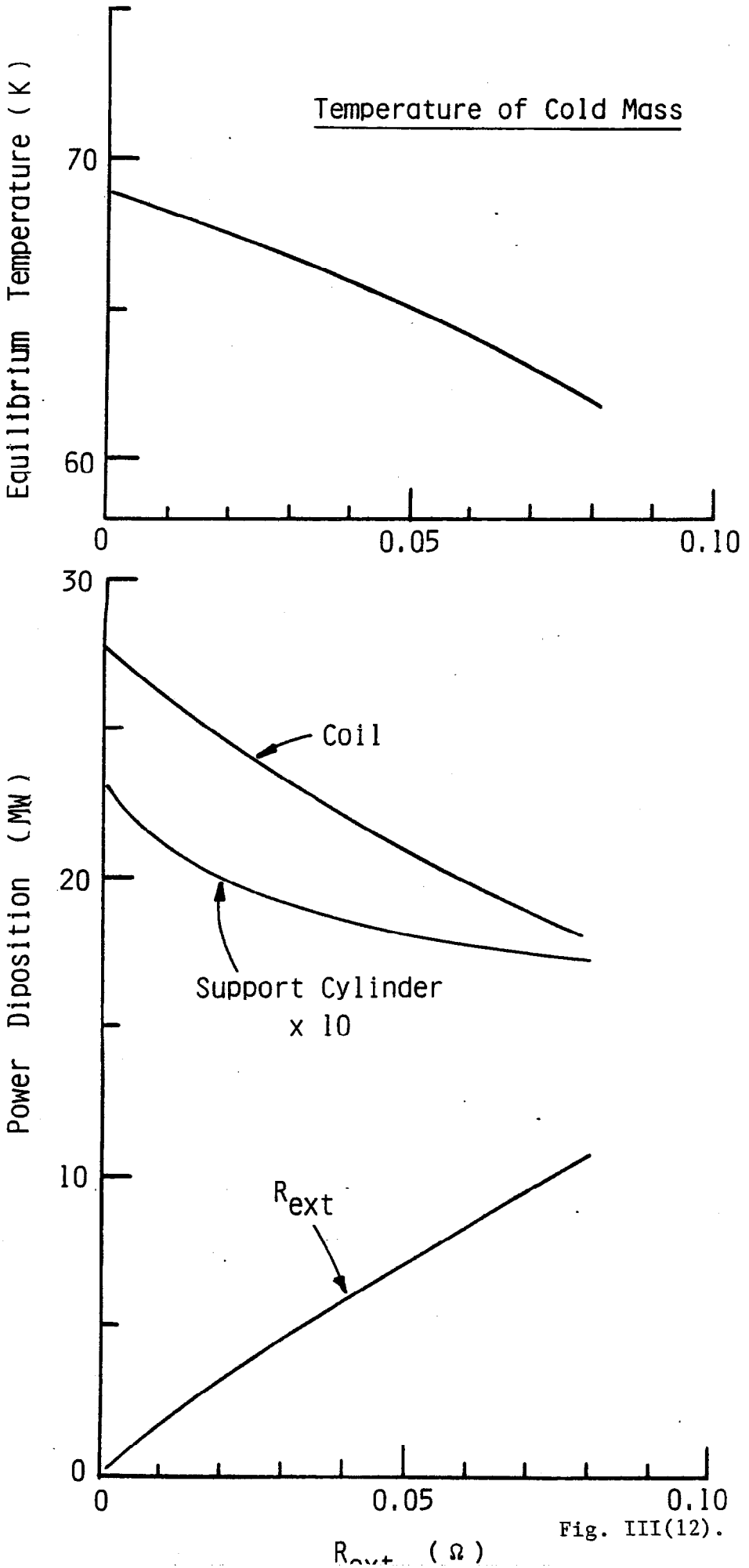

Fig. III(12). Temperature and power during quench

Simulations of Quench Properties of Thin, Large Superconducting Solenoid Magnets", TSUKUBA-HEAP-5, May 1982.

CHAPTER IV: CRYOSTAT DESIGN

General Features

The cryostat consists of four functional components: (1) The vacuum vessel, (2) the coil support system, (3) the helium cooling tube and (4) the liquid nitrogen cooled intercepts and radiation shield. This chapter summarizes the basic design features of the components, while detailed discussion and calculations are found in the appendixes. Design details are the responsibility of the vendor.

Vacuum Vessel

General Design Philosophy. Fermilab Engineering Standards (SD-24 and SD-37) require that all room temperature pressure vessels in use at Fermilab be designed and constructed in accordance with the American Society of Mechanical Engineers (ASME) Boiler and Pressure Vessel Code, Sec. VIII, Div. 1 (the "Code"). We have investigated the penalty paid with respect to radiation transparancy by following these standards. We found that for the outer shell the difference in radiation or absorption thickness between a non-code design (safety factor = 1.2) and a Code design (safety factor $\sim$ 3) is 0.052 λ_r, (0.013 λ_a). Because of the uncertainties inherent in aluminum tank construction, we designed the vacuum vessel in accordance with the Code. This design is shown in Fig. IV (1).

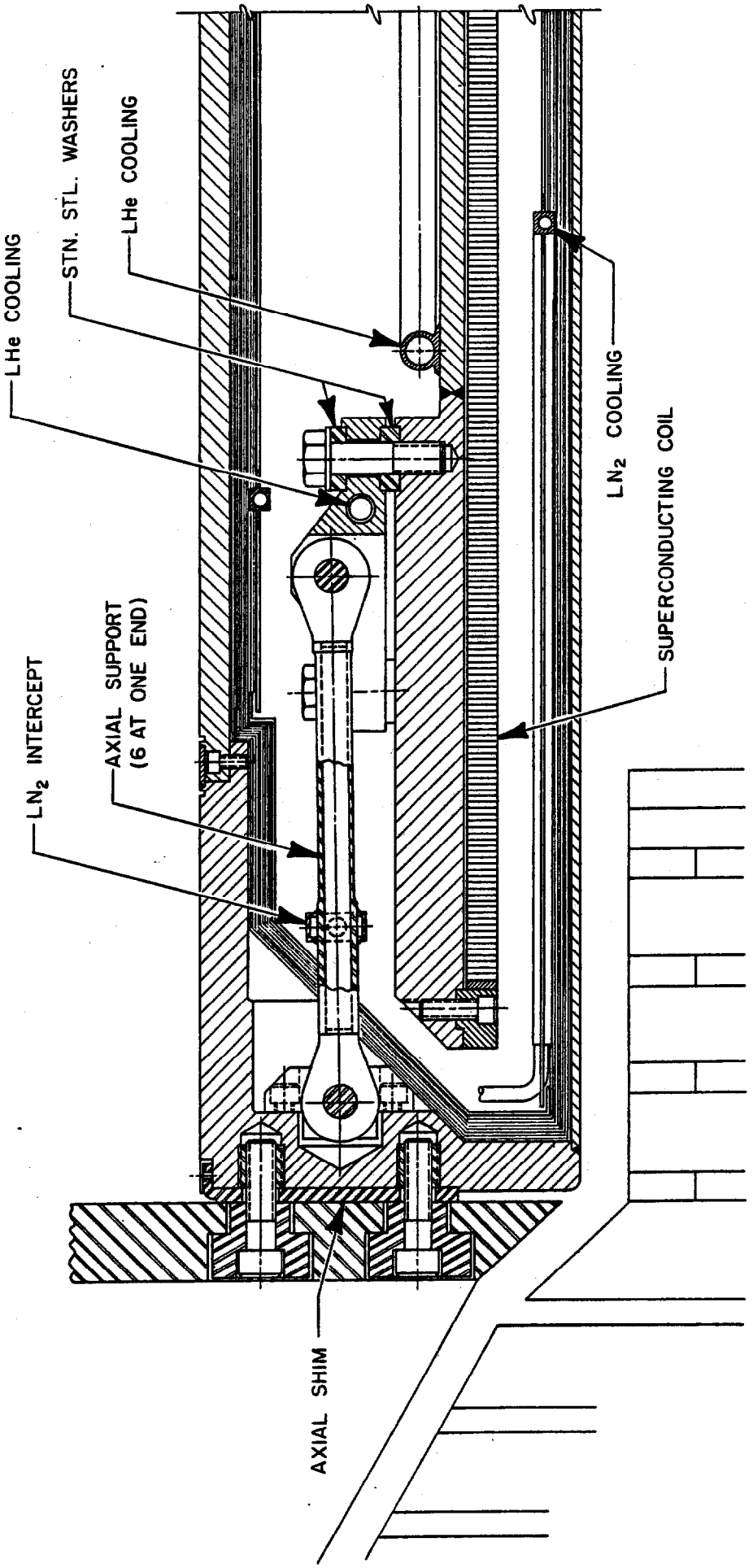

Fig. IV(1). Section view of proposed coil and cryostat

Inner Shell. The inner shell is fabricated of 6061-T6 or 5083-0 aluminum alloy, rolled and welded to form a cylinder. The shell is held circular by the end flanges, but does not have additional stiffening rings.

The inner shell dimensions are given in the table:

Inner Shell Dimensions

Inner diameter	112.5 + 0.25, - 0 inch (2858 + 6.4, - 0 mm)
Outer diameter	113.0 inch (2870 mm)
Wall thickness	0.25 inch (6.4 mm)

We note that with these dimensions the maximum Code allowable positive pressure in the vacuum annulus is 1.17 psig (8.09 kPa-gauge) and the vessel must be protected accordingly. Detailed calculations are found in Appendix F.

Outer Shell. The outer shell is also fabricated of 6061-T6 or 5083-0. The outer shell dimensions are given in the table. It has end flanges on both ends to which the radial supports are attached.

Outer Shell Dimensions

Inner diameter	130.50 inch (3315 mm)
Outer diameter	132.0 + 0, - 0.25 inch (3353 + 0, - 6.4 mm)
Wall thickness	0.75 inch (19 mm)

Shell Tolerances. In order to satisfy the Code the inner diameter of the shells must be constant to with $\pm$ 0.625" (15.9 mm) and the shells must not deviate from circular by more than 0.375 in (9.5 mm) over an chord length of 30 inches (762 mm). However

in order to prevent interference with the central tracking chamber the actual tolerances on the inner shell are much tighter than those required by the Code.

Penetrations into Outer Shell. The vacuum vessel of the chimney is attached to the top of the outer vacuum shell. This penetration of the shell is reinforced as necessary to conform to the Code.

Annular End Covers. The annular end covers serve as closures for the vacuum space and as the attachment for the axial and radial supports. They are essentially flat annular plates attached to the ends of the two shells. The flange thickness is 1" (25.4 mm) which is in excess of the Code requirement (see Appendix F). The overall length of the vacuum vessel is 199.5" + 0 , - 0.25" (5067 + 0, - 6.35 mm). It will be inserted into the yoke in a space 200" + 0, - .25" long (5080 + 0, - 6.35 mm). The overall clearance is therefore seen to be between 0.25" (6.35 mm) and 0.75" (19.05 mm).

Welded Fabrication. The detailed design of all weld joints in the vacuum vessel will be in accordance with the Code, Part UW (Welded Vessels). The intention is also to follow the fabrication and inspection provisions of Part UW.

Code Stamping. Fermilab would like that the vacuum vessel either (1) be ASME Code stamped or (2) be stamped in accordance with the Japanese pressure veessel code and that documentation be provided to show that the Japanese code is at least as stringent

as the ASME Code.

Support System

The purpose of the coil support system is to transmit both gravitational and electromagnetic loads from the 4.2 K coil package to the magnet yoke which is at 300 K. The gravitational loads are due to the weight of the outer support cylinder, conductor and insulation. The sum of these weights is expected to be about 5568 kg (12250 lb). The magnetic forces are much larger than the gravitational forces and thus dominate the design of the coil support structure.

The magnetic field produced by the coil/yoke combination has been calculated using TRIM as described previously. The expected magnetic field distribution is such that if the geometric center of the coil were located at the magnetic center of the yoke, the coil would be in unstable equilibrium with no net electromagnetic body forces acting upon it. However, if the coil were displaced from its equilibrium position, forces would act upon the coil in such a way as to increase the displacement. The magnitude of these forces has been estimated using TRIM (see Chapter II) and for displacements of interest was found to be linear with displacement with spring constants $k_z \backsim$ 17.6 MN/m (10.1×10^4 lbf/inch) of axial displacement and $k_r \backsim$ 12.3 MN/m (7.0×10^4 lbf/inch) of radial displacement. Clearly, if the support system is to be stable and deflections kept small the support system must be stiffer than these magnetic spring constants. In addition to this stiffness requirement, the support system must have

sufficient strength so that if the coil is not positioned at the magnetic center, it can safely handle the resultant body forces on the coil.

For the purposes of designing the support system, we have assumed that the coil may be located as much as 1" (25.4 mm) from the yoke magnetic center in any direction. This choice is somewhat arbitrary but is based on the following considerations: (1) The coil can only be located to $\pm$ 1/4" (6.4 mm) of the geometric center of the yoke due to tolerances in the yoke itself. (2) The geometric center of the yoke may not coincide with the magnetic center. The steel to be used for the yoke is such that considerable variation in magnetic properties may exist in the yoke. These variations in magnetic properties may cause the position of the magnetic center to vary somewhat as the magnet is excited. (3) The return paths contain several air gaps whose dimensions could change, especially the air gaps between the movable calorimeterized end plugs and the yoke or coil. (4) The space available to attach the coil to the yoke and the limited access to this space makes attractive a design that does not require careful adjustment of the coil position to place it on magnetic center.

The support system consists of 6 axial and 24 radial metallic supports. This system is shown schematically in Fig. IV (2). All 6 axial supports are located at the power chimney end of the coil, and are designed to work either in tension or compression. There are 12 radial supports at each end of the coil which are connected

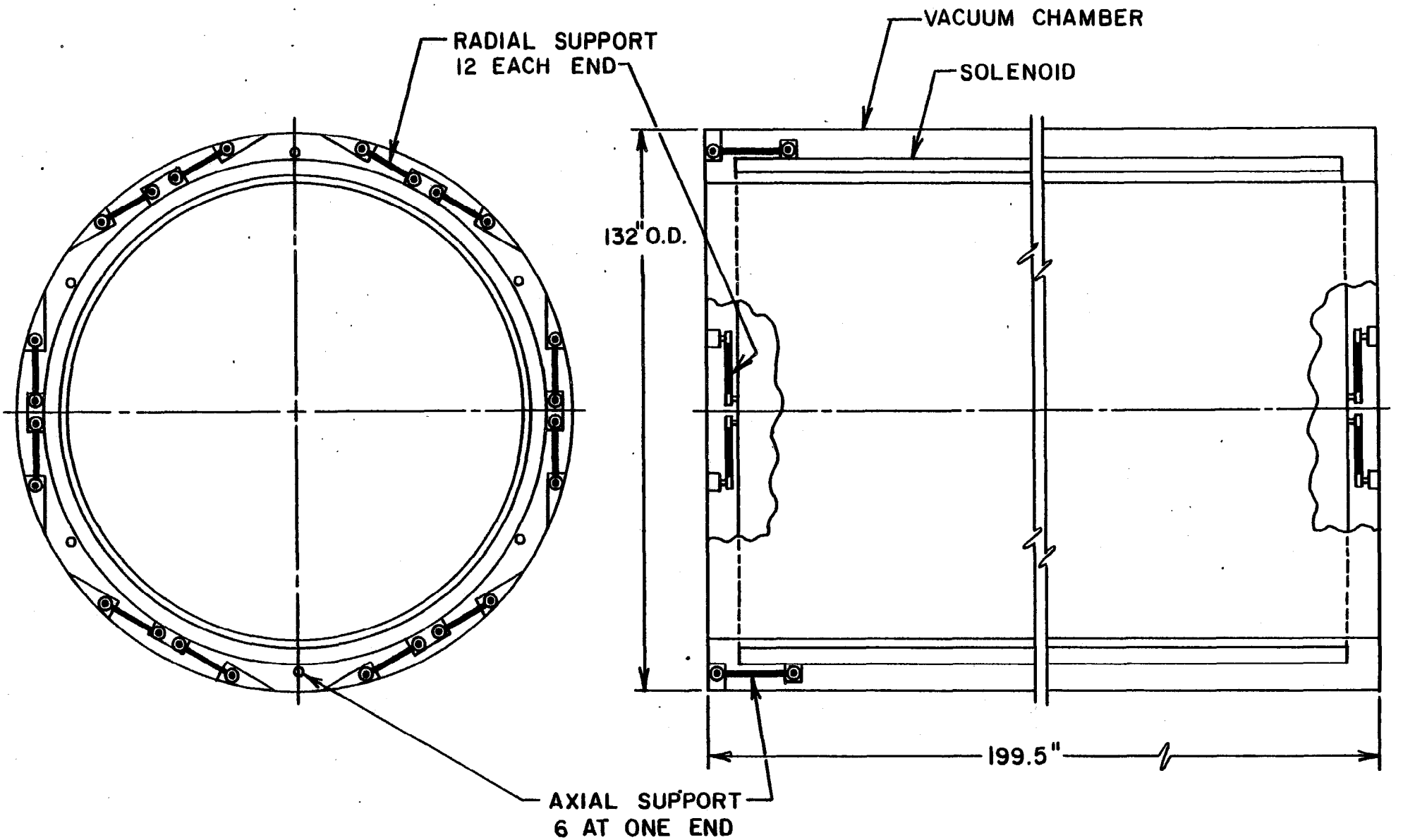
RADIAL SUPPORT
12 EACH END
VACUUM CHAMBER
SOLENOID
132" O.D.
199.5"
AXIAL SUPPORT
6 AT ONE END

approximately tangentially between the coil package and the vacuum vessel and which are preloaded so that they are always in tension. The axial supports determine the axial position of the coil. The coil position with respect to the vacuum chamber is fixed by these supports but the entire package can be shimmed by about 1/4" (6.4 mm) axially if necessary. Similiarly the radial position of the coil is adjustable by $\pm$ 1/4" (6.4 mm) during installation, in the cryostat, but is then fixed.

Differential thermal contraction of the coil in the radial direction is taken care of by allowing both the radial and axial supports to rotate about spherical bearings on the end of each support. The spherical bearings insure that stresses due to bending in the supports are small. The axial supports rotate through an angle of 1.2^{o} during cooldown while the radial supports rotate through angles of 1.3^{o} on the chimney end and 4.1^{o} on the non-chimney end of the coil.

The preload on the radial supports will be adjusted while the magnet is cold during its first cryogenic test. Thereafter, Belleville washers located on the radial support adjustment bolts would compensate for elongation of the radial supports when the magnet is warmed up. All 30 supports will contain strain gauges so that the forces on the support elements can be monitored during magnet excitation. The supports themselves are fabricated from an alloy that exhibits a high strength to thermal conductivity ratio such as Inconel 718. The properties of this material are given in Appendix B. Stress, deflection, and elastic buckling calculations

and a thermal analysis for the supports are presented in Appendix G. The calculated heat load for these supports is 6.3 watts to 4.4 K and 91 watts at 80 K.

Attachment of Cryostat to Yoke

The cryostat is attached axial to the yoke at the chimney end. The six attachments are placed midway between yoke ribs and are located in a 2" (50.8 mm) thick mild steel ring end plate as can be seen in Fig. IV(3). The attachments are equally spaced 60° apart starting at top or zero degrees. Each attachment has two support knobs bolted to the cryostat with 3/4" diameter (≃ 20 mm) bolts which will allow ± 1/8" (3.2 mm) radial movement but will restrict axial motion. The internal axial dimension of the yoke is 200 + 0.0, - 1/4" (5080 +0.0, - 6.35 mm) while the length of the cryostat is to be 199.5 + 0.0, - 1/4" (5067.3 + 0.0, - 6.35 mm). An axial shim will be installed so as to center the cryostat axially within the yoke. This nominal 1/4" (6.35 mm) shim should be mounted with a radial fastener on the outer diameter of the cryostat.

The cryostat is attached radial to the yoke at both ends. Since any radial attachment must have complete freedom in the axial direction six keys are used at each end. The keys are 6" wide x 3/4" thick (152.4 mm x 19 mm) and are mounted centered on six equally spaced radial lines (30°, 90°, etc). They are bolted with four 3/4" (≃ 20 mm) bolts for each key. The keys also allow thermal contractions in the radial direction.

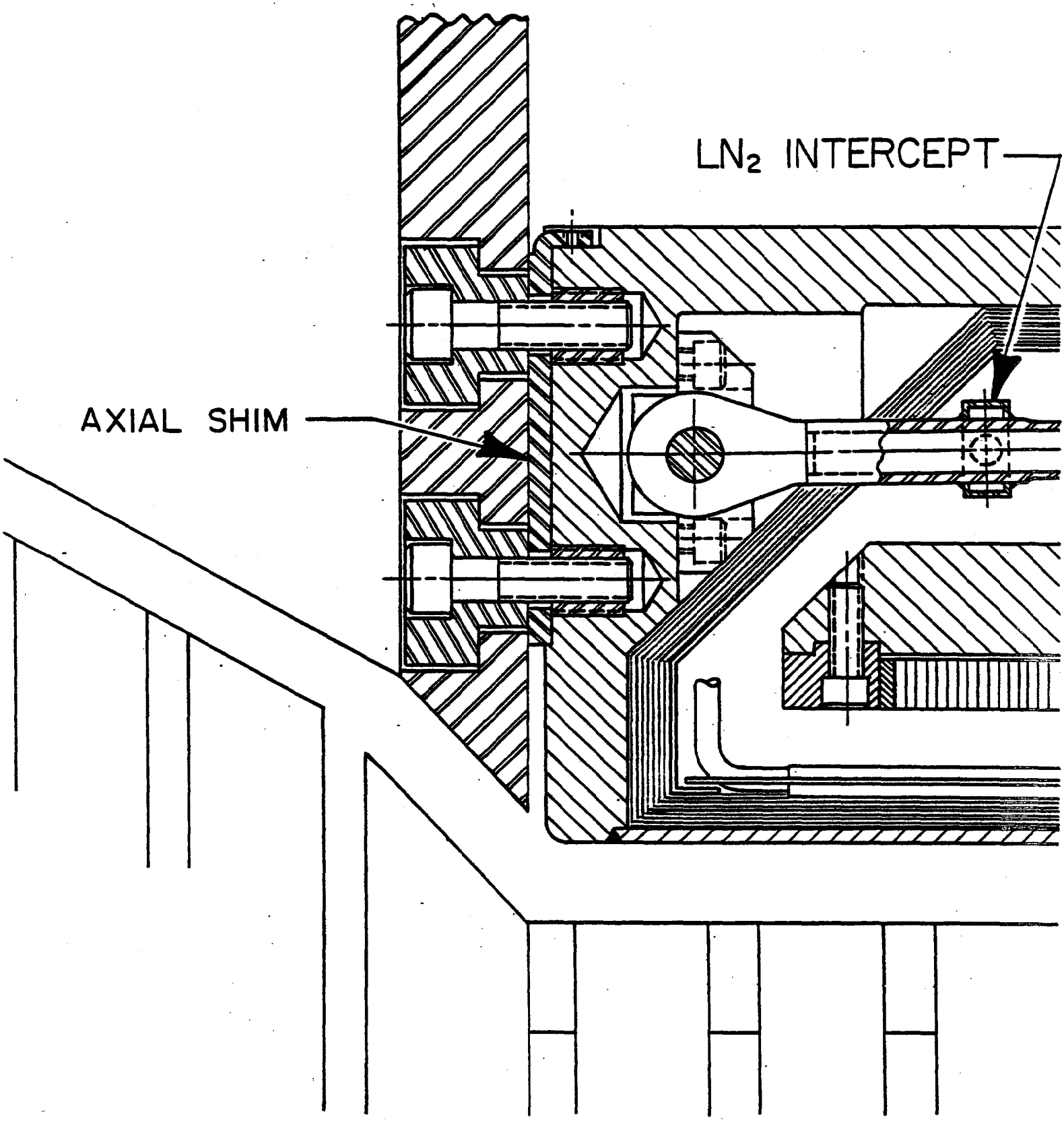

Fig. IV(3). Cryostat to yoke attachment

The cryostat must be capable of being installed in a horizontal manner with the knobs, shims and keys added when the coil is located in its nominal position. It is intended that the yoke, namely the end walls and return legs, will be assembled prior to receipt of the cryostat and present plans do not call for any disassembly of the yoke for cryostat installation. Figure IV(4) shows present yoke configuration.

Liquid Helium Cooling Tube

Description. The helium refrigeration system absorbs heat from the coil and outer support cylinder by means of LHe circulated through a cooling tube attached to the support cylinder. Thermal radiation and conduction through the supports constitute a steady state heat load. Heat is generated in the coil and support cylinder by charge and dicharge eddy currents and by joule heating during a quench. A 0.79" (20 mm) inner diameter aluminum tube is routed longitudinally on the outer support cylinder with the 24 straight sections separated by approximately 16" (400 mm) and then circumferentially to the axial and radial support intercepts as shown in Fig. IV(5) . The flow direction is such that the support intercepts are cooled by two phase LHe of the highest gas fraction. The cooling tube is welded to the support cylinder for good thermal contact. A finite element calculation was used to help choose the cooling loop pattern. A cool down pressure drop calculation and consideration of the pressure rise during a quench helped determine the tube diameter and wall thickness.

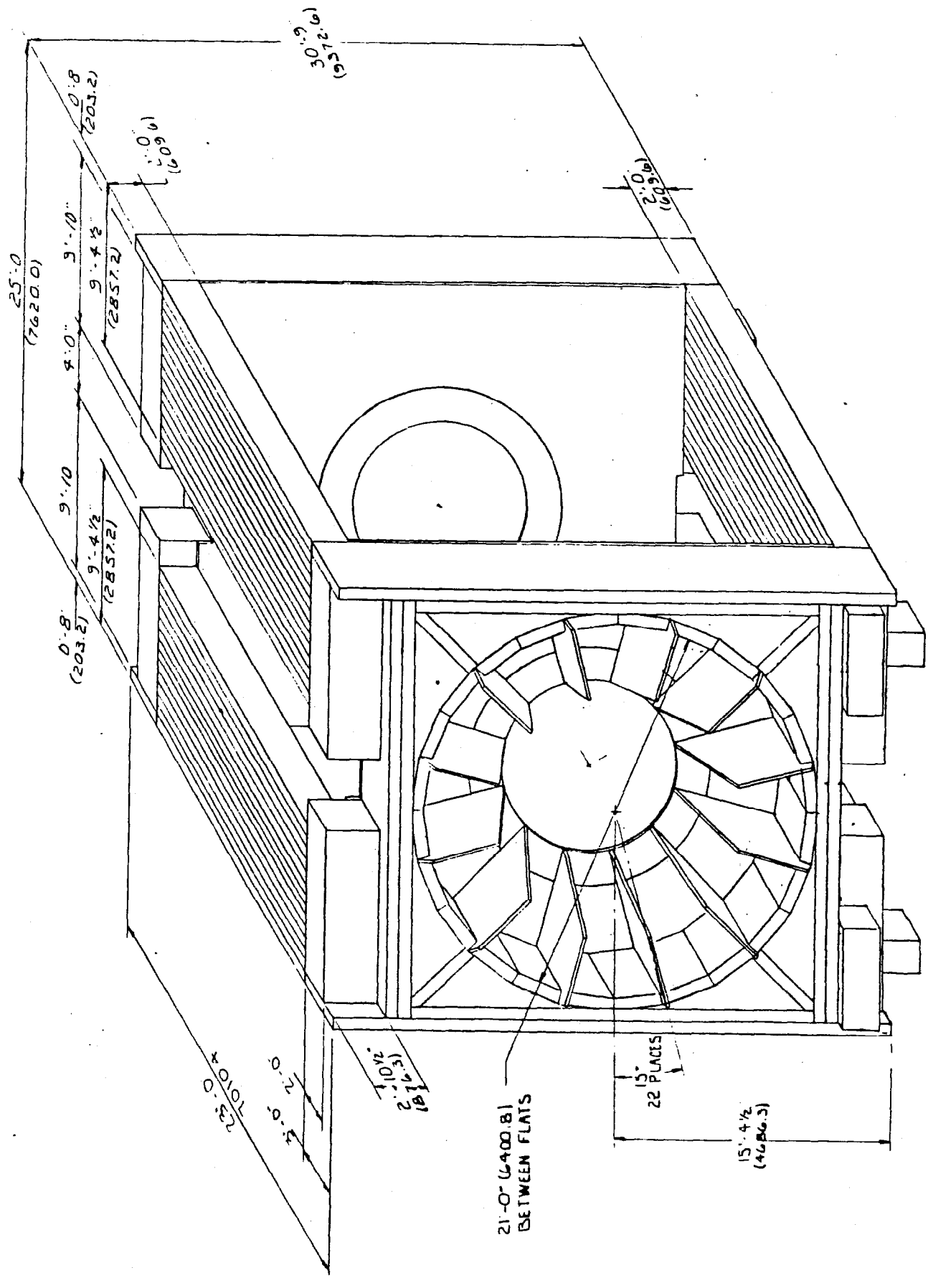

Fig. IV(4). Isometric view of bare yoke

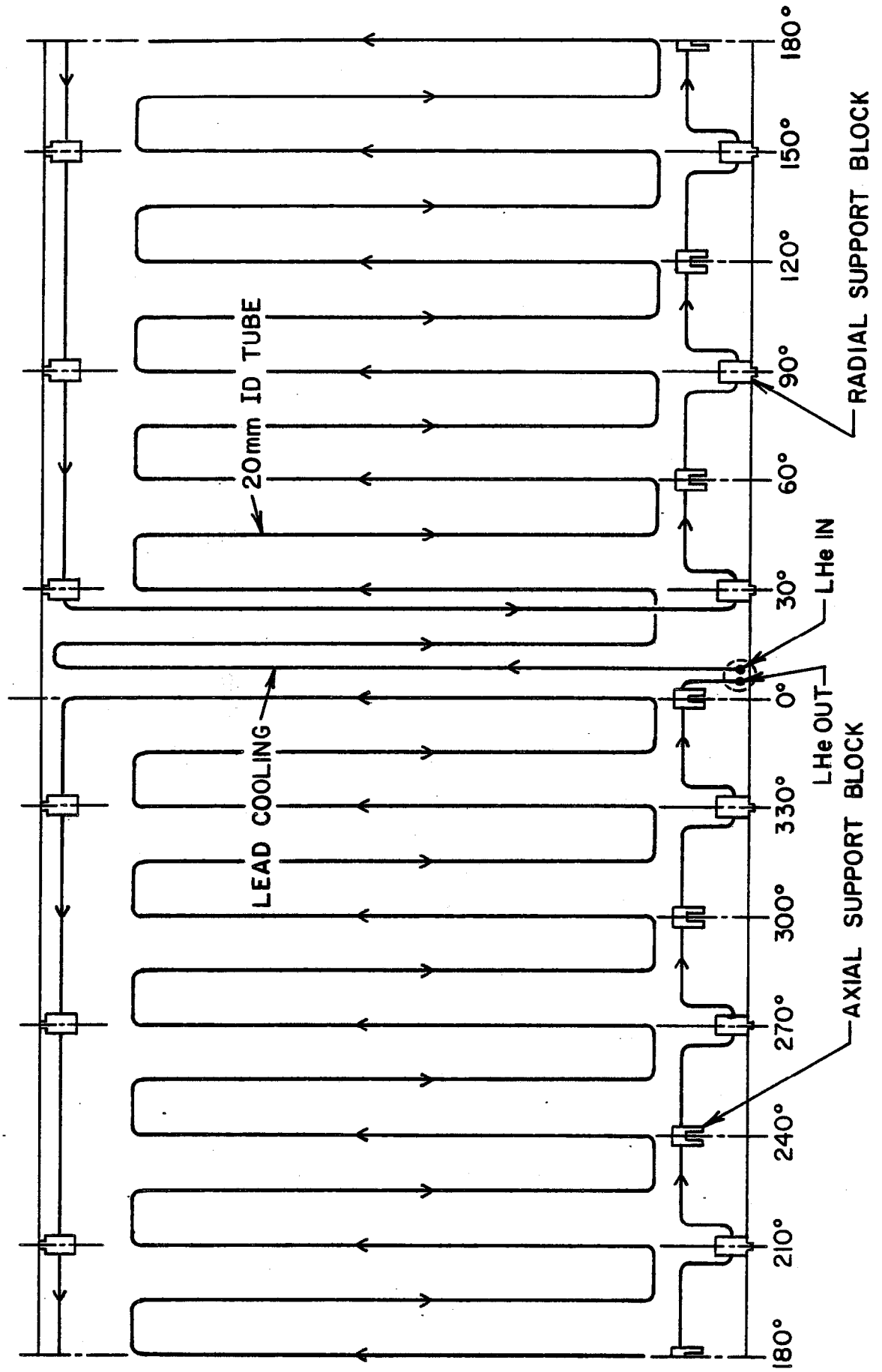

Fig. IV(5). Routing of LHe cooling tube on support cylinder

Finite Element Thermal Analysis. Finite element models were generated to study the thermal behavior of the solenoid under a linear ten minute charge and under a concentrated external heat flux. A liquid helium temperature of 4.4 K in the cooling tube was assumed. These calculations, in Appendix H, indicate that during the charge, when eddy current heating is ~ 100 watts, the maximum support cylinder temperature is approximately 4.90 K and occurs at a bolting location for the radial support pad. Support rod heat fluxes were calculated to be 0.16 W for the radial support rod and 0.21 W for the axial support rod. These figures agree well with those calculated analytically in Appendix M.

The maximum concentrated external heat flux which the support cylinder can absorb while maintaining a maximum temperature of 6.5 K midway between two of the 24 cooling paths is 0.43 watts. Should this flux result from a resistive section of conductor, then the conductor temperature may exceed 6.5 K since the heat must be transferred through the conductor and insulation into the support cylinder. However, conduction of heat along the high purity aluminum conductor stabilizer should provide some beneficial effect, although no attempt has been made to model the solenoid in this detail.

Pressure Rise During Quench. The initial pressure at the quench initiation point is determined by the force required to accelerate the liquid in the tube to a velocity adequate to clear

the tube of liquid in some specified time. Calculations given in Appendix I show that for a liquid expulsion time of one second the maximum internal pressure is approximately 60 atm. It is shown in Appendix K that a wall thickness of 0.125" (3.2 mm) satisfies the USA Standard Code for Pressure Piping (USAS B31.1.0-ASME) for a pressure of 180 atm.

Due to uncertainties in the pressure rise calculation, we recommend this wall thickness.

Radiation Shield and Thermal Intercepts

General Features. In order to reduce the thermal radiation load on the 4.2 K helium vessel, a radiation shield cooled by force flow LN_2 is provided. It consists of cylindrical aluminum inner and outer shields, and a series of segmented copper shields at each end of the magnet. There are two separate LN_2 circuits, one cooling the aluminum shields in series and the other handling the end copper shields and the LN_2 temperature intercepts on the axial and radial supports.

Inner Shield Design. The inner shield is designed to be supported from the inner vacuum shell by (G-10) epoxy-fiberglass standoffs. The shield is made of two semi-cylindrical 0.080" (2.0 mm) thick 6061-T6 aluminum panels. The support standoffs, shaped like single leaf springs, are fastened to the aluminum shield, and only rest on the inner vacuum shell with small contact areas. The shield is securely fastened to the vacuum shell at one location only. This fixed point is located at the top of the shield near

the chimney. The shield is split at the top and bottom. A G-10 piece is used to fasten the halves together at the top. At the bottom, the halves are connected with stainless steel tension springs, which keep the diameter of the shield constant during cooldown and hence maintain the relative position of the shield and shell. The LN_2 coolant flows through two loops consisting of 3/8" (9.5 mm) diameter extruded aluminum tubes. The extrusion is 6063 aluminum and is mechanically fastened and welded to the edge of each panel. The extrusion provides a curved frame to maintain the shield curvature. Conduction heat transfer is adequate to maintain the panels at an effective temperature.

Outer Shield Design. The outer shield also consists of two .080" (2.0 mm) thick 6061-T6 aluminum semi-cylindrical panels which are edge cooled with liquid nitrogen. As in the inner shield the panels are cooled along the perimeter. The shields are fastened to the outer vacuum shell with G-10 bolts, through holes in the panel which are slotted to allow contraction towards a fixed point near the chimney.

Column Intercepts and End Shields. The axial and radial supports are intercepted with the nitrogen circuit that also cools the pie-shaped end shields. For the expected heat loads and strap geometry, we calculate the intercept temperature to be 80 K. The end shields are made of 0.060" (1.5 mm) thick copper and are not connected to the two inner and outer aluminum shields.

Flow Pattern. A schematic of the flow pattern is shown in Fig. IV(6). Each circuit has a modulating valve on the supply line which is controlled by the temperature of the exhaust gas. The valve dynamically regulates the liquid flow to keep the shields at some preset temperature. Chapter VI gives details of the nitrogen refrigeration system.

Performance. The shields have conduction heat loads from the supports in addition to the radiation load. Heat load by radiation from 300 K to 78 K depends on the choice of insulation system which is treated in Appendix L. The thermal analysis of the shields and support intercepts, presented in Appendix H, shows that the maximum temperature in the inner shield is 85 K and in the outer shield is 88 K. The heat load to the nitrogen system is considered in Appendix M.

a) INTERCEPT CIRCUIT

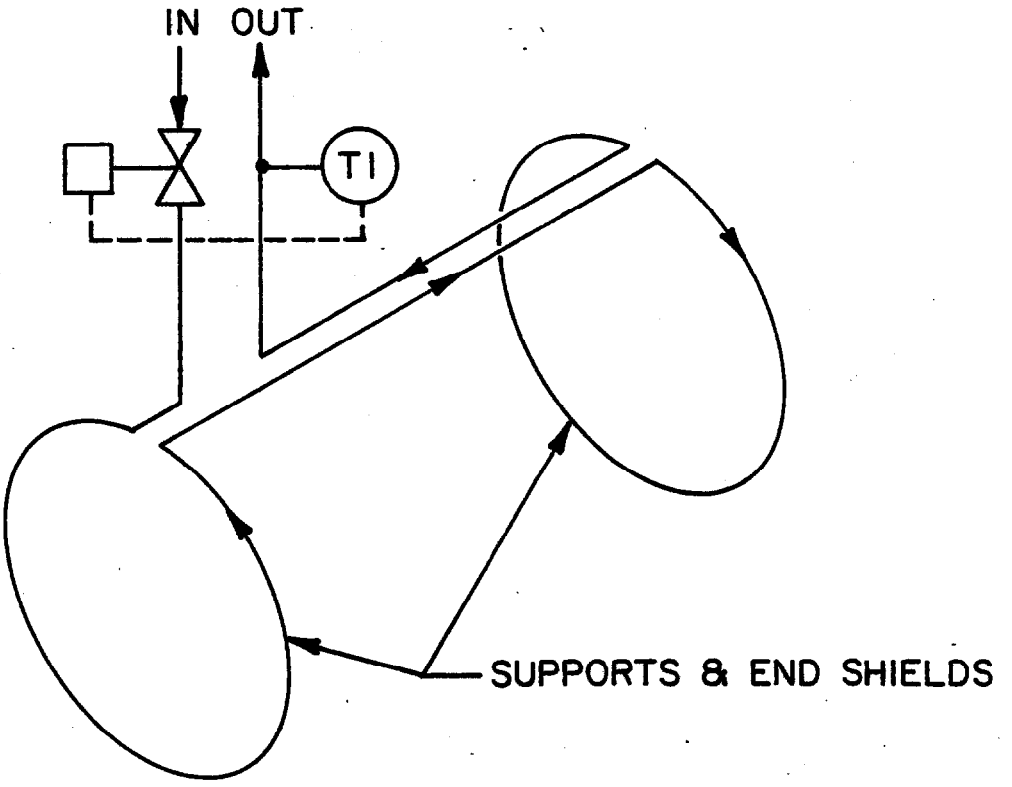

b) INNER & OUTER SHIELD CIRCUIT

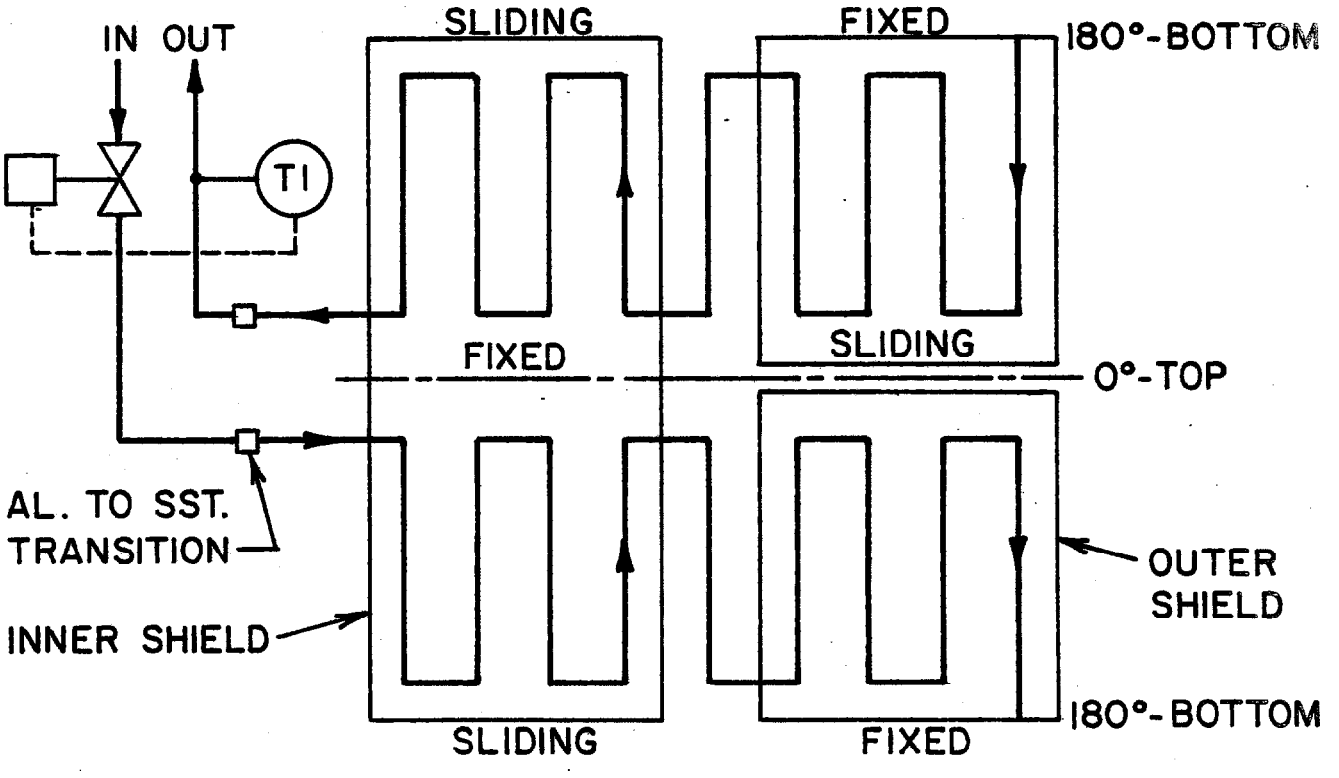

Fig. IV(6). Liquid nitrogen circuits

CHAPTER V: CHIMNEY AND CONTROL DEWAR DESIGN

Chimney

The chimney is the vacuum vessel that carries all cryogenic and electrical lines to the coil from the control dewar. It also serves as a relief channel for the vacuum space. Since the chimney requires a hole in the central calorimetry of the detector, it is important to make the chimney as small as possible consistent with safety and structural integrity. The chimney must come out of the detector through an opening in the magnet iron yoke on the east side of the magnet which is 3 x 5 ft^2 (0.91 x 1.5 m^2). The design to meet these requirements is shown in Fig. V (1). The 8" (203 mm) pipe contains LHe supply and return lines, LN_2 supply and return lines, instrumentation wires and two superconducting bus bars. Design details are given in Appendix K.

Protection against vacuum space over-pressure is provided both by relief valves and an 3" dia. (76 mm) relief disk. We have calculated that this combination of relief valves and relief disk should comfortably handle "worst case" cryogenic failures, such as ruptured LHe and LN_2 lines under the maximum flow rates.

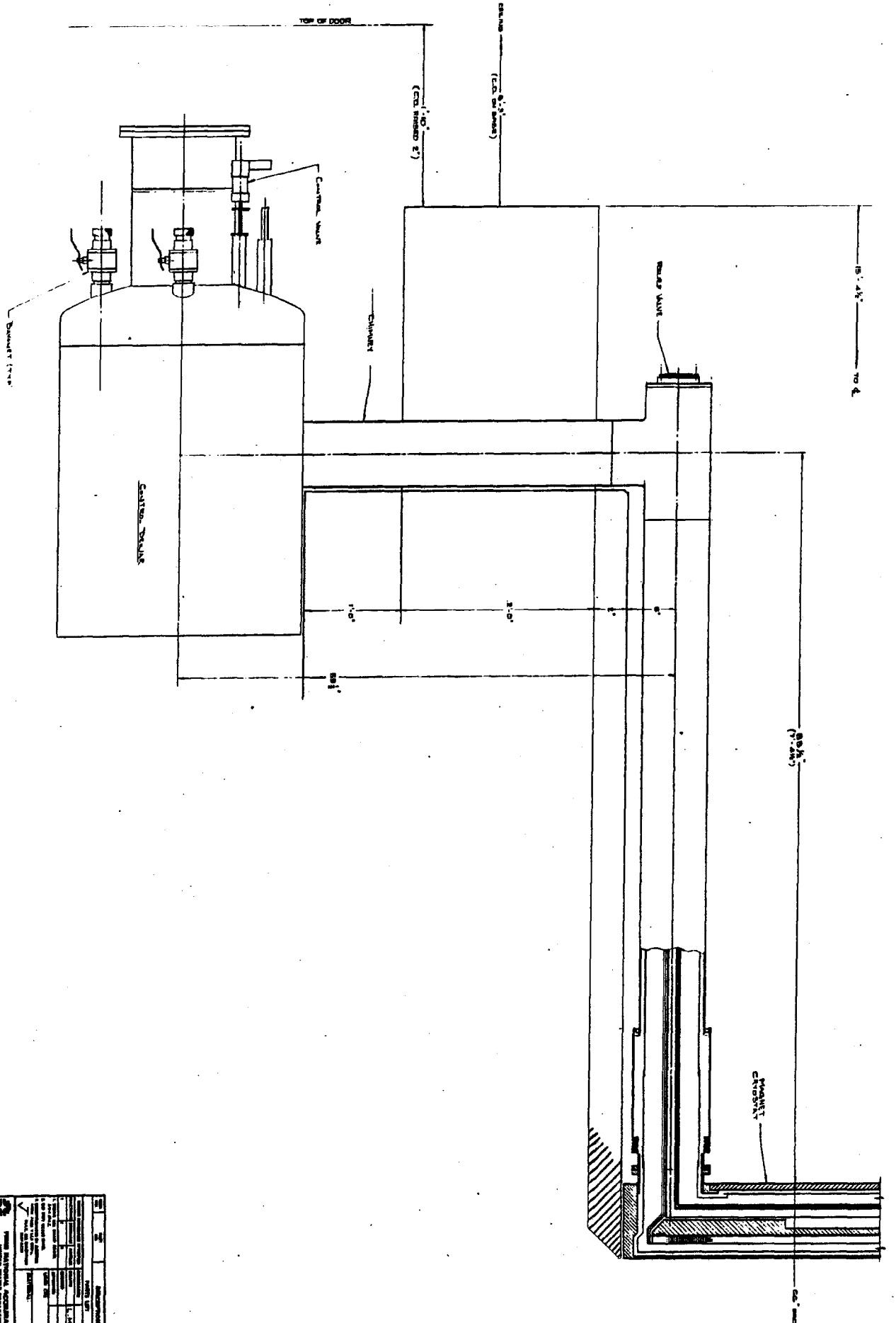

Fig. V(1). Chimney

Control Dewar

The control dewar, located just outside the magnet yoke, at the end of the chimney is the interface between the permanently installed cryogenic transfer line and the movable magnet. It has bayonet couplings for the helium supply, return, and cool down lines and the liquid nitrogen supply and return lines. It contains a LHe reservoir fed from the helium return line with an internal supply line heat exchanger and J-T valve. The purpose of the heat exchanger is to insure that the helium stream supplied to the magnet is >80% liquid for mass flows of 10-50 g/s. The J-T valve provides a temperature difference across the heat exchanger. The superconducting bus bars from the coil enter the helium vessel through insulating feed-throughs and connect with gas cooled current leads leading to 300 K through a 4" (102 mm) neck. The helium vessel has a liquid volume of approximately 35 L and is relieved through the neck. The control dewar is shown schematically in Fig. V(2), with details in Appendix K. The control dewar and chimney have common vacuum with the cryostat. The vacuum shell of the control dewar has pumping ports and appropriate vacuum instrumentation.

Transition Joints

Each of the liquid and gas lines in the chimney (six in total) and the chimney vacuum vessel has an aluminum to stainless transition joint. In general these joints are located either in the control dewar or in the chimney-to-cryostat junction area at the base of the chimney. The location of specific transition

1 Female Bayonet Ass'y
2 Control & Shut-Off Valve Ass'y
3 Cryogenic Check Valve
4 Alum. to Stainless Stl. Transition
5 1" Vacuum Valve
6 Vacuum Seal-Off Valve
7 Ion Gage
8 Thermocouple Vacuum Gage
9 Electrical Feed-Thru
10 Temperature Sensor

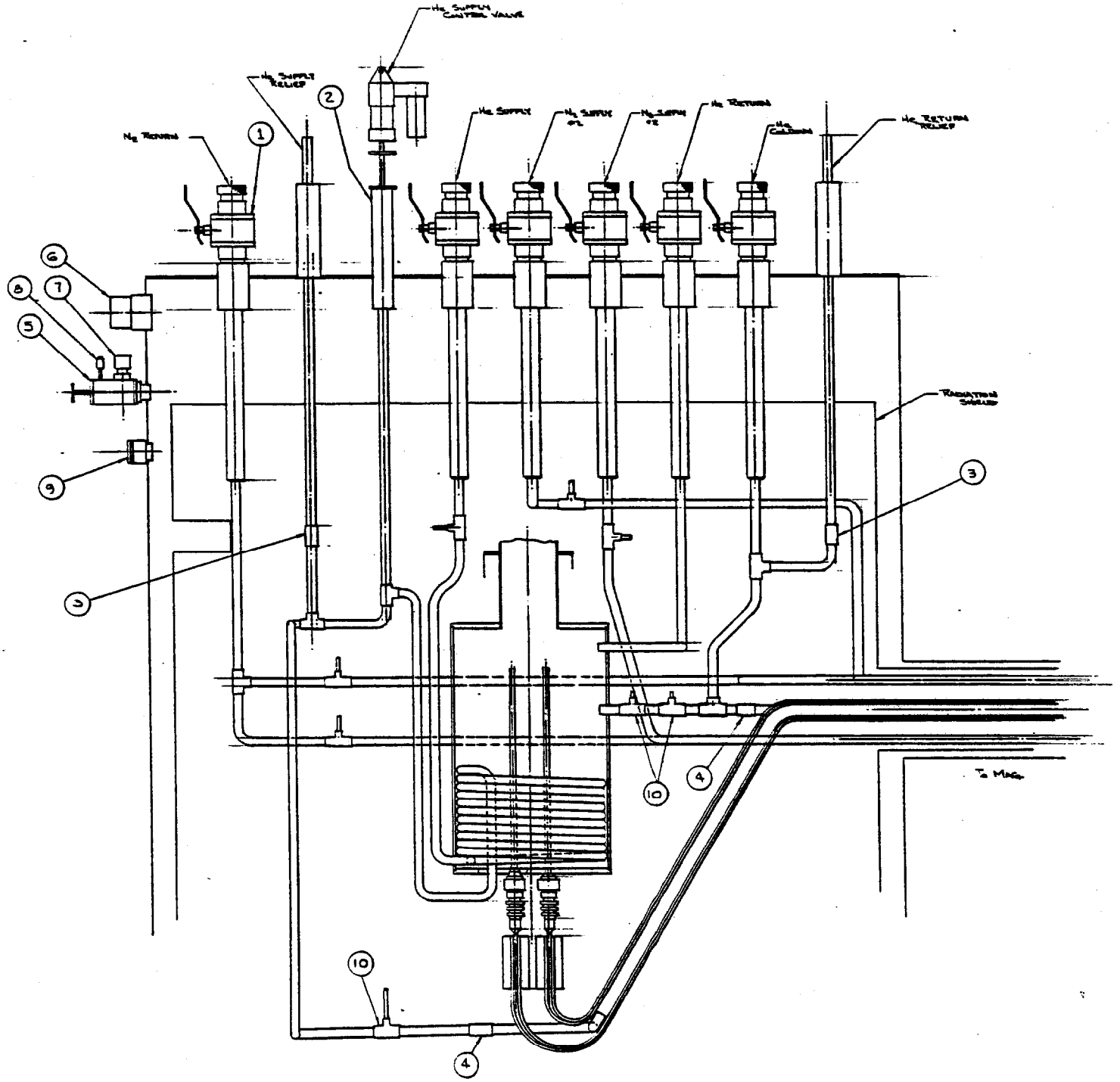

Fig. V(2). Control dewar schematic

joints is given in this table:

Location of Aluminum/Stainless Transition Joints

Line	Location of Joint
Chimney vacuum vessel	Base of chimney
Helium supply	In control dewar
Helium return	In control dewar
Nitrogen shield supply	Base of chimney
Nitrogen shield return	Base of chimney
Nitrogen intercept supply	None required
Nitrogen intercept return	None required

Assembly/Disassembly Joints

These joints are made initially by the vendor prior to his testing the coil. The control dewar/chimney assembly is separated from the magnet cryostat at these joints for shipping. The joints are remade at Fermilab when the chimney is reinstalled. The joints in the helium supply and return lines are in the aluminum tubing, all other joints occur in stainless tubing.

CHAPTER VI - REFRIGERATION SYSTEM

Description.

The refrigeration system that has been chosen for the CDF solenoid is based on a Fermilab "Satellite" refrigerator. The solenoid refrigeration system will be independent of the Energy Saver and low-beta quadrupole refrigeration systems. The system will be controlled by the Accelerator Division control system. We have attempted to copy existing hard- and soft-ware as much as possible.

Flow Diagram

A box diagram is given as Fig. VI(1) and a simplified flow diagram as Fig. VI(2).

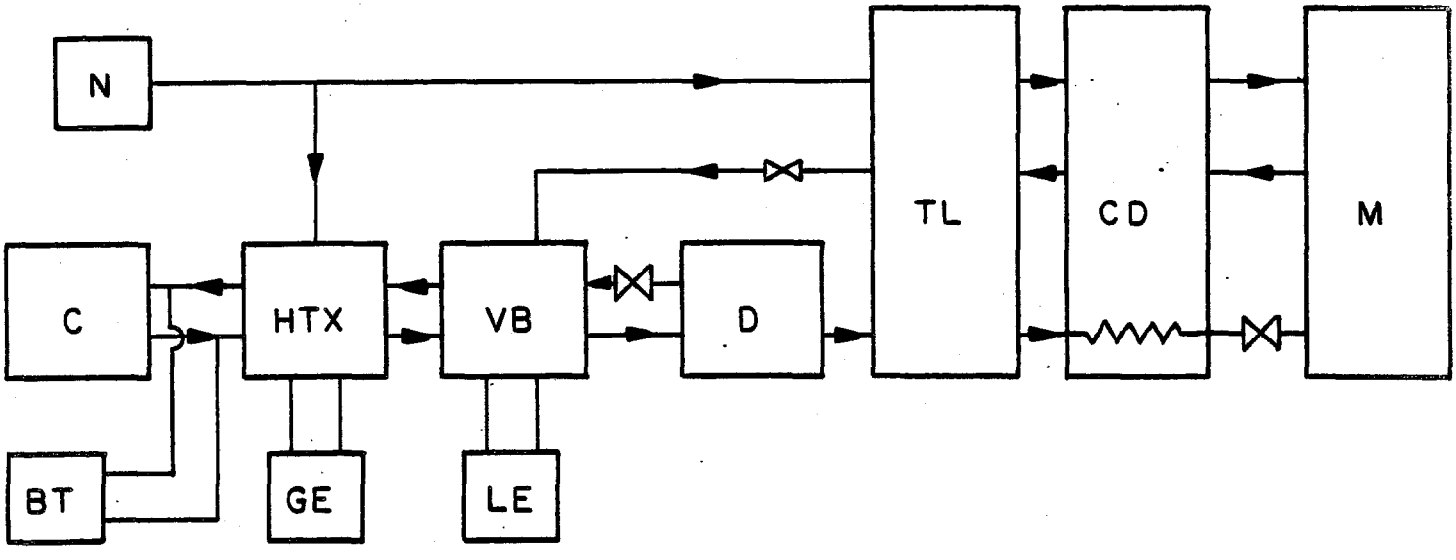

Fig. VI(1) Refrigeration System - Box Diagram
Symbols: N=liquid nitrogen tank; C=compressor; BT=buffer tank; HTX=heat exchanger; GE=gas expansion engine; LE=liquid expansion engine; VB=valve box; D=dewar; TL=transfer line; CD=control dewar; M=magnet

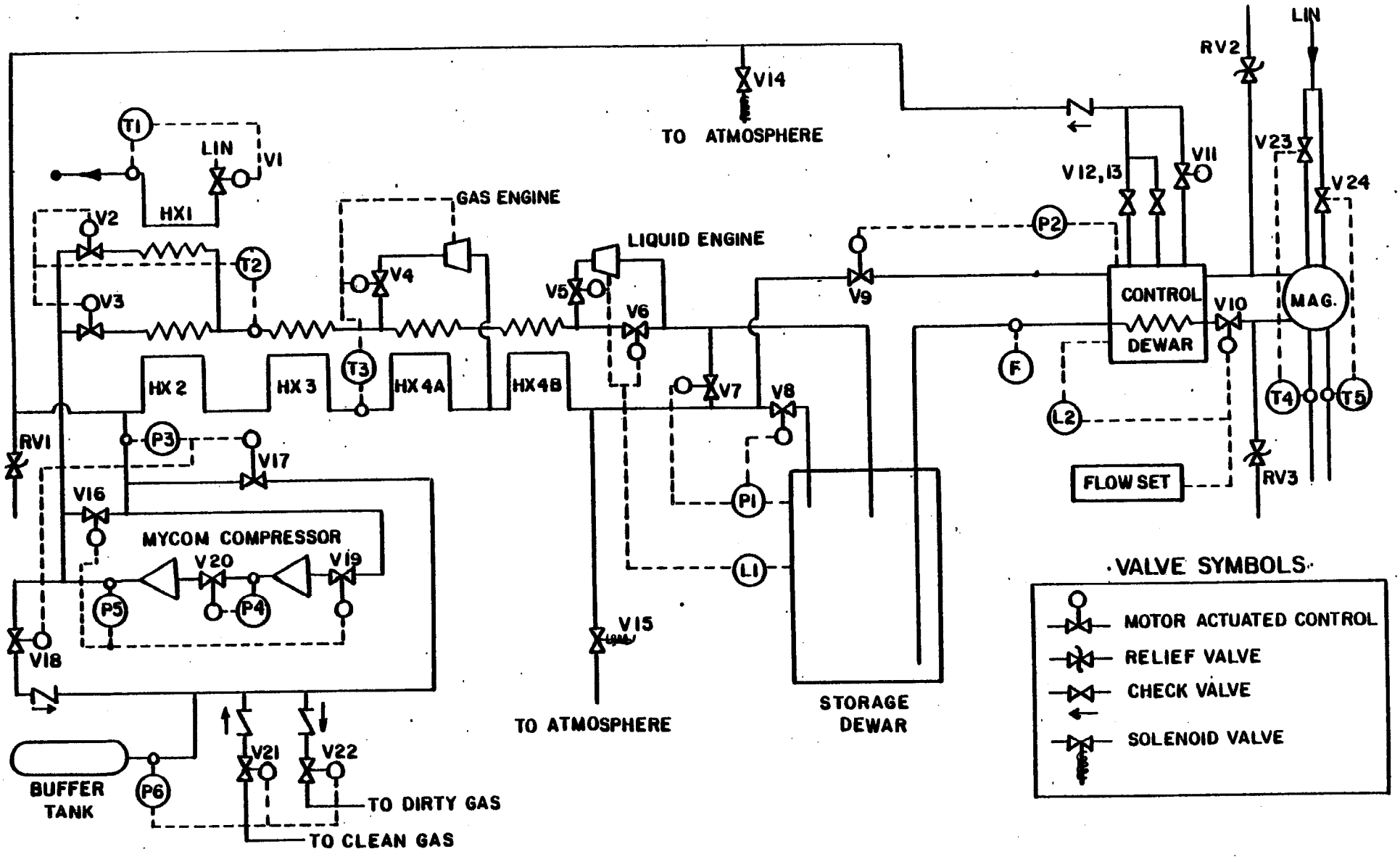

Fig. VI(2a). Simplified flow schematic

Valve Legend

V1	Heat exchanger LIN control valve
V2	HX1 flow control valve
V3	HX2 flow control valve
V4	Gas engine flow control valve
V5	Liquid engine flow control valve
V6	J-T valve
V7	By pass valve
V8	Storage dewar pressurizing valve
V9	Control dewar pressurizing valve
V10	Magnet flow control valve (J-T valve)
V11	Cool-down valve
V12,13	Current lead flow control valves
V14,15	Solenoid valves for open cycle operation
V16	Compressor by pass valve
V17	Suction-side inventory control valve
V18	Discharge-side inventory control valve
V19	1st stage slide valve
V20	Interstage slide valve
V21	Clean gas supply valve
V22	Dirty gas discharge valve
V23,24	Magnet LIN control valves

Valve numbering valid for this drawing only.

Fig. V(2b). Valve legend

Hardware Components

Compressor. A 350 hp two-stage Mycom compressor has been ordered for the system. It is identical to those used for the Saver. It is specified for a discharge pressure of 20 atm at 600 SCFM (50.5 g/s). The existing units have measured capacities of ∿ 57 g/s. The compressor will be located in a new annex to the B0 accelerator service building. A standard, full-flow, three-stage purifier will treat the discharge flow to remove oil and water. The purifier is also located in the service building annex. The piping within the service building will be such that the CDF compressor can be plugged into the Saver system at some later time. Compressor discharge and suction lines run across the berm to the CDF Assembly Hall, along with a "dirty gas return" line and an inventory management line to a gas buffer tank, located north of the berm and possibly parallel to it.

Heat Exchanger. A so-called "STAR" (STand Alone Refrigerator) heat exchanger has been ordered. This is a horizontal vacuum vessel containing the LIN/He and He/He heat exchangers. It will be located on the East Mezzanine of the Assembly Hall (elevation 743 ft).

Expansion Engines. The STAR uses a dry reciprocal expansion engine across the process stream and a wet reciprocal expansion engine in the process stream. These engines are installed in individual vacuum vessels, connected to the heat exchanger through

bayonets and U-tubes. Two dry (one spare) and one wet engine assembly have been ordered from Koch Process Systems, Inc. (formerly CTI Process Systems). The engine vacuum vessels will also be located on the mezzanine.

Valve Box. A valve box serves as a junction between the heat exchanger, wet engine, storage dewar and transfer line with the interconnections made with U-tubes. It is a vacuum box with bayonet fittings on the top and internal cold piping. The box contains four electrically operated control valves: the high-to-low pressure by-pass valve, a J-T valve in parallel with the wet engine, a storage dewar pressurizing valve, and a control dewar pressurizing valve.

Storage Dewar. The STAR will make LHe into a 1000 to 2000 L storage dewar. We hope this item can be commercially procured. The pressure rating must be appropriate for pressures encountered during cooldowns. In cold, steady-state the dewar will operate at $\sim$ 1.8 atm, (4.91 K) which will be the driving pressure for LHe flow through the magnet, i.e. no LHe pumps will be used. The storage dewar will be located on the mezzanine.

Liquid Nitrogen Storage Tank. A liquid nitrogen (LIN) tank located outdoors along the east side of the Assembly Hall provides LIN for the heat exchanger and magnet. The commercial tank, either horizontal or vertical, will have a volume of 2000 - 10,000 gal (8 - 38 cubic meters). A vacuum insulated LIN header with liquid withdrawal bayonets runs along the mezzanine.

Transfer Line. U-tubes will connect the storage dewar, heat exchanger and LIN header to the LIN/LHe/GHe transfer lines. One line reaches north to the magnet test position in the Assembly Hall and another south to the Collision Hall. U-tubes connect the transfer line to the control dewar.

Control Dewar. The control dewar, described in Chapter V, is the interface between the permanently installed cryogenic transfer line and the movable magnet.

System Heat Loads and Capacity.

A detailed description of the low-temperature components and the identified heat loads to the nitrogen and helium systems are given in Appendix K. The total identified steady state helium heat load is 40 W + 14 L/h with an additional 100 W during charge. The nitrogen heat load is approximately 600 W, equivalent to approximately 16 L/h.

Figure VI(3) shows the nominal capacity of the STAR with the identified and expected heat loads. It can be seen that there is adequate excess refrigeration to cool the magnet system from room temperature and to quickly recover from a quench.

Steady-State Operation of Helium System.

Although not completely finalized, steady-state operation of the system will probably be approximately as follows. Referring to Fig. VI(2), the refrigerator will be running to maintain the liquid level and pressure in the storage dewar at preset values, approximately 90% full and 1.8 atm, respectively. Valve V10 will maintain a given mass flow through the magnet and liquid level in

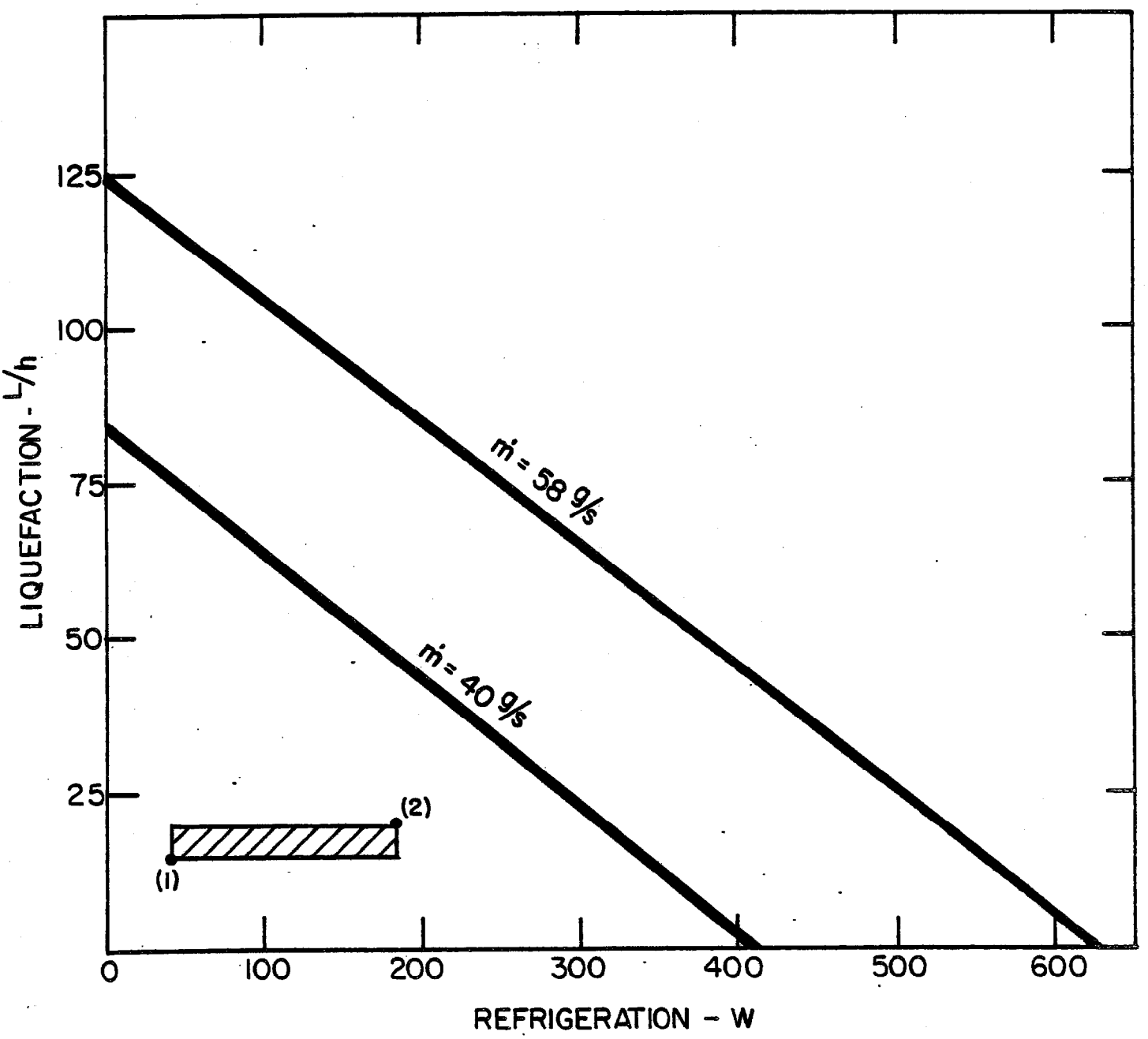

Fig. VI(3). Capacity of star refrigerator and (1) identified steady state heat load, (2) max. expected charging heat load.

the control dewar. Valve V9 will keep the control dewar pressure at about 1.2 atm. The control dewar heat exchanger will remove the heat picked up by the supply stream in the transfer line and will subcool the stream slightly. Following the expansion in valve V10 the stream will be about 80-85% liquid. The stream will absorb heat in the magnet and return to the control dewar at about 70-75% liquid. The stream returning to the heat exchanger will probably contain some liquid which will permit operating the gas engine at less than full capacity. Approximately 14 L/h or 0.5 g/s will flow out the current leads to compressor suction.

Non Steady-State Operation of Helium System.

Cooldown from 300 K. The Energy Saver computer controlled cooldown sequence will be modified for use with the solenoid. Basically the cooldown will use refrigeration from the LIN/He heat exchanger, HX1 in Fig. VI (2), and the gas engine. The entire compressor flow, approximately 50 g/s, can be directed through the magnet cooling tube. The magnet cold mass is 12250 lb (5568 kg) which corresponds to a thermal energy of approximately 1 GJ from 300 K to 80 K and 52 MJ from 80 K to 4.4 K. The cooldown rate will be determined by thermal stresses in the magnet coil, which will be calculated later. A cooldown time of 2 to 4 days should be achievable, depending on thermal stresses.

Magnet Charge. During a 10 min charge eddy currents in the outer support cylinder cause an additional heat load of 100 W or 60 kJ for the charging process. If necessary, the mass flow through the magnet can be automatically increased to insure that

the flow remains two phase. The refrigerator will increase its production to maintain the storage dewar liquid level.

Superconducting Discharge. The refrigeration system will behave the same as for a charge.

Quench and Recovery. Upon detection of a quench, valve V10 closes. As the quench proceeds the pressure in the magnet cooling tube will rise, some liquid will be vaporized and some blown out to the control dewar. Valve V9 opens to maintain 1.2 atm in the control dewar and some liquid is carried back to the refrigerator. Relief valves RV2 and RV3 open if necessary. Calculations given in Appendix I show that the maximum pressure to be expected in the cooling tube is 900 psi (60 atm).

Following the quench discharge the magnet will be at a temperature of 50 to 80 K. A cooldown sequence will take over and restore the system to steady state, removing the 9.5 MJ (50 K) in approximately 4-6 hours.

Loss of Compressor Flow. If the helium flow in the refrigerator (not magnet) circuit is lost due to a plug in the heat exchanger or power loss to the compressor, or if refrigeration capacity is lost due to a failed or inefficient gas engine, the storage dewar acts as a buffer supply of LHe for the magnet. Solenoid valves V14 and V15 open, V9 continues to maintain the pressure in the control dewar and V8 along with an electrical heater in the storage dewar maintains the delivery pressure at 1.8 atm. The flow through the magnet cooling tube is not interrupted and so the magnet need not necessarily be turned

off. If the refrigerator is out of service for a protracted length of time and if it is desired to run the magnet, liquid helium from an external source (a commercial vendor or the central helium liquifier) can be added to the storage dewar through the valve box. The LHe use rate of the system in this open cycle mode is at least 100 L/h.

Moving the Detector to and from Collision Hall. When the detector, with the attached solenoid cryostat, is moved, the helium system will be shut down and the helium U-tubes between the transfer line and the control dewar removed. The current lead return lines and the vent lines will be valved off and disconnected. The magnet coil will warm toward 80 K during the move because liquid nitrogen refrigeration is provided during that time (see the following paragraph).

Liquid Nitrogen System Operation.

The two nitrogen circuits in the magnet cryostat (the intercept circuit and the radiation shield circuit) are independently refrigerated by valves V23/24 on the LIN supply and temperature sensors T4/5 on the return or discharge. In either operating position, LIN is supplied from the bulk tank via the transfer line and U-tubes. When the detector is moved, smaller (125 L) LIN dewars ride along to maintain flow to the shield and intercepts.

CHAPTER VII: DC CIRCUIT, POWER SUPPLY, BUS CONDUCTOR AND DUMP RESISTORS

DC Circuit

The proposed DC circuit is given in Fig. VII(1). The circuit provides two discharge modes; a slow dump (switch S1 closed) that will cause sufficiently small eddy current heating that the coil will not quench and a fast dump (switch S2 open) for use when the coil has quenched or in other cases where the magnet must be discharged quickly to prevent damage to the system. The fast dump mode will cause eddy current heating and the coil will quench if it has not done so already.

The components of the DC circuit are described below. The power supply control and interlock system is discussed in Chapter VIII.

Prime Mover

The prime mover is a current/voltage controlled power supply. It will be rated for 5000 A continuous service, at approximately 20 V and 100 kW. The specified current regulation should be $\pm$ 0.1% at full current. The prime mover would be purchased from a commercial source and is expected to be approximately 48" (1.2 m) x 48" (1.2 m) x 72" (1.8 m) high and weigh 4000 lbs (1818 kg). It will be located on the mezzanine of the Assembly Hall.

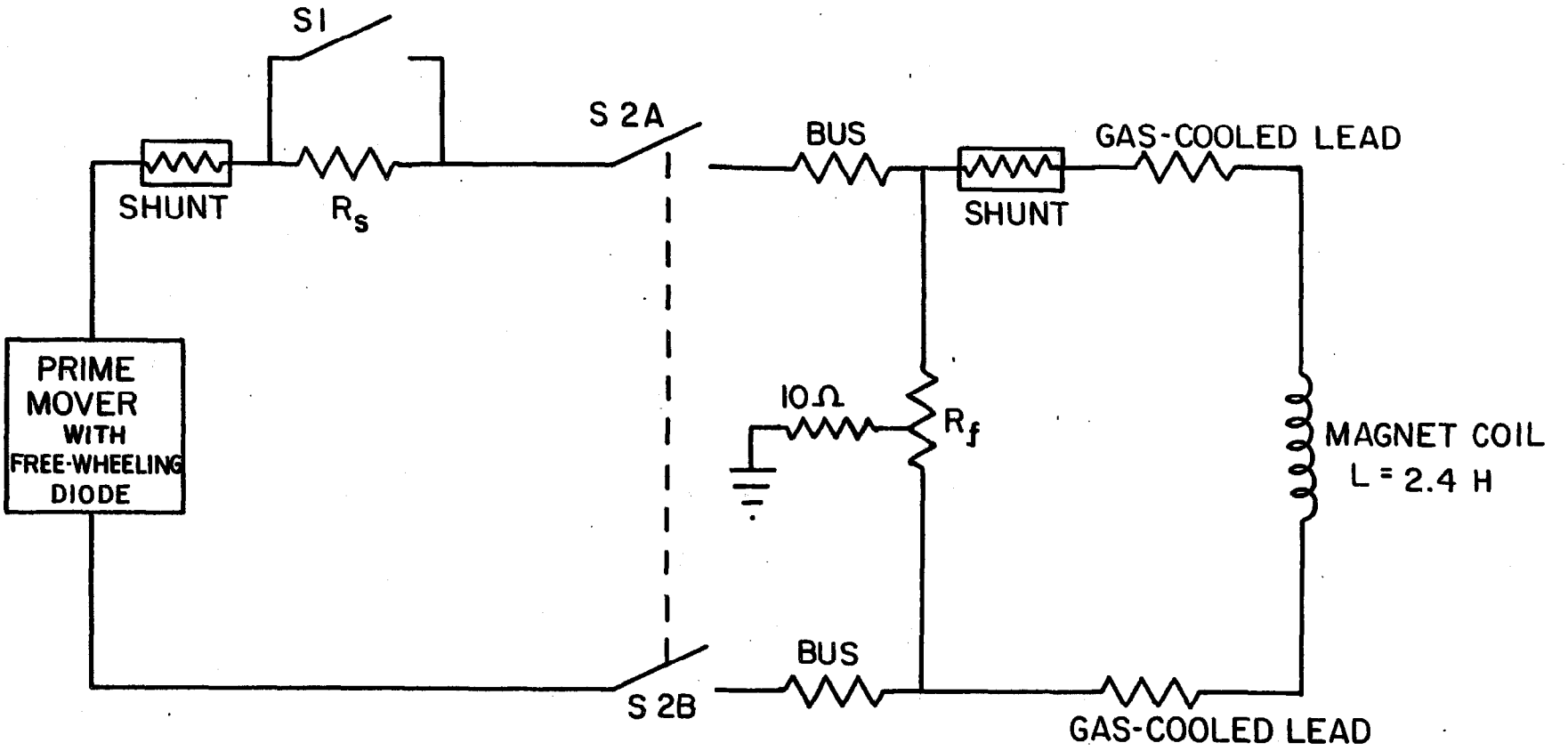

Fig. VII(1). DC circuit

Total power to Collision Hall and return	6.2 kW 21300 BTU/hr	5.75 kW 19800 BTU/hr
Water required at $\Delta T = 50^{\circ}F$	57 gal/hr (3.5 L/min)	53 gal/hr (3.3 L/min)

Fast Dump Resistor

This dump resistor (R_f) is connected across the coil terminals at all times. Present plans locate the resistor on the east side of the magnet so that the bus to the magnet leads is short and therefore reliable. The resistor we propose to use is similar to that used by the Energy Saver and will be procured from the same vendor. It is of an "adiabatic" type, i.e. no heat is dissipated to any great extent during magnet discharge and the final resistor temperature is determined by the energy and resistor mass. Following the heat pulse the resistor cools to ambient temperature by natural convection. The parameters of the dump resistor are:

Energy	=	30 MJ
Resistance	=	72 mΩ at $20^{\circ}C$
Final temperature	=	$232^{\circ}C$ ($450^{\circ}F$)
Cooldown time or time between coil discharge pulses	=	10 min.

The resistance element will be made of 70% Ni - 30% Fe alloy known as "Balco" which has a high temperature coefficient of resistance. This will cause the resistance to increase from 72 mΩ at $20^{\circ}C$ to

Bus Circuit

The DC circuit consists of water cooled bus conductor with flexible connecting cables at each end.

The water-cooled bus runs to both magnet operating locations. The one-way distance to the Collision Hall location is about 90 ft (27.4 m) and to the Assembly Hall location, about 45 ft (13.7 m). The bus is sized to reduce the voltage drop and power. Two strands of either (1) original CCM copper conductor, 2" (50.8 mm) square x 1.125" (28.6 mm) hole diameter or (2) aluminum conductor, 2.42" (61.5 mm) square x 0.55" (14 mm) hole diameter are required. Since adequate amounts of both these conductors already exist at Fermilab, the choice will be made on the basis of ease of installation. The bus parameters are given in the table below. The bus conductors will be insulated with epoxy glass tape to provide a moisture barrier and personnel safety.

Bus Conductor Parameters

Material	Copper	Aluminum
Number of bars	2	2
Size	2" sq x 1.125" ϕ	2.42" sq x 0.55"ϕ
Resistance length at 100°F	4.5 $\mu\Omega$/m	4.2 $\mu\Omega$/m
Resistance to Collision Hall and return	0.25 mΩ	0.23 mΩ
Total voltage drop to Collision Hall and return	1.24 V	1.15 V

about 144 mΩ at 220°C during the discharge and will tend to maintain the terminal voltage constant, thus reducing the discharge time as compared to a constant resistance. The resistivity of Balco as a funtion of temperature is given in Fig. VII(2).

The resistor box will have dimensions 25" (0.6 m) x 96" (2.4 m) x 40" (1 m) high and will weigh about 1500 lbs (680 kg).

Slow Dump Resistor

The resistance (R_s) of the slow dump resistor is chosen so that the maximum eddy current heating during a slow discharge is equal to that during the constant voltage portion of the nominal 10 minute charge, approximately 100 W. The slow discharge time constant, τ_s, is therefore 600 seconds and the total resistance of the discharge circuit is 4 mΩ. A simple series-parallel resistance calculation shows that R_s = 4 mΩ. The slow dump resistor should probably be specified for 5000 A steady-state operation (100 kW). It will be located near the prime mover.

5000 A Switches

Switches S1 and S2 are either mechanical or SCR types. Neither switch has to break 5000 A, since both are shunted by resistors.

Magnet Charge Time

With the circuit parameters given in Fig. VII(1), the power supply set for 20 V and 5000 A, and the switch S2 closed at t=0, various currents and voltages are given as a function of time in Fig. VII(3) for a 10 min charge. Under these conditions the

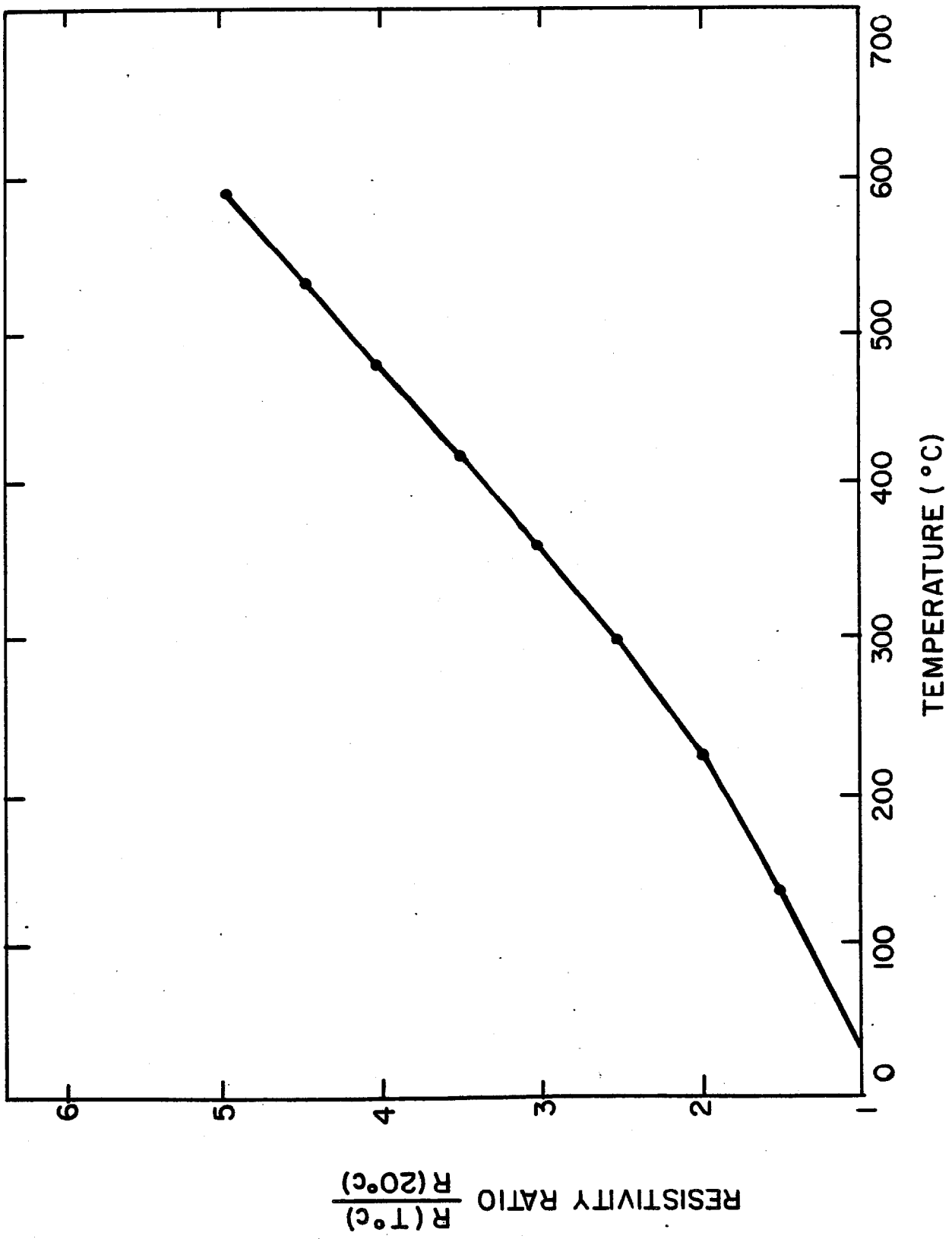

Fig. VII(2). Resistivity of Balco (70% Ni/30% Fe) vs. temperature

constant voltage to constant current transition occurs at t = 568 seconds. A magnet current of 4995 A is reached in 700 sec (11.7 min). A current of 3500 A can be reached in 420 seconds with a 20 V constant voltage charge.

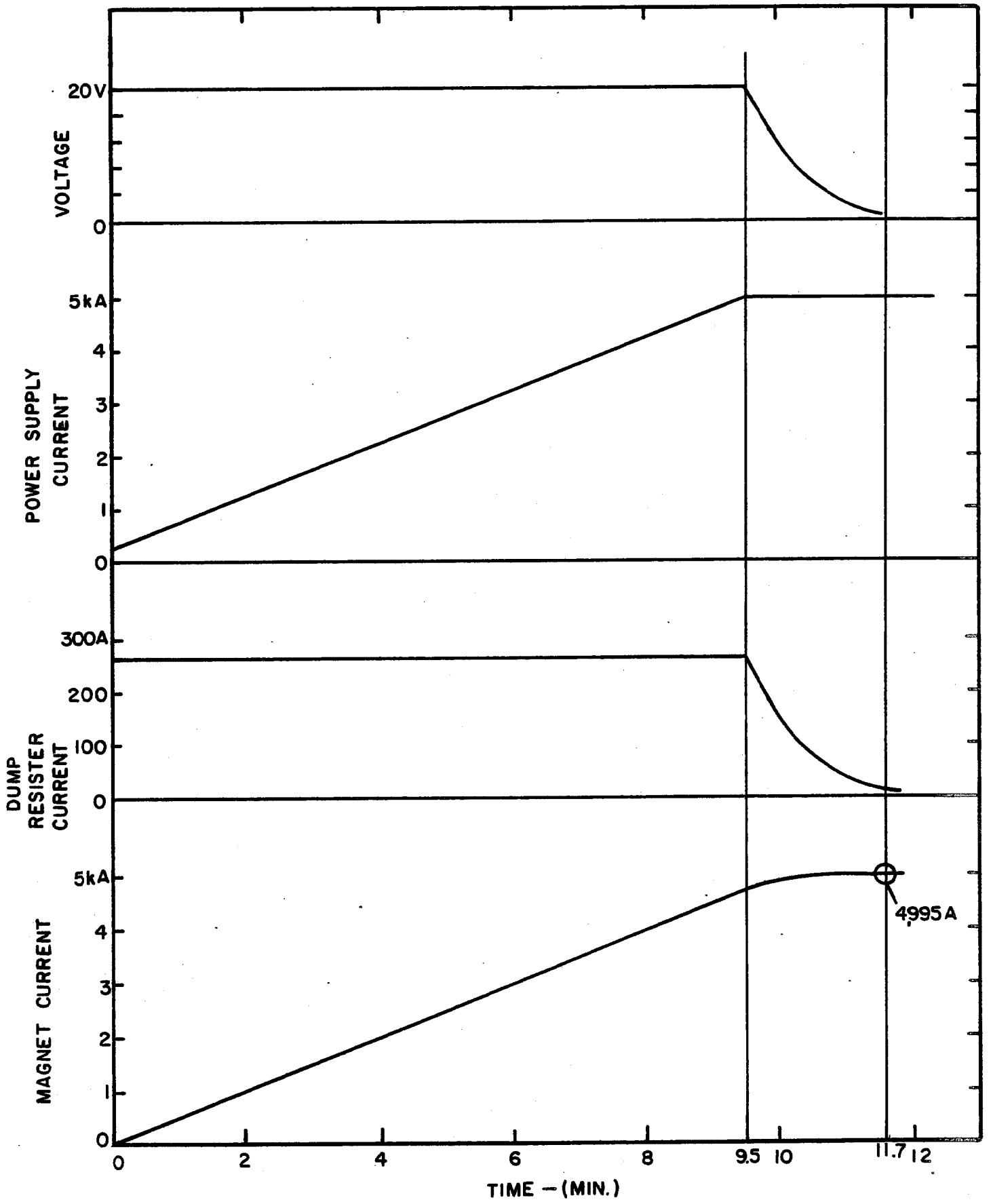

Fig. VII(3) Charging of CDF solenoid

CHAPTER VIII: INSTRUMENTATION AND CONTROLS

Magnet and Refrigerator Instrumentation

A variety of instrumentation is necessary to provide the following five basic functions:

1. Monitor the magnet, refrigerator and other cryogenic systems during cooldown.
2. Monitor the steady state electrical and cryogenic performance of the magnet and its subsystems during normal operation.
3. Provide feedback information for the control of the magnet refrigerator and cryogenic systems.
4. Provide information for the magnet safety and interlock system (e.g. quench detection, current lead gas flow, cryostat vacuum etc.).
5. Provide information for initial magnet testing and if necessary diagnose to the origins of any coil faults.

A variety of devices will be used to provide these functions. Primarily they consist of devices to measure voltage, current, strain, pressure and temperature at strategic points in either the coil proper or its associate subsystems. A substantial portion of the instrumentation listed below is intended for use during the initial testing and debugging period of the magnet, and therefore only a smaller subset is required for normal operation.

Voltage Taps. A total of three taps will be used for each current lead. They will be located at the top and bottom of the gas cooled lead and at the bus bar/superconductor joint located just below the control dewar. In addition, five more voltage taps

will be installed at regular intervals along the coil. These taps will be used to study the magnetic quench behavior and if necessary to locate faults. One of these five will serve as the coil center tap and will be used to detect quenches by looking for voltage imbalances between the two coil halves. In addition, voltage taps will be located to measure the voltage drop across the bus work, shunt (to determine the current) and power supply.

Thermometry. Temperatures will be measured using carbon resistors (4 - 80 K), platinum resistors (80 - 300 K) and vapor pressure thermometers (VPT) as sensors. These choices are dictated by the desire to use existing hardware and software developed by the Accelerator Division for ES/D Satellite Refrigerators to read and calibrate these sensors. This control system will be explained in detail in the following section. The control module designed to read carbon and platinum resistor values and convert these to temperatures has a total of 48 available channels. Table VIII(1) lists our assignment of these channels. VPT outputs are converted to voltages which are read out via the control system analog to digital (A/D) converters. These assignments are given in Table VIII(2).

In general the temperature sensors are located so that the following temperatures can be measured:

1. The temperature of the He stream at various points as it circulates through the refrigerator, the coil cooling loop and the 4 K support intercepts. Of particular interest is the ability to detect "hot spots" in the coil or outer support cylinder which might prevent the magnet

TABLE VIII(1)
CDF REFRIGERATOR & MAGNET TEMPERATURE MONITORING CHANNELS
Platinum (TP) & Carbon (TR) Resistors Only
(48 available)

NAME	DESCRIPTION
0	TR 1 - Wet Engine Input Temperature (in valve box)
1	TP 20 - EX 1 Nitrogen Return
2	TP 16 - Storage Dewar Temperature
3	TR 17 - Control Dewar Inlet Temperature
4	TR 18 - HX5 Outlet Temperature
5	TR 19 - Chimney Supply Temperature
6	TR 30 - Magnet Inlet Temperature
7	TR 31 - Magnet Return Temperature
8	TR 23 - Transfer Line Return Temperature
9	TR 24 - Storage Dewar Return Temperature
10	TP 31 - Magnet Return Temperature
11	TP 32 - Outer Support Cylinder Temperature
12	TR 32 - Outer Support Cylinder Temperature
13	TR 33 - Axial Support #1 - Support Bracket
14	TR 34 - Axial Support #1 - Outer Support Cylinder
15	TR 35 - Axial Support #2 - Support Bracket
16	TR 36 - Axial Support #2 - Outer Support Cylinder
17	TR 37 - Radial Support #1 - Support Bracket
18	TR 38 - Radial Support #1 - Outer Support Cylinder
19	TR 39 - Radial Support #2 - Support Bracket
20	TR 40 - Radial Support #2 - Outer Support Cylinder
21	TR 41 - Radial Support #3 - Support Bracket

TR 42 - Radial Support #3 - Outer Support Cylinder

TR 43 - Radial Support #4 - Support Bracket

TR 44 - Radial Support #4 - Outer Support Cylinder

TP 51 - Inner Radiation Shield #1

TP 52 - Inner Radiation Shield #2

TP 53 - Outer Radiation Shield #1

TP 54 - Outer Radiation Shield #2

TP 55 - End Radiation Shield #1

TP 56 - End Radiation Shield #2

TP 57 - LIN Shield Supply Temperature

TP 58 - LIN Intercept Supply Temperature

TP 59 - LIN Shield Return Temperature

TP 60 - LIN Intercept Return Temperature

TP 61 - Radial Intercept #1

TP 62 - Radial Intercept #2

TP 63 - Radial Intercept #3

TP 64 - Radial Intercept #4

TP 65 - Axial Intercept #1

TP 66 - Axial Intercept #2

TABLE VIII(2)
CDF REFRIGERATOR A/D CHANNEL ASSIGNMENTS
(64 available)

	NAME	DESCRIPTION
0	EVX1	EX#1 Helium Valve
1	EVX2	EX#2 Helium Valve
2	EVLN	EX#1 Nitrogen Valve
3	EVLH	Central Helium Liquefier Valve
4	EVJT	Cold Box JT Valve
5	EVBY	Cold Box Bypass Valve
6*	EVBP	Storage Dewar Back Pressure
7*	EVCP	Control Dewar Pressure
8*	EVNX	Nitrogen Shield
9*	EVNI	Nitrogen Intercept
10*	EVCV	Cooldown Valve
11*	EVMF	Magnet Flow Regulator
12	_____	_____
13	_____	_____
14*	PI1	Nitrogen Supply Tank Pressure
15*	LL1	LIN Tank Liquid Level
16	TI3	EX#2 Shell Temperature
17	TI4	EX#1 Output Temperature
18	TI5	EX#3 Return Temperature
19	TI6	EX#3 Supply Temperature
20	TI7	EX#4 Return Temperature
21	TI8	EX#4 Supply Temperature

*New or redefined

22 TI9 - Dry Engine Output Temperature

23 TI11 - Cold Box Return Temperature

24 TI12 - Wet Engine Input Temperature

25 PI20 - EX#1 Nitrogen Pressure

26 PI6 - EX#3 Supply Pressure

27 PI8 - EX#4 Supply Pressure

28 PI12 - Wet Engine Supply Pressure

29 LL20 - EX 1 Nitrogen Liquid Level

30 _____

31 _____

32 SPDE - Dry Engine Speed

33 PWDE - Dry Engine Power

34 SPWE - Wet Engine Speed

35 PWWE - Wet Engine Power

36 PI11 - Cold Box Return Pressure

37* TI13 - Wet Engine Output Temperature

38* PI13 - Wet Engine Output Pressure

39* PI16 - Storage Dewar Pressure

40* LL16 - Storage Dewar Liquid Level

41* FI16 - Magnet Flow Indicator

42* TI17 - Control Dewar Inlet Temperature

43* PI17 - Control Dewar Inlet Pressure

44* PI19 - Chimney Supply Pressure

45* PI22 - Control Dewar Pressure

46* LI22 - Control Dewar Liquid Level

47* FI21 - Current Lead Flow #1

48* FI22 - Current Lead Flow #2

49 FI4 - Total Bldg Helium Gas Input Flow

50 TSV - Transducer Supply Voltage

51 ASV - Actuator Supply Voltage

52 _____

53 _____

54 _____

55 _____

56 _____

57 _____

58 _____

59 _____

60 _____

61 _____

62 _____

63 _____

from operating at full current or which might make it more likely to quench. In addition a few of these sensors are used to control the refrigerator.

2. The temperatures in the two LN_2 cooling loops are monitored. Here the desire is to insure that the coil supports are effectively being intercepted by LN_2 and that the coil radiation shields are near 80 K.

Strain Guages. Strain guages will be located on some of the radial and axial supports to measure the total forces acting on the coil. In addition it may be desirable to locate strain guages either on the outer support cylinder or the bolts on the thrust ring to monitor the coil axial preload. These strain guages will be read out via a special purpose module included as part of the power supply package.

Quench Monitors. In addition to the voltage taps mentioned above several other devices will be installed to detect and induce quenches in the coil. These devices will be used both during the initial testing of the coil (to measure its quench behavior) and later as part of the coil safety system. These devices are still under review but the following represents one suggested set:

1. Two heater type quench starters on the outer support cylinder, one at center and another at one end of the coil.

2. A pick up coil wound on the outside surface of the coil for detecting the start of a quench.

3. Small inductive coils embedded either in slots milled into the outside surface of the support cylinder or at the spacer locations for conductor joints. They would be arranged in pairs on the same turn, about 1/2 m apart and at 5 different positions along the coil axially so that both the axial and circumferential velocities of propagation of quench can be measured. If this scheme is

adopted, the voltage taps for doing the coil for performing the same function could be eliminated.

Power Supply Instrumentation Package

In addition to the prime mover with its current and voltage regulation circuitry the magnet power supply package will contain a variety of other electronics whose purpose is to detect unsafe operating conditions and take appropriate action to protect the magnet from damage.

Quench Detector. The power supply package will contain circuitry that will be able to detect whether a portion of the superconducting winding has gone "normal". This will be done by looking for small voltage changes across the coil and by monitoring the "difference voltage" between each lead and the coil center tap. These signals will be sent to an integrating amplifier with a time constant of about one second. If a quench is detected then a "fast dump" sequence will be initiated to discharge the magnet into the 72 mΩ dump resistor. A great deal of care is required in the design of this system since we need to detect quenches reliably but must also avoid the initiation of a fast dump because of electrical "noise" or other spurious signals.

Interlock Systems. The magnet has an extensive protection system. Various sensors monitor important system parameters and can initiate a discharge if an unacceptable value is detected. Depending on the fault detected or the value of the measured parameter either a fast or a slow discharge will occur. A fast

discharge can be initiated at any time even while a slow discharge is in progress. It may be possible to recover quickly from a slow discharge, however a fast discharge sequence will quench the coil and recovery will not be possible until after the magnet is fully discharged and recooled to operating temperature.

The magnet will fast discharge if any of the following conditions occur:

1. Quench detected.
2. Excessive ground current.
3. Excessive lead voltage.
4. Excessive voltage drop across bus work.
5. AC LINE voltage to supply interrupted.

A slow discharge will be initiated by the following:

1. Excessive operating current.
2. Excessive ground current.
3. LHe probe in control dewar reads low.
4. LHe probe in storage dewar reads low.
5. LHe supply temperature is high.
6. LHe intercept temperature is high.
7. Excessive pressure in control dewar.
8. Insulating vacuum failure.
9. Power supply over heats.

It will not be possible to turn the magnet on unless the following interlocks are satisfied:

1. Both end plugs properly in place (microswitches).

2. Dump resistor temperature less than 35°C.

3. Doors on the power supply and switch gear closed for personnel safety.

Control System

The CDF solenoid refrigerator and power supply package will be controlled by a modified version of hardware and software developed for the Energy Saver/Doubler*. A block diagram of this system is shown in Fig. VIII(1) and of the refrigerator multibus crate in Fig. VIII(2). A Z80 microprocessor located in a multibus crate controls refrigerator feedback loops locally. Input to these loops is received via two 32 channel analog to digital converter modules and a 48 channel thermometry module located in the multibus crate. Output is via four digital to analog converters (engine speed control) and two 8 channel valve actuator modules. In addition the multibus crate contains a digital I/O module to monitor up to 40 status bits and output up to 24 control bits. The Z80 software is contained in PROM and RAM. The code resident in RAM will be "down loaded" from the accelerator control system higher level computers, (VAX 11/780's). After the software is loaded, the Z80 is able to function by itself without continuous intervention from the main computer system.

*J.C. Gannon, Computer Operated Control System for the Energy Saver Satellite Refrigerators, Fermilab TM-1024 (1981).

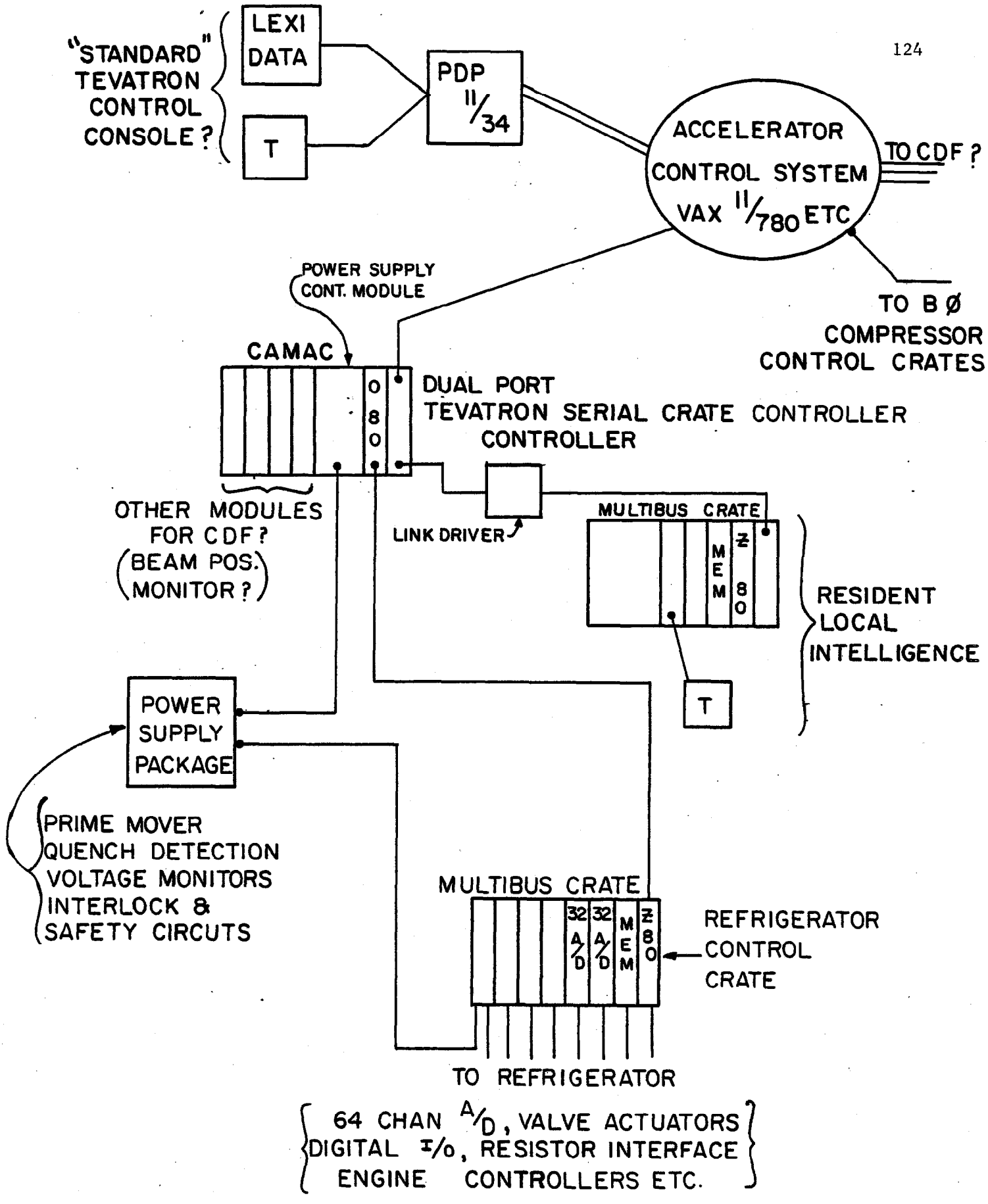

Fig. VIII(1). CDF control system block diagram

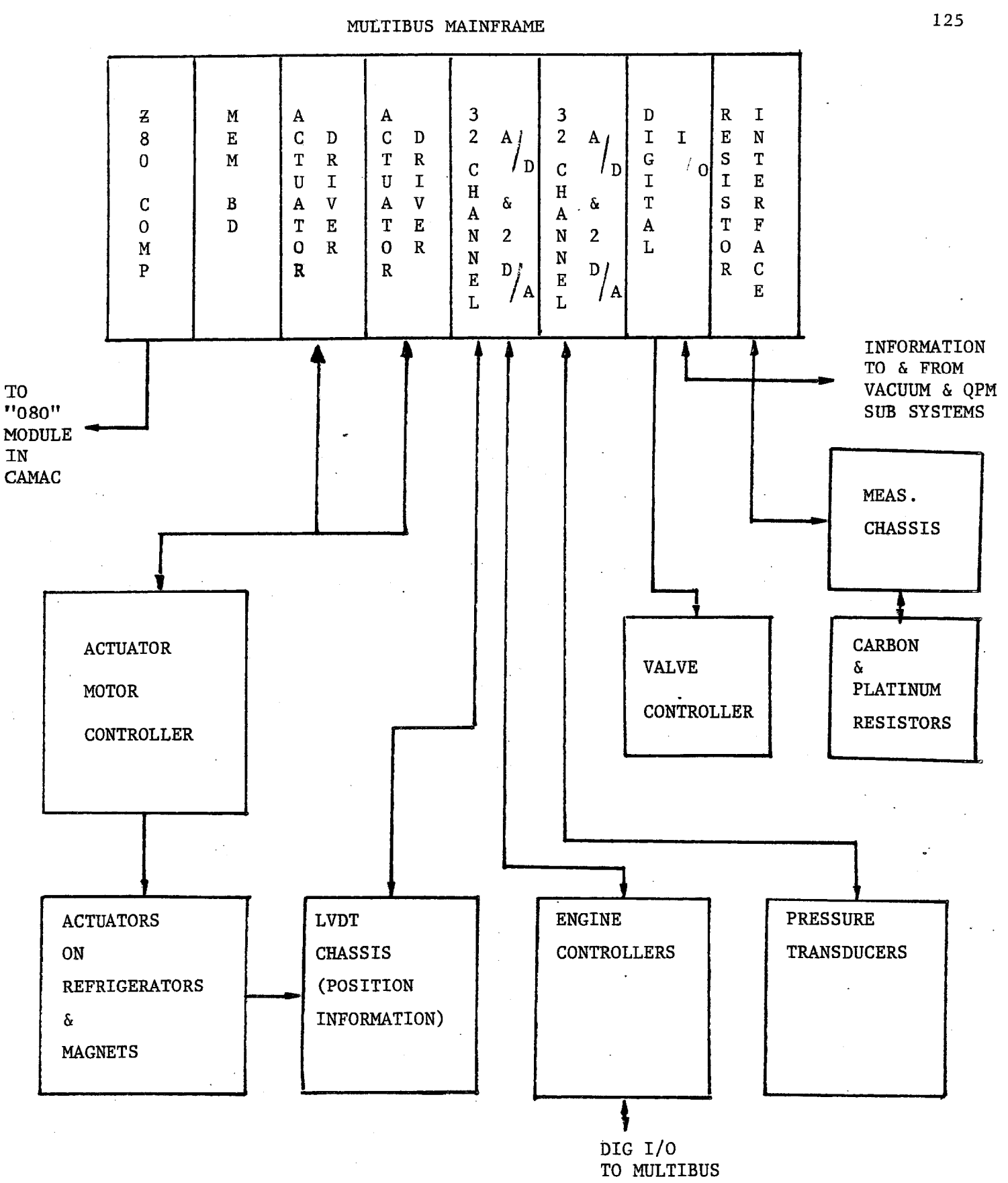

REFRIGERATOR CONTROL SYSTEM
BLOCK DIAGRAM
Fig. VIII(2)

Communication with the Z80 is via an 0-8Ø module residing in a CAMAC crate connected to the accelerator system via a serial link. The control module for the power supply will reside in this same CAMAC crate. The connection to the accelerator control system is then made via a dual port Tevatron Serial Crate Controller (TSCC). The other port of this controller is connected to another small Z80 system and terminal called the "resident local intelligence" (RLI). This small system allows the user to control the refrigerator even if the accelerator control system is unavailable (i.e. system fault or maintenance period). In normal operation all control changes, alarms and monitoring, data logging and graphics will be done using the accelerator control system. The refrigerator and power supply will not be able to be controlled remotely from any other accelerator control console.

CHAPTER IX: TESTING

There will be two major tests of the solenoid before its acceptance by Fermilab. The first test will take place at the manufacturing company (Hitachi, Ltd, Japan) and will consist of a full cryogenic test of the coil done with Hitachi's test refrigeration system and a low current test of the coil. Specifically, the goals of this test are:

1. To verify that there are no mechanical problems associated with the cooldown of the coil.
2. To check the proper performance of all instrumentation installed in the magnet.
3. To show that the magnet heat load is acceptable.
4. To verify that there are no breaks or "normal" regions in the superconducting winding.
5. To demonstrate that no eddy current associated problems exist. This will be done by ramping the magnet power supply up and down.
6. To verify proper operation of the magnet safety circuits.
7. To study quench behavior during induced quenches.
8. To verify the stable operation of the coil. The coil will be operated for about 24 hours without interruption for this test.

When this test is complete the coil will be shipped to Fermilab, installed in the steel yoke and the final acceptance tests performed. This acceptance test will repeat those tests done at Hitachi. In addition the coil will be excited to the

guaranteed current (4.5 kA) and long term stability tests of the coil and refrigeration system will be conducted. When these tests are completed the coil will be excited to the design current (5 kA). The coil must not be damaged by a quench at this current.

Before attempting these two major tests several subsystems will be tested independently:

1. The refrigerator and transfer lines will be tested with a dummy load.

2. The chimney and control dewar will be tested at Hitachi. For this test the power lines and LHe and LN_2 lines will be temporarily shorted at the bottom of the chimney and a heater installed to simulate the magnet load. The system will be cooled with a refrigerator and tested for 24 hours at 110% of the maximum magnet operating current. In addition the leads should be tested at 1 KV for 10 minutes and the system pressurized to verify proper operation of reliefs.

3. The power supply and safety circuits will be thoroughly tested before being connected to the magnet.

4. The refrigerator and magnet control system hardware and software will be carefully tested and debugged before the tests.

In addition to these planned tests, whatever additional tests are required by the Fermilab or DOE safety committee will be performed at Hitach, Ltd or at Fermilab before the magnet is commissioned.

ACKNOWLEDGEMENTS

We wish to thank A.V. Tollestrup, R.F. Schwitters, D. Theriot and the members of the Collider Detector Department for the stimulating discussions which helped us to clarify the solenoid design. We want to acknowledge the contributions of Mike Mruzek and John Rauch to the mechanical design. Ray Carra and Phil Calahan are thanked for their drafting assistance. We thank Terry Gutierrez for word processing this document and making the innumerable revisions.

We would also like to thank Drs. H. Hirabayashi, K. Morimoto, T. Tominaka, M. Wake and A. Yamamoto for their valuable contributions to the R&D solenoid. We also would like to thank Profs. K. Kikuchi, E. Matsuura, T. Nishikawa and S. Ozaki for their support and encouragement for this project.

APPENDIX A: SYSTEM PARAMETERS

General

Overall inner diameter:	2858 mm (112.5")
Overall outer diameter:	3353 mm (132")
Overall length (nominal):	5067 mm (199.5")
Design central field:	1.5 T
Guaranteed central field:	1.35 T
Approximate weight of cryostat:	11,100 kg (24500 lb)

Coil

Inner diameter (cold):	2965 mm (116.75")
Mean diameter of conductor (cold):	2975 mm (117.05")
Circumference of support cylinder (warm):	9575 mm (376.99")
Winding length (cold):	4794 mm (188.75")
Linear current density: (required)	1200 A/mm for 1.5 T
Design operating current:	5000 A
Guaranteed operating current:	4500 A
Winding scheme:	Single layer helix
Number of turns:	1150
Inductance:	2.4 H
Stored energy:	30×10^6 J at 1.5 T
Charge time:	10 - 20 min

Coil discharge

Time constant:	10-30 sec
Dump resistor:	72 mΩ at 20°C
Max. discharge voltage:	360 V

Conductor

General:	Cu/NbTi coextruded with high purity aluminum stabilizer
Overall dimensions:	3.89 mm x 20 mm .153 in x .7874 in
Al:Cu:Nb-Ti area ratios:	21:1:1
Peak field at conductor:	1.5 T
Bare conductor current density:	6427 A/cm^2 at 5000 A
Total weight:	2994 kg (6586 lbs)
Total length:	11.2 km (36800 ft)

Cu/NbTi Components

Alloy:	Nb 46.5 a/o Ti
Matrix:	copper ASTM B170-1; CDA 101
Bare width:	3.85 mm
Bare thickness:	1.8 mm
Short sample current:	10.4 kA at 1.5 T, 4.2 K
NbTi short sample current density:	2.64×10^9 A/m^2 at 2 T and 4.2 K
Filament diameter:	50 μm

No. filaments:	1700
Twist pitch:	25 mm

Aluminum Stabilizer

Alloy:	99.99 + %
Residual resistivity ratio:	$\geq$ 1000

Electrical Insulation (not completely specified)

Coil to support cylinder:	epoxy-polyester
Turn to turn:	Half lapped Kapton film

Forces Acting on Coil

Total compressive axial force at midplane:	0.95 MN (2.1×10^5 lbf)
Axial decentering force:	17.6 MN/m (10.1×10^4 lbf/in)
Max. radial decentering force:	12.3 MN/m (7.0×10^4 lbf/in)

Vacuum Vessel

Inner vacuum shell material/ OD/thickness	5083 aluminum/ 2870 mm (113.0")/ 6.4 mm (0.25")
Outer vacuum shell material/ OD/thickness:	5083 aluminum/ 3353 mm (132")/ 19.0 mm (0.75")

Radiation Shields

Inner radiation shield material/thickness:	6061-T6 aluminum/ 2 mm (0.078")
Outer radiation shield material/thickness:	6061-T6 aluminum/ 2 mm (0.078")
Outer Support Cylinder Material/ OD/thickness:	5083-0 aluminum/ 3048 mm (120")/ 16.0 mm (0.630")

Thermal Insulation Vacuum Plus Multilayer Insulation

Between 4.2 and 77 K:	Aluminum tape 3M#425 $\sim$12 layers NRC-2 (500 Angstrom)
Between 77 and 300 K:	$\sim$30 layers NRC-2 (300 Angstrom)

Liquid Nitrogen Cryogenics

Cooling mode:	Forced flow
Liquid reservoir:	$8 m^3$ $\sim$ 2000 gal
Steady state heat load:	600 W (est.)

Liquid Helium Cryogenics/Refrigeration

Coil cooling mode:	Forced flow LHe 10-20 g/s at 1.2 atm
Liquid temperature:	4.4 K
Steady state heat load:	40 W + 14 L/h
Inlet quality:	80-85%
Outlet quality:	70-75%
Steady state pressure drop across magnet at 4.4 K (approximately)	1.03 psi (0.07 atm) at 10 g/s

Length of cooling loop on magnet:	∿ 140 m
Diameter:	20 mm ID
Liquid capacity of cooling loop:	45 L
Liquid capacity of control dewar:	35 L
Storage dewar capacity:	2000 L
Cold mass (magnet):	5568 kg (12250 lb)
Cooldown time:	300 K to 80 K ≤ ∿ 6 days 80 K to 4.2 K ≤ 2 days

THICKNESS

ITEM	MATERIAL	INCHES	CM	RADIATION LENGTH	ABSORPTION LENGTHS
Inner vacuum shell	Aluminum	0.250	0.64	0.071	0.0170
Inner shield	Aluminum	0.080	0.20	0.022	0.0053
Conductor	Aluminum Copper NbTi	0.787	2.0	0.312	0.0605
Coil insulation	Epoxy/fiberglass, etc.	0.080	0.20	0.011	0.004
Outer support cylinder	Aluminum	0.629	1.6	0.179	0.0430
Outer shield	Aluminum	0.080	0.20	0.022	0.0053
Outer vacuum shell	Aluminum	0.750	1.90	0.214	0.0512
TOTALS				0.831*	0.186

(λ_R = 8.9 cm) (λ_a = 37.2) for Aluminum

(λ_R = 1.6 cm) (λ_a = 15.0 cm) for Cu/NbTi

(λ_R = 18 cm) ($\lambda_a \sim 45$) for G-10

* Particles passing through 20 mm of cooling tube will pass through an additional thickness $\gtrsim 0.07\ \lambda_R \lesssim 3\%$ of all particles will do so (24 paths).

MATERIAL	Specific Gravity	Young's Modulus of Elasticity E at 4.2 K 10^6 psi	E at 77 K 10^6 psi	E at 300 K 10^6 psi	Yield Strength at 4.2 K ksi	at 77 K ksi	at 300 K ksi	Code Allowable Stress ksi
Pure aluminum	2.65	---	---	---	---	6.5 (RRR = 1200)		---
Al 6061-T6	2.65	11.3	11.2	10.2	51.8	47.8	39.2	6.0 (welded)
Al 5083-0	2.65	11.7	11.6	10.4	25.0	23.0	21.0	10.0
Al 7075-T6	2.65	12.0	11.2	10.6	99.6	89.5	73.0	---
SS 304	8.9	30.5	31.1	28.9	70.0	60.0	35.0	18.8
Inconel 718	8.5	32.0	31.5	31.0	199.0	186.0	157.0	---
Ti(6Al4V)	4.5	19.1	17.2	15.7	278.0	229.0	138.0	---
Epoxy-Fiberglass Nema G-10	1.8	3.9 ‖ "CR"	3.7 ‖ "CR"	3.2 ‖ "CR"	---	---	---	---
Cu (OFHC)	8.9	21.5	20.0	17.2	13.1	12.8	10.9	6.7

MATERIAL	Radiation Length mm	$\frac{\Delta L}{L}\Big\|_{4.2\,K}^{300\,K}$	Electrical Resistivity at 4.2 K $\mu\Omega$-m	at 77 K $\mu\Omega$-m	at 300 K $\mu\Omega$-m	Integrated Thermal Conductivity $\int_{77}^{300K} k(T)dT$ W/cm	$\int_{4.2}^{77K} k(T)dT$ W/cm	$\int k(T)dT$ W/cm	Enthalpy $\Delta H_{4.2\,K}^{300\,K}$ J/g
Pure Aluminum	90.0	0.0043	0.000018	0.0020	0.025	---	---	---	170.4
Al 6061-T6	90.0	0.0042	0.014	0.017	0.039	---	---	---	170.4
Al 5083-0	90.0	0.0043	0.030	0.033	0.057	169.0	25.5	---	170.4
Al 7075-T6	90.0	0.0042	0.028	0.030	0.053	---	---	---	170.4
SS 304	17.3	0.00304	0.496	0.514	0.704	27.5	3.18	---	76.6
Inconel 718	---	0.0024	1.18	1.19	1.25	22.0	3.5	---	
Ti(6Al4V)	37.2	0.00154	1.47 at 20K	1.50	1.675	13.5	1.8	---	101.4
Nema G-10	180.0	0.0071 ⊥ 0.0025 ‖	Insulator	Insulator	Insulator	0.96 ⊥ 1.41 ‖	0.139 ⊥ 0.20 ‖	---	91.1
Cu (OFHC)	14.5	0.00325	0.00016	0.002	0.0156	934.0	586.0	---	79.6
Nb-Ti	16.0	---	---	---	---	---	---	---	80.3

REFERENCES:

1. Mech. Prop. of Structural Materials at Low Temperatures, R. Michael McClintock and Hugh P. Gibbons, NBS Monograph 13, June 1, 1960.
2. Handbook on Materials for Superconducting Machinery, James E. Campbell, Metals and Ceramics Information Center, Battelle-Columbus Laboratories, November 1974.
3. A Compedium of the Properties of Materials at Low Temperature (Phase I) Part II. Properties of Solids, Victor Johnson, General Editor, NBS, October 1960.
4. LNG Materials and Fluids, Douglas Mann, Louis Diller, Hassell Ledbetter, Cryogenics Division, Inst. for Basic Standards, NBS, First Edit. 1977.
5. Standard Handbook for Mechanical Engineers, Baumeister and Marks, Seventh Ed., McGraw Hill.
6. Lawrence Berkeley Lab., Engineering Note, Michael Green. Minimag Experiment, Large Superconducting Solenoid Magnet, Code AB0103, Serial M4835, March 21, 1975.
7. ASME Boiler and Pressure Vessel Code, Section VIII, Division 1

APPENDIX C: COMPUTER ANALYSIS OF QUENCHES

There is a possibility that an indirectly cooled solenoid will quench during operation due to malfunctioning of the cooling system and the power supply system. Therefore the solenoid should be designed to be completely safe from quenching. During design stage an extensive study was carried out on the quench behavior of the CDF solenoid in many different independent ways. All the results show that with the selection of optimized parameters the CDF solenoid can be designed and constructed quite safe from the effect of quenches.

The design parameters of the solenoid, namely the conductor dimensions and the resistance of the external dump resistor, were selected after many programs on quench were run.

In some cases quenches without a quench-back effect were studied.[1,2,3] But it was found out that the CDF solenoid even with a support cylinder of high resistance aluminum would quench-back after the start of a quench.[2,4] And the quenches with quench-back effect were analyzed.[5,6] In some cases the propagation of the normal zone is analyzed using a one-dimensional model.[1,5] In other cases it is treated in two-dimensional model.[2,3] In a simplified case an instantaneous quench is assumed at the beginning, and the subsequent conditions are analyzed.[6]

(1) Quench Calculation by One-dimensional Approximation

This method was developed originally for the one-meter R&D coil, successfully applied to interpret the detailed experimental data of voltage shapes, and applied to the CDF solenoid.[1,5] In this model the normal zone is assumed to propagate only along the conductor in the circumferential direction. The thermal propagation in the axial direction through the insulation layer is completely neglected. In the analysis the rate of heat transfer through thermal diffusion along the conductor is also neglected.

The voltage curves are fitted using the following approximate relation of thermal diffusion in one dimension

$$\frac{\Delta T}{\Delta t} = \frac{RI^2}{mAC} - \alpha (T - T_o)$$

where

T = temperature of the conductor

T_o = temperature of the materials which are in contact with the conductor, about 4.5 K,

R = resistance per unit length of the conductor

I = excitation current

m = average density of the conductor

A = cross sectional area of the conductor

C = average specific heat of the conductor

α = thermal diffusion rate out of the conductor

And the propagation speed U (m/s) of the normal zone was derived from the experimental data in the following form,

$$U\ (m/s) = 6.9 \times I\ (kA)^2$$

The detailed calculations applied to the CDF solenoid are summarized elsewhere.[1)]

In the modified version of this approximation, the quench-back effect is included in the calculations, by increasing the propagation velocity of the normal zone after the quench back and by defining T_o as the temperature of the support cylinder. Maximum voltages and temperatures are substantially reduced with the quench-back effect compared with those calculated without it.

The calculated quench results with the designed parameters are explained in Chapter III.

(2) Quench Calculation by Two-Dimensional-Approximations without Quench-Back Effects

As a comparison, quench simulations for the CDF solenoid with the design parameters were done using the standard Wilson's QUENCH program,[7)] and the Cornell's QUENCH program[8)] without quench-back effect. In these cases we assumed no quench-back effect, and there is no thermal nor electrical effect from the support cylinder.

The quench velocity U along the conductor is given by the initial propagation velocity U_o as follows

$$U(t) = U_o \frac{I(t)}{I_o}$$

Where $I(t)$ and I_o are the magnet current at t and t=o, respectively.

U_o is given by

$$U_o \simeq \frac{I_o}{AmC_p} \sqrt{\frac{LT_t}{T_t - T_o}}$$

where

A = Cross sectional area of the conductor (cm^2)

m = Average density of the conductor (g/cm^3)

C_p = Averaged specific heat of the conductor (J/g)

L = Lorentz number (= 2.45×10^{-8} $W\Omega/K^2$)

T_t = Transition temperature (K)

T_o = Operational temperature (K)

The transverse quench velocity U_t in the axial direction is given by

$$U_t(t) = \varepsilon\, U(t),$$

$$\varepsilon = \sqrt{k_L/k}$$

where k_L, and k are the averaged thermal conductivity in the axial direction and that in the conductor direction.

The calculated results are shown in Fig. C(1). The quench results by Cornell's program are shown by solid lines, and results by Wilson's program are indicated by dotted lines. Their differences are due to the different two-dimensional propagation mode of the normal zone.

(3) Quench Calculation by Two-Dimensional Approximation with Quench-Back Effect

When the start of a quench is detected, the power supply is turned off and the magnet current starts to flow through the external dump resistor R_1. The initial decay time constant of the

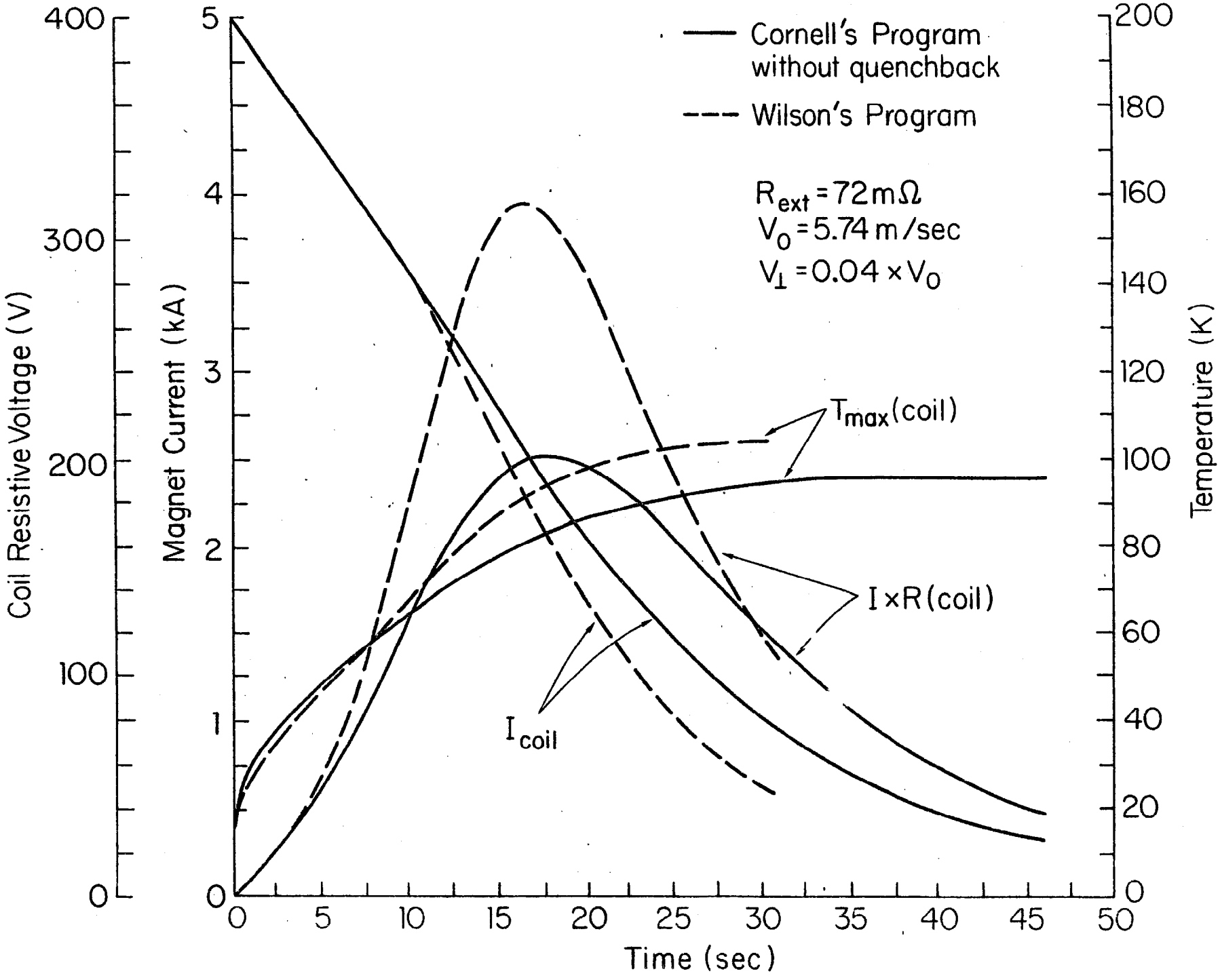

Fig. C(1). Quench behavior without quench back

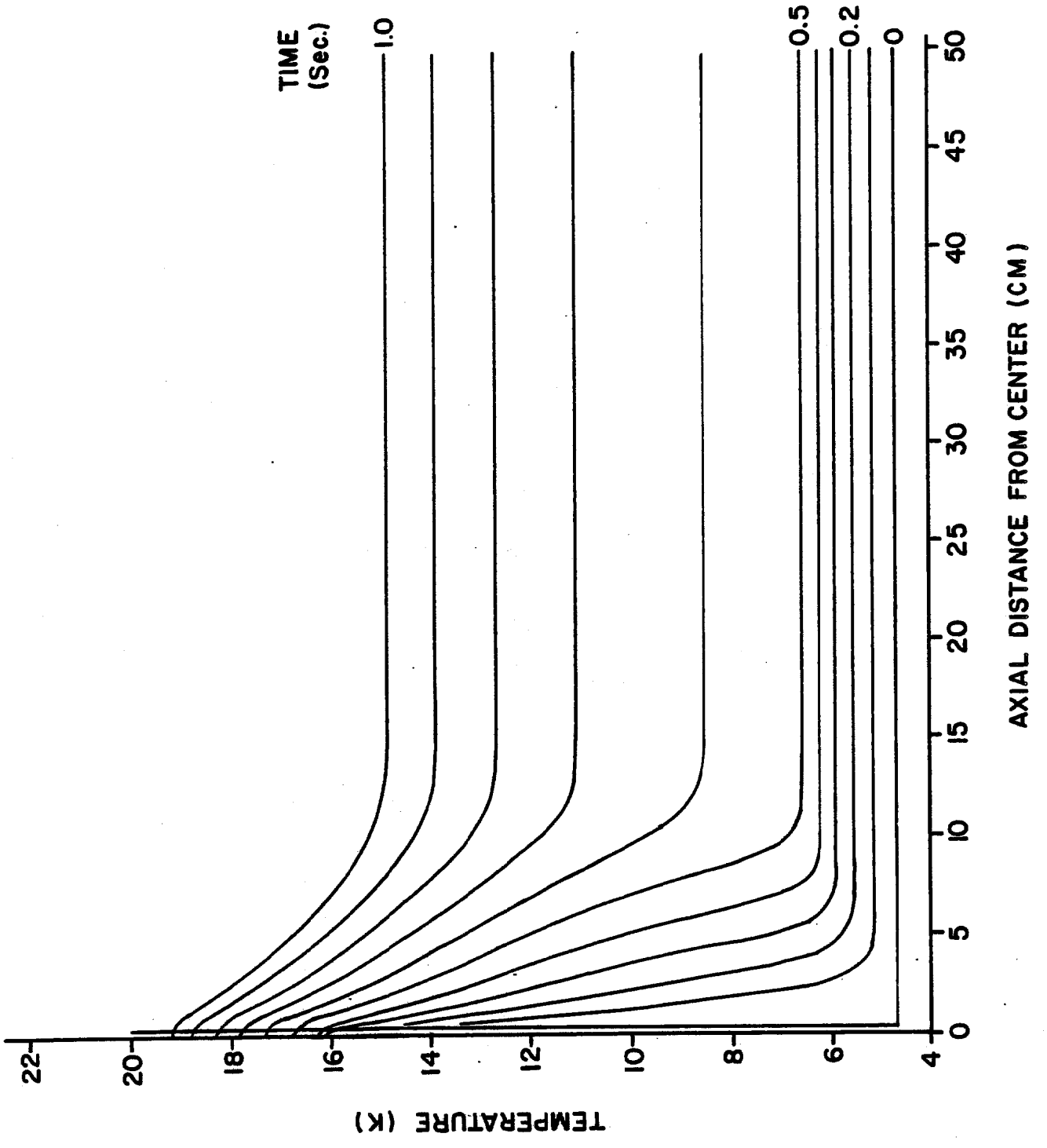

Fig. C(2). Temperature distribution with quench back effect

magnet current is determined by L_1/R_1, where L_1 is the inductance of the coil.

Then the eddy current is induced in the support cylinder, and effectively a part of the coil current is transfered into the cylinder. Therefore at the beginning of a quench (within a second) the current and voltage shapes of the coil are affected. In addition to the support cylinder, the aluminum cryostat cylinder, flanges of the cryostat, the aluminum end plates of the central tracking chamber and yoke iron, will also affect the current and voltage shapes of the coil.

Meanwhile the normal zone is propagating by itself. And the support cylinder is gradually warming up due to its eddy current and starts warming up the adjacent conductor. In one to two seconds after the start of the quench, the temperature of the conductor, including the aluminum stabilizer and the superconductor reaches near its transition temperature (about 8 K). Then the quench-back occurs over the whole conductor in a very short time (in less than 0.1 second). A computer simulation was done using a program called NOPRO, and its results are shown in Fig.C(2). The temperature variation around the origin is shown in the axial direction and in time. In this special case the quench back is observed to take place at 0.5 sec.

After the quench-back, the whole conductor is going to warm up uniformly by the Joule loss of the current in the aluminum. And the stored energy is dissipated uniformly over the whole conductor, as well as in the dump resistor.

Compared with the case without quench-back, a part of the stored energy is absorbed more or less uniformly over the whole conductor and the support cylinder. The localized maximum temperature rise around the origin of the quench is decreased. Since the resistance of the coil grows approximately uniformly over the entire coil, the coil voltage to ground is minimized with cancellation of resistive voltage by inductive voltage.

The coil is closely coupled with the support cylinder as shown in Fig. C(3), and they can be represented by the following equations:

$$L_1 \frac{dI_1}{dt} + M \frac{dI_2}{dt} + \left[R_1 + R_c(t)\right] I_1 = 0 \quad \text{----------(1)}$$

$$M \frac{dI_1}{dt} + L_2 \frac{dI_2}{dt} + R_2 I_2 = 0 \quad \text{----------(2)}$$

Fig. C(3) Coupling of Coil and Support Cylinder

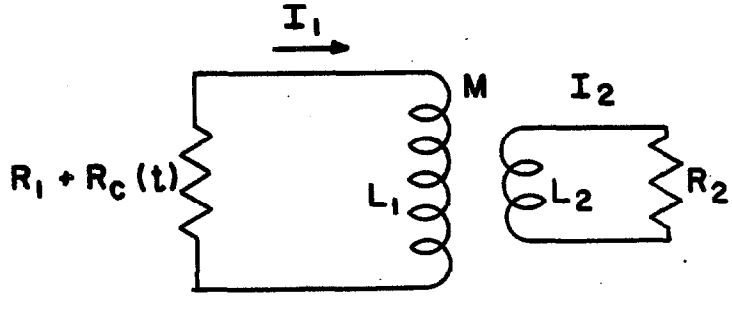

where L_1, L_2 and M are the self inductances of the coil and the support cylinder, and their mutual inductance. R_1, R_2 and R_c (t) are the resistance values of the external dump resistor, the support cylinder, and the normal zone developed in the coil, which will increase gradually at the beginning of the quench, jump up at the quench-back, and steadily increase until the current decays. I_1 and I_2 are the currents in the coil and the support cylinder.

The support cylinder is made of 1.6 cm thick high strength aluminum alloy A-5083. Its resistivity is high, 3.05×10^{-8} Ωm at liquid helium temperature and stays almost constant up to the room temperature. The inductance and resistance of the cylinder are $L_2 = 1.8 \times 10^{-6}$ H and $R_2 = 3.6 \times 10^{-6}$ Ω. Therefore its time constant $\tau_2 = L_2/R_2 = 0.50$ sec.

The ratio of ampere-turn in the support cylinder and that in the coil is determined by the ratio of decay time constants in these systems. As the initial decay time constant of the coil $\tau_1 = L_1/R_1 = 2.48/0.072 = 34$ sec, and $\tau_2 = 0.50$ sec, there will be about 1.5% current transfer from the coil to the support cylinder at the beginning of the quench. This ratio changes as the resistances of the coil and the cylinder change during the development of the quench.

The quench behavior of the CDF solenoid with the design parameters is simulated by the quench program with quench-back effect, which was originally developed at Cornell[8] and modified at KEK. The results are shown in Fig. C(4), where the current and the maximum temperature of the conductor, the resistive voltage of

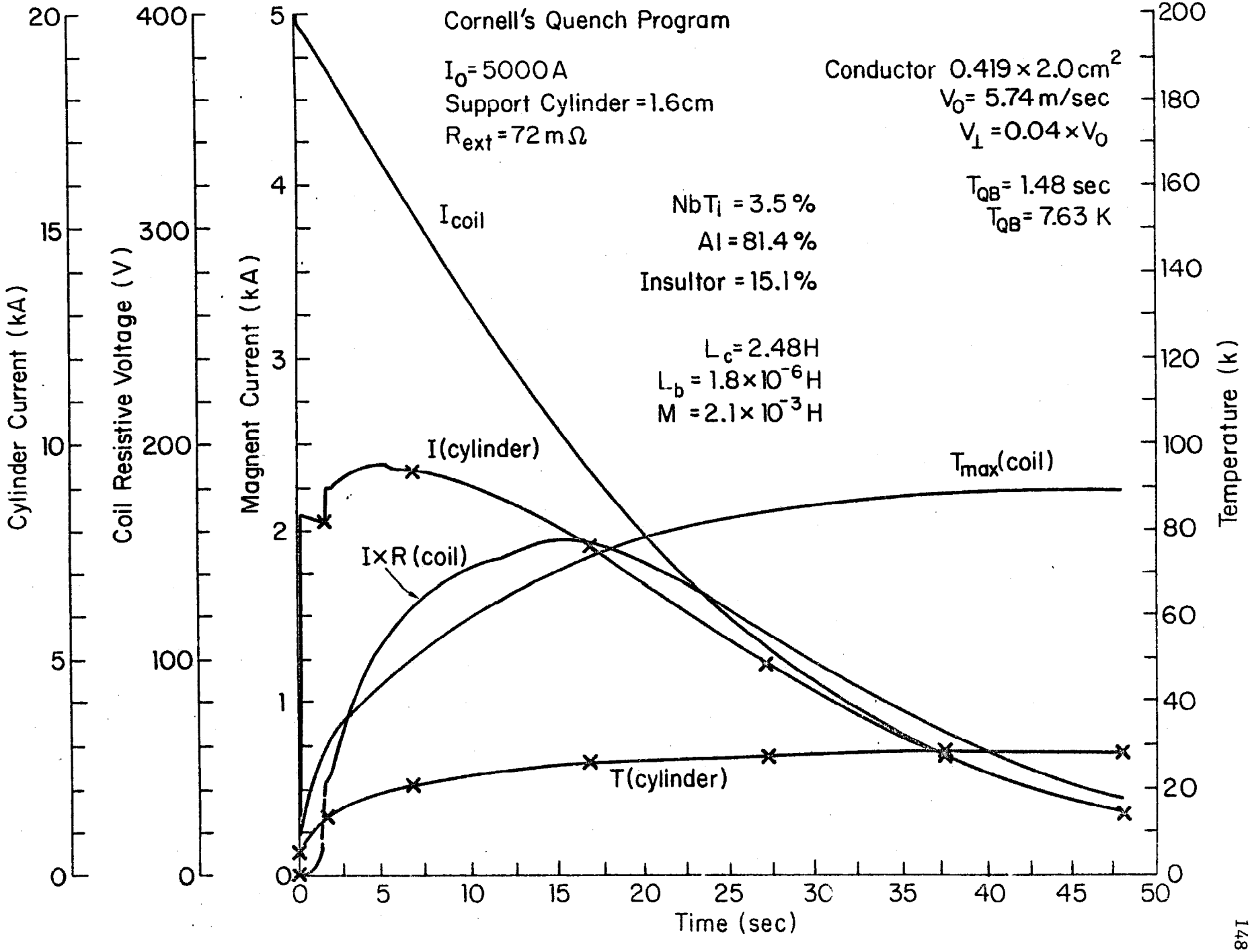

Fig. C(4). Quench behavior with quench back

the coil $I_c \times R_c$ are shown. The current and the temperature of the support cylinder are shown with x marks.

In this figure, we can see the eddy current of 8.4×10^4 A starts to flow in the support cylinder at the start of the quench, which is 1.5% of the total ampere-turns. Corresponding to it, there is a sudden decrease of 1.5% in the coil current at the beginning, which will be about 5 in the actual case due to other components, such as the outside cylinder of the aluminum cryostat and other. At about 1.5 sec there occurs a quench-back, as can be seen in the resistive voltage of the coil. The current in the support cylinder also shows a sudden change at the quench-back time reflecting to the sudden change of the resistance of the conductor.

In this simulation the conductor and the support are separated by 2.5 mm thick epoxy with $k = 8 \times 10^{-4}$ W/cm K. There is enough heat exchange between them to cause quench-back, but time is required to equalize their temperatures.

The calculated maximum temperature of the conductor is about 90 K. The maximum resistive voltage of the coil is about 130 V, and the maximum terminal voltage is 360 V. We feel these voltages are quite safe.

References

1. T. Kishimoto, S. Mori and M. Noguchi, "Computer Simulations of Quench Properties of Thin, Large Superconducting Solenoid Magnets", TSUKUBA-HEAP-5, May 1982, also as CDF-SDS-10.

2. T. Tominaka et. al., "Quench Simulation in Thin Solenoid," CDF-SDS-6B, May 25, 1982.

3. R.D. Kephart and E. Leung, "Comments on the Choice of Operating Current for the CDF Solenoid", CDF Solenoid Engineering Note 35, May 18, 1982, also as CDF-SDS-7.

4. R. Yamada, "The Current and Voltage Shapes of Coil During Quenches and Quench-Backs", CDF Solenoid Engineering Note 37, June 8, 1982, also as CDF-SDS-12.

5. S. Mori and M.Noguchi, "Computer Simulations of Quench Properties of Thin, Large Superconducting Solenoid Magnets with Quench-Back Effects", TSUKUBA-HEAP-6, June 1982; also as CDF-SDS-14.

6. R. Yamada "Simple Computer Simulation of Quench-Back Effect of CDF Solenoid", CDF Solenoid Engineering Note 39, July 12, 1982.

7. M.N. Wilson "Computer Simulation of the Quenching of a Superconducting Magnet". RHEL/M 151, Rutherford Lab., Internal Report, (1968).

8. D. Andrews, CBX-77-1, Cornell Internal Report, (1977).

APPENDIX D: MAGNETIC FORCES ON DETECTOR COMPONENTS

Magnetic Force in Ideal Case

If the iron surfaces of the end plug and the end wall were completely flat and uniform without the hole in the end plug, with infinite permeability iron, and if the end of the coil conductor were up to the iron surface, the magnetic field inside the coil would be completely parallel in the axial direction and uniform. Then there would be no axial forces acting on the coil. There would, however, be a uniform radial force on the conductors that would produce a hoop load in the coil, but there would be no eccentric net radial force on the coil. In this case the total inward force on the end plug will be given by

$$\frac{B_o^2}{2\mu_o} \times \pi R^2$$

which is about 645 metric tons, for a central field of $B_o = 1.5$ T and the end plug radius of R = 1.5 m.

Magnetic Force in Real Cases

In reality the iron has finite permeability. There are holes in the end plug plates, and a gap between the iron surface and the end of the coil conductor as shown in Fig. D(1). This introduces a radial field component B_r near the end of the coil, which will cause an axial force on the coil. In order to make more uniform

field at the end, and reduce the fringing field and its resulting axial force, four iron plates are introduced inside the bore of the coil.

Axial Force on Conductor

The axial force on the coil for different iron/coil geometries was calculated using TRIM and FORGY programs. The proposed design has the axial gap of 4.75" and the radial gap of 3.75" with the resulting axial force of 97 metric tons.

With the proposed four reentrant plates the axial force F_z is directed toward the longitudinal center [to the bottom in Fig. D(1)] of the coil. This compressive force could be made zero or changed into a tensile force by increasing the number of plates, if we had enough space for locating extra reentrant iron plates.

Axial Decentering Force on Coil

If the coil is displaced axially from the center position, then there is unbalance between two big competing forces at the ends of the coil, and that will cause as a result an axial decentering force on the coil assembly. In our case, the force between the iron and the end of the coil, where a radial magnetic field component exists, is repulsive in the axial direction. The more the coil moves away from the one end, the stronger the repulsive force becomes. Therefore, if the coil is displaced axially, the coil will not be pulled to the pole piece where the gap is decreasing but rather the coil will be pushed from the other end of the coil, where the gap is increasing.

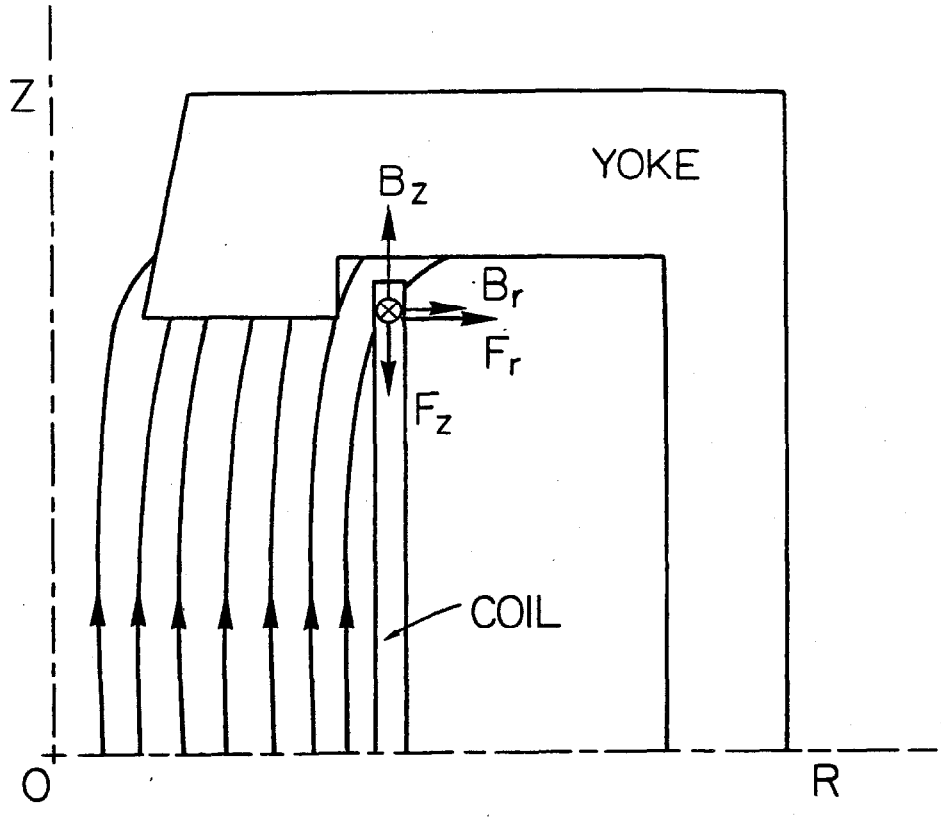

Fig. D(1). Simplified iron geometry - one quadrant

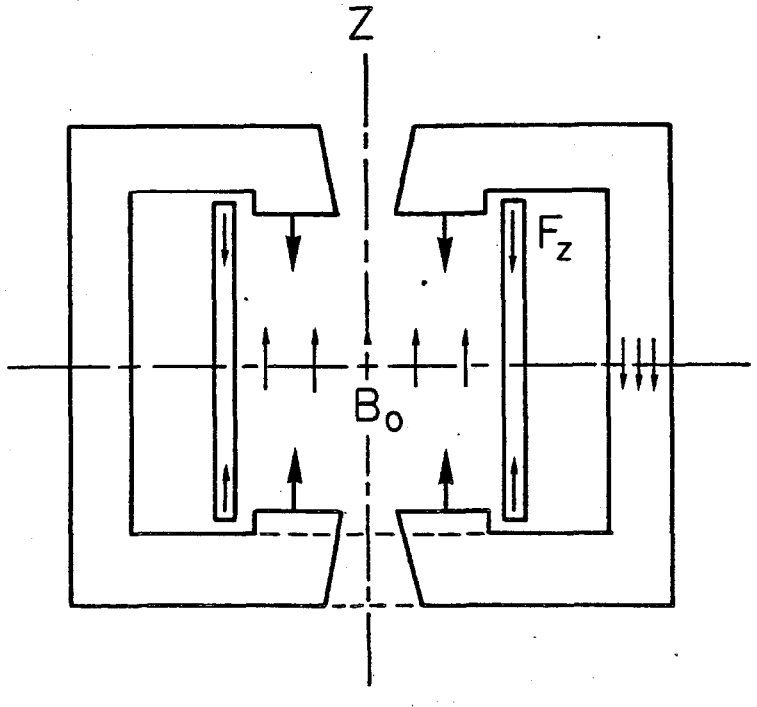

Fig. D(2). Simplified iron geometry - total forces

Radial Decentering Force

If the coil is displaced radially with respect to the yoke, or if the coil is not made axially symmetric, then there will be a net radial decentering force on the coil.

The Total Axial Force on the Magnet System

Assume a cylindrically symmetric magnet system with fairly uniform field B_o on the median plane inside the coil radius R, as shown in Fig. D(2). If we do the surface integration of Maxwell stress on the median plane of this figure and on the surface of a hemisphere with infinite radius

then

$$\underset{\text{system}}{\int}\frac{B^2}{2\mu_o}\,ds = \underset{\text{coil}}{\int}\frac{B_o^2}{2\mu_o}\,ds + \underset{\text{yoke}}{\int}\frac{B^2}{2\mu_o\mu}\,ds + \underset{\text{between}}{\int}\frac{B^2}{2\mu_o}\,ds + \underset{\text{outer}}{\int}\frac{B_o^2}{2\mu_o}\,ds \sim \underset{\text{coil}}{\int}\frac{B_o^2}{2\mu_o}\,ds$$

or

$$\underset{\text{coil}}{\int}\frac{B_o^2}{2\mu_o}\,dS = \frac{\pi R^2}{2\mu_o}B^2{}_o \sim \Sigma \text{ (axial forces on all components of magnet)}$$

The major components for the summation include the axial forces on the coil, the end plug and the end wall. There are also some small forces on the surfaces of the yoke and the central calorimeter.

Even if the shape of the end plug and/or the geometry at the end of the coil is changed, the total of the axial forces of the components is the same, as long as the magnetic field B_o is kept the same by adjusting the magnet current. The total axial force is the same as in the ideal case.

In the ideal case with no holes in the end plug, the axial force on the end plug is 645 metric tons as explained earlier. The axial force distribution for several other cases with holes in the end plug was calculated with TRIM and FORGY, with the ideal case with finite permeability the total force on the end plug was calculated 679 metric tons. In our design, the summation of the axial forces of the coil, the end plug, and the end wall is about 630 metric tons. The coil has an axial force of 110 metric tons, and the end plug has an axial force of about 490 metric tons. In the extreme case when there is no yoke, the axial force on the coil is about 700 metric tons for B_o = 1.5 T. In this case it is bigger than 645 metric tons because the return flux is not contained in the yoke. There is substantial magnetic field outside the coil on the median plane.

Number of Plates in Magnet Bore

This effect was studied in detail with the "505 CBD" series of TRIM runs. In this old series, the thickness of the re-entrant iron plates is 2 inches with a half inch spacing between them. The width of the coil conductor is one inch and the radial gap is 4 inches. There is no air gap between the end plug and the end wall as in the present design.

For cases with three, four, five and seven plates, the axial gap D is changed and the resultant axial forces on the coil are shown in Fig. D(3). Except for the seven plate case all the axial forces are negative, indicating a compressive force on the coil. In the case of seven plates, the integrated total force becomes positive, meaning a tensile force on the coil. As can be seen in Fig. D(3), there exist cases with zero total axial force on the coil, if we can afford to install as many re-entrant plates as needed. In this case the integrated axial force will be zero, but locally there are regions in compression and regions in tension within the coil.

In this series the axial spring constant is about 50 metric tons/inch for all the cases, independent of the number of re-entrant plates, as shown in the same slopes.

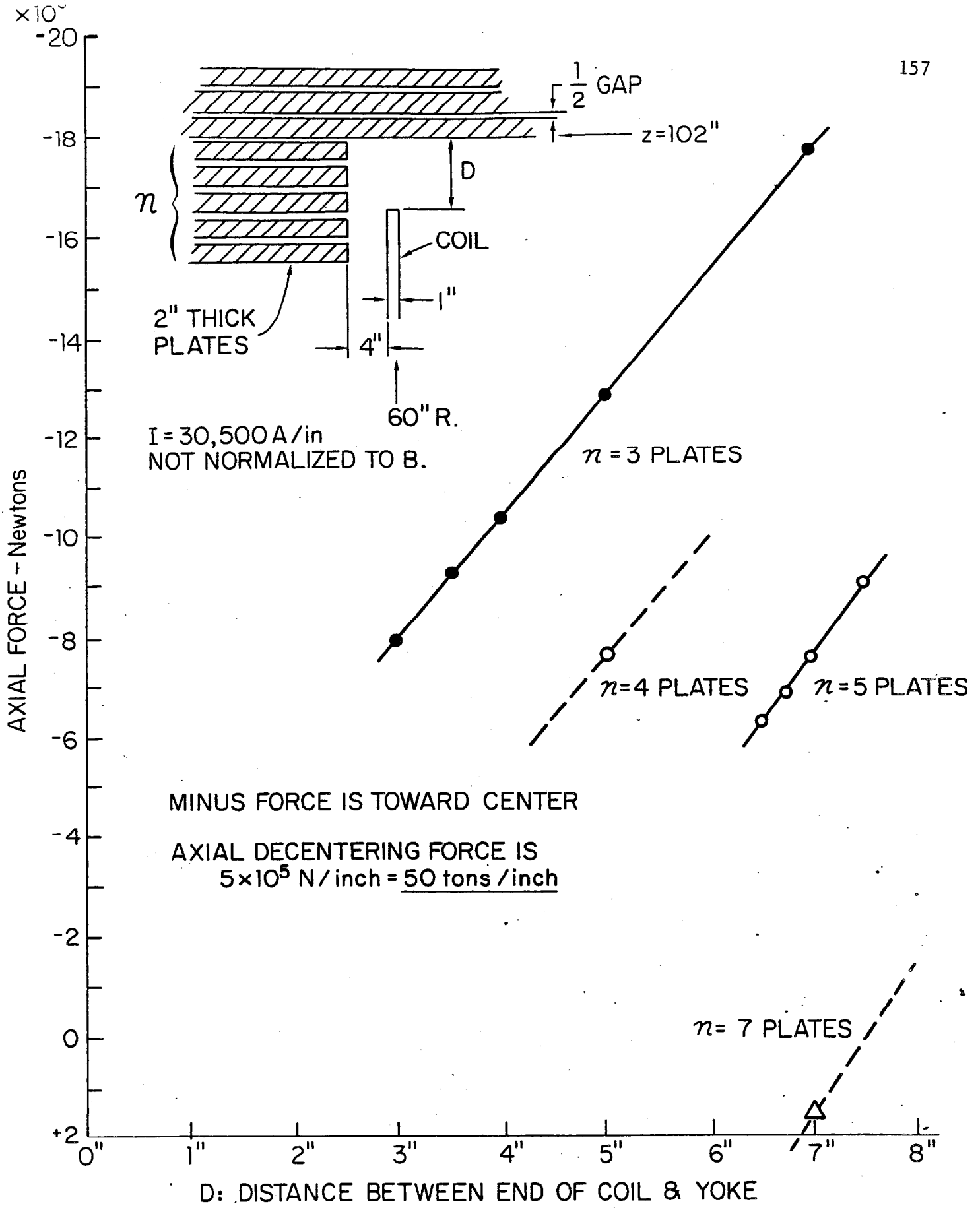

Fig. D(3). Axial force on CDF solenoid as a function of axial coil-iron separation and number of plates

APPENDIX E: RESIN IMPREGNATION

General Description

The gap between the outer surface of the conductor winding and the inner surface of the support cylinder will be filled via epoxy resin impregnation. The size of this gap depends ultimately upon the mechanical tolerances of the winding and the support cylinder, and upon the vendors ability to impregnate the gap such that it is free of voids. While ease of assembly argues that this gap be large, a variety of other factors require that it be minimized. In particular the gap should be minimized for the following reasons:

1. All mechanical forces between the conductor and support cylinder are transmitted through this layer. These forces can originate from temperature differences between the support cylinder and winding (e.g. during cooldown or a quench) or may occur during coil excitation. When the coil is energized the conductor is pressed out radially with a magnetic pressure that is $B^2/2\mu_o$ ($\sim$ 130 psi) against the support cylinder. In addition, due to the fringing field at the ends of the coil, there is an axially compressive force on the winding that results in a shear force between the conductor and the support cylinder. Moreover, since the support cylinder is mechanically connected to the yoke through the axial and radial supports, then whatever forces result from the coil being off magnetic center must be carried through the material that fills the gap.

2. It is also desirable to minimize the gap for thermal reasons. Since the cooling pipe is mounted on the support cylinder, the conductor is conduction cooled through the epoxy and other materials that fill the gap.

Requirements for the Resin

In view of the above considerations the resin shoud have the following properties:

1. It should provide a strong bond between the conductor and support cylinder. In particular the shear strength should be good. (Note that since the resin actually bonds to the turn to turn conductor insulation, this insulation must also be well bonded to the conductor).
2. The resin should have good thermal conductivity.
3. The thermal expansion coefficient of the resin should be about equal to that of aluminum so that the bond does not peel off during cooldown.
4. The resin should not crack or peel when thermally cycled.

The most likely material that wil satisfy these requirements is an epoxy resin highly filled with silica powders or glass fibers.

Vacuum Impregnation

The gap will be filled by resin using vacuum impregnation techniques. These techniques have been used on other large coils, e.g the TPC magnet, with good results.[1)] Since the resin layer should never be placed in tension or have to resist a peeling force, we are confident that this technique will be satisfactory.

Shear Strength of Resin

Measurements of the shear strength of epoxy impregnants have been made and reported.[2)] With the combination of Araldite CY 22Y, Hardner CY 225 and Filler K13, the best bond shear stress at 4.2 K

reported is 6.0 MPa (≃ 61 kg/cm^2) and 3.3 MPa (≃ 34 kg/cm^2) for 0.5 and 1.0 mm gaps respectively. The strength of this material should be about 17 kg/cm^2 for a 2.0 mm gap, assuming that the strength depends on the gap. Other combinations tested by these authors do not seem to have as strong a bond shear stress. We need extensive study of this property before finally selecting the resin we use.

Cracking Energy of Bonding Resins

The heater test results on the R and D model magnet indicate the energy required to start a quench is about 10 joules.[3] In this coil a heater was imbedded in the conductor and pulsed with successively increasing energy until a quench started. The energy was quite localized and the pulse width was about 0.1 second.

The cracking energy of epoxy resins has been measured and is reported to be less than 18 kJ/m^3.[4] If we assume the thickness of the insulation layer is 3 mm, then it can release an energy of about 54 J/m^2 if it cracks. If we assume the thickness of the conductor is 2 cm and the cylinder is 1.6 cm, and we assume that whole resin volume cracks and releases energy uniformly, then the enthalpy rise is 0.56 mJ/g, corresponding to a temperature rise from 4.7 K to a 6.0 K. Such a situation is unlikely to happen. The expected temperature rise will be controllable as long as it is uniform, as is shown in Fig. E(1), but it is preferable to minimize the thickness of resin impregnation to minimize the temperature rise. In this figure the conductor specification for the short sample data at 4.2 K is shown. The estimated

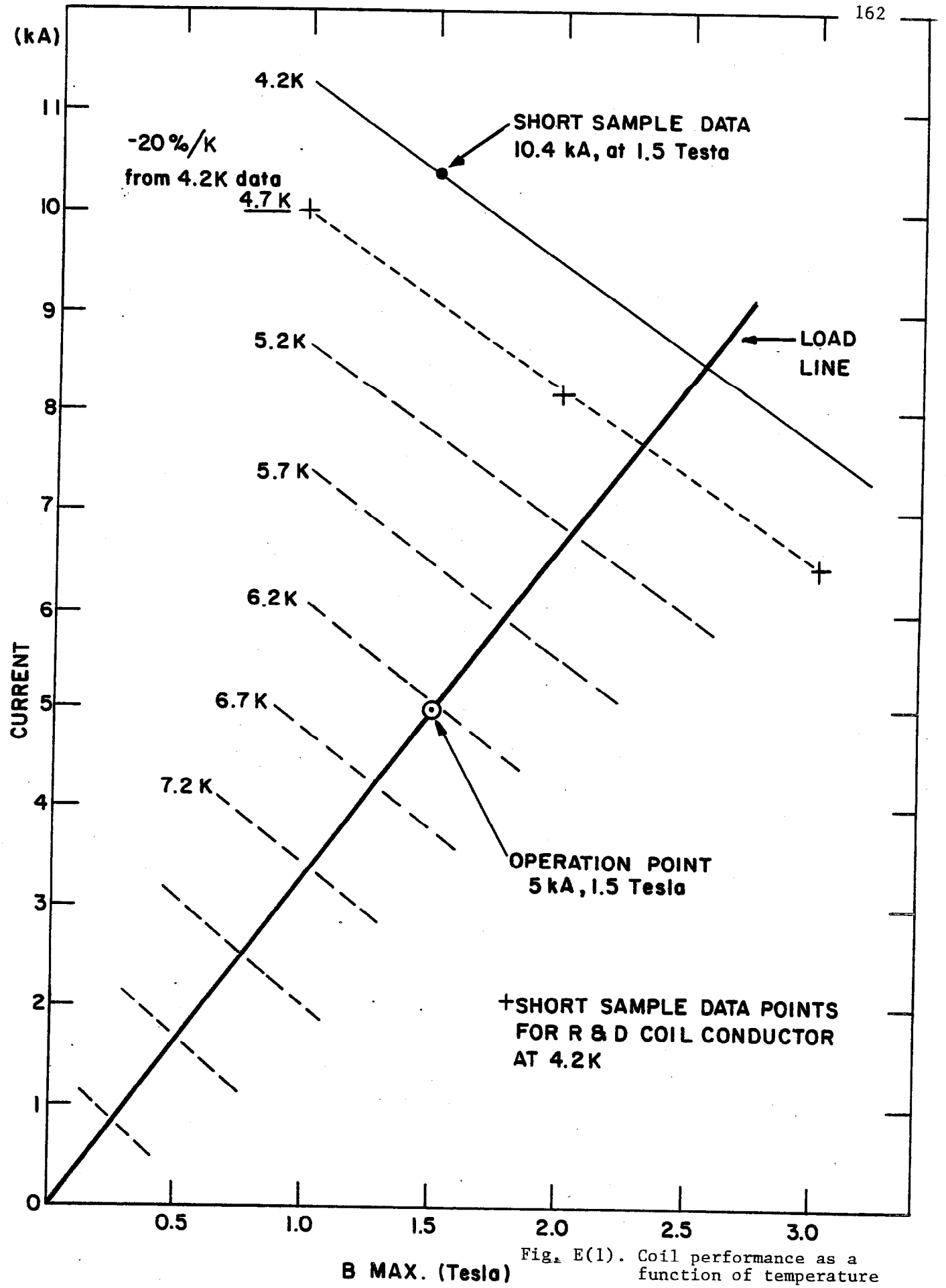

Fig. E(1). Coil performance as a function of temperature

corresponding short sample currents at different temperatures are shown, assuming a 20% decrease per degree.

There are also data on the debonding energy of epoxy which are kJ/m^3 reported to be 3 kJ/m^3.[5] This number gives 9 J/m^2 for the 3 mm thick insulation layer. In the same way, for the 2 cm thick conductor and 1.6 cm cylinder, ΔE is 0.09 mJ/g and the corresponding temperature is 4.9 K. Another quoted data for epoxy debonding is 0.05 mJ/cm^2.[5] This corresponds to 0.5 J/m^2, which is much smaller than the previous value.

In our case we will select the resin, which will neither crack nor debond from the conductor during operation, but however even in the worst case in which the whole bonding surface debonds all over the entire surface, and the whole resin layer cracks simultaneously, the temperature rise is not large enough to cause a quench due to the large heat capacity of the conductor.

References

1. M.A. Green, et.al., "Vacuum Impregnation with Epoxy of Large Superconducting Magnet Structures", LBL-7931 (1978).

2. H. Brechna and P. Turowski "Training and Degradation Phenomena in Superconducting Magnets", Pro. 6th Int. Conf. Magnet Tech., Batislava (1981).

3. T. Kishimoto et. al., "Design Report for an Indirect Cooling Superconducting Solenoid Magnet for the CDF Detector" TSUKUBA HEAP-4, March 15, 1982.

4. H. Maeda and Y. Iwasa "Heat Generation from Epoxy Cracks and Bond Failures" to be published in Cryogenics.

5. Y. Iwasa "Diagnostic Requirements and Mechanical Disturbances in Superconducting Magnets" to be published in the Pro. of ICEC9-ICMC, Kobe, 1982.

APPENDIX F: CODE* DESIGN OF VACUUM SHELLS

Inner Vacuum Shell

Shell under external pressure i.e., vacuum annulus at a pressure greater than one atmosphere. Code Paragraph UG-28.

$t = 0.25"$ (6.4 mm), $D = OD = 113"$ (2870 mm)

$L = 198"$ (5029 mm)

$L/D = 1.75 \curvearrowright 1.8$ $\quad D/t = 452 \curvearrowright 450$

From Fig. F(1) and F(2), which are Code Fig. UGO-28.0,

A factor = 0.0000775

and

P_a = maximum allowable pressure differential

$$= \frac{2\,AE}{3(D/t)}$$

for 5083-0 aluminum alloy $E = 10.4 \times 10^6$ psi (71.7 GPa) so

$P_a = 1.19$ psi (8.25 kPa).

The critical collapse pressure of the inner shell is

$$P_{crit} = 0.807 \frac{Et^2}{LR} \left[\left(\frac{1}{1-\nu^2}\right)^3 \frac{t^2}{R^2}\right]^{0.25} **$$

$$= 3.4 \text{ psi } (23.2 \text{ kPa}).$$

Shell under internal pressure i.e., vacuum annulus evacuated. Code Paragraph UG-27

*ASME Boiler and Pressure Vessel Code, Sect. VIII, Div. 1.

**R.J. Roark and W.C. Young, "Formulas for Stress and Strain, McGraw-Hill, New York (1975), p. 556.

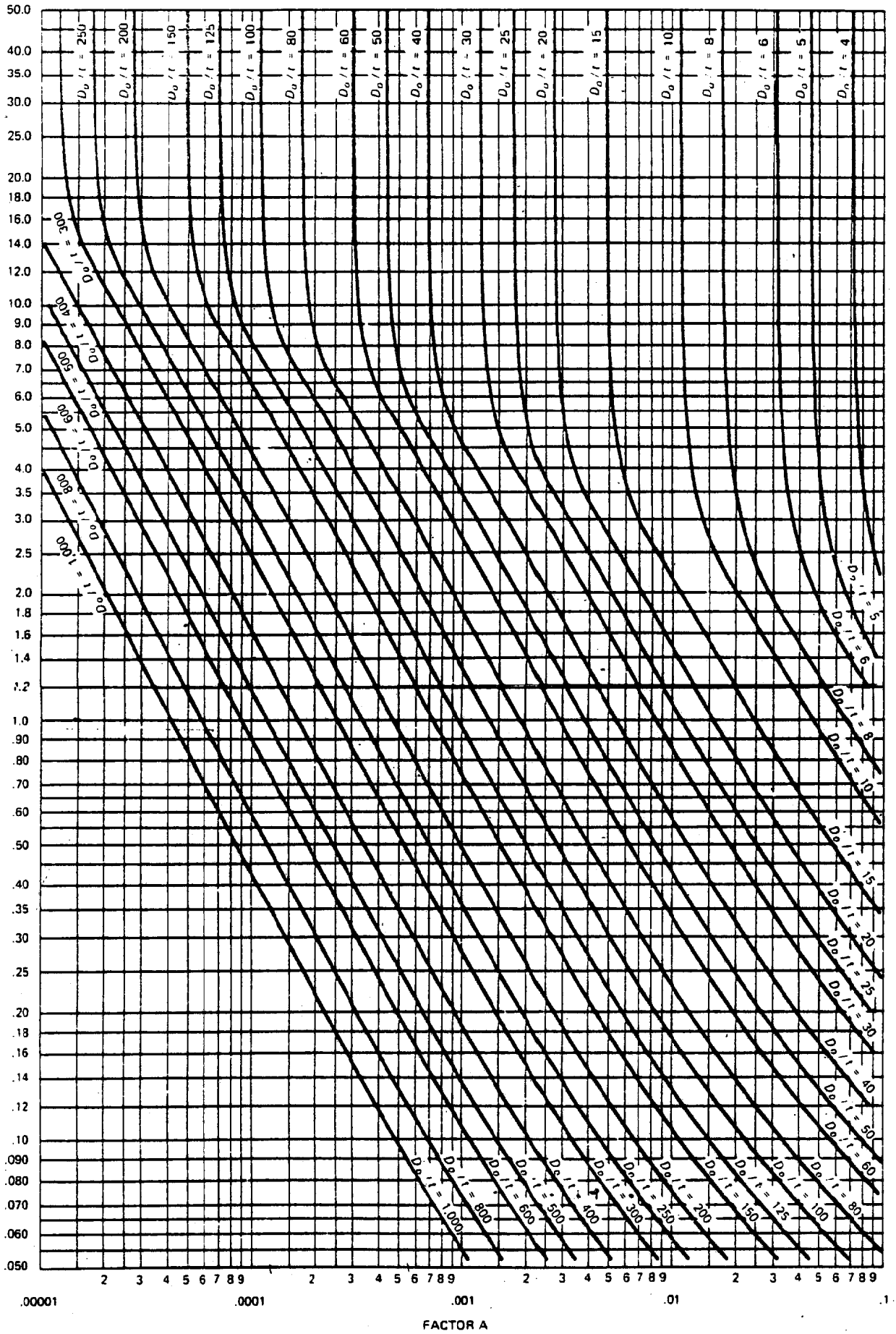

Fig. F(1) From ASME Code

FIG. UGO-28.0 GEOMETRIC CHART FOR CYLINDRICAL VESSELS UNDER EXTERNAL OR COMPRESSIVE LOADING (FOR ALL MATERIALS)

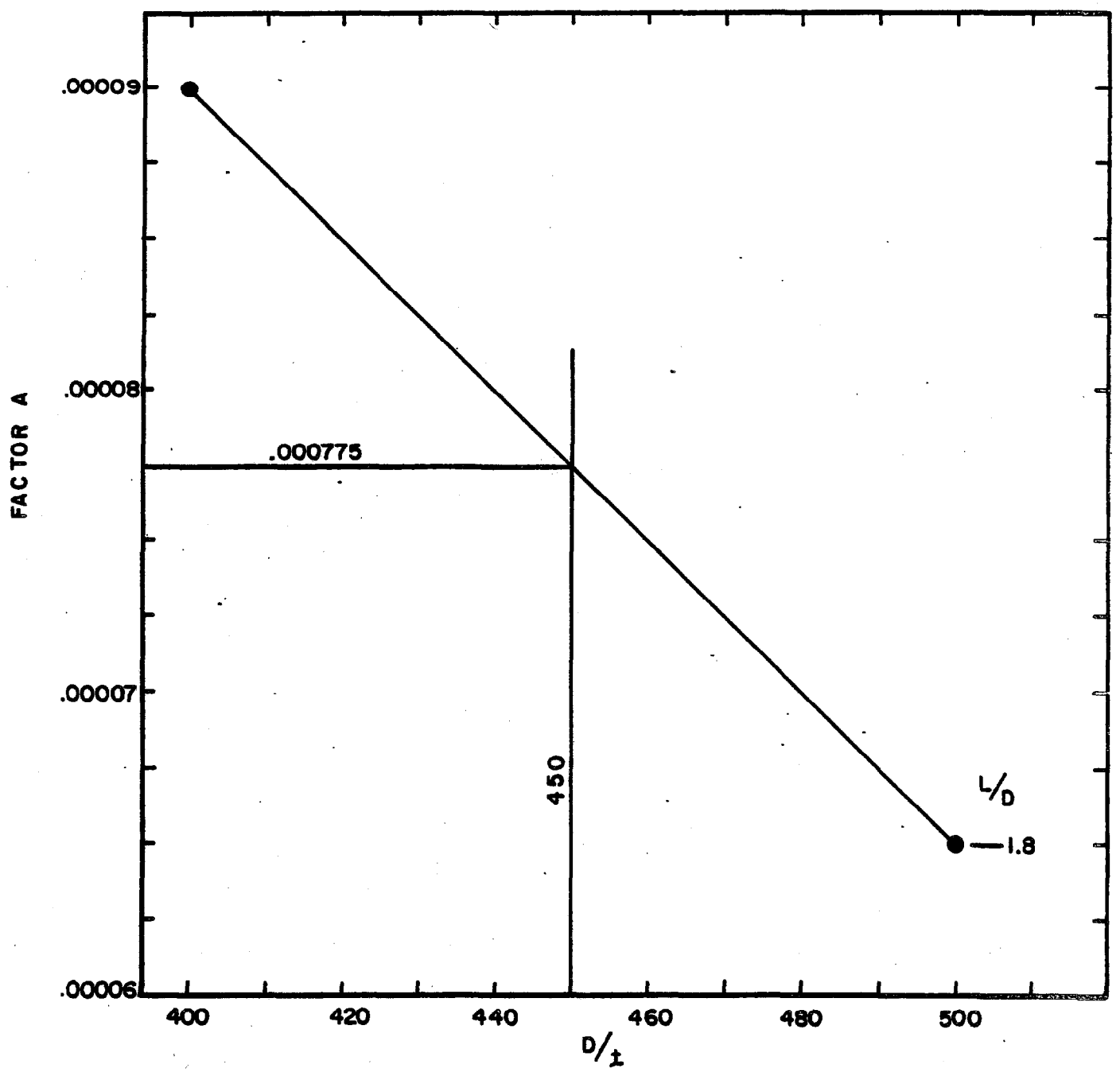

Fig. F(2). Inner vacuum shell, external pressure from: Fig. UGO-28.0, ASME Code

t_{min} = minimum allowable thickness

$$= \frac{PR}{SE-0.6\ P}$$

where

P = design pressure = 15 psi (103.4 kPa), vacuum load

R = inner radius of shell = 56.25" (1429 mm).

S = maximum allowable stress

= 10000 psi (69 MPa) for 5083-0

E = joint efficiency at = 0.80

and

t = 0.105" (2.7 mm)

from which it is seen that the external pressure criteria dominates the design.

Outer Vacuum Shell

Shell under external pressure, vacuum annulus evacuated. Code Paragraph UG-28.

t = 0.750" (19.0 mm)

D = OD = 132" (3353 mm)

L = 188" (4775 mm)

L/D = 1.42 ≯ 1.5, D/t = 176

From Fig. F(1) and F(3), which are Code Fig. UGO-28.0,

A factor = 0.000380

From Fig. F(4) which is Code Fig. UNF-28.31, for 5083-0.

B factor = 1900

and

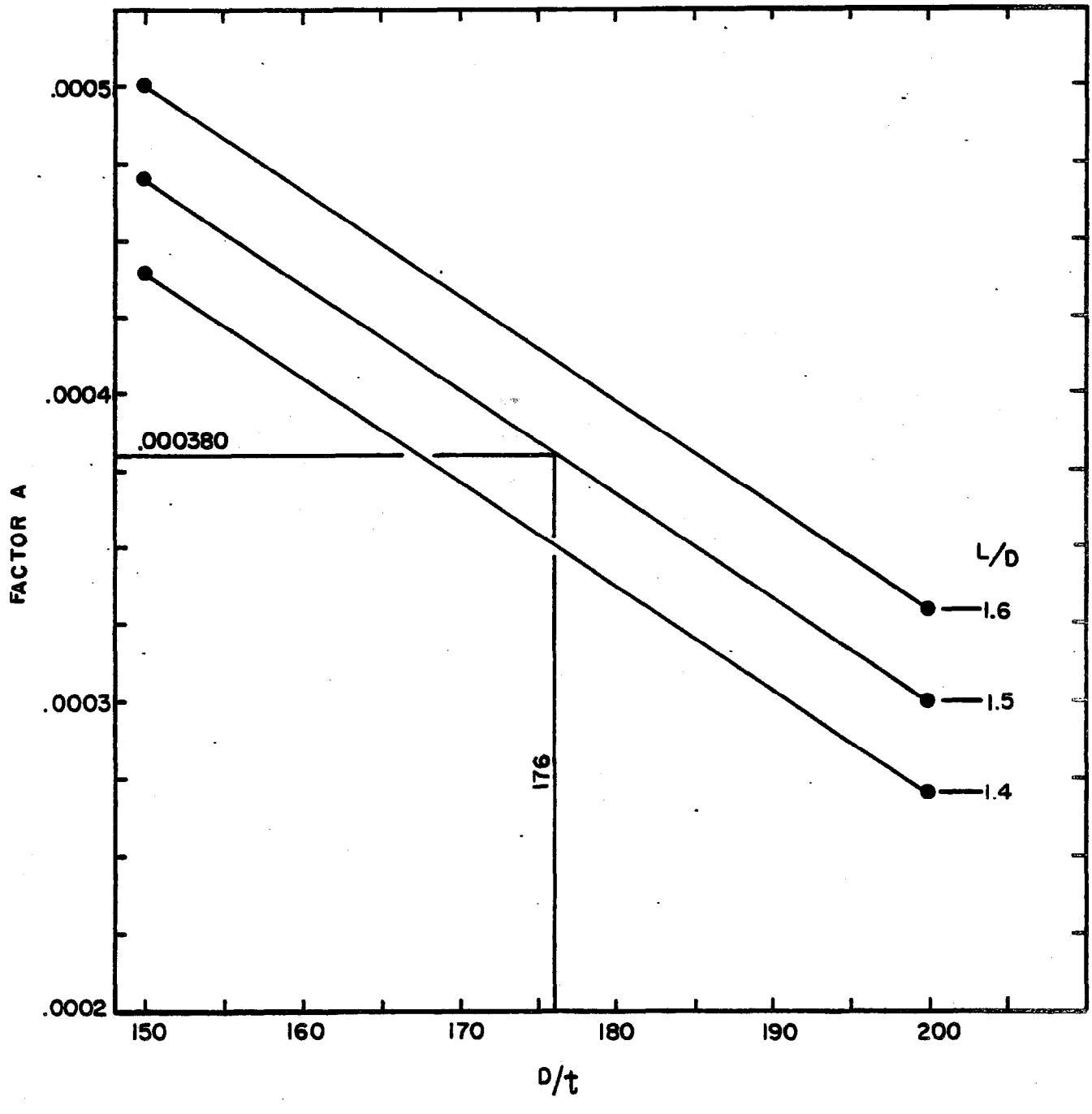

Fig. F(3). Outer vacuum shell under external pressure from: Fig. UGO-28.0 ASME Code

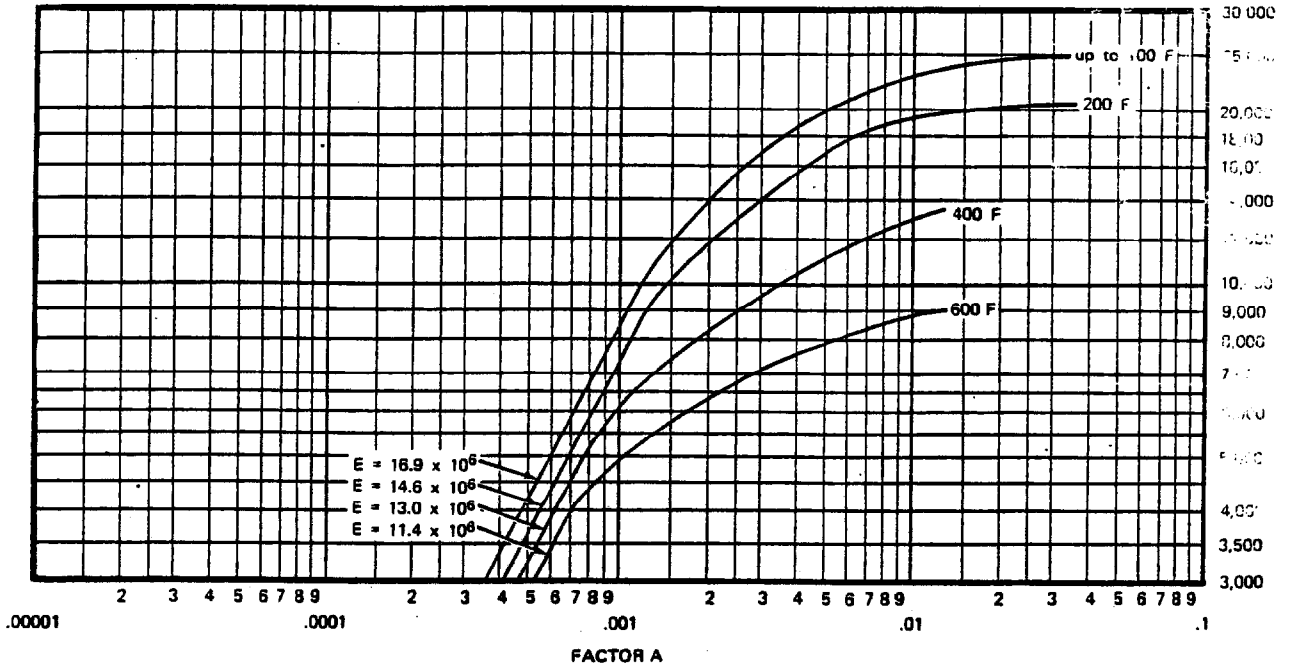

FIG. 5-UNF-28.22 CHART FOR DETERMINING SHELL THICKNESS OF CYLINDRICAL AND SPHERICAL VESSELS UNDER EXTERNAL PRESSURE WHEN CONSTRUCTED OF UNALLOYED TITANIUM, GRADE 3 [NOTE (7)]

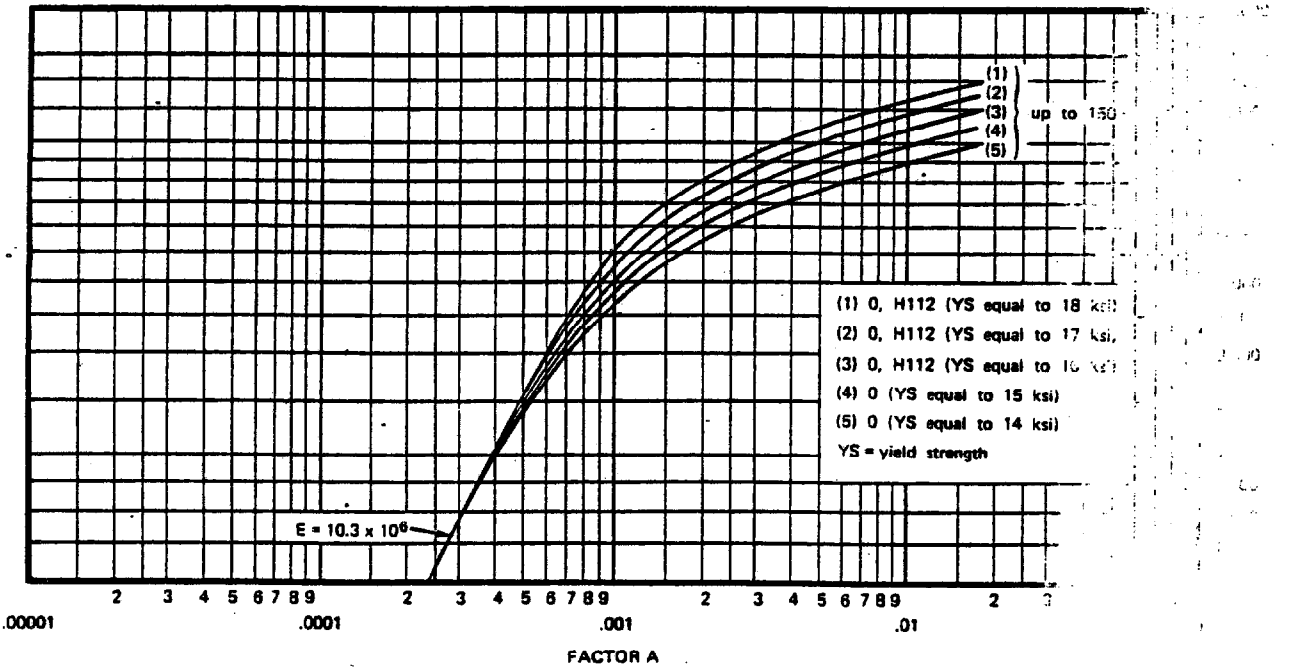

FIG. 5-UNF-28.23 CHART FOR DETERMINING SHELL THICKNESS OF CYLINDRICAL AND SPHERICAL VESSELS UNDER EXTERNAL PRESSURE WHEN CONSTRUCTED OF ALUMINUM ALLOY 5083 IN O AND H112 TEMPERS [NOTE (4)]

Fig. F(4). From ASME Code

P_a = maximum allowable pressure differential

$$= \frac{4B}{3(D/t)} = 14.4 \text{ psi } (99.29 \text{ kPa})$$

Since the operating pressure differential across the shell is atmospheric pressure, which at the Fermilab elevation of 767 ft (233.8 m) above sea level is 29.2" Hg or 14.35 psi (98.94 kPa), this shell is in accordance with the Code.

Shell under internal pressure, i.e., vacuum annulus at a pressure greater than one atmosphere. Code Paragraph UG-27.

p = pressure rating of shell

$$= \frac{SE\ t}{R + 0.6\ t}$$

where

S = max. allowable stress = 10000 psi (69 MPa)

E = weld efficiency = 0.80

t = shell thickness = 0.750" (19.0 mm)

R = inner radius of shell = 65.25" (1657 mm)

and

p = 92 psi (0.63 MPa)

Permissible out-of-roundness of shells permitted by Code, Code Paragraph, UG-80,

$$\text{Maximum ID} - \text{Minimum ID} \leq 1\% \ D_{nominal}$$

For the inner shell,

$$\text{Maximum ID} - \text{Minimum ID} \leq 1.12" \ (28.4 \text{ mm})$$

and for the outer shell,

Maximum ID - Minimum ID $\leq$ 1.30" (33.0 mm)

The maximum radial deviation from circular for L/D = 1.50, D/t = 176 (the outer shell) is 0.7 t = 0.394" (10.0 mm) and for L/D = 1.8, D/t = 450 (the inner shell) is $\sim$ 1.4 t = 0.350" (8.9 mm). This deviation is measured with a template which has a chord length of at least 30".

Tolerances on shells.

The tolerances on the diameters of the shells and the out-of-roundness is determined by the requirement that there be no thermal shorts between 300 K, 77 K and 4.5 K components and that there be no interference with other components of the detector.

Openings in outer shell, Code Paragraph UG-37

The opening in the outer shell for the 8" (200 mm) vacuum shell of the chimney must be reinforced in accordance with the Code. A 6" (150 mm) long sleeve with a wall thickness of 0.375" (9.5 mm) appears to be adequate to reinforce the chimney.

Annular end flanges, Code Paragraph UG-34

t_{min} = minimum thickness of flat circular head required by Code

$$= d\sqrt{\frac{CP}{SE}}$$

where

d = span between shells = 10" (254 mm)

C = geometry factor = 0.5

P = design pressure = 15 psi (103.4 kPa)

S = maximum permissible stress

= 10000 psi (69 MPa)

E = weld efficiency = 0.8

so

t_{min} = 0.306" (7.8 mm)

and the flange thickness is greatly in excess of this minimum thickness.

APPENDIX G: MECHANICAL ANALYSIS OF SUPPORTS

In this appendix we calculate the stresses and deflections for the support system described in the text. For the purposes of clarity, we assume that all 6 axial and 24 radial supports are made of Inconel 718 which has the following material properties.

	300 K	4 K
σ_{yield}	157 ksi (1080 MPa)	199 ksi (1372 MPa)
$\sigma_{ultimate}$	190 ksi (1310 MPa)	268 ksi (1848 MPa)
$\sigma_{allowable}$	52 ksi (360 MPa)	67 ksi (462 MPa)

Minimum elongation at 4 K: $\sim$ 14%

Young's modulus, E, at 300K: $\sim 3 \times 10^7$ psi (207 GPa)

In addition we use magnetic spring rates of 10.1×10^4 lb/in (17.6 MN/m) axially and a maximum 7.0×10^4 lb/in (12.3 MN/m) radially, see Chapter II.

Radial Supports

A schematic of the radial support system at one end of the coil is shown in Fig. G(1). The 12 identical supports are attached tangentially to the coil at 6 points. Each support is assumed to be preloaded so that it always remains in tension and since each support is attached via spherical bearings, stresses due to bending are assumed to be neglible.

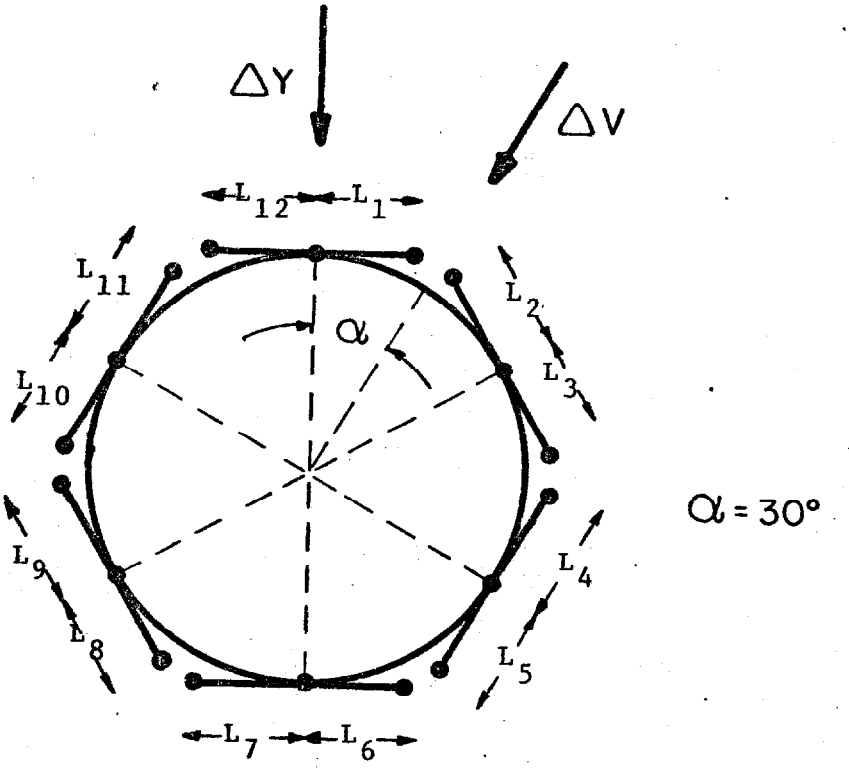

Fig. G(1). Radial Support System

We consider forces acting in two possible radial directions Y and V in Fig. G(1) but note that arbitrary azimuthal directions yield results intermediate to these two cases. For purposes of these calculations the coil itself is assumed to be perfectly rigid. Finite element analysis of the coil package with ANSYS indicates this to be a good assumption.

Magnetic force in the V Direction. Consider a force F_V that causes the coil to be displaced by a distance ΔV. Then each support changes its length by an amount

$$\Delta L_1 = \Delta L_2 = \Delta V \cos 60^\circ$$
$$\Delta L_3 = \Delta L_{12} = -\Delta V \text{ cox } 60^{0^\circ}$$
$$\Delta L_4 = \Delta L_{11} = \Delta V$$
$$\Delta L_5 = \Delta L_{10} = -\Delta V$$
etc

The change in tension produced in each support by these deflections is given by

$$T = AE\ (\Delta L/L) \qquad (1)$$

where

T = Tension produced by displacement ΔL

E = Young's modulus

A = Cross sectional area of the supports

thus

$$T_1 = T_2 = \frac{AE}{L} \Delta V \cos 60^\circ$$

$$T_3 = T_{12} = -\frac{AE}{L} \Delta V \cos 60^\circ$$

$$T_4 = T_{11} = \frac{AE}{L} \Delta V$$

$$T_5 = T_{10} = -\frac{AE}{L}\Delta V$$

Thus taking the components of these tensions in the V direction gives

$$F_V = 4\ T_4 + 8\ T_2 \cos 60^\circ = 4\ T_4 + 8\ (T_4 \cos 60^\circ) \cos 60^\circ$$

$$= 6\ T_4 = 6\ \frac{AE}{L}\Delta V \qquad (2)$$

We observe that the stiffness of the system in this direction is six times the stiffness of one radial support member.

Next we calculate the required cross sectional area of the supports. If we assume that the magnet is 1" (25.4 mm) from magnetic center so that a force of $F_V = 7.0 \times 10^4$ lb acts upon it, then the supports with the highest tension supplies

$$T = \frac{AE}{L}\Delta V = 11{,}667 \text{ lbs } (51890 \text{ N})$$

which is 1/6 of the total force applied by the V direction. Using a 4 K working stress of 67 ksi (462 MPa) for Inconel 718 it follows that the required cross section area of a support is

$$A = T/\sigma = 11{,}667/67000 = 0.174 \text{ in}^2 = 1.12 \text{ cm}^2 \text{ (1-77 K)}$$

$$A = T/\sigma = 11{,}667/52000 = 0.224 \text{ in}^2 = 1.45 \text{ cm}^2 \text{ (77-300 K)}$$

the former corresponds to rods .47" (12 mm) in diameter. With this choice the spring constant of the support system in the V

direction can be calculated from equation (2) using L = 11.25" (286 mm) yields

$$K_V = \frac{F_V}{\Delta V} = \frac{6AE}{L} = \frac{6(0.174\ in^2)\ (3.0 \times 10^7\ lb/in^2)}{11.25\ in}$$

$$= 2.8 \times 10^6\ lb/in \qquad (3)$$

clearly this is large compared to the radial magnetic spring of 7.0×10^4 lbs/in thus the system is stable.

Finally from (3) we can calculate the deflection of the coil assuming that it is 1" from magnetic center

$$\Delta V = \frac{F_V}{K_V} = 0.025\ in \quad (0.64\ mm)$$

Magnetic force in the Y direction. Here we repeat the previous calculation for forces in the Y direction

$$\Delta L_1 = \Delta L_{12} = \sqrt{L_1^2 + \Delta Y^2} - L_1 \backsim \frac{\Delta Y^2}{2L_1}$$

$$\Delta L_2 = \Delta L_{11} = \Delta Y \cos 30^\circ = (3/2)\ \Delta Y$$

$$\Delta L_3 = \Delta L_{10} = -\Delta Y \cos 30^\circ$$

$$\Delta L_4 = \Delta L_9 = \Delta Y \cos 30^\circ$$

$$\Delta L_5 = \Delta L_8 = -\Delta Y \cos 30^\circ$$

$$\Delta L_6 = \Delta L_7 = \Delta L_1$$

thus

$$T_1 = \frac{AE}{L} \left(\frac{\Delta Y^2}{2L}\right)$$

$$T_2 = \frac{AE}{L} \frac{\sqrt{3}}{2} \Delta Y$$

$$T_3 = \frac{-AE}{L} \frac{\sqrt{3}}{2} \Delta Y \quad \text{etc.}$$

Noting that since ΔY is small the terms proportional to ΔY^2 are negligible and taking the components of these tensions in the Y direction gives

$$F_Y = 8\ T_2 \cos 30^\circ$$

$$= 8 \frac{AE}{L} \left(\frac{\sqrt{3}}{2}\right)^2 \Delta Y$$

$$= 6 \frac{AE}{L} \Delta Y \qquad (4)$$

comparing equation (4) with (2) we see that the support system has the same stiffness in both dirrections. (If the coil were off magnetic center by 1" then ΔY = .025" similiarly, the maximum tension that one support suppies is

$$T = \frac{F_Y}{8 \cos 30^\circ}$$

$$= \frac{7.0 \times 10^4}{8 \left(\frac{\sqrt{3}}{2}\right)} = 10,100 \text{ lbs}$$

This tension corresponds to a maximum stress of $\sigma = T/A = 10,100/.174$ = 58 KPSI (400 MPa)

Axial Supports

Next we calculate the forces and deflections on the axial support members. If the coil is 1" off magnetic center in the axial direction and the magnetic spring constant is 10.1×10^4 lb/in. Then,

$$F_z = 10.1 \times 10^4 \text{ lb (450 kN)}$$

if this force is divided equally among the 6 axial supports, then

$$T = \frac{10.1 \times 10^4}{6} = 16800 \text{ lbs (75 kN)}$$

The force applied to the supports may be either compressive or tensile.

The required cross section of the supports is given by

$$A = \frac{T}{\sigma_a} = \frac{16800 \text{ lbs}}{6.7 \times 10^4 \text{ lb/in}^2} \simeq 0.25 \text{ in}^2 = 1.62 \text{ cm}^2 \quad (4\text{-}77 \text{ K})$$

$$A = 0.320 \text{ in}^2 = 2.1 \text{ cm}^2 \quad (77\text{-}300 \text{ K})$$

The deflection in the Z direction is

$$\Delta z = \frac{\sigma_a L}{E} = \frac{6.7 \times 10^4 \text{ psi}}{3 \times 10^7 \text{ psi}} (12.5 \text{ in})$$

$$= 0.028 \text{ in (0.71 mm)}.$$

where we have used L = 12.5" (317.5 mm) as the length of the axial supports. The axial spring constant of this support system is

$$K_z = \frac{F_z}{\Delta z} = \frac{10.1 \times 10^4 \text{ lbs}}{0.028 \text{ in.}} = 3.6 \times 10^6 \text{ lb/in} \quad (630 \text{ MN m})$$

is 35 times stiffer than the magnetic spring constant.

Finally, since the axial support may operate in compression, we must consider elastic buckling of the supports. The critical stress in the support which would lead to elastic buckling is given by the Euler formula*.

$$\sigma_{crit} = \frac{c\pi^2 E}{(L/r)^2} \qquad (6)$$

where

L = length of the support

r = radius of gyration = I/A

I = moment of inertia

c = constant = 1 for free ends

Then for a support with the following cross section:

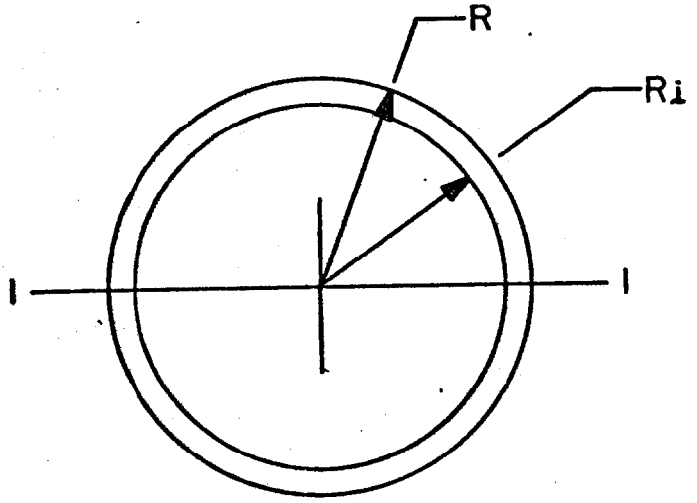

OD = 7/8" (22.2 mm)

R = 0.4375 (11.1 mm)

R_i = 0.334" (8.5 mm)

Wall thickness = $R-R_i$ = 0.103" (2.6 mm)

*Roark and Young, "Formulas for Stress and Strain", Fifth Edition, McGraw-Hill, New York, (1975), p. 415

the cross sectional area is

$$A = \pi \ (R^2 - R_i^2) = 0.25 \text{ in}^2 \ (1.62 \text{ cm}^2)$$

thus the radius of gyration about axis 1-1 is

$$r = \frac{1}{2}\left(R^2 + R_i^2\right) \ 1/2$$

$$r = 0.28 \text{ in } (7 \text{ mm})$$

using this value in equation (6) and L=11.5" for the effective length of the support

$$\sigma_{crit} = \frac{\pi^2 \ (3 \times 10^7 \text{ psi})}{(11.5/0.28)^2} = 176 \text{ ksi } (1200 \text{ MPa})$$

which is above the yield point of the material, thus, the support would fail by yielding rather than elastic buckling in compression.

APPENDIX H: FINITE ELEMENT THERMAL ANALYSIS OF SOLENOID

Introduction

Finite element models were generated to determine temperature profiles in the support cylinder and support pads during a linear ten minute magnet charge, and the maximum concentrated heat flux which the support cylinder can absorb under steady state operating conditions while maintaining superconducting temperature. It was assumed that, due to the attachment of the supports to the support cylinder and the non-existence of a conventional internal bobbin, the thermal behavior of the solenoid (conductor and support cylinder) could be accurately determined by consideration of the support cylinder alone.

The Patran-G finite element model generator was used to create the finite element models. The ANSYS large scale finite element program was used to perform the finite element calculations.

Finite Element Thermal Analysis of Solenoid and Supports During Charge

The charging of the CDF solenoid will impose eddy current heating on the support cylinder, in addition to the support and radiation heat loads already present. Two finite element models were used to analyze solenoid thermal behavior during charge.

Refined Axisymmetric Model of Bolt/Stainless Steel Spacer Combination. This model, Fig. H(1), was used to determine the effective resistance of the bolt/stainless steel spacer so that simple conducting bar elements of equivalent resistance might be used in the solenoid thermal analysis. The aluminum and stainless steel were assigned thermal conductivities which represent an average over the narrow temperature range of interest. A ΔT of 5 K was applied, as shown in Fig. (H)1, and the resulting temperature and flux values as calculated by ANSYS were used to determine the appropriate thermal resistance. This was then expressed as ℓ/KA, where K is the thermal conductivity, and ℓ and A are the length and cross sectional area of the equivalent resistance bar elements used in the solenoid thermal analysis.

Three Dimensional Model of Solenoid. This model, shown in Fig. H(2), was used to determine the temperature profile in the support cylinder and support fixtures during a linear ten minute magnet charge. Due to symmetry, only 1/6 of the solenoid was modeled circumferentially. Also, it was assumed that at a distance of 50 cm from the end of the solenoid, the support cylinder temperature would be that of the helium in the support cylinder cooling pipe, or 4.4 K for this analysis.

The support pads were modeled with a much finer grid than the support cylinder, due to the high thermal gradients expected there. Heat leak into the fixtures from the Inconel 718 support rods was provided by fixing the temperature of the nitrogen

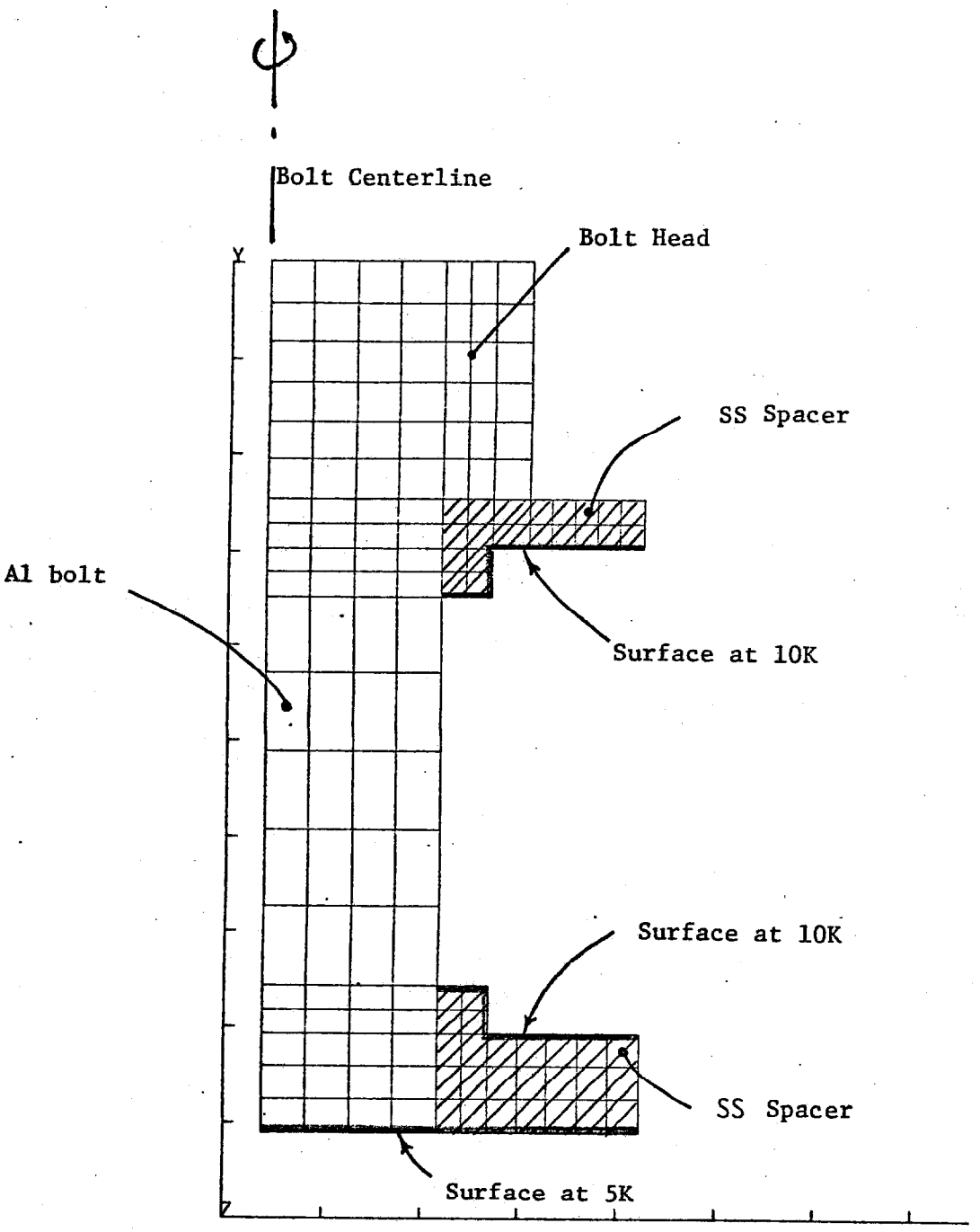

Fig. H(1) Axisymmetric SS Spacer/Bolt Model

intercept point on the rods at 80 K. Each rod was modeled with four thermal bar elements, and the thermal conductivity was input as a fourth order function of temperature. This non-linearity required an iterative solution, with four iterations required for convergence.

The attachment of support pads to support cylinder was done using bar elements having resistances equal to those calculated by the refined axisymmetric model discussed previously.

The eddy current thermal load was calculated for the case of 1.5 cm support cylinder assuming a linear charge over a ten-minute period to a field of 1.5 T. The calculated eddy current power dissipation in the support cylinder is 98.8 W. To this power was added the estimated radiation heat load of 4.4 W. The power dissipation was modeled as heat generation per unit volume and applied to all support cylinder elements.

The support fixture cooling tubes were represented by assigning a temperature of 4.4 K to the line of nodes corresponding to the cooling tube center in each support pad. Calculations indicate that for the flow rate and materials considered, the heat-sink assumption is valid.

Results. The maximum support cylinder temperature occurs at the attachment bolt location #3, Fig. H(2) and is 4.90 K. Figure H(3) shows the temperature distributions in the support cylinder along an axial cut in the plane of the attachment bolts for both the radial and axial supports. The bolts at locations #2 and #4

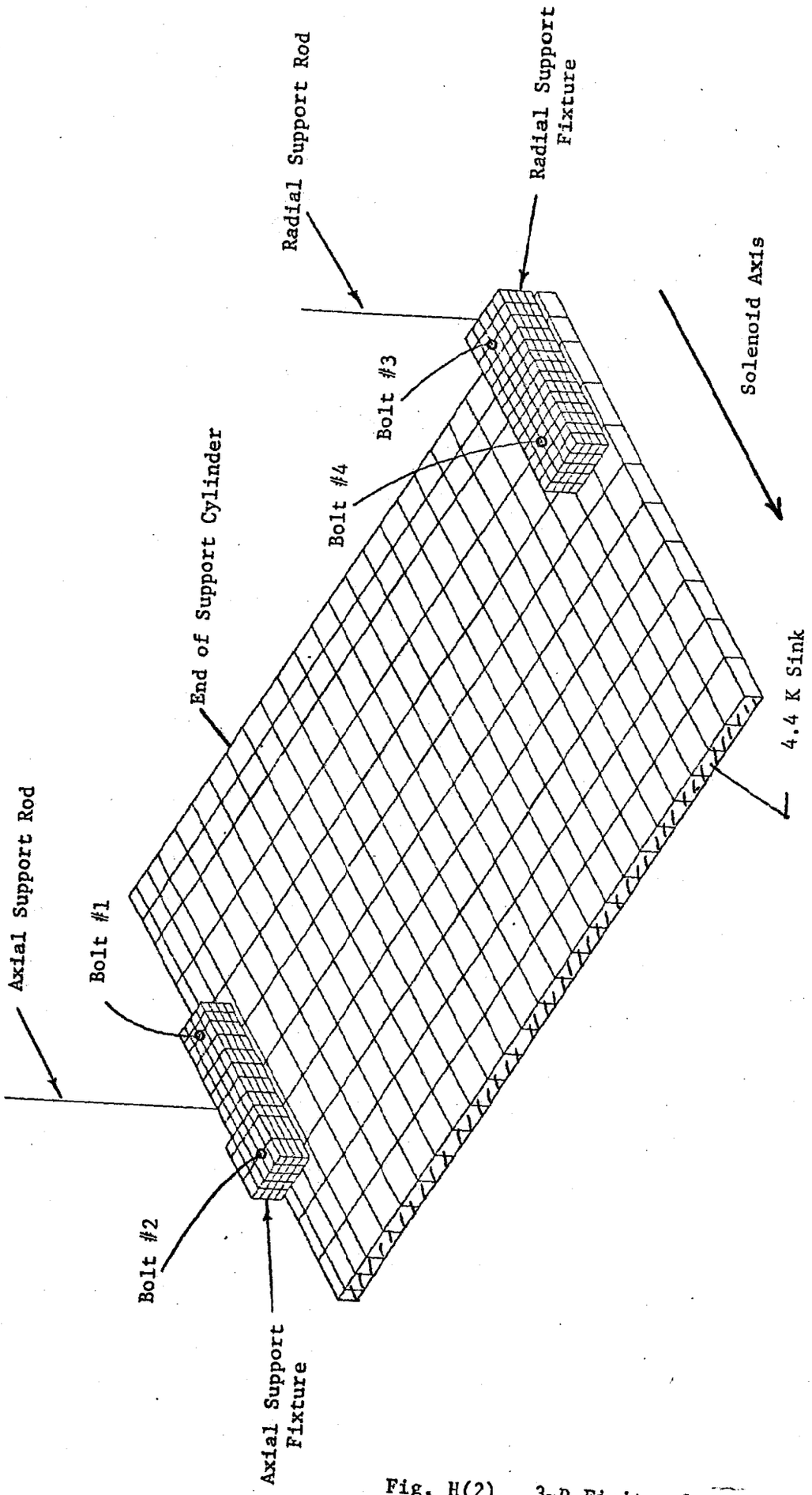

Fig. H(2). 3-D Finite element model of support tube

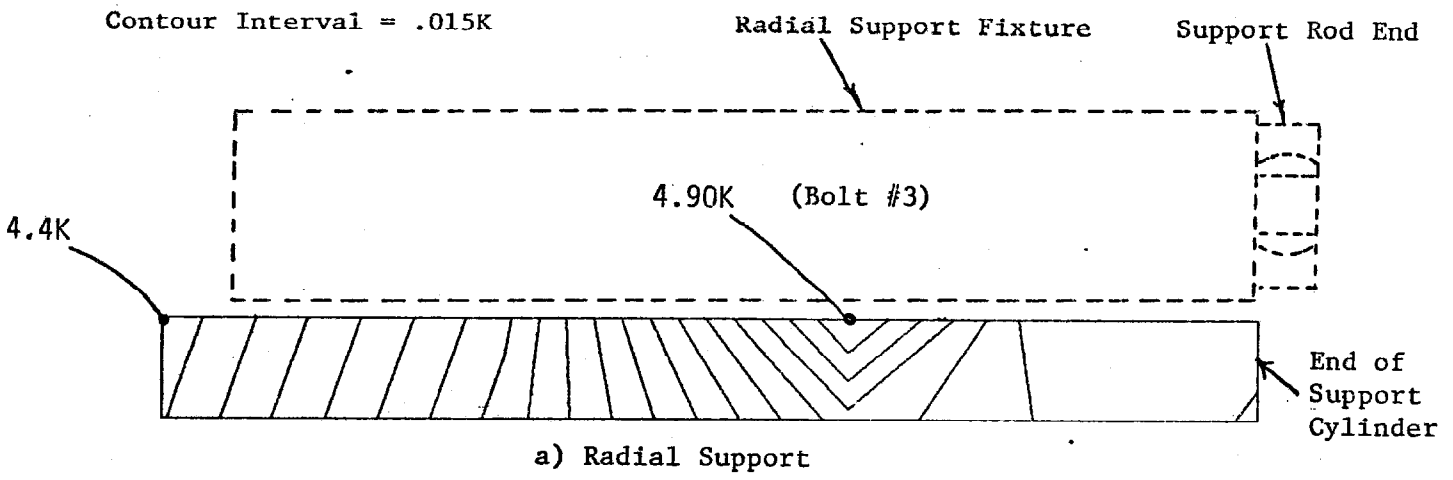

a) Radial Support

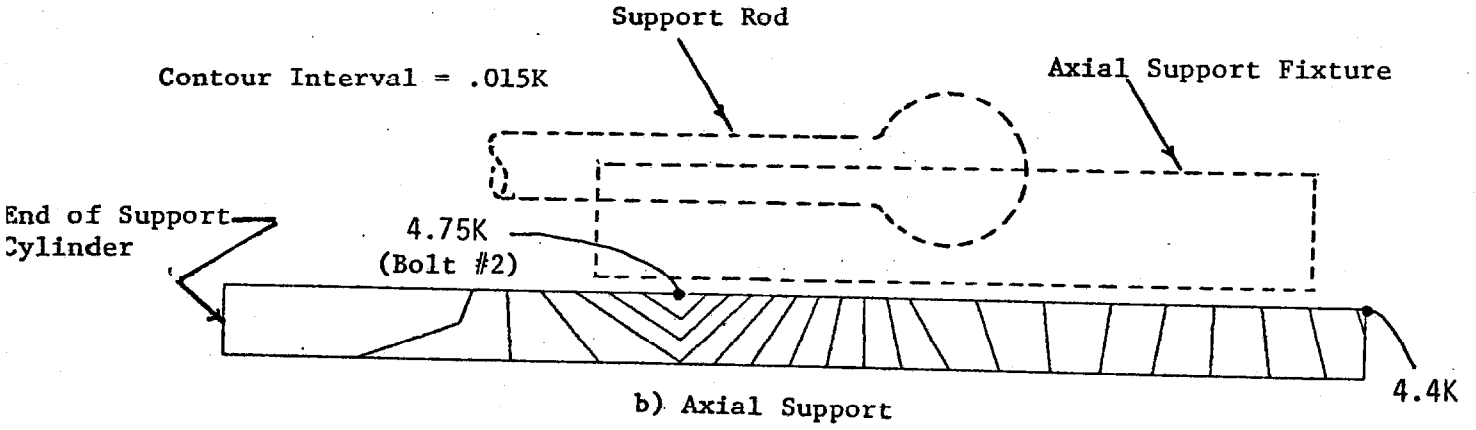

b) Axial Support

Fig. H(3) Temperature Distribution at Support Fixture Locations on Support Cylinder

conduct heat out of the support cylinder. This is reasonable given the relative locations of the bolts and the support pad cooling tube.

The heat flux through the radial and axial support rods for this model is 0.16 W and 0.21 W respectively for the model. These figures are in good agreement with those presented in Appendix M. Figure H(4) shows the temperature distribution calculated along the support rods. Figure H(5) shows the temperature distribution in the support fixtures along an axial cut in the plane of the support rod attachment point.

Finite Element Thermal Model of Solenoid with Concentrated Heat Source

The purpose of this analysis is to determine the maximum concentrated heat leak which the support cylinder can tolerate while maintaining a maximum temperature of 6.5 K.

The Finite Element Model. A finite element model composed of plate elements was constructed to represent one half of the circumferential support cylinder area bounded by the axially oriented cooling tube paths. This model is shown in Fig. H(6). Although originally designed to model a cooling geometry of six axial traverses, the model was easily modified for the current geometry of 24 axial traverses. A single node was assigned a temperature of 6.5 K, as shown in the figure, and a line of nodes representing the cooling tube was assigned a temperature of 4.4 K as indicated. Other edges of the model were assumed insulated.

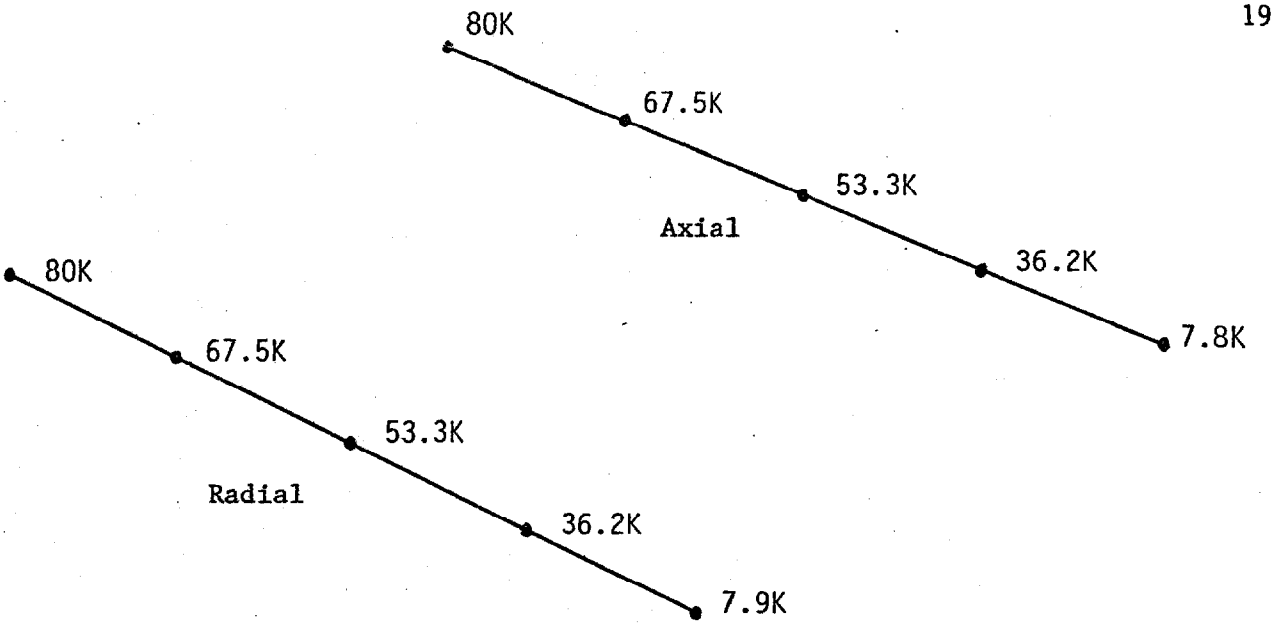

Fig. H(4) Temperature Distribution Along Support Rods

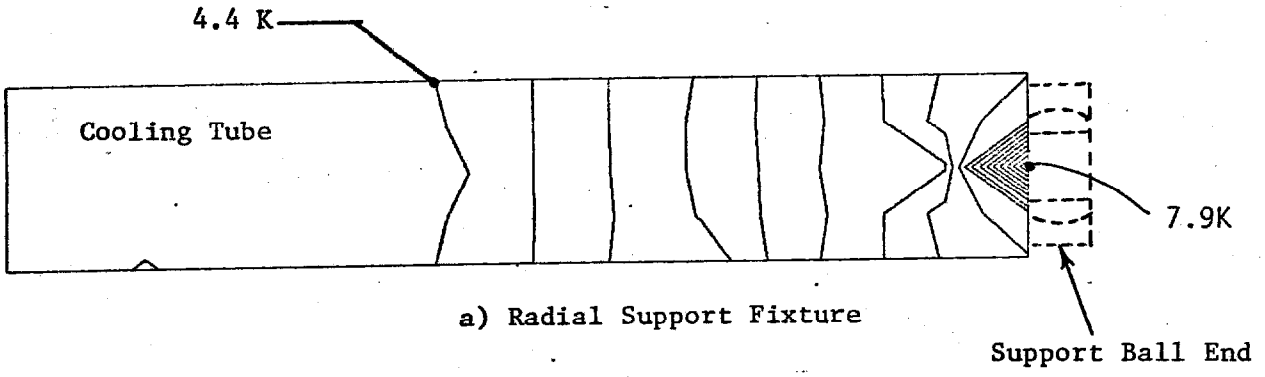

Contour Interval = .2K

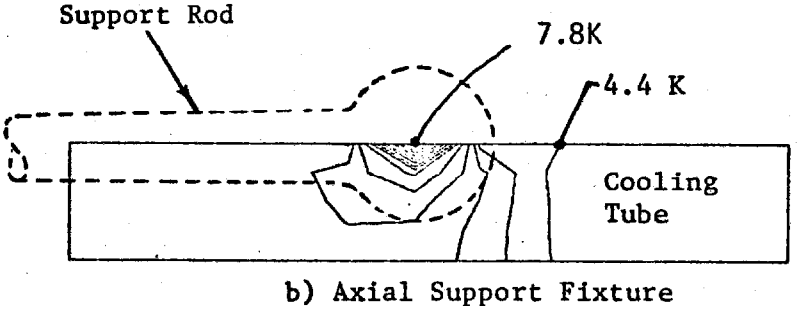

Fig. H(5) Temperature Distribution in Support Fixture in Plane of Support Rod Attachment

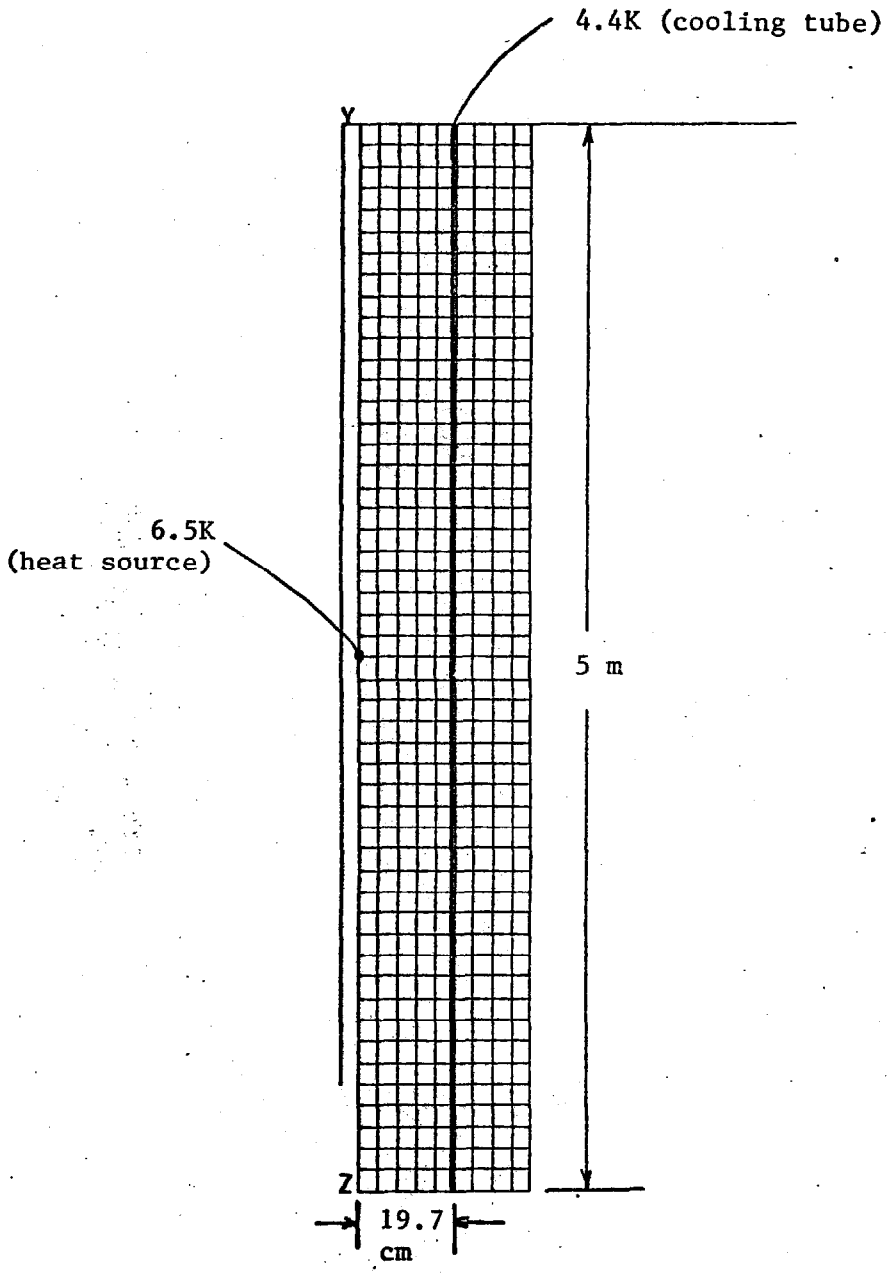

Fig. H(6) Finite Element Support Cylinder Model

This model will accurately represent an external heat flux directly to the support cylinder surface. However, should the heat flux result from a small locally resistive section of conductor, then the heat must transfer through the conductor and insulation to reach the support cylinder, hence, conductor temperature may exceed 6.5 K temperature used here, although conduction through the pure aluminum stabilizer in the direction of winding should provide some help in keeping conductor temperature down.

Results. The ANSYS solution calculated a flux at the 6.5 K nodal location of 0.4 W.

Conclusions

The proposed cooling tube geometry will provide adequate cooling for a ten minute linear charge of the solenoid, with support cylinder temperatures not in excess of 4.90 K. Support pads will operate at a higher temperature, but due to the separate support fixture cooling loop and stainless spacers at the bolted locations will not affect support cylinder temperature greatly. The ^{24} axial cooling paths provide the capability of absorbing a 0.4 W concentrated heat load on the support cylinder as might result from a thermal short.

APPENDIX I: PRESSURE RISE DURING QUENCH

Formulation

The purpose of this section is to estimate the maximum pressure rise in the cooling tube during a quench and hence to choose the appropriate wall thickness for the tube. The inner diameter of the tube is assumed to be 0.79" (20 mm). The cooling circuit, shown in Fig. I(1) with approximately 140 m of tubing is considered.

The approach is to calculate the pressure rise, ΔP, required to expel all the liquid from the cooling tube in a short time, Δt. From the quench calculations (Appendix C) it is known that quench back occurs approximately one second after the quench is started and so we will use $\Delta t = 1s$. The temperature of the fluid is assumed to be the same as the coil.

The ΔP is calculated from Newton's second law:

$$\Delta P = \frac{F}{\pi R^2} = \frac{ma}{\pi R^2} \qquad (1)$$

where

F = force necessary to expel fluid in Δt

R = inner radius of tube

m = mass of fluid expelled

a = acceleration of fluid

Since $a = d^2s/dt^2$,

$$L = 1/2\ a\ (\Delta t)^2 \qquad (2)$$

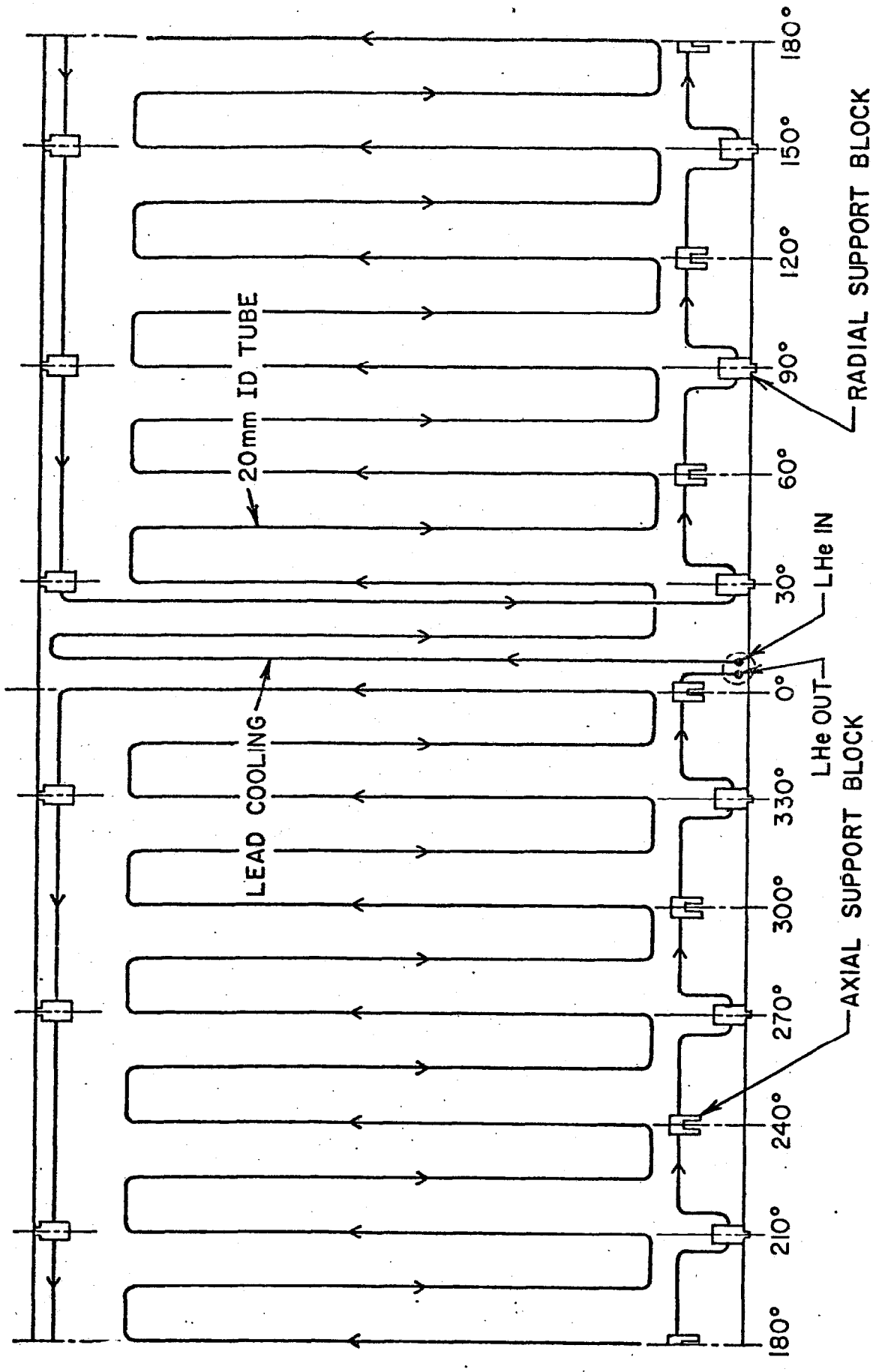

Fig. I(1) Routing of LHe cooling tube on support cylinder

Also $m = \rho \pi R^2 L_1$ (3)

Combining (1), (2) and (3),

$\Delta P = 2\rho L^2 / (\Delta t)^2$

where

L = distance over which fluid is accelerated

ρ = density of 100% LHe at 4.4 K = 121 kg/m^3

The initial (operating) pressure and the relief valve cracking pressure must be added to ΔP to get the maximum total pressure at the quench initiation site.

Relief valves are located at both ends of the cooling tube, in the control dewar approximately 4.5 m from the coil. The total length of the tube involved = 24 (5 m) + 2 (3 π m) + 2 (4.5 m) $\sim$ 150 m, neglecting the effect of the bends.

Two-Way Fluid Acceleration

If both relief valves are set for exactly the same presure, fluid will be accelerated both ways from the quench or L = 150/2.

$P = (2)(121\ kg/m^3)(75\ m)^2/1\ s^2$

$= 1.36$ MPa

$= 200$ psi

$= 13.6$ atm

and P = 13.6 + 1.2 + relief valve cracking pressure 20 atm (300 psia)

One-Way Fluid Acceleration

If the relief valves are not set for the same pressure, one will open before the other and venting will, initially at least, take place through only one vent. In this case L = 150 m.

and ΔP = 5.44 MPa = 790 psi = 53.7 atm

P $\sim$ 60 atm (750 psia)

Wall Thickness

Appendix K gives the sizes of the helium supply and return lines in the chimney. For ease of fabrication, i.e., bending and welding, a wall thickness of 0.125" (3.2 mm) was recommended. A 1" (25.4 mm) OD x 0.125" (3.2 mm) wall aluminum tube is shown to have a code-allowable internal pressure of 180 atm. We recommend using the same tubing, or its metric equivalent, for the cooling tube.

APPENDIX J: THERMAL ANALYSIS OF RADIATION SHIELDS AND LN_2 INTERCEPTS

Performance of the Inner Shield

Total heat load. The heat load into the shield consists of two components:

(i) thermal radiation across the gap of 0.72" (18.3 mm) between the inner vacuum wall and the inner shield. Using 30 layers of NRC-2 300 Angstrom superinsulation, a heat flux of 0.63 W/m^2 (58 mW/ft^2) is possible (see Appendix L). To include the effects of penetrations and corners, 80 mW/ft^2 is used for calculation.

Total heat load = (.080 W/ft^2) (2 π x 57.25" x 195.5")

= (.080 W/ft^2) (488.4 ft^2)

= 39.1 W

(ii) conduction through the shield supports:

(a) the leaf-spring type standoffs: The heat leak through each of these G-10 standoffs, which is designed to take at least 25 lbs in compression without appreciable deflection, is

$$Q = 2\left(\frac{bt}{\ell}\right) \int_{78}^{300} K_{k(T)}dT$$

where

b = width of the standoff ⇝ 3/4" (19 mm)

t = thickness of the standoff ⇝ 3 x .032" (2.4 mm)

ℓ = conduction path ⇝ 2.5" (63.5 mm)

$$\int_{78\ K}^{300\ K} k(T)dT$$ = thermal conductivity integral from 300 K to 78 K for G-10 (parallel to glass fibers) = 1.41 W/cm

$$Q = 2\left(\frac{0.24 \times 1.9\ cm^2}{6.35\ cm}\right)\ (1.41\ W/cm)$$

$$= 0.20\ W$$

There are a total of 170 standoffs so

$$Q_{total} = 0.20 \times 170$$

$$= 34.4\ W$$

(b) the top support: as the worst case, assume stainless steel 5/32" (4 mm) bolts as supports, each 3/4" (19.1 mm) long.

$$Q = \frac{.25\ \pi\ (0.4\ cm)^2\ (27.5\ W/cm)}{1.91\ cm}$$

$$= 1.8\ W$$

Eleven of these supports gives $\sim$ 19.8 W

The total heat leak into the inner shield

$$= 39.1 + 34.4 + 19.8$$

$$= 93.3\ W$$

Maximum Temperature in Shield. If there were two cooling loops 20" (0.5 m) from each end of the shield, then maximum thermal path would be 2 m. We assume that the shield at the cooling loop is held at 78 K and that the total heat load to the shield may be averaged out over the entire length of the shield.

The maximum temperature Tmax, found at the center of the shield, can be calculated from:

$$\int_0^{2\ m} (Q/\ell)\ z\ dz = A \int_{78\ K}^{Tmax} k(T)dT$$

A = cross section area for heat transfer

= (2 π x 57.25") (0.080") = 28.8 in^2 (186 cm^2)

Q/ℓ = 93.4 W/5m = 18.7 W/m

$$\int_{78\ K}^{Tmax} k(T)dT \simeq (k_{av})\ (Tmax - 78)$$

where k_{av} for aluminum ∿ 80→90 K

≃ 250 W/m-K

$$(Tmax - 78) = \frac{(18.7\ W/m)\ (2\ m)^2}{2} \frac{1}{(0.0186\ m^2)\ (250\ W/m\text{-}K)}$$

= 8.0 K

Tmax= 86 K

Performance of Outer Shield

The outer shield is evaluated in a similar fashion and the maximum temperature in the center is found to be 86.5 K.

Peformance of End Shields.

There are 18 end shields at each end. Each is made with 0.060" (1.5 mm) thick OFHC copper and cooled by the same nitrogen supply circuit that cools the support intercepts. Heat load into each shield (a) by conduction is equal to that via six leaf-spring style standoffs: .20 x 6 = 1.20 W, (b) by thermal radiation is (using 0.150 W/ft^2 beause of penetrations) 1/18 (0.150 W/ft^2) (2 π) (5') (7/12') = 0.15 W. The total heat load is 1.35 W. The distance of the farthest corner from the cooling tube on the copper shield is approximately 21 in (53.34 cm). Using the same analysis as before, the maximum temperature on the shield is estimated to be about 87 K.

LN_2 Temperature Intercepts on the Support Columns

The purpose of this section is to verify that it is reasonable to assume the nitrogen intercepts on the magnet supports operate at 80 K. The present design calls for direct feeding of liquid nitrogen through an annular region of approximately 1/2" (12.7 mm) long along the length of each radial and axial support column. The surface area for heat transfer is approximately (π/2) in^2 (10 cm^2). For liquid nitrogen, the heat transfer capacity for nucleate boiling is $\sim$ 0.6 W/cm^2; hence there is enough surface area for removing 6 W of heat. The calculated heat conduction down an axial support is 3.5 W and 2.4 W for a

radial one. The the cooling scheme therefore has sufficient operational margin (especially since our system uses forced flow).

APPENDIX K: DESIGN OF CHIMNEY AND CONTROL DEWAR

CHIMNEY

Physical Arrangement

Figure K (1) shows the over-all arrangement, and Fig. K(2) is a cross-section. The chimney is basically an 8" (200 mm) vacuum pipe with cryogenic lines and superconducting bus inside. The vacuum pipe and liquid nitrogen lines are stainless steel with transition joints at the magnet cryostat. The radiation shield is copper and the helium lines are aluminum. The current bus is two parallel strands of magnet conductor, wrapped with insulation and clamped to the helium supply line.

Pressure Ratings of Components

Vacuum pipe. The vacuum pipe is ASME Code designed for vacuum load (15 psi external pressure). From Section VIII, Paragraph UG-28, considering the vertical section, D_o = 8" (200 mm), L = 84" (2134 mm). With t = 0.125" (3.2 mm), A = 0.0003 and for 304 stainless B = 4200. The allowable external pressure is P_a = $4B/3\ (D_o/t)$ = 87 psi. The wall thickness could be less, but 0.125" is chosen because of the movable detectors nearby. The vacuum pipe is Code rated for an internal presure of P = SEt/(R + 0.6 t) = 510 psi where S = maximum allowable stress = 17.5 ksi; E = weld efficiency = 0.95; t = wall thickness = 0.125"; R = tube radius = 4".

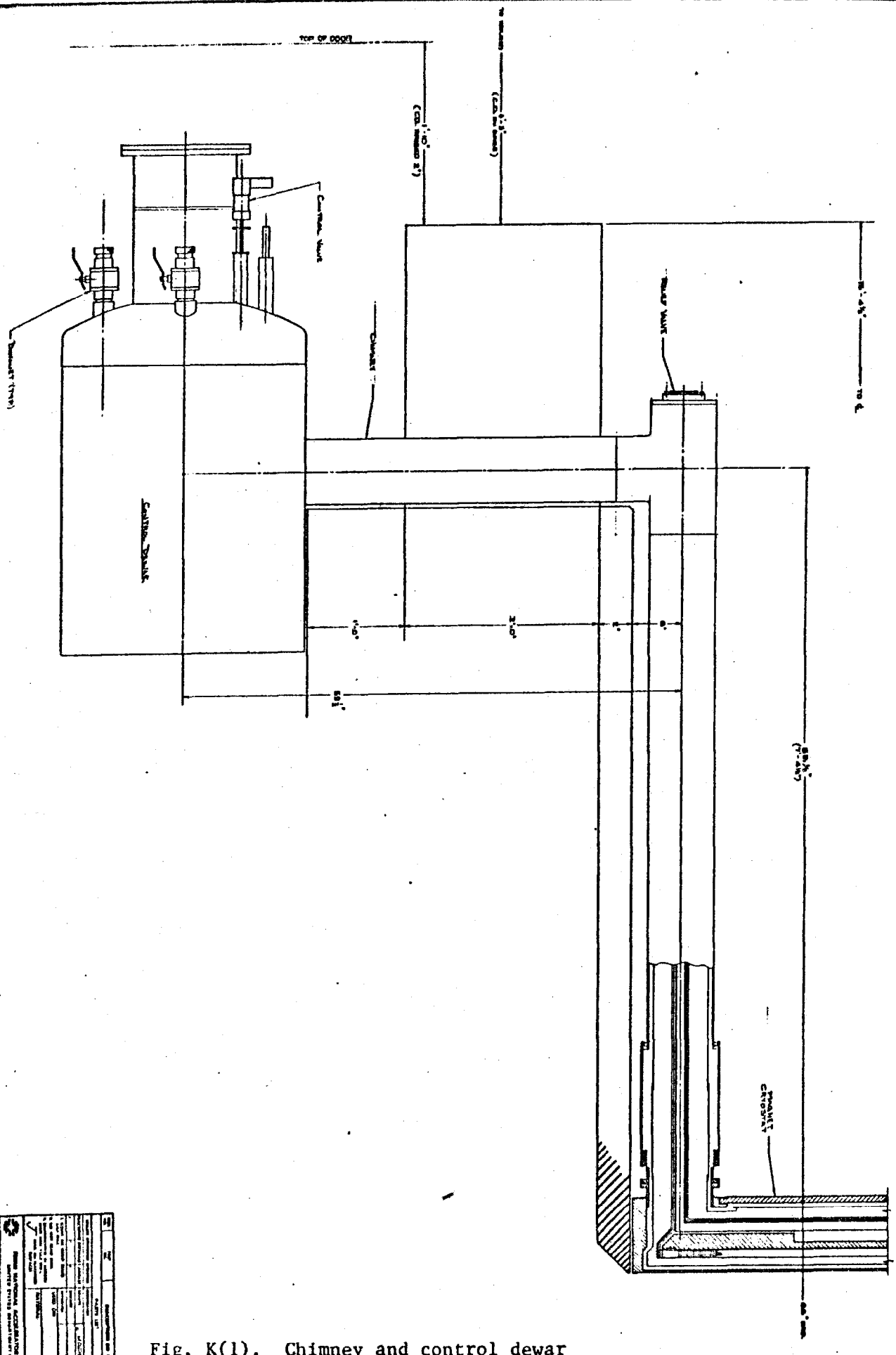

Fig. K(1). Chimney and control dewar

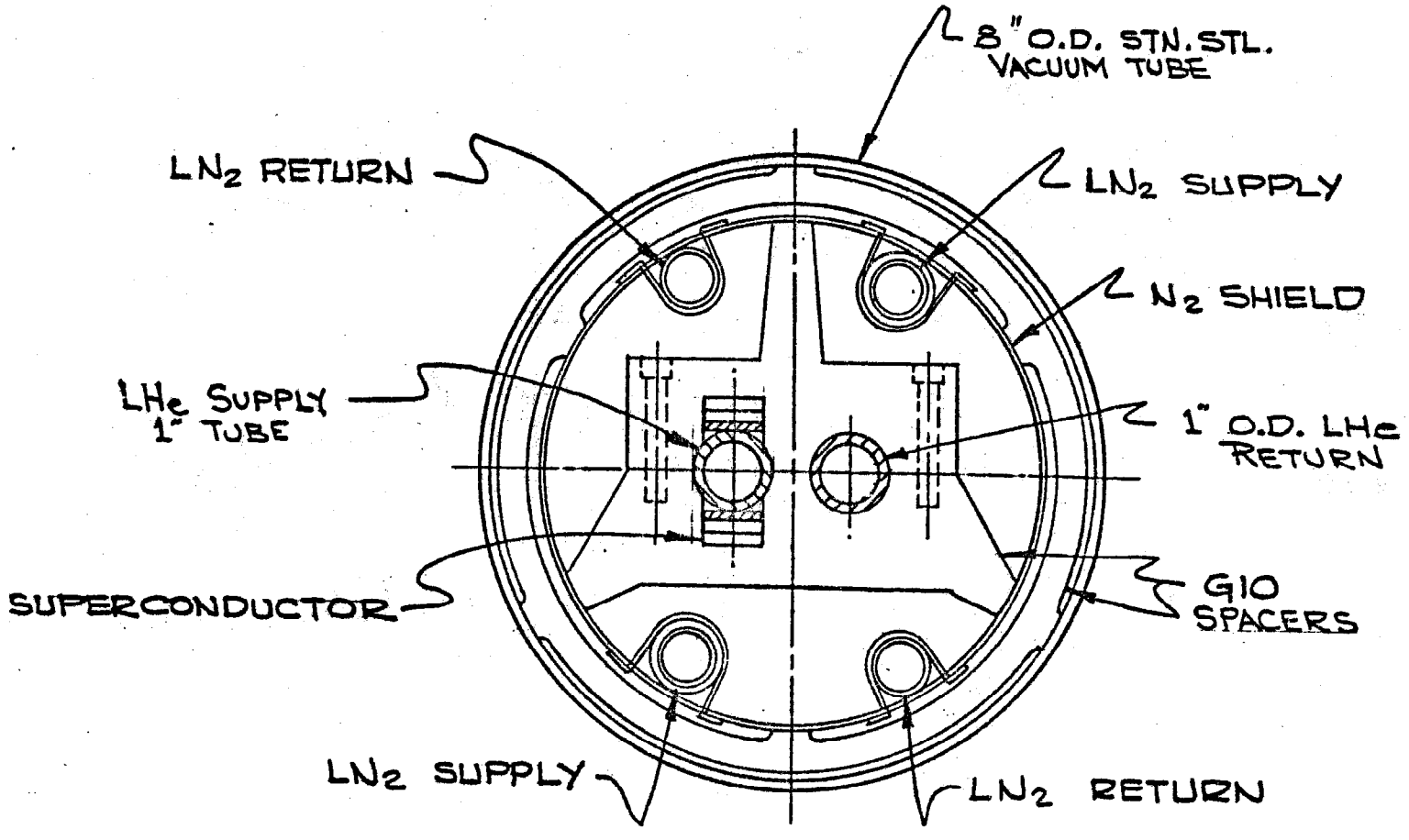

Fig. K(2). Chimney cross section

1 Female Bayonet Ass'y
2 Control & Shut-Off Valve Ass'y
3 Cryogenic Check Valve
4 Alum. to Stainless Stl. Transition
5 1" Vacuum Valve
6 Vacuum Seal-Off Valve
7 Ion Gage
8 Thermocouple Vacuum Gage
9 Electrical Feed-Thru
10 Temperature Sensor

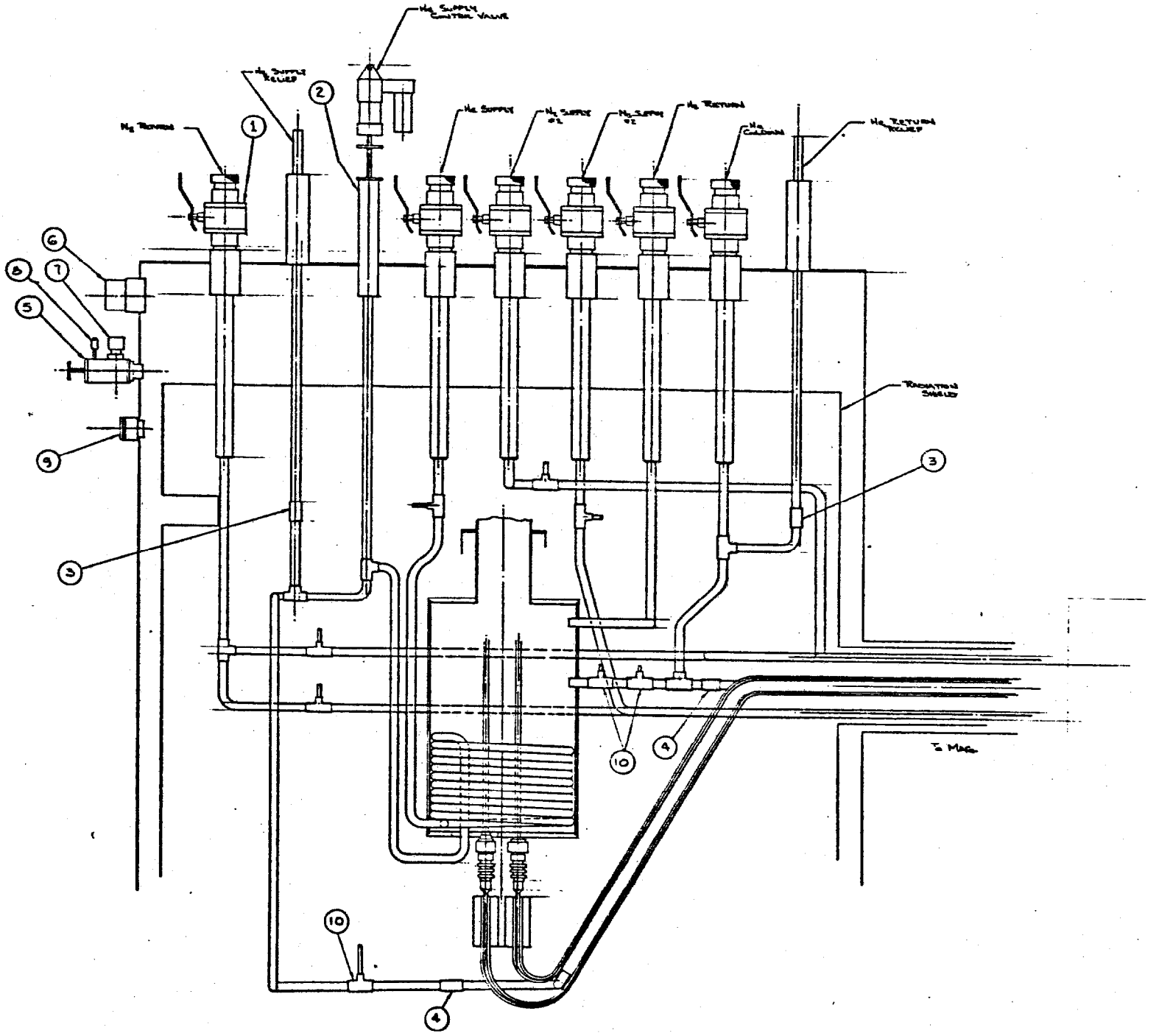

Fig. K(3). Control dewar schematic

Nitrogen lines. These lines are all 0.75" (19 mm) OD 304 stainless tubing. A wall thickness of 0.035" (0.9 mm) has been chosen and can be shown to be in accordance with the USA Standard Code for Pressure Piping, USAS B31.1.0 for an internal pressure differential of 2800 psi (186 atm) and an external pressure differential of 750 psi (50 atm). We choose this wall thickness for ease of fabrication.

Helium return line. This line is 1" (25.4 mm) 5083 aluminum tubing. The wall thickness was chosen for ease of welding during assembly. With a wall thickness of 0.125" (3.2 mm) the line is Code rated for 2644 psi (180 atm) internal pressure and 1688 psi (115 atm) external pressure at 77 K and 20% less at 310 K.

Helium supply line. The supply line is the same size as the return line, but with flat plates welded to the tubing to which the electrical bus is clamped.

Venting of Vacuum Space Through Chimney.

The insulating vacuum of the storage dewar, magnet cryostat and chimney is vented through relief valves on the control dewar and a burst disk at the top of the chimney. These pressure relief devices are primarily to protect the inner vacuum shell of the magnet cryostat against collapse, the critical pressure for which is about 3 psi (0.2 atm). (See Appendix F). We propose to use a spring-loaded resealable disk.

As a worst-cast failure mode for venting the vacuum space a simultaneous rupture of the helium supply line and one of the nitrogen supply lines is postulated. This discharges helium into

the cryostat vacuum space at 50 g/s, which is the maximum flow rate possible from the compressor. A maximum nitrogen flow rate of 50 g/s was assumed. A gas temperature of 300 K was assumed. If the vent system removes gas at 100 g/s the pressure in the vacuum space will not rise. The chimney has a venting area of 11.2 in^2 (72.2 cm^2). The steady state pressure drop up the chimney is approximately 2 x 10^{-3} psi (14 Pa). A preliminary calculation of the pressure required to accelerate the gas up the chimney gives a value of about 150-200 Pa. It therefore appears that the pressure drop is negligible, but further calculations are required.

In the Collision Hall the chimney vent is connected to a vent pipe which leaves the hall through a 24" (600 mm) opening in the ceiling which extends to the top of the berm. The vent pipe is 23 ft (7 m) long, and 4" (100 mm) in diameter. The preliminary calculations described above were modified to include the vent pipe, but the pressure drop was still negligible.

CONTROL DEWAR

Physical Arrangement

Figure K(1) is an overall view of the control dewar and Fig. K(3) is a schematic view. The vacuum vessel is a 30" (760 mm) diameter stainless steel shell 36" (914 mm) long with a dished head on the top and a flat, grind-off closure plate on the bottom. The dished head has six standard Fermilab Energy Saver bayonets; helium supply, helium return, helium cooldown, two nitrogen supply

and nitrogen vent. The nitrogen cooled shield is copper, 26" (660 mm) in diameter. The stainless helium vessel is 12" (300 mm) in outer diameter, 20" (500 mm) long, and has a 4" (100 mm) neck connecting to a room temperature "top hat". Gas-cooled current leads enter the top of the helium vessel. Two superconducting bus leave the helium vessel through insulated feed-throughs in the bottom of the vessel and join the helium supply pipe at the bottom of the dewar. It is suggested that a superconducting wire go through the feed-throughs. The helium supply line forms a heat exchanger coil inside the helium vessel. A standard Fermilab motor actuated J-T valve is located in the helium supply line after the heat exchanger. The top hat contains relief vents for the helium vessel and there are also pressure relief lines on the helium supply and return lines.

Pressure Ratings of Components

Vacuum vessel. The vessel is designed in accordance with the Code. For the shell with D_o = 30", L = 36" and t = 0.125" (3.2 mm) the maximum allowable external pressure P_a = 22.2 psi (1.48 atm) which is satisfactory for the vacuum load. Using Section 33(e) of the Code for the dished head, with R_o = 24" (600 mm) and t = 0.125"; A = 0.033, B (for 304 stainless) = 15000 and P_a = 41.2 psi (2.75 atm). The bottom plate has a closure joint that can be easily ground off with the magnet installed in the detector. A flat plate is required because of over-all and interior height limitations on the control dewar. It is clear that the maximum bending stress and deflection occur with a simply supported edge.

Using

$$\sigma_c = \text{stress at center of dish}$$

$$= \frac{6}{t^2} \frac{PR^2 (3 + \nu)}{16}$$

and

$$y_c = \text{maximum deflection}$$

$$= \frac{PR^5 (5 + \nu)}{64 D (1 + \nu)}$$

where

$$D = Et^3/12 (1 - \nu^2)$$

For t = 9/16" (14.3 mm), R = 15" (381 mm), p = 15 psi (1 atm), ν = 0.3.

$$\sigma_c = 13200 \text{ psi } (91 \text{ MPa})$$

$$y_c = 0.105 \ (2.7 \text{ mm})$$

The maximum Code-allowable stress for welded 304 stainless is 16000 psi, so 9/16" plate is acceptable.

Helium vessel. This vessel is Code designed for 15 psi (1 atm) external (internal vacuum) and 100 psi (6.7 atm) internal pressure differential. For the shell, D_o = 12" (300 mm), L = 20" (508 mm) and t = 0.0625" (1.6 mm), the maximum allowable external pressure is 25.3 psi; A = 0.00028, B = 3800, $P_a = 4B/3 (D_o/t)$. This wall thickness has a Code-allowable internal pressure P_a = (SE)t / (R + 0.6 t), which for S = 16000 psi / 110 MPa (304 stainless at room temperature) and E = 0.80 is 132 psi (8.8 atm). The flat top and bottom plates, under a simply-supported-edge/

worst case criteria have σ_c = 14100 psi (97 MPa) and y_c = 0.018" (0.46 mm) for a plate thickness of 9/16" (14.3 mm). The 4" (100 mm) neck with L = 18" (460 mm) and t = 0.035" (0.9 mm) has an external allowable pressure of 35 psi (0.24 MPa) and an internal allowable pressure of 111 psi (0.77 MPa). The weight of the helium vessel (metal + LHe) is about 50 lbs (22 kg), which is a negligible tensile stress on the neck.

Piping. The piping is considered under the chimney section of this appendix and the lines in the control dewar have the same dimensions as those used in the chimney, with the exception of the helium supply line which is stainless steel 0.75" (19 mm) ϕ x 0.035" (0.9 mm) wall from the bayonet to an adapter after the relief line tee.

Heat Exchanger Design. Assume that the helium supply line is at 1.8 atm and that the helium return line and the helium vessel are at 1.2 atm. Assume also that the quality of the supply and return streams is less than one, i.e. the streams have a non-zero liquid fraction. The temperatures of the streams are then 4.91 K and 4.42 K.

From Scott,* for a tube/evaporating liquid heat exchanger

$$UA = q \ln \frac{\Delta Tw}{\Delta Tc} / (Tw - Tc)$$

*R.B. Scott, "Cryogenic Engineering", D. Van Nostrand, Princeton, NJ, (1967), p. 23.

where

U = overall heat transfer coefficient

A = heat exchanger area

q = rate of heat transfer to boiling liquid

ΔT_w = warm stream temperature - bath temperature

ΔT_c = cold stream temperature - bath temperature

$T_w - T_c$ = warm stream temperature - cold stream temperature

For the expected head loads (Appendix M), a mass flow of 8 g/s, magnet inlet and exit qualities of 82% liquid and 75% liquid respectively should be adequate and is assumed here. For a typical case

q = heat picked up in supply transfer line = 27 W (see Appendix M)

T_w = 4.91 K

T_c = 4.88 K (subcooled)

ΔT_w = 4.91 K - 4.42 K = 0.49 K

ΔT_c = 4.88 K - 4.42 K = 0.46 K

and UA = 60 W/K

To get A, we must calculate U, from

$$\frac{1}{U} = \frac{1}{u_i} + \frac{1}{u_w} + \frac{1}{u_o}$$

where

u_i = heat transfer from fluid in tube to the wall

u_w = heat transfer across wall

u_o = heat transfer from wall to outside fluid

with

$$u_i = 0.023 \frac{k}{D} \left(\frac{DG}{\mu}\right)^{0.8} \left(\frac{C_p \mu}{k}\right)^{0.4}$$

where

k = thermal conductivity

μ = viscosity

C_p = specific heat at constant pressure

D = tube diameter

G = mass velocity of fluid in tube

For helium at 1.8 atm and 4.91 K (saturated liquid) $k = 0.211 \times 10^{-3}$ W/cm-K, $\mu = 27.3 \times 10^{-6}$ g/s-cm^2, $C_p = 14.11$ J/g-K. At $D = 1.7$ cm and $\dot{m} = 10$ g/s, $G = 4.406$ g/s-cm^2.

then

u_i = 0.0813 W/cm^2-K

u_w = k (wall material) / wall thickness

= 3.94×10^6 W/cm^2 K (for stainless tubing with 0.035" wall)

u_o = (q/A) / ΔT, where (q/A) is the nucleate boiling heat flux at $\Delta T = 0.05$ K and 1.2 atm. From Smith* (q/A) = 0.0075 W/cm^2.

*R.V. Smith, Cryogenics 9:11 (1969)

$= 0.15 \quad W/cm^2\text{-}K$

Assuming inside and outside areas the same, i.e. not finned tubing

$$\frac{1}{U} = \frac{1}{0.0813} + \frac{1}{3.94 \times 10^6} + \frac{1}{0.15}$$

and $U = 0.0527 \ W/cm^2\text{-}K$

The heat exchanger coil as presently designed has a length of approximately 35 ft (10.7 m), A = 990 in^2 (6380 cm^2) and UA = 342 W/K.

APPENDIX L: RECOMMENDED THERMAL INSULATION SCHEME

This note describes the insulation schemes for (a) the space between the vacuum shell (300 K) and the nitrogen (78 K) radiation shield (b) the space between the radiation shield (78 K) and the coil and outside support cylinder (4.2 K). NRC-2^R superinsulation made by King-Seeley Thermos Co.* of Massachusetts, U.S.A., is the multilayer insulation chosen on account of its superior performance and relatively low price.

Between the inner vacuum shell and inner radiation shield

Use 30 layers of 300-Angstrom NRC-2 superinsulation in a gap 0.72" (18.3 mm) wide, giving a density of $\sim$40 layers per inch. The estimated heat load could be 0.63 W/m^2 (58 mW/ft^2). For heat load calculations we will use 80 mW/ft^2.

Between the outer vacuum shell and outer radiation shield

It is recommended that we move the outer shield inwards such that we may employ 40 layers of 300-Angstrom NRC-2 in a 1 inch gap for a heat load of 0.49 W/m^2 (46 mW/ft^2).

*King-Seeley Thermos Co.
37 East Street
Winchester, Mass 08190
U.S.A
Phone: (617)-727-8300

If the existing gap width (23/32") must be kept, again use 30 layers of 300 Angstrom NRC-2. This is the optimal density and number of layers to be used.

Between the vacuum shell and the pie-shaped end shields

Use 20 layers of 300-Angstrom NRC-2 superinsulation in the 1/2" (12.7 mm) gap, a density of $\sim$ 40 layers per inch. The estimated heat load $\sim$ 1.2 W/m^2 (112 mW/ft^2).

Between the outer radiation shield and the outside support cylinder

A scheme developed by E. Leung et. al.,** to reduce the heat load in multi-shield vessels, by using pure aluminum tape, is applicable here. This scheme was used on the superconducting Chicago Cyclotron Magnet and it worked quite well. The 5083 aluminum surface is to be taped with 3M industrial aluminum tape #625 and then wrapped with 12 layers of 500-Angstrom NRC-2. The extra thickness of aluminum on the superinsulation would help to reduce transmission of infra-red radiation. The estimated heat load for this scheme is < 1.2 mW/ft^2 (13 mW/m^2). One must make sure that the outermost layer of the NRC-2 does not touch the inside of the outer radiation shield.

**E.M.W.Leung, R.W.Fast, H.L.Hart and J.R.Heim, "Advances in Cryogenic Engineering, Vol. 25", Plenum Press, New York (1980), p. 489.

Between the inner radiation shield and the inner surface of the coil

A thin sheet of insulating material (e.g. G-10 or G-11) is secured on the coil surface with the aluminum applied to it. This is to provide additional electrical insulation between the Kapton-wrapped conductor and the conductive tape. Twelve layers of 500-Angstrom superinsulation are wrapped around the outside of the inner radiation shield. It is important to make sure that the superinsulation does not touch the tape surface.

APPENDIX M: HEAT LOAD INTO CRYOGENIC SYSTEMS

Heat Load to 4.5 K

In this section we evaluate the heat loads from all the components of the system shown in Fig. M(1), starting at the bayonets on the valve box, with all the U-tubes in place. The heat leak of individual components is calculated or estimated and summed for the entire system. These heat load values should be taken as reasonable lower limits, since fabrication errors or poor craftsmanship can easily inflate them by factors of two or more.

Bayonets. The standard Energy Saver bayonet, with a 2 ft (600 mm) stinger, is used throughout the system. The heat leak of a disconnected female bayonet is 0.69 W and of a male/female bayonet pair is 1.33 W. A female bayonet with a vacuum plug is 1.39 W.

U-tubes. Energy Saver style U-tubes, with modified horizontal and vertical dimensions are used. The inner line is 1.25" (32 mm) OD tubing. The line is not shielded with liquid nitrogen, but uses multilayer insulation only. The heat load of such a U-tube has a component due to the stinger and a component proportional to the length. The stinger component is included here with the value for the bayonet and the length component is 0.10 W/ft (0.328 W/m).

Storage dewar. The 2000-L storage dewar will be built to the ASME Pressure Vessel Code for a working pressure of 8 atm (105 psig). It has not yet been designed or fully specified, but will

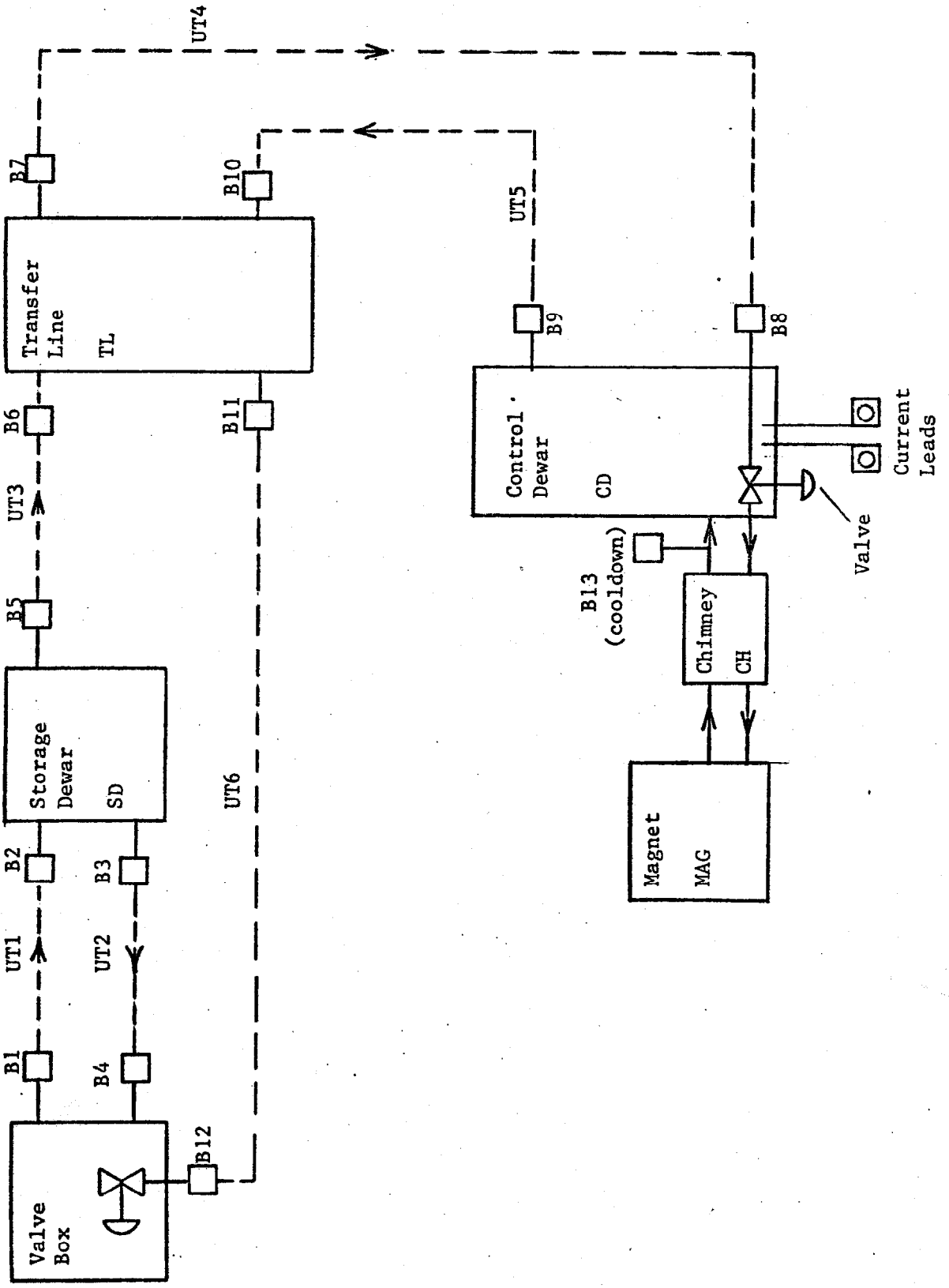

Fig. M(1). Liquid helium circuit

either have a neck large enough to accomodate three U-tubes, liquid level probes and reliefs or will have individual bayonets or feed-throughs. With a boil-off of 5% of the capacity per day (a standard 1000-L low-pressure dewar might have a boil-off of 1% per day), the heat load is 1.5 W.

Transfer line. The transfer line consists of a feed can, an end box and the horizontal portion. It contains two liquid nitrogen lines, which shield the inner lines, helium supply and return lines. There are two nitrogen and two helium bayonets in the feed can and end box. The horizontal distance into the Collision Hall is approximately 80 ft (25 m). At a linear heat flux of 0.01 W/ft (0.033 W/m) the transfer line to the Collision Hall is estimated as 0.8 W. Due to the field assembly of the line, we shall use 2 W for the transfer line. The final design (yet to be done) will determine whether this heat load appears on the supply or return line.

Control dewar. The control dewar contains a 35-L liquid helium vessel with a heat exchanger, helium supply, return and cool-down bayonets, motor actuated control valve and a pair of 5 kA current leads exiting through a 4" (100 mm) diameter neck. The low-temperature components are shielded by a liquid nitrogen cooled shield.

The estimated heat leak of the stand-alone control dewar is:

Female Bayonets (3: B8, B9, B13)	2.1 W
Control valve stem	0.5 W
Current leads (5 kA at 2.8 L/h-kA-pr)	14 L/h

Neck *	0.3 W
Helium supply relief line †	0.3 W
Helium return relief line	0.3 W
Radiation §	Negligible
	3.5 W + 14 L/h

without the bayonets the heat load is 1.4 W + 14 L/h.

Chimney. The 8" (200 mm) diameter chimney is a transfer line between the control dewar and magnet cryostat. It has helium supply and helium return lines, two aluminum-stabilized conductors, two liquid nitrogen supply lines and two nitrogen return lines which shield the low temperature lines. It has insulating vacuum common with the control dewar and magnet cryostat, and so has no bayonets. The expected heat leak is 0.033 W/m for each helium line or 0.22 W for the 3.25 m chimney.

*Conduction (4"Ø x 0.030 wall x 11") $= \frac{A}{L} \int_{4.2}^{77} k(T)dT = \frac{2.42\ cm^2}{28\ cm}$ (3.18 W/cm)

†Conduction (1" Ø x 0.032 wall x 26") $= \frac{A}{L} \int_{4.2}^{300} k(T)dT = \frac{0.65\ cm^2}{66\ cm}$ (30.68 W/cm)

§Radiation (4 mW/ft^2, 26" Ø x 26" long) = .06 W

Since the joint between the chimney and magnet cryostat must be made after installation in the detector, use 0.5 W for each line.

Magnet cryostat. The primary components of the heat load are conduction from radial and axial supports, radiation and joule heating in the conductor joints.

Axial supports. The axial supports are intercepted with flowing liquid nitrogen. If we assume that the intercepts are at 80 K then the conduction heat load per support is $(A/L) \int k\,(T)\,dt$, with $A = 1.62\ cm^2$, $L = 23$ cm, $\int k\,(T)\,dt = 3.5$ W/cm for Inconel 718. This is 0.25 W per support and 1.5 W for all six supports.

Radial supports. The radial supports are also intercepted by flowing liquid nitrogen. Assuming an intercept temperature of 80 K and with $A = 1.12\ cm^2$, $L = 20$ cm, the heat load per support is 0.20 W and for all 24 supports is 4.8 W.

Radiation from outer shield. Using 3M aluminum tape on the surface of the outer support cylinder plus 12 layers of NRC-2 (500 Angstrom), the heat flux can be as low a 1.5 mW/ft^2 (16 mW/m^2) and 3.0 mW/ft^2 can easily be achieved. The surface area of the outer support cylinder is π (120") (196") = 513 ft^2 (47.6 m^2) and so this component of the heat load (at 3 mW/ft^2) is 1.54 W.

Radiation from inner shield. At 3.0 mW/ft^2 (32 mW/m^2) this component is 1.54 W.

Radiation from shield ends. Due to difficulty in properly insulating this area, assume a heat flux of 30 mW/ft^2 (320 mW/m^2). The heat load on each annular coil end (4 ft^2 of surface area) is 0.120 W and for both ends 0.24 W.

Conductor joints. Assuming an individual conductor piece length of 500 m, the coil will contain 16 joints. This will lead to joule heating of $(5000\ A)^2\ (6.5 \times 10^{-10}\ \Omega/\text{joint})$ (16 joints) = 0.26 W.

The magnet cryostat heat load is

Axial supports	1.5 W
Radial supports	4.8 W
Radiation	3.3 W
Joints	0.3 W
Total	9.9 W

Heat Load Summary

Item see Fig. M(1)	Heat Load to 4.4 K
B1	1.3 W
UT1 (4 m)	1.3 W
B2	1.3 W
B3	1.3 W
UT2 (4 m)	1.3 W
B4	1.3 W
SD	1.5 W
B5	1.3 W
UT3 (4 m)	1.3 W
B6	1.3 W
TL	2.0 W
B7	1.3 W
UT4 (4 m)	1.3 W
B8	1.3 W
CD (operating)	1.4 W + 14 L/h
CH	1.0 W
MAG	9.9 W

B9	1.3 W
UT5 (4 m)	1.3 W
B10	1.3 W
B11	1.3 W
UT6 (4 m)	1.3 W
B12	1.3 W
B13	1.3 W
Total	≈ 40 W + 14 L/h

This can be further summarized:

Magnet cryostat, chimney, control dewar	12.3 W
	+ 14 L/h
Storage dewar	1.5 W
Transfer line, U-tubes, bayonets	26.7 W

Heat load to 77 K - Fig. M(2)

Tank. A liquid nitrogen tank located outside the east side of the BØ Assembly Hall, filled by the commercial vendor, provides liquid nitrogen for the refrigerator and magnet. A tank in good condition should have a heat load of 0.5% per day. Using a surplus 2000 gal tank at 1% per day is a heat load of 140 W.

Bayonets. The bayonets used are the same as those used for LHe service, the standard Saver design. The heat leak of the female bayonet is 0.62 W, of a male/female pair is 1.19 W, and of a male bayonet with vacuum plug is 1.24 W. The coupling between the tank and the liquid header is estimated as 5 W.

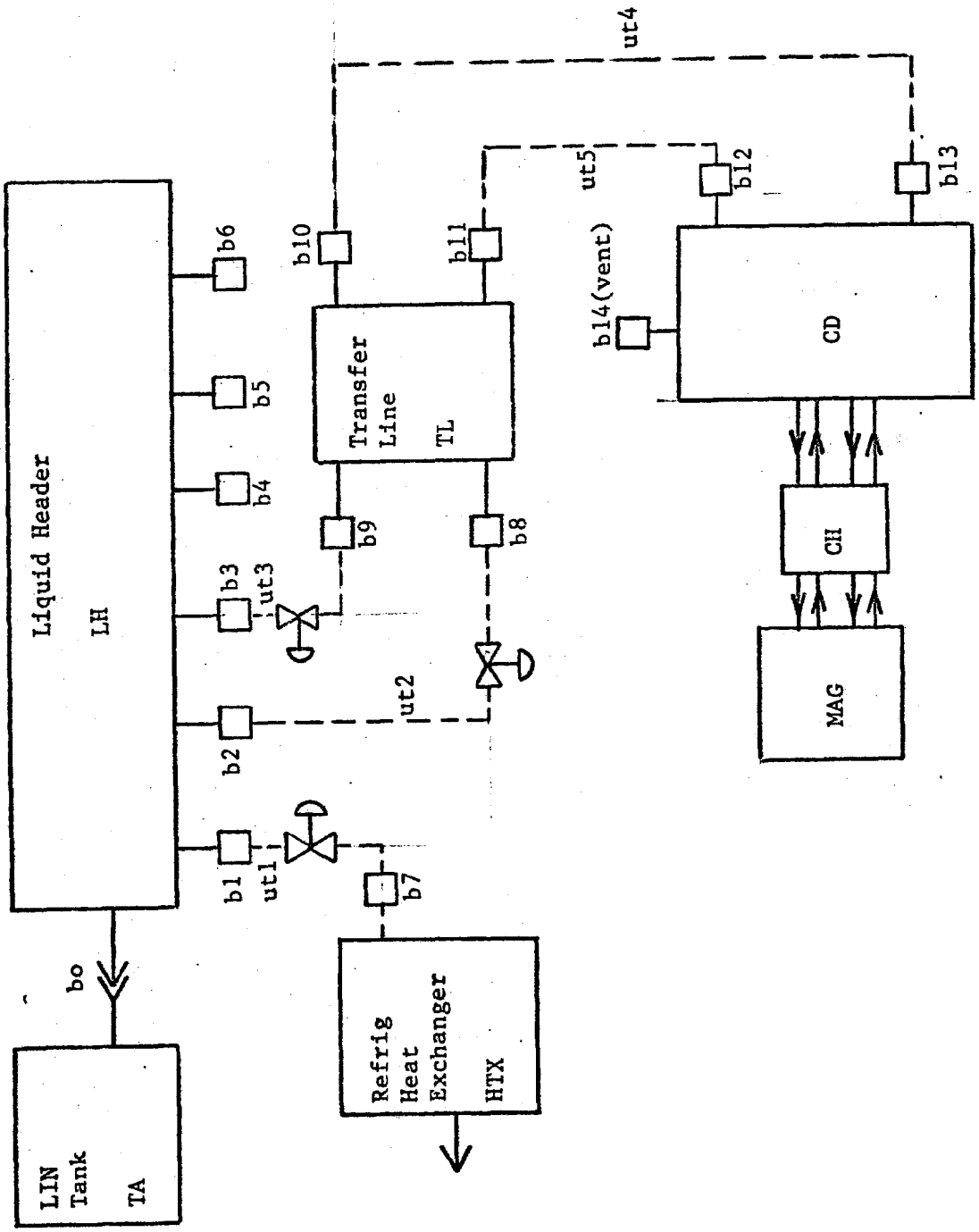

Fig. M(2). Liquid nitrogen circuit

Liquid header. This is an insulated line with a through-the-wall penetration and a fitting to connect to the bulk tank. It has several (approximately 6) vertical risers with bayonets for liquid withdrawal. The heat load of just the line itself with 1.0 W/m (vacuum and multilayer insulation) and a total length of approximately 38 ft (12 m) is 12 W.

U-tubes. Standard Energy Saver U-tubes with a linear heat load of 0.080 W/ft (0.262 W/m) will be used. Three of the U-tubes are special with flow control valves, these are expected to have an additional heat load of 0.7 W.

Refrigerator, heat exchanger #1. The liquid nitrogen usage is a function of helium mass flow, and hence of helium refrigeration. For the helium heat load given previously the nitrogen usage is expected to be 4 L/h.

Transfer line. The transfer line has a linear heat load of 0.155 W/ft (0.51 W/m) or 12.8 W for a 25 m line.

Control dewar. There are two nitrogen supply bayonets and one nitrogen vent bayonet in the control dewar. The dewar has a shield, with 40 layers of multilayer insulation, cooled by the return line. The estimated heat load of the stand-alone control dewar is:

Female liquid bayonets (2: b9, b11)	1.2 W
Vent line bayonet (b14)	.6 W
Radiation *	.8 W
Neck intercept†	5.0 W
	7.6 W

Without the bayonets, the heat load is 5.8 W.

Chimney. Assume that the chimney has the same linear heat load as the transfer line, (0.51 W/m) leading to a heat load of 1.8 W for the 3.5 m chimney.

Magnet cryostat

Axial supports. With A = 2.1 cm^2 , L = 11.4 cm, $\int k\ (T)\ dt$ = 22.0 W/cm for Inconel 718, the heat load per support is 4.0 W and for the six supports is 24 W.

Radial supports. With A = 1.45 cm^2, L = 11.4 cm, the heat load per support is 2.8 W and for all 24 supports is 67 W.

Radiation to inner shield. With 30 layers of NRC-2 (300 Angstrom) in the 18 mm gap, giving an area heat flux of approximately 80 mW/ft^2 (0.86 W/m^2), the estimated heat load is 39 W.

*Radiation (50 mW/ft^2, 26" Ø x 26" long) = 0.74 W

†Conduction (4" Ø x .030" wall x 6" long) = $\frac{2.42\ cm^2}{13\ cm}$ (27.5 W/cm) = 5 W

Radiation to outer shield. With 30 layers of NRC-2 in the 18 mm gap, the estimated heat load is 39 W.

Radiation to end shields. Using 150 mW/ft^2 (1.4 W/m^2) because of penetrations, the estimated heat load is 2.8 W/end or 5.5 W total.

Conduction to inner shield. With 11 fixed supports and 170 G-10 leaf-spring type standoffs the conduction heat load is 65.5 W.

Conduction to outer shield. Same as to inner shield, 65.5 W.

Conduction to end shields. Each end shield consists of 18 sectors which have leaf-spring type standoffs. The total heat load for both ends is 45 W.

The magnet cryostat therefore is (rounding off to next highest integer)

Axial supports	24 W
Radial supports	67 W
Radiation to shells	84 W
Conduction to shells	176 W
Total	351 W

Heat Load Summary

Item see Fig. M(2)	Heat load to 77 K
TA	140 W
b0	5 W
LH	12 W
b1	1.2 W
b2	1.2 W

b3	1.2 W
b4 (with vacuum plug)	1.24 W
b5 (with vacuum plug)	1.24 W
b6 (with vacuum plug)	1.24 W
ut1 (4 m with valve)	1.7 W
b7	1.2 W
HTX	4.0 L/h
ut2 (4 m with valve)	1.7 W
b8	1.2 W
ut3 (4 m with valve)	1.7 W
b9	1.2 W
TL	12.8 W
b10	1.2 W
ut4 (4 m)	1.7 W
b13	1.2 W
b11	1.2 W
ut5 (4 m)	1.7 W
b12	1.2 W
b14	1.2 W
CD	5.8 W
CH	1.8 W
MAG	351 W
Total	$\overline{\sim 560}$ W + 4 L/h = 16 L/h

This can be summarized:

Magnet cryostat, chimney, control dewar 360 W

Refrigerator heat exchanger #1 4 L/h or 24 gal/day

Transfer line, U-tubes, header, tank 198 W

Note: The liquid nitrogen usage will be substantially higher than this if the nitrogen flow is in the slug flow regime.

APPENDIX N - PRESSURE RELIEFS

General

This appendix describes the pressure relieving devices (relief valves and disks, burst disks) on the vacuum, helium and nitrogen systems. Not all of the sizes and pressures of the reliefs are known at this time, but those on the magnet cryostat/chimney/control dewar package are tentatively specified. The ASME Code, Section VIII, Paragraph UG-125 to -136 and Appendix M is followed for the relief devices. The total system is considered on an individual component or subsystem basis. Special care is given to relieve all trapped liquid volumes (TLV), i.e., those components or sections of piping or transfer lines in which liquid nitrogen or helium may become trapped (typically between valves).

Compressor Subsystem

This subsystem includes the Mycom compressor skid, purifier skid and associated piping in the BØ Compressor Building. The helium suction line has a relief valve at approximately 3 atm. The helium discharge line has a relief valve on the compressor at approximately 21-22 atm, since the Code rating of the compressor and purifier skids is 350 psig (24.8 atm).

Buffer Tank

The buffer tank is code-rated for a maximum allowable working pressure of 250 psig (17 atm). A relief valve at 17 atm, sized for 50 g/s of helium gas at 300 K is used.

Liquid Nitrogen Tank

Both the insulating vacuum space and the liquid vessel are relieved by appropriate relief valves and rupture disks.

Refrigerator Heat Exchanger

Relief valves are located on the tube-side inlet lines to HTX1 and HTX2 and on the shell-side outlet of HTX2. The nitrogen supply lines are relieved against TLV. The vacuum vessel is also appropriately relieved to protect against simultaneous rupture of a high pressure helium and liquid nitrogen line.

Gas and Liquid Engine

The helium supply and return lines to both expansion engine modules have relief valves and the liquid engine is relieved against TLV. Both vacuum vessels are relieved by means of a combination pump-out/relief-valve assembly.

Valve Box

The vacuum vessel has a pump-out/relief assembly sized for 50 g/s of liquid helium. The various helium lines are relieved against TLV between bayonet valves and between bayonet valves and control valves.

Storage Dewar

The vacuum vessel has a pump-out/relief assembly and relief disk to protect against a catastrophic rupture of the helium vessel. The helium vessel, Code-rated for 8 atm, has redundant relief valves and perhaps a Fermilab "Kautsky" valve in the neck to guard against a quench-induced over pressure.

Nitrogen/Helium Transfer Line

The helium supply and return lines and both LIN supply lines are relieved to avoid TLV. The insulating vacuum space has a pump-out/relief assembly.

Control Dewar, Chimney and Cryostat

The common vacuum is relieved by a 3" (76 mm) pump-out/relief assembly which opens at 2 psig (1.16 atm). The vacuum space is also relieved by a 3" (76 mm) relief disk or rupture disk at the upper end of the chimney. Calculations given in Appendix K show an insignificant pressure drop across the chimney at a combined helium/nitrogen flow rate of 100 g/s.

The control dewar helium vessel is relieved through the 4" (100 mm) control dewar neck. Both helium supply and return lines have relief lines and "Kautsky" valves.

All helium and nitrogen piping is relieved against TLV.

U-Tubes

The U-tubes have a combination pump-out/relief assembly on the insulating vacuum. The U-tubes do not have reliefs on the inner (liquid) lines since in proper operation TLV do not occur.

APPENDIX O: PRESSURE DROP DURING NORMAL OPERATION

In the present calculations we consider two-phase (liquid-gas) flow of helium. For simplicity we assume a straight horizontal tube for the cooling tube.

For turbulent flow of liquid in circular tubes we have a basic relation[1)]

$$- dp = G\, dV + \frac{f\, G^2\, v}{D/2}\, dz$$

where

G : mass flow

V : average velocity

f : friction factor

v : specific volume

D : tube diameter

z : coordinate of straight pipe

We neglected a term corresponding to gravitation. The contribution from the first term is generally small for long tubes. For example, even when saturated liquid helium changes into saturated vapor at 4.5 K for G = 5 g sec^{-1} cm^{-2},

$$- \frac{\Delta p}{p} = \frac{G}{p}\, \Delta V \simeq 2 \times 10^{-3}$$

Therefore, we have an approximate relation

$$-\frac{dp}{p} = \frac{2 f G^2 v}{D p} dz \qquad (1)$$

or

$$-dp = \frac{32}{\pi^2} \frac{f M^2}{D^5} v \, dz \qquad (2)$$

where M is the net mass flow rate and $M = \pi D^2 G/4$.

The friction factor f can be computed by an empirical relation

$$f = 0.00140 + 0.125 / Re^{0.32} \qquad (3)$$

where Re is the Reynolds number

$$Re = D G/\mu = 4 M / (\pi D \mu)$$

and μ is the viscosity.

The pressure drop of isothermal two-phase flow can be approximated by the following relations:[2)]

$$-\frac{dp}{dz} = -\left.\frac{dp}{dz}\right|_g \Phi_g^2$$

$$\Phi_g^{2/n} = 1 + X^{2/n}$$

$$X^2 = \frac{1-x}{x} \frac{\mu_\ell \rho_g}{\mu_g \rho_\ell}$$

$$x = G_g / G$$

where $\left.\frac{dp}{dz}\right|_g$ is the pressure drop for the gas phase alone, x the quality factor of gas, ρ the density, and the suffixes ℓ and g stand for iquid and gas, respectively. The parameter n is approximately 4 for turbulent flow.

We assume that flow velocities of liquid and gas are identical in the two phase flow of helium. Then the effective tube diameter and friction factor for gas phase D_g and f_g can be computed by

$$D_g^2 = \frac{x\, v_g}{(1-x)\, v_\ell + x\, v_g} D^2$$

$$f_g = 0.00140 + 0.125 / (D_g\, G_g / \mu_g)^{0.32}$$

Figure 0(1) shows $-\frac{1}{p}\frac{dp}{dz}$ and $\left.-\frac{1}{p}\frac{dp}{dz}\right|_g$ computed as a function of gas quality factor x. The flow rate is assumed to be 10 g/sec for the tube diameter of 2 cm.[3)]

For a gas quality of about 30% (70% liquid) and a cooling tube length of 150 m, the pressure drop is approximately 0.45×10^{-5} atm/cm $\times$ 1.5×10^4 cm $\sim$ 0.07 atm (1.03 psi).

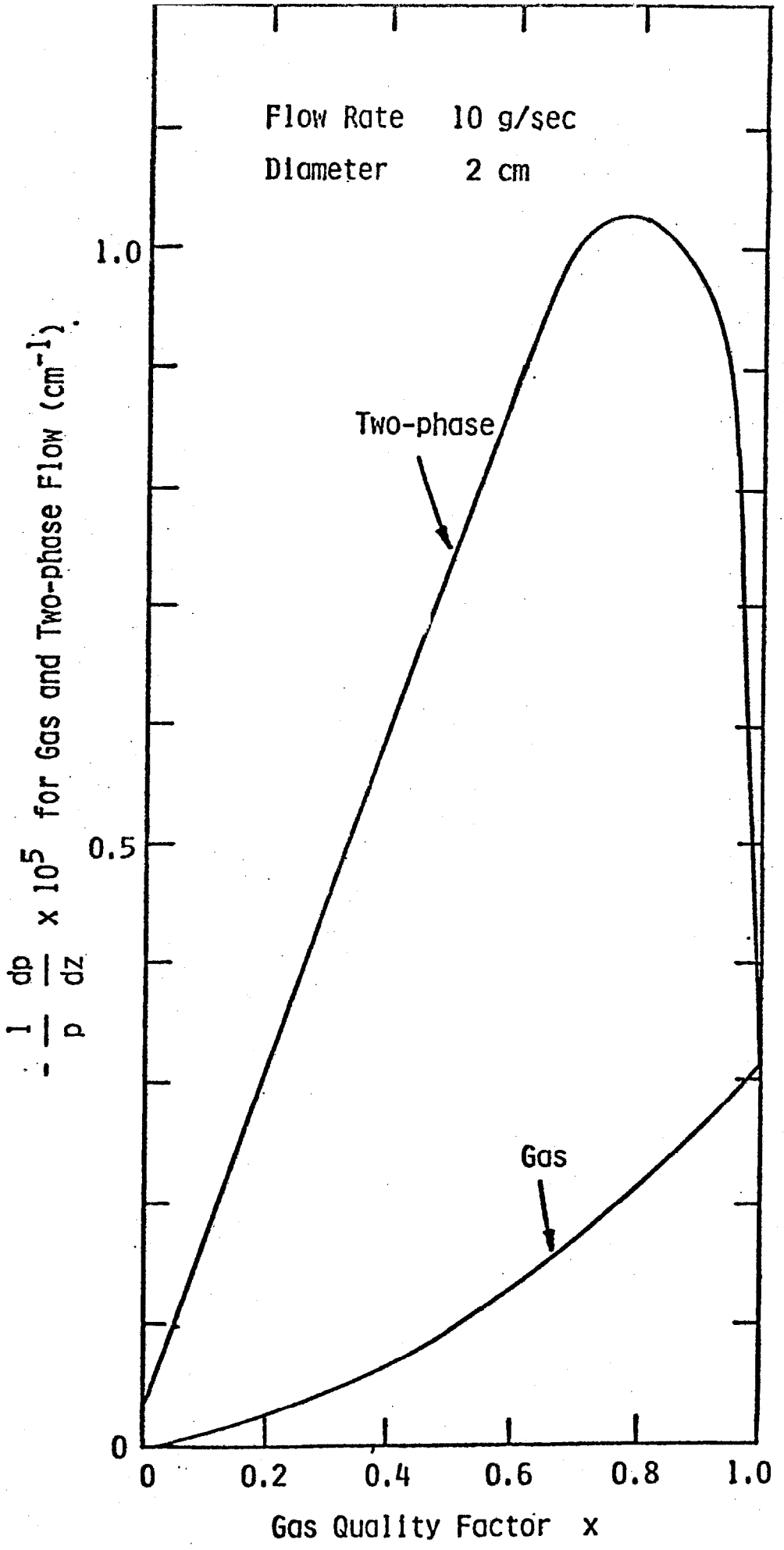

Fig. 0(1). Steady state pressure drop in helium cooling tube

References

1. W.H. McAdams, "Heat Transmission", 3rd ed., McGraw-Hill Book Co., Inc., N.Y. 1954, Chapter 6.

2. Y. Mori and K. Hijikata, "Nagare to Netsu no Kogaku (in Japanese) (Engineering of Flow and Heat)", 2nd ed., Kyoritsu Publishing Co., Inc., Tokyo, 1978, Chapter 7.

3. Properties of helium are summarized in R.B. Scott, "Cryogenic Engineering", D. Van Nostrand Co., Inc., Princeton, N.J., 1059, Chapter 9.

APPENDIX P: LOCAL HEAT SOURCE INSIDE THE CDF SOLENOID COIL

Introduction

We consider the case in which the coil of the CDF solenoid has a local heat source. It can be due to a bad conductor spot or discontinuity of superconductor caused by inclusion. We estimate the upper limit of temperature rise at the conductor under various conditions.

Method of Calculations

The effective thermal conductivity inside the coil in the solenoid axial direction κ_{ax} can be given by

$$\kappa_{ax} = (t_{Al} + t_{Ins}) \frac{\kappa_{Al} \times \kappa_{Ins}}{t_{Al}\,\kappa_{Ins} + t_{Ins}\,\kappa_{Al}}$$

$$\simeq \frac{t_{Al}}{t_{Ins}} \kappa_{Ins}$$

$$= \frac{0.39}{0.01} \times 0.001 = 0.04 \text{ W cm}^{-1} \text{ K}^{-1}$$

where t and κ are the material thickness and thermal conductivity, respectively, for aluminum stabilizer (Al) and insulator (Ins).

Since $\kappa_{Al} > 10 \text{ W cm}^{-1} \text{ K}^{-1}$ for high-purity aluminum stabilizer near 4.5 K as shown in Fig. 1, thermal conduction of the coil proceeds predominantly in the conductor direction.

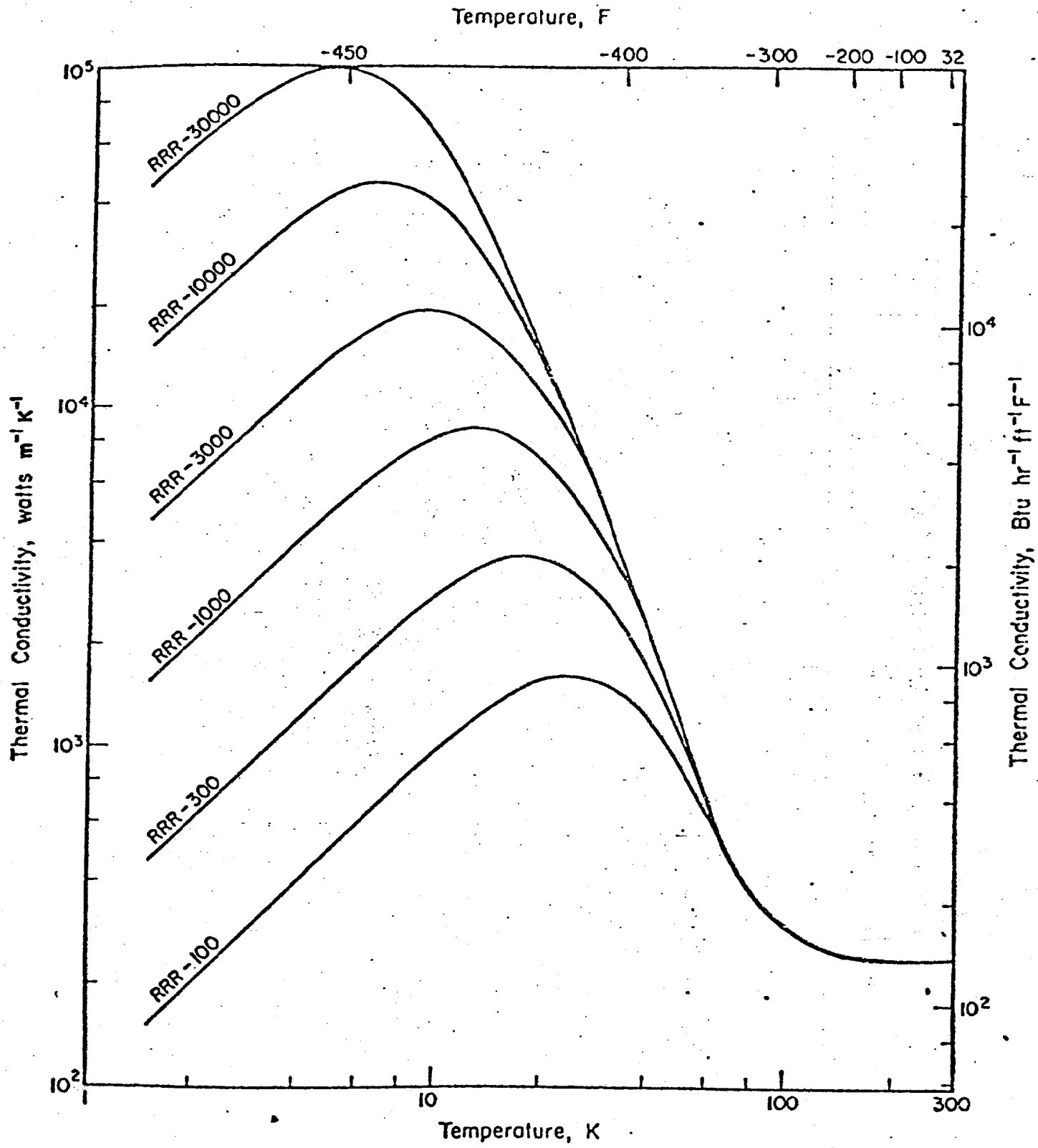

Fig. P(1). Thermal conductivity versus temperature for aluminum

Calculations are made in two steps. First we assume that the support cylinder is an infinite heat sink and has a uniform temperature despite of heat flow from the conductor due to a local heat source. We also assume thermal conduction in the conductor direction only and no thermal coupling between the adjacent turns. Therefore, the coil appears from the support cylinder as if it had a line heat source in the conductor direction. Second we evaluate the temperature gradient in the support cylinder for the line heat source obtained in the first step.

Results

First Step. We assume that the conductor has uniform temperature distribution in the plane perpendicular to the conductor current direction. The heat flow q per unit length from the conductor to the support cylinder is given by

$$q(x) = \kappa_{Ins} \frac{t_{Al}}{\delta} \Delta T(x) \qquad (1)$$

where δ is the thickness of insulator and $\Delta T(x)$ the temperature difference between the conductor and the support cylinder at x as shown below.

The heat flow inside the conductor Q(x) is given by

$$Q(x) = \kappa_{Al} S \frac{d\ \Delta T(x)}{dx} \qquad (2)$$

where S is the conductor cross section and S = 0.39 x 2.0 cm^2. We neglected effects due to the NbTi/Cu conductor.

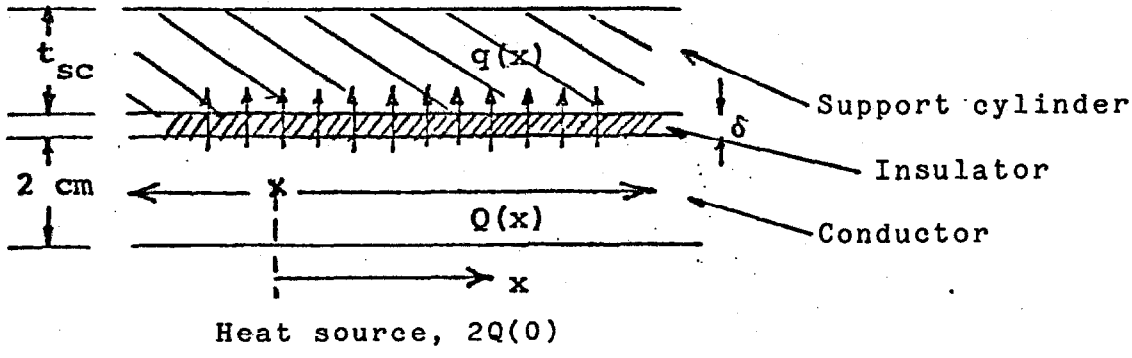

The temperature distribution ΔT(x) can be calculated numerically for a given heat source using Eqs. (1) and (2). The source power corresponds to 2Q(0). Figure P(2) shows computed maximum temperature ΔT(0) as functions of source powers for δ = 0.2, 0.3, and 0.5 cm, and $\kappa\kappa_{Al}$ = 10, 30, and 60 W cm^{-1} K^{-1}. We used κ_{Ins} = 0.001 W cm^{-1} K^{-1}.

Figure P(3) shows computed temperature distributions and net heat flow rates (Q) for δ = 0.3 cm and κ_{Al} = 10 and 30 W cm^{-1} K^{-1}. The source power is 0.8 W for κ_{Al} = 30 W cm^{-1} K^{-1} and 0.6 W for κ_{Al} = 10 W cm^{-1} K^{-1}. Figure P(4) shows the heat flow rate to the support cylinder for δ = 0.3 cm and κ_{Al} = 30 W cm^{-1} K^{-1} as a parameter of the source power.

Second Step In the case of the CDF solenoid the cooling tube will be placed outside the support cylinder perpendicularly to the line heat source shown in Fig. P(4). Since calculations are difficult in this case, we consider a much more severe case in

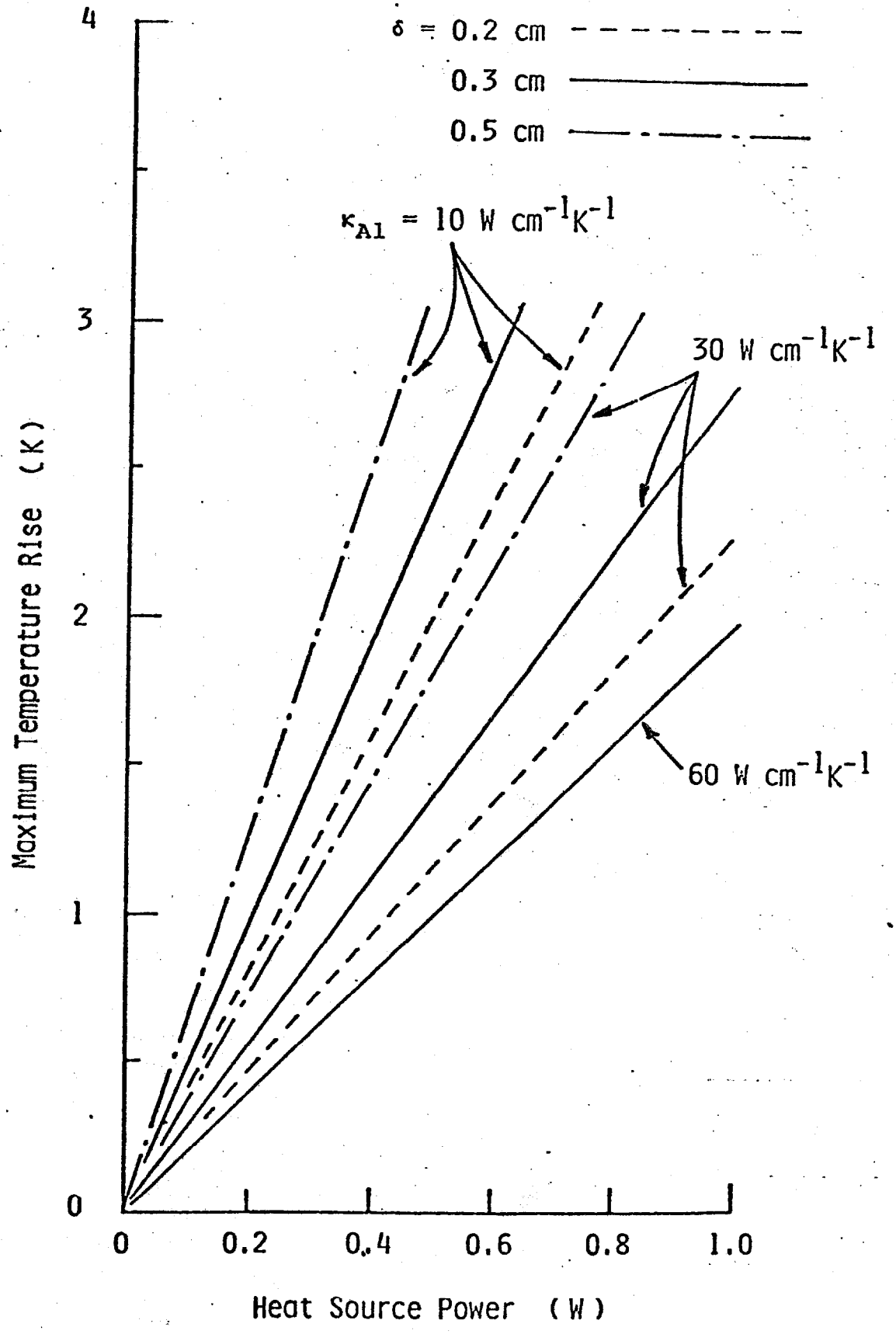

Fig. P(2). Maximum temperature as a function of source power with source power = 2Q(0)

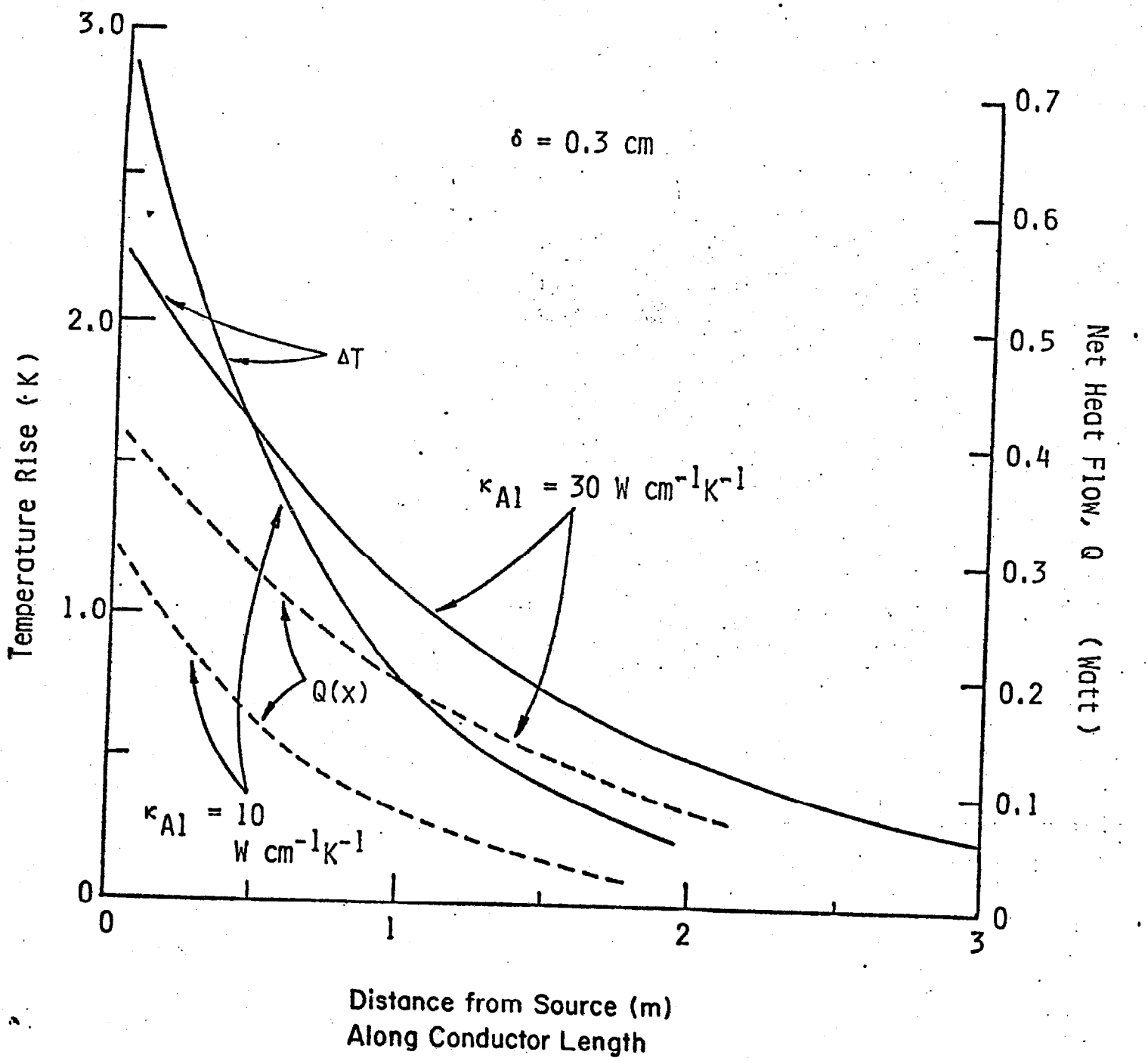

Fig. P(3). Computed temperature distribution

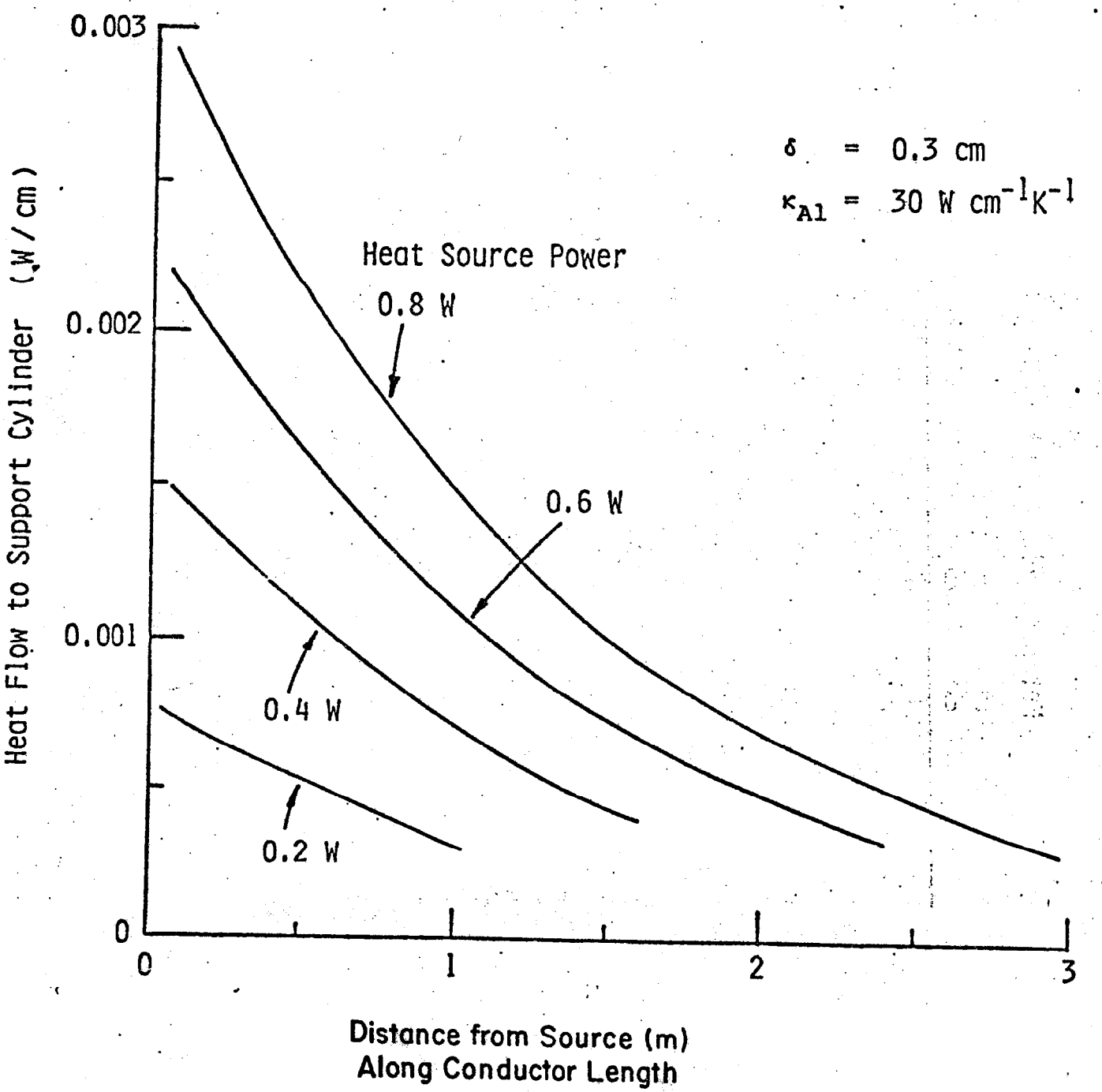

Fig. P(4). Heat flow distribution with heater source power = 2Q(0)

which the line heat source lies parallel to the cooling tube and at the middle of two cooling paths with an interval of s. Then the maximum temperature rise can be given approximately by

$$|\delta T|_{max} \lesssim q(0) \frac{1}{\kappa_{sc} t_{sc}} \frac{s}{2} \qquad (3)$$

where κ_c and t_c are the thermal conductivity and thickness of the support cylinder.

For a local heat power of 0.8 W in the conductor, $q(0) = 0.003$ W cm^{-1} as shown in Fig. P(4). With $\kappa_c = 0.04$ W cm^{-1} K^{-1}, $t_c = 1.6$ cm, $s = 40$ cm, and $q(0) = 0.003$ W cm^{-1}, we get

$$|\delta T|_{max} \lesssim 0.94 \text{ K}$$

For a local heat power of 0.6 W, $|\delta T|_{max} \lesssim 0.72$ K. Therefore, the overall maximum temperature rise is less than 0.7 K.

Conclusions

The temperature rise due to a local heat source in the coil depends upon the thermal conductivity of aluminum stabilizer, thickness of the support cylinder and insulator, and interval of the cooling path of two-phase helium. The present calculations are made very conservatively. Nevertheless, for a set of reasonable parameters a heat source of 0.5 W gives a temperature rise of about 0.5 K or less.

Figure P(5) shows the temperature rise measured in the quench test of the R&D solenoid at 5000 A. The interval of the cooling path was 10 cm. The heat power was applied with a pulse of about 110 msec. It can be said from this measurement that the DC heat power of roughly 1 W probably would not quench the R&D solenoid which has a similar aluminum-stabilized superconductor to that of the CDF solenoid.

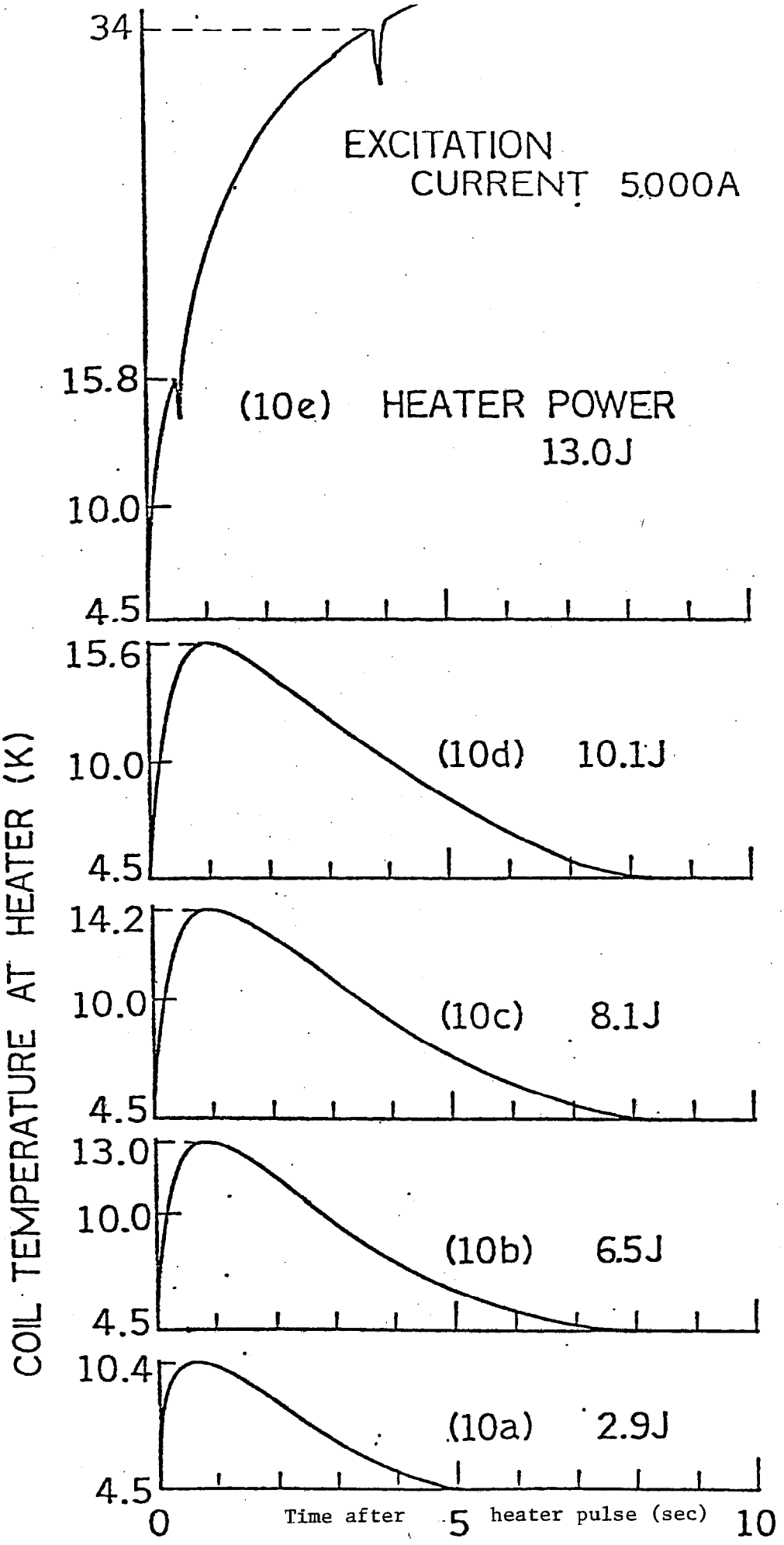

Fig. P(5). Temperature rise in R&D solenoid